NUREG/CR-3915
PNL-5184

Acoustic Emission Results Obtained From Testing the ZB-1 Intermediate Scale Pressure Vessel

Prepared by P. H. Hutton, R. J. Kurtz, R. A. Pappas,
J. F. Dawson, L. S. Dake, J. R. Skorpik

Pacific Northwest Laboratory
Operated by
Battelle Memorial Institute

Prepared for
U.S. Nuclear Regulatory Commission

NUREG/CR-3915
PNL-5184
R5, GS

Acoustic Emission Results Obtained From Testing the ZB-1 Intermediate Scale Pressure Vessel

Manuscript Completed: April 1985
Date Published: September 1985

Prepared by
P. H. Hutton, R. J. Kurtz, R. A. Pappas,
J. F. Dawson, L. S. Dake, J. R. Skorpik

Pacific Northwest Laboratory
Richland, WA 99352

Prepared for
Division of Engineering Technology
Office of Nuclear Regulatory Research
U.S. Nuclear Regulatory Commission
Washington, D.C. 20555
NRC FIN B2088

ABSTRACT

Acoustic emission (AE) monitoring of flaw growth in an intermediate scale vessel during cyclic loading at 65°C and 288°C is described in this report. The report deals with background, methodology, and results. The work discussed is of major significance in a program supported by NRC to develop and demonstrate application of AE monitoring for continuous surveillance of reactor pressure boundaries to detect and evaluate growing flaws. Several areas of technical concern are addressed. Results support the feasibility of effective continuous monitoring.

TABLE OF CONTENTS

TABLE OF CONTENTS

(cont'd)

LIST OF FIGURES

LIST OF FIGURES

(cont'd)

LIST OF FIGURES

(cont'd)

LIST OF FIGURES

(cont'd)

LIST OF FIGURES

(cont'd)

LIST OF FIGURES

(cont'd)

LIST OF FIGURES

(cont'd)

LIST OF FIGURES

(cont'd)

LIST OF FIGURES

(cont'd)

LIST OF FIGURES

(cont'd)

LIST OF FIGURES

(cont'd)

LIST OF FIGURES

(cont'd)

LIST OF FIGURES

(cont'd)

LIST OF TABLES

ACOUSTIC EMISSION RESULTS OBTAINED FROM TESTING THE ZB-1 INTERMEDIATE SCALE PRESSURE VESSEL - AN INTERIM REPORT

EXECUTIVE SUMMARY

1.0 INTRODUCTION

A program devoted to developing and demonstrating the use of acoustic emission (AE) methods for continuous surveillance of reactor pressure boundaries to detect flaw growth is in progress at the Pacific Northwest Laboratory (PNL). This work is sponsored by the U.S. Nuclear Regulatory Commission. In an initial phase, technology was developed in the laboratory to identify AE from crack growth and to utilize that AE information to estimate flaw severity. Two key subsequent phases are concerned with evaluating the technology through testing on an intermediate scale test vessel (Phase 2) and finally, demonstrating the technology on an operating reactor (Phase 3).

Phase 2 has been accomplished by testing an intermediate scale vessel. This test and the associated results constitute the subject of this report.

Theoretical transfer of laboratory test results to a full size structure is complex and uncertain particularly in the case of AE. Phase 2 was designed to be an experimental transfer step to validate laboratory relationships on a structure wherein conditions could be controlled and adjusted to provide a simulation of a range of reactor monitoring conditions. Additionally, it was intended to identify limitations in the AE technology for structural monitoring and develop improvements to overcome these limitations. Key considerations in the work included:

- reliability of flaw detection and location
- ability to detect AE signals in the presence of reactor background noise
- separation of crack growth AE signals from similar acoustic signals produced by innocuous sources (slag inclusions, insulation rubbing, etc.)
- ability to interpret AE data in terms of source significance
- effect of temperature on detection of AE from crack growth.

The decision was made to perform Phase 2 by participating in testing of a German vessel (ZB-1). Arrangements were made under the NRC-BMFT Safety Research Exchange Agreement. The site of the test was a test bunker at the Grosskraftwerk Mannheim facility in Mannheim, West Germany. This provided the necessary facilities for performing high temperature testing. The test vessel was located about 18 meters (60 feet) underground in the test bunker with the AE instrumentation located in a trailer at ground level adjacent to the test bunker.

2.0 TEST EQUIPMENT AND INSTALLATION

The ZB-1 vessel, with a 120 mm thick wall, is 1713 mm O.D. and 3750 mm long. An A533B steel section 1500 mm x 700 mm x 120 mm containing I.D. and O.D. machined flaws (a machined groove which was fatigue precracked prior to testing) was inserted in the vessel wall. A second insert, designated KS07C, fabricated from degraded A508 German steel was also installed. This insert was 1500 mm x 700 mm x 120 mm and was placed in the vessel wall on the side opposite the A533B insert.

Other special features designed into the test were:

- A slag inclusion placed into the A533B insert weld.
- An I.D. clad section intended to contain areas of underclad cracking and poor clad-to-vessel bonding.

The AE monitoring/analysis system consisted of a special data acquisition front end developed and fabricated by PNL, a PDP 11/23 computer for data analysis, a waveform digitizer and recorder, and a PDP 11/03 computer for waveform pattern recognition analysis. A special feature of the data acquisition front end instrument was a high density tape cartridge recorder with a 67 Mbyte storage capacity. This facilitates making a backup record of all raw data as well as performing on-line data analysis.

Waveguide sensors made up of 3.2 mm (0.125 in.) diameter by 605 mm (23.8 in.) long stainless steel wire with a piezoelectric crystal and amplifier integral on one end were used to accommodate the high temperature test conditions. Part of these sensors were pressure coupled in the same fashion they are being applied for reactor monitoring. The waveguide sensors were tuned to operate at about 400 kHz frequency.

A special set of commercial sensors with peak response at 110 kHz were installed on the vessel surface for each hydro test. The intent here was to provide a monitoring regime similar to what would normally be applied in a preservice hydro test.

All sensors were characterized at the time of installation and periodically during the test.

Crack opening displacement (COD) gauges were installed on the three machined defects in the A533B insert. The smaller of the flaws was designated Flaw A and was located on the insert I.D. The middle sized flaw (Flaw B) was also on the I.D. Flaw C, which was the largest flaw, was located on the insert O.D. The flaws were sized to produce a wide range of flaw growth rate under the cyclic load test conditions. The COD gauges provided a continuous measure of crack growth which was then related to the AE information.

3.0 TEST CONDITIONS

The ZB-1 vessel test was designed to provide a variety of test conditions (loading, temperature, R-ratio, noise sources, etc.). Water was used as an internal pressurizing medium to stress the vessel in both static and cyclic loading. The test matrix consisted of five hydrostatic tests separated by blocks of cyclic loading which total 28,000 cycles. Testing temperatures of 65°C and 288°C with an operating pressure of 250 bar (3675 psig) were used.

Cyclic loading was tension-tension with planned changes in R-ratio. Cycle rate varied from a maximum of 1 cycle/78 seconds during 65°C testing to a minimum of 1 cycle/120 seconds during 288°C testing.

4.0 TEST RESULTS

4.1 HYDROSTATIC TEST RESULTS

Six hydrostatic tests were performed as shown below.

Step	Overpressure, %	Temperature, °C
1	0	65
4	2	65
7	4	65
9*	10	240
10	15	65
13	36	65

*Not planned as a part of the original test matrix.

The AE results from the six hydro tests performed in the course of the ZB-1 test lead to the following conclusions:

- AE appeared to be sensitive to the KS07R weld crack in the second part of Step 1. The flaw was estimated to have been about 5 mm deep at that time, yet the AE from the 1.0 x operating pressure hydro showed indications of the crack. Also in the first part of Step 1, the KS07 degraded material produced an abundance of AE even before reaching the 1.0 x operating pressure level. The machined defects did not produce AE in Part 2 of Step 1 because they were previously stressed in Part 1 of Step 1 (some flaw indications noted at that time).

- The hydro results raise a serious question about the effectiveness of AE monitoring during inservice hydrostatic testing to 1.15 x operating pressure. Steps 4, 7, and 10 produced no notable indications from the known flaws. In Step 13, AE was identified with Flaw B at about 1.0 x operating pressure; however, it was 83% through-wall at this point. The stress intensity level required to activate Flaw B was about 70 ksi$\sqrt{in}$. Flaws A and C barely exceeded this level during the Step 13 hydrotest. Since no notable AE was detected for any of the flaws below this stress intensity level, small flaws do not appear to be detectable at low overpressure levels during an inservice hydrotest. As the level of inservice hydro test overpressure increases, the flaw detection resolution could be expected to increase.

It must be noted that the above conclusions do not apply to AE monitoring of vessels during preservice acceptance testing where the flaw areas generally would not have been previously stressed to a high level. AE monitoring under these conditions should be effective for flaw detection.

4.2 SPECIAL TEST FEATURES

There were several special features of the test. These features include:

- flow noise simulation
- slag inclusion
- weld cladding
- nozzle cracks
- blind test.

The flow noise simulator was effective in testing the influence of reactor coolant flow noise on detection of AE from crack growth. It had little affect on AE detection with sensors tuned to 400 kHz; however, low frequency (150 kHz) sensors were

saturated. The results were consistent with subsequent data obtained during hot functional testing at Watts Bar, Unit 1 nuclear reactor in indicating that the flow noise is a manageable problem.

A slag inclusion placed in the A533B insert weld partially accomplished its purpose. It indicated that a small slag inclusion (100 x 3 mm) should not interfere with AE detection. Due to the small size, however, essentially no AE was detected which precluded assessing the similarity between AE which might be produced by a major slag inclusion and that from crack growth.

Weld cladding did not fulfill its intended purpose of evaluating AE detection of possible noise from defective cladding areas and detection of underclad crack growth due to the lack of intended flaws. Detection of underclad cracking should not be a problem, however, since the AE signals would not traverse the defective area to reach AE sensors on the vessel O.D.

Unplanned cracking in the KS07R insert installation weld provided an effective "blind" test of AE detection of crack growth which gave very positive results. AE detected and located the growing crack significantly before it was confirmed by ultrasonic testing.

Cracking in the bore of blind nozzles on the vessel was not clearly indicated by AE. This, however, appears to be due to a unique geometry effect wherein the discontinuity of the nozzle bore interferred with propagation of signals to some of the AE sensors installed to monitor the vessel cylinder.

4.3 AE MONITORING AT 65°C

The first two-thirds of the ZB-1 vessel cyclic loading test was performed at 65°C (150°F). This consisted of four elements designated as Steps 2, 3, 5, and 6. The cyclic loading steps were alternately low (0.1) and high (0.6) R-ratio to produce crack front marking between steps as a result of the different crack growth rate. The maximum pressure for all low temperature cyclic loading was 240 bar (3530 psig).

AE from growth of Flaws A and B was detected by both the AE array (Array 2) on the A533 insert and the AE array (Array 3) monitoring the vessel cylinder. The crack growth AE assumed consistent characteristics of high amplitude and of occurring at or near peak load.

Noise from a manhole cover assembly was an intermittent problem throughout the low temperature testing. Generally, this

noise could be handled by filtering with parametrics (load position and signal amplitude). This, however, underscores the need for real-time AE identification by pattern recognition to isolate crack growth AE. Generally, parametrics such as load position in particular will be of little use in a general reactor monitoring situation.

There was some evidence of the KS07R weld crack becoming active during Step 6. The indications were not sufficiently prominent to draw attention at that time, however.

Point location of AE sources was not always as concise as desired. Point source location using a two-dimensional concept on a heavy section, complex structure is a significant challenge. This is an aspect of established AE technology that needs to be reassessed and upgraded.

The need to exercise special care in mounting pressure coupled waveguide AE sensors was evident. Performance of Array 3 (pressure coupled) was marginal until the waveguide-to-vessel interface pressure was corrected. This resulted in a significant improvement in array performance.

4.4 AE MONITORING AT 288°C

High temperature - 288°C (550°F) - test conditions were imposed during the last one-third of the cyclic loading. This constituted Steps 8, 9, and 11 for a total of 7300 load cycles. R-ratios of 0.4 and 0.6 were applied alternately during this period. The maximum cyclic pressure was 250 bar (3675 psig).

The dominant sources of acoustic emission during the high temperature portions of the test were manhole noise during Step 8, and KS07R weld cracking during Steps 9 and 11. Flaw growth activity from A, B, and C was detected by all arrays during Steps 8 and 9, but was overshadowed by the large amount of activity from the KS07R weldment during Step 11. In the hot phase of the test, Array 3 was most effective at detecting and locating activity from the KS07R weld cracking and least effective at detecting events from Flaws A, B, and C under the given circumstances. Overall, Array 3 (cylindrical array) performed better than Arrays 1 and 2 (quad arrays). The latter two showed a tendency to mislocate data originating outside of the array to show it inside the array. This was not the case with Array 3. The amplitude and load position characteristics of the AE signals from Flaws A, B, and C were similar to signals detected during 65°C testing. Signal attributes for events from the KS07R weld cracks were different than for Flaws A, B and C. The difference in signal amplitudes was probably [illegible] due to the large source-to-sensor distance. The substantially higher

event rates from the KS07R weld cracks may have resulted from differences in material chemistry, heat treatment, and flaw geometry.

4.5 AE/FLAW GROWTH INTERPRETATION

Flaw growth characteristics for Flaws A, B, C, and KS07R weld cracking have been determined from NDE, crack-opening-displacement and fractographic measurements. This information was used to establish crack growth rates for comparison with predictions derived from the AE/flaw severity relationship. The near field array (Array 2) consistently detected more AE events than the far field array (Array 3). Both arrays failed to detect any notable AE from Flaw C at 65°C test conditions, but this was probably due to the small amount of crack growth produced by this defect. The amount of AE caused by large crack jumps varied, which matches experience with laboratory specimens.

A test of the flaw severity relationship indicates that the model underpredicted crack growth rates at 65°C test temperature. This result was not anticipated but may not seriously impair the utility of the relationship for use at operating pressure and temperature. When the relationship was applied to 285°C data, the crack growth rate was consistently overpredicted by the near field array as was expected. The far field array results were not conservative in that the crack growth rate was underpredicted in half the cases. Clearly the source-to-sensor distance was largely responsible for this effect. The range of predicted crack growth rates were within the normal variation observed during laboratory testing. It is significant to note that the relationship tends to compensate for the range of absolute number of AE signals detected by the two arrays for the same two installed flaws.

A test of the relationship on the weld cracking in the KS07R replacement patch was attempted and indicated a significant overprediction of the crack growth rate. The magnitude of the overprediction was beyond our expectations based upon the laboratory data. Possible explanations for the difference in behavior are material chemistry, heat treatment, and the extremely complex geometry of the KS07R weld crack.

4.6 CRACK GROWTH AE SIGNAL IDENTIFICATION

One of the key requirements of this program is to develop a method of separating AE signals produced by crack growth from acoustic signals produced by innocuous sources. Signal pattern recognition using signal processing techniques to generate features related to spectral content was chosen initially. This did not produce satisfactory results during the test. A second

set of features consisting of the parameters of a 10th order autoregressive model of each waveform was developed out of analysis of initial ZB-1 data. This approach showed some improvement in identification of acoustic signals from the ZB-1 test, but still did not produce the performance level considered necessary ($\geq$90% correct classification).

In the course of reassessing the problem, waveform by waveform source location made possible the identification of a consistent three-pulse signal pattern present in practically all waveforms originating near known and suspected regions of crack growth. This is a function of the waveguide sensor response to excitation by a fast rise time, short duration signal. A signal classification method developed around this phenomenon has produced over 90% correct classification of recorded acoustic signals examined. This meets the required level of accuracy for an effective working tool.

5.0 CONCLUSIONS

The ZB-1 test results provide strong support to the feasibility of flaw surveillance in reactor pressure boundaries using AE. Key points of the test results are highlighted below.

The ability of an AE monitor system to perform over a long period under adverse conditions was demonstrated.

Generally, detection of AE from growing flaws was good at all stages of the test. One of the major achievements was detection of an unexpected crack growing in the KS07 replacement weld. This was clearly detected by AE well before it was confirmed by ultrasonics. Some of the AE sensors were 3 meters from the source.

Analysis of the test data to identify AE signals from crack growth has underscored the need for a method to isolate crack growth AE signals in real time. The pattern recognition algorithms applied for this purpose during the test performed discrimination correctly for many of the signals, but the overall performance was not acceptable. Post test analysis of recorded waveforms has, however, produced a modified approach which achieves a correct classification level greater than 90% for the ZB-1 data.

A test of the flaw evaluation model was performed. The relationship underpredicted the crack growth rate at 65°C (150°F) test temperature and overpredicted the crack growth rate at 285°C (550°F) test conditions. The high temperature results were within the expected range based upon the observed variations in laboratory data. The low temperature results were below the expected range. This may be due to a change in the

power-law relationship at low crack growth rates and/or that the relationship based on 20°C (70°F) data should be corrected for use on 65°C (150°F) data.

A test of the relationship on weld cracking in the KS07R replacement patch was attempted and indicated a significant overpredciction of the crack growth rate. The magnitude of the overprediction was beyond our expectations based on laboratory data. This result may have been due to differences in material chemistry, heat treatment, and flaw geometry.

Results from the hydrostatic tests lead to three conclusions.

- For preservice hydro testing to detect flaws where the vessel has not been previously stressed to operating conditions, AE monitoring should be an effective technique to detect and locate flaws because the flaws and surrounding material will be experiencing a new level of stress.

- Application of AE monitoring to inservice hydros limited to an overpressure of 1.15 x operating pressure appears to be of questionable effectiveness.

- In the case where higher hydro overpressures are used (i.e., in the order of 1.4-1.5 x operating pressure), AE monitoring appears to offer a useable degree of flaw detection resolution.

The AE event rate at a constant crack growth rate was not dependent upon temperature.

The high AE event rates from the KS07R weld cracks suggest that material chemistry and heat treat condition combined with complex flawed geometry may also significantly affect the AE event rate.

The results from the ZB-1 test have identified areas of technology which need to be improved. These areas do not preclude useful application of the technology at this time, but they are improvements needed to enhance the effectiveness and maturity of the technology.

Overall, the ZB-1 test is considered to be an unquestionable success. It provided valuable information to support continuous AE monitoring for flaw detection and it showed limitations which need to be observed in application of the technology and ultimately eliminated. Much of this information could not have been practically obtained in any way other than a test such as ZB-1.

ACOUSTIC EMISSION RESULTS OBTAINED FROM TESTING THE ZB-1 INTERMEDIATE SCALE PRESSURE VESSEL - AN INTERIM REPORT

1.0 INTRODUCTION

A program devoted to developing and demonstrating the use of acoustic emission (AE) methods for continuous surveillance of reactor pressure boundaries to detect flaw growth is in progress at the Pacific Northwest Laboratory (PNL).[1] This work is sponsored by the U.S. Nuclear Regulatory Commission. In an initial phase, technology was developed in the laboratory to identify AE from crack growth and to utilize that AE information to estimate flaw severity.[2] Two key subsequent phases are concerned with evaluating the technology through testing on an intermediate scale test vessel (Phase 2) and finally, demonstrating the technology on an operating reactor (Phase 3).

Phase 2 has been accomplished by testing an intermediate scale vessel. Results from the test constitute the subject of this report.

Phase 3 of the program is being performed at the Watts Bar Unit 1 Nuclear Plant through the cooperation of the Tennessee Valley Authority. Progress on Phase 3 is reported separately.[3,4]

1.1 PHASE 2 CONCEPT AND APPROACH

Theoretical transfer of laboratory test results to a full size structure is complex and uncertain particularly in the case of AE. Phase 2 was designed to be an experimental transfer step to adjust and validate laboratory relationships on a structure wherein conditions could be controlled and adjusted to provide a simulation of a range of reactor monitoring conditions. Pertinent test vessel design criteria included the following:

- Wall thickness - greater than 100 mm (4 inches) thickness.
- Vessel diameter and length should be sufficient to test AE detection over a representative distance - at least 3 meters (10 feet).
- Vessel material should be representative of U.S. reactor pressure vessel steel - A533 Grade B, Class 1 steel.
- Vessel should be cyclically and monotonically loaded.

- Flaws will be exposed to pressurized water at temperatures up to 288°C (550°F).

- Cyclic stressing at R-ratios ranging from 0.1 to 0.7 (R = minimum pressure/maximum pressure) shall be employed.

- Nominal stress levels should be representative of those in operating reactor pressure vessels.

- Innocuous noise sources representative of reactor environment - e.g., coolant flow noise, insulation rubbing, slag inclusions, base metal-to-cladding interface noise, and electrical transients should be simulated.

The objective of Phase 2 was to determine the effectiveness of laboratory developed relationships and methods for monitoring flaws in a structure which simulated the conditions of monitoring a reactor pressure vessel. Additionally, to identify limitations in the AE technology for structural monitoring and develop improvements to overcome these limitations. Key considerations in the work included:

- reliability of flaw detection and location

- ability to detect AE signals in the presence of reactor background noise

- separation of crack growth AE signals from similar acoustic signals produced by innocuous sources (slag inclusions, insulation rubbing, etc.)

- ability to interpret AE data in terms of source significance

- effect of temperature on detection of AE from crack growth.

Three approaches to accomplishing Phase 2 were considered.

1. Install a test facility at PNL capable of performing the required testing.

2. Utilize test facilities at another national laboratory site (Oak Ridge National Laboratory).

3. Participate in vessel tests planned as part of the Federal Republic of Germany's program to investigate pressure boundary integrity issues. This included the

HDR test vessel at Kahl and a vessel test (ZB-1) to be performed at the Materialpruefungsanstalt (MPA) facilities at Stuttgart.

The choices were analyzed from the standpoint of test features available, timing, and estimated cost.[5] Based on this analysis, the decision was made to participate in testing of the German ZB-1 vessel. Arrangements were made under the NRC-BMFT Safety Research Exchange Agreement. In the course of negotiations with MPA on test plans, the site of the test was changed to a test bunker at the Grosskraftwerk Mannheim facility in Mannheim, West Germany (Figure 1.1). This provided the necessary facilities for performing high temperature testing. The test vessel (Figure 1.2) was located about 18 meters (60 feet) underground in the test bunker with the AE instrumentation located in a trailer at ground level adjacent to the test bunker. This involved using signal cables about 45 meters (150 feet) in length between the AE sensors on the vessel and the AE monitoring instruments. Fortuitously, this simulates the length of cable required to reach outside of containment in an actual nuclear reactor.

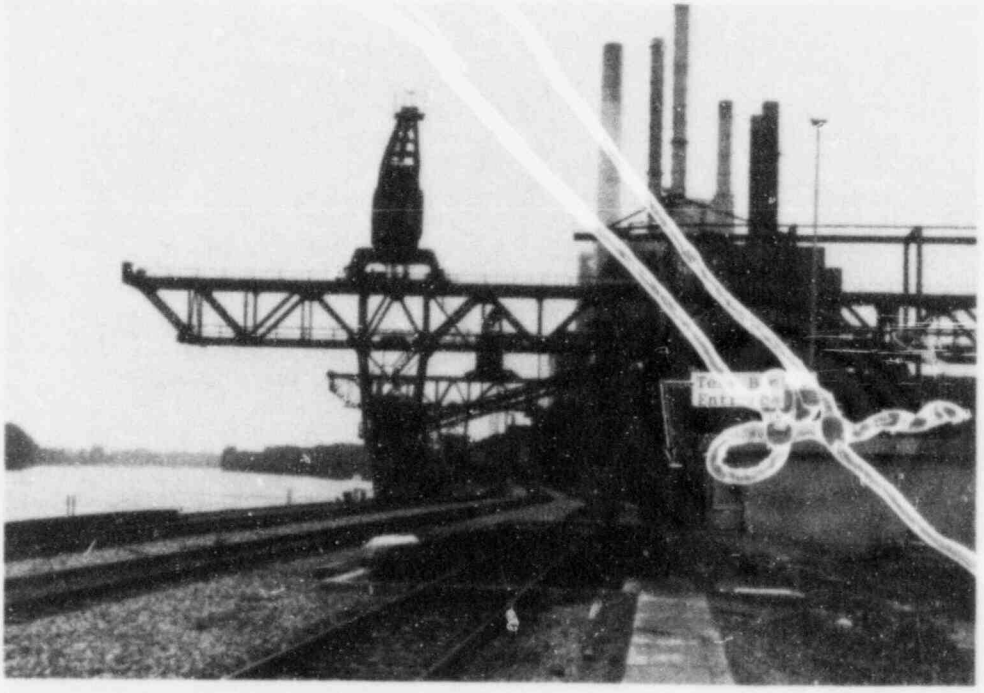

Figure 1.1. ZB-1 Test Site.

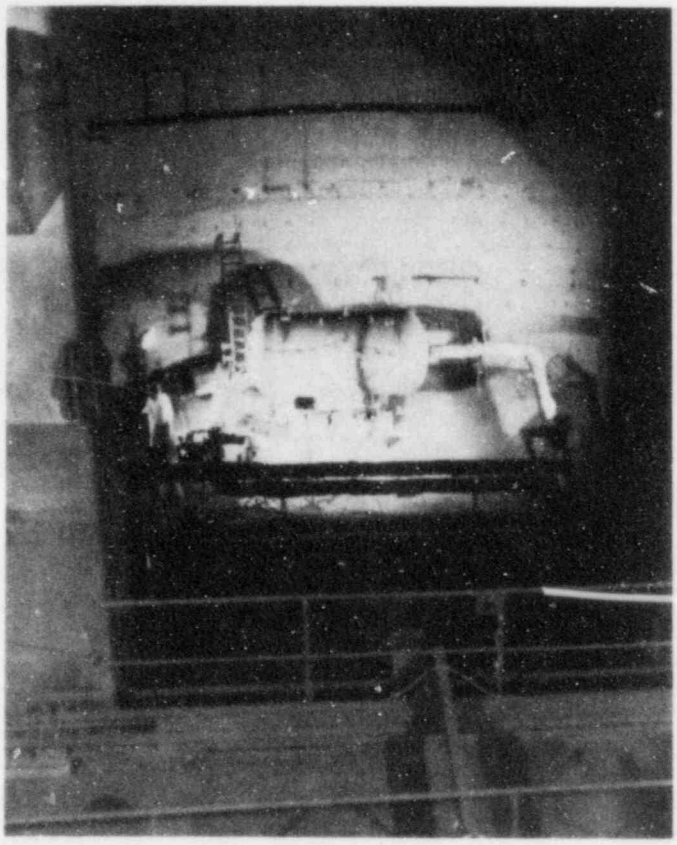

Figure 1.2. ZB-1 Vessel in the Test Bunker.

1.2 TEST PLAN

The complexity of the test together with the remoteness of the test site from PNL served to emphasize the necessity that a test plan be prepared in advance and approved by the participants. The test plan is included as Appendix A of this report. There were some deviations from the plan during the course of the test. The most notable was that the test sequence was shortened from that shown in the test plan. Steps 12, 14, 15, 16, and 17 were eliminated. A practical method for reducing the fluid volume in the tank during the high temperature part of the test could not be devised. Without this, bursting the vessel was not acceptable because the immense stored energy release might have destroyed the test bunker. With this in mind, the test was shortened when unanticipated cracks in the vessel grew significantly during high temperature testing to the point where the integrity of the vessel was in question by the end of Step 11. Step 13 was the final step.

2.0 TEST EQUIPMENT AND INSTALLATION

This section focuses on describing the test vessel and the special features included, the PNL measurement instrumentation, and preparation for test monitoring.

2.1 TEST VESSEL

The ZB-1 vessel shown in Figure 2.1 was fabricated from the German equivalent to A508 steel. The wall thickness is 120 mm (4.7 inches) and the outside diameter is 1712 mm (67.4 inches).

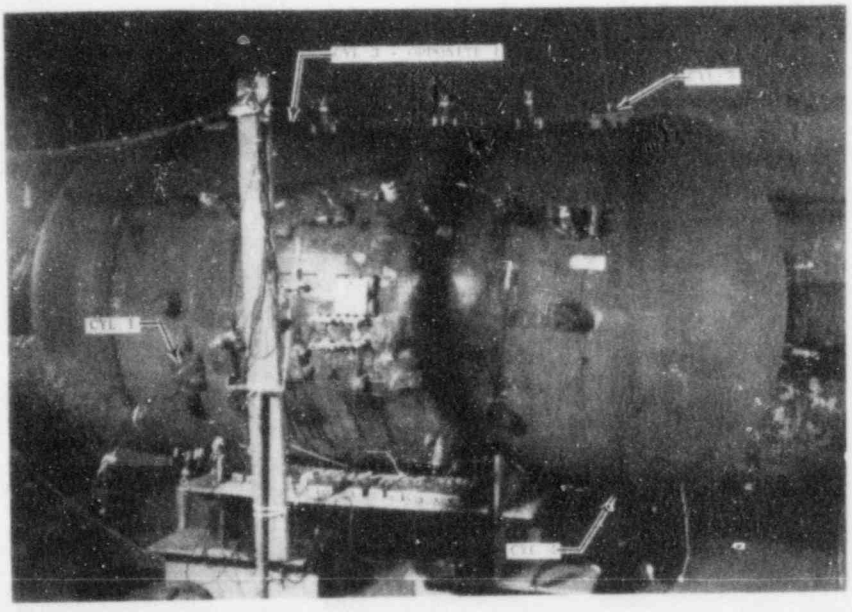

Figure 2.1. ZB-1 Test Vessel with AE Sensors Installed.

The length of the cylindrical section is 2280 mm (89.8 inches). Figure 2.2 shows a roll-out of the cylindrical portion of the vessel. Special features included in support of the test objectives are identifed. These are:

- two special inserts
- an intentional slag inclusion in a weld
- a stainless steel weld clad area on the vessel I.D.

An insert of A533 Grade B, Class 1 steel was included to relate to U.S. pressure vessel steel. The insert contained two I.D. (Flaws A and B) and one O.D. (Flaw C) part-circular surface notches that were fatigue presharpened. The insert was 1500 x 700 mm and 120 mm thick. Fabrication of this insert was

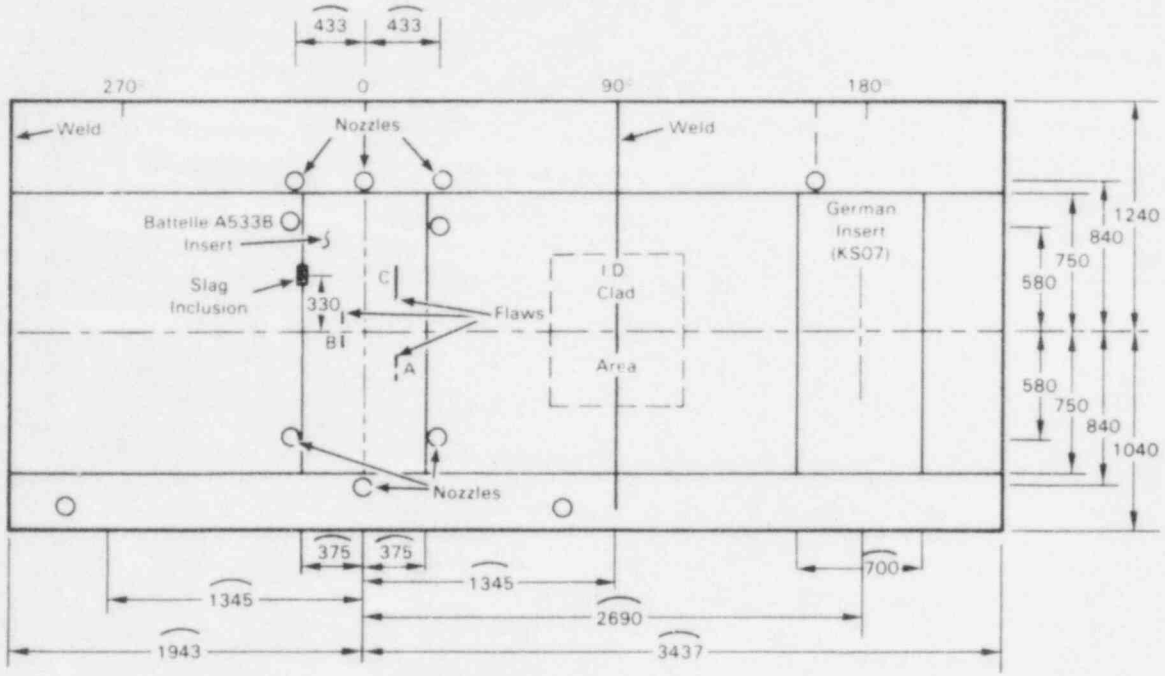

Note

1) Illustration is a Roll-Out of Vessel Cylinder
2) Dimensions in Millimeters

Figure 2.2. Test Features of the ZB-1 Vessel.

performed under contract with the German Materialpruefungsanstalt (MPA), Stuttgart using material supplied by PNL. A report detailing the fabrication process is included as Appendix B.

A second insert designated KS07 of A508 degraded German steel was also included. This insert was 1500 x 700 mm and 120 mm thick. The material was degraded by modified fabrication heat treatment to produce extensive micro and macro cracking. The purpose in testing the material was to evaluate its ability to withstand test conditions and thereby provide an experimental benchmark of the degree of material deterioration that could be tolerated in a reactor pressure vessel. An example of degraded material is shown in Figure 2.3.

The approach to fabrication of the KS07 insert is illustrated in Figure 2.4. The insert was fabricated from two sections machined from a very large block of material. As shown, these two curved sections were selected from the edge of the degraded area in the block. They were then welded end-to-end to produce a finished insert 700 mm x 1500 mm x 120 mm thick. The KS07 insert played a key role in the test.

The area in Figure 2.2 identified as "Slag" is the location of an intentional slag inclusion. The intent was to generate a

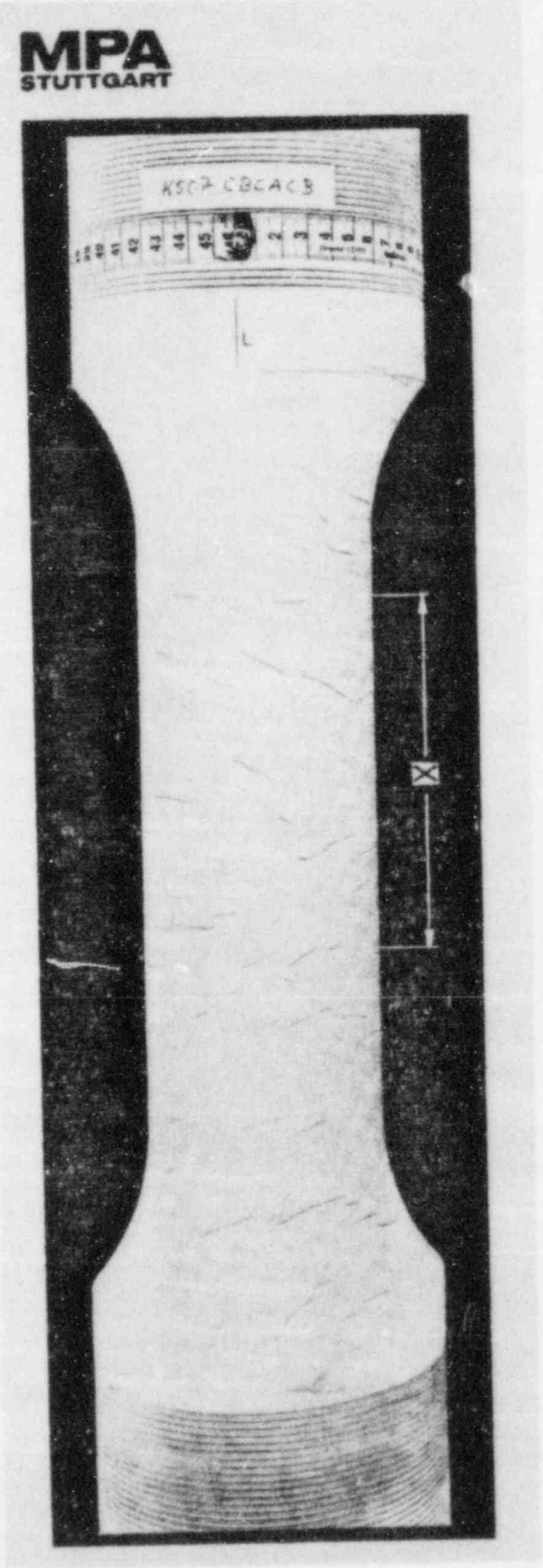

Figure 2.3. Specimen of the KS07 Degraded German Steel.

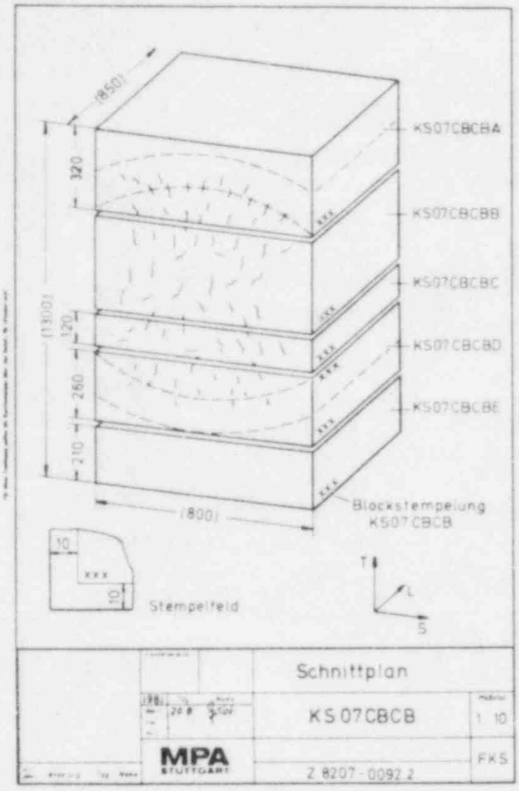

Figure 2.4. KS07 Insert Cutting Plan.

slag inclusion about 100 mm long by 10-15 mm wide near the mid-wall of the vessel. Pretest inspection of the vessel by the Fraunhofer Institut fuer zerstoerungsfreie Pruefverfahren (IzfP), Saarbruecken, West Germany indicated the slag was narrower than planned. Figure 2.5 shows an image of the slag by a synthetic aperture focusing technique (SAFT). This indicates that the slag is about 7 mm wide by 110 mm long. Subsequent destructive examination after the test showed that the slag inclusion was in reality only about 3 mm wide.

An area on the inside of the vessel was clad with stainless steel weld overlay in the location shown in Figure 2.2 The intent was to produce an area about 50 x 100 mm with underclad cracking and another similar size area with poor clad-to-vessel wall bonding.

Both the slag inclusion and the faulty cladding were being viewed as potential noise sources which might affect identification of AE from crack growth. A second consideration for the underclad cracking is whether or not AE monitoring would be responsive should the cracks grow.

Vessel fabrication was performed by a German firm (Thyssen Henrichshutte AG in Hattingen/Ruhr). Nondestructive inspection

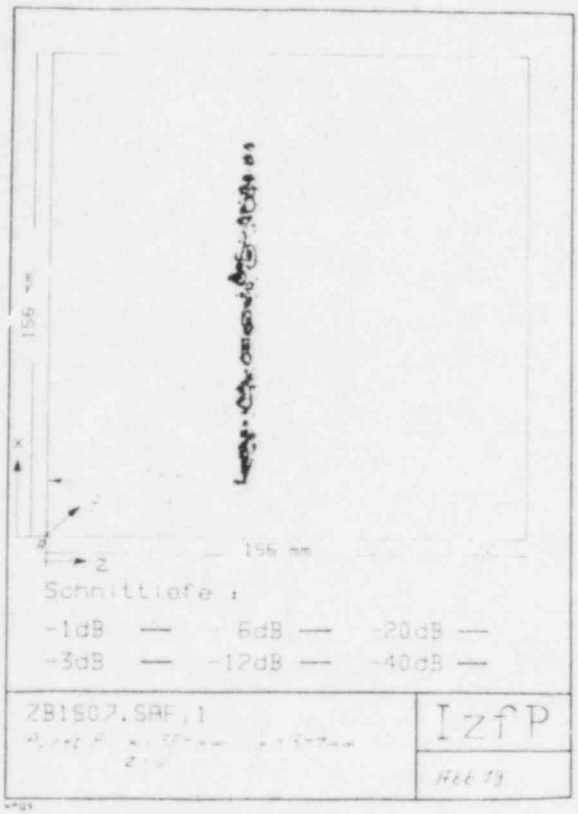

Figure 2.5. SAFT Image of Intentional Slag Inclusion, ZB-1 Vessel.

was performed during fabrication to assure weld quality and the vessel was stress relief heat treated at the end of fabrication. Fabrication was completed in February 1982.

2.2 AE INSTRUMENT SYSTEM

The total AE monitoring system is shown in Figure 2.6 in the trailer adjacent to the test bunker. It consists of a data acquisition front end, a PDP 11/23 computer for data analysis, a waveform recorder, and a PDP 11/03 computer for waveform pattern recognition analysis.

2.2.1 AE Data Acquisition System

The system concept for the AE data acquisition and recording instrument, known as System-81, is shown in Figures 2.7 and 2.8. This is a Battelle-built and owned instrument. The unit is a 12-channel instrument subdivided into three arrays. Each array may consist of 2, 3, or 4 channels. The arrays are hardware configured as opposed to software configured. The hardware concept with the design philosophy chosen has performance features discussed below.

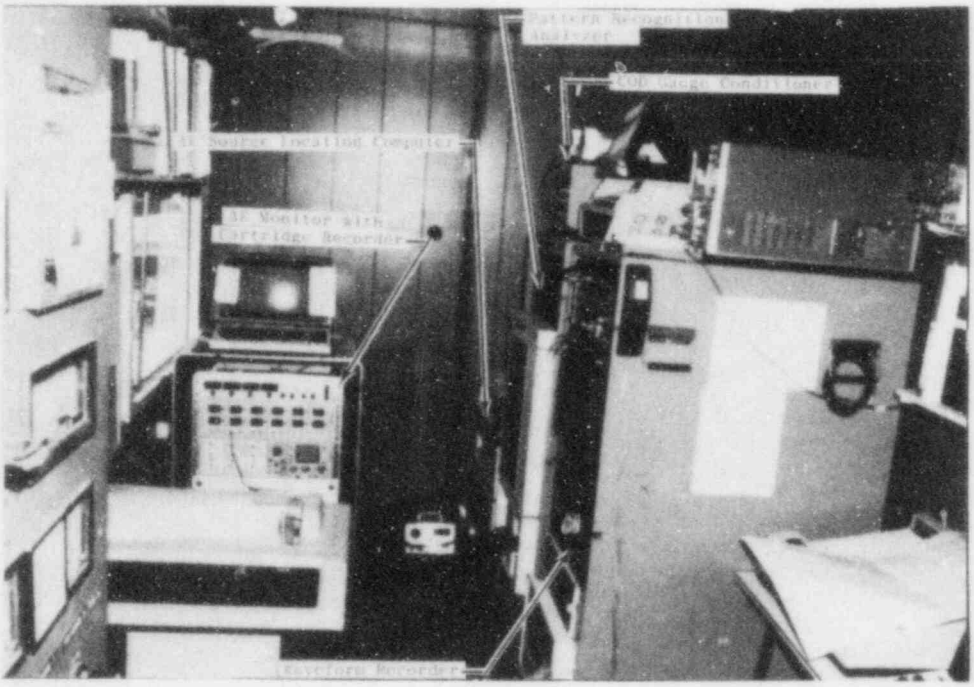

Figure 2.6. AE Monitoring and Analysis System for ZB-1 Vessel Test.

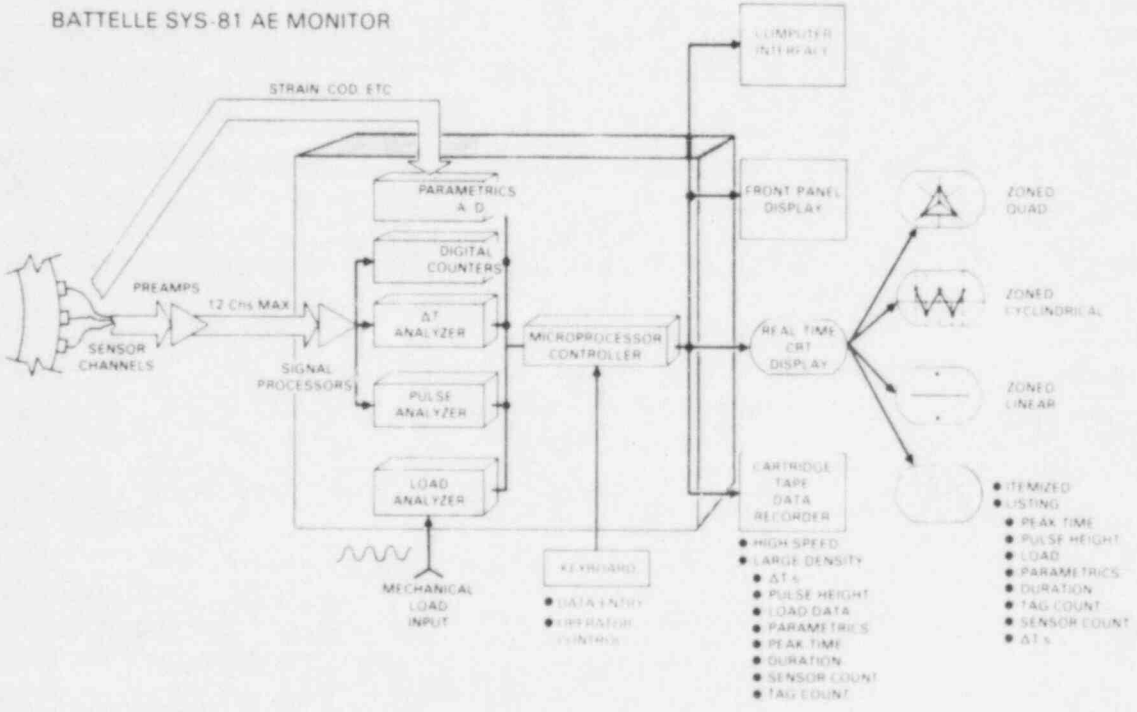

Figure 2.7. Battelle Sys-81 AE Monitor.

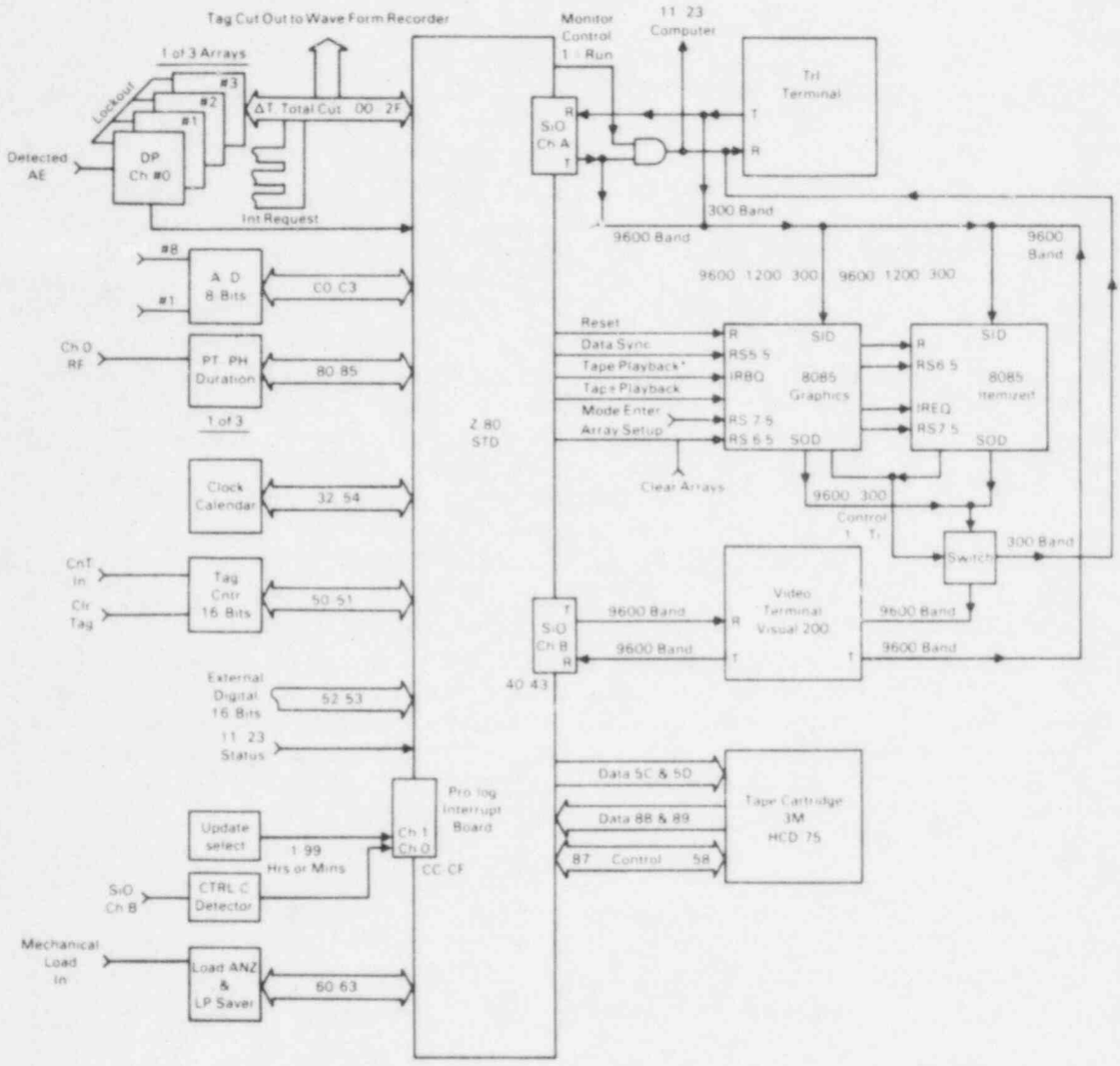

Figure 2.8. Layout of System-81.

The unit is controlled and set up by the operator with a keyboard and front panel controls. All pre-run and post-run operations are performed with the keyboard and a video message CRT display. A menu (procedure choices) is displayed on the CRT. The operator selects a desired operation prompting the system controller to respond back with a new menu or a sequence of questions that must be answered. Since the system is self-prompting and instructive, the unit can be operated without an operation manual. The front panel controls are used during the running of a test and are used in conjunction with counter displays and the CRT data displays. Use of the keyboard would require service time by the system controller and thus could slow down the data acquisition rate.

Processed data which can consist of up to eight different types is sent three separate places: 1) cartridge recorder, 2) real-time CRT display, and 3) 11/23 computer interface. The cartridge recorder is a high density storage (67 Mbytes) unit for collection of all raw data. It is extremely fast and does not slow down the system processing rate. The tape cartridges themselves are protected by a self-enclosure which enhances field reliability. The real-time display has four different output formats as shown in Figure 2.7. These outputs give a visual overview as to the status of the system and the general location of any AE activity. The location displays operate on a zone principle; not point source location. The zone concept is easier to implement and is adequate for operator confirmation of the test performance. Figure 2.8 provides further detail of the System-81 design. All of the real-time display formats are handled by two slave microprocessors. This is done to maximize acquisition rate by limiting tasks from the main system controller. The 11/23 interface is a link to a minicomputer for point source location, data analysis, and plotting. This is a serial link and has the potential of slowing down the data acquisition rate when the 1600 event acquisition buffer is full and a high data rate continues. The serial link limits the rate at which the buffer can be emptied. As a stand alone, System-81 could conceivably accommodate a continuous data rate of 800 events/second total. Since signal duration affects array lockout time, a typical rate would be more like 400 events/second. If more than one array is employed, the 400 would be divided among them. With the 11/23 connected, the data rate would be equal to 400/sec. until the buffer is filled. The continuous rate would then drop from 400 to 50 until the buffer starts to empty. An expediency is to disconnect the 11/23 during high data activity periods. Data acquired during this period can be linked to the 11/23 from the cartridge at a later time.

2.2.1.1 System Amplification

The instrument has a maximum total linear gain of 90 dB. There is 60 dB of preamplifier gain and 30 dB of gain in the main instrument. The main instrument gain can be attenuated in 2 dB steps down to 14 dB. The 60 dB preamp gain is divided in two subunits; a microamp of 20 dB and a midamp of 40 dB. The microamp incorporates a special front end with sensor impedance matching. Power for the preamps resides on the same cable as buss data. Each channel has its own voltage regulator and a current limiting circuit. Power to all channels is monitored with front panel LEDs.

2.2.1.2 Signal Detection

Data is detected by comparing event amplitude to a fixed threshold level. The threshold can be adjusted at any time by the operator, but it is not a floating threshold.

2.2.1.3 Delta-Time Analysis

Delta-time measurements are made between channels of each array. The first hit channel starts a 1 MHz clock for calculating the time differences for later hit channels. If all sensors of the array are hit, an interrupt is generated as a request for the times to be read. Maximum time between sensors is 65,535 microseconds with resolution of 1 microsecond. Each array lockout time is controlled by each channel lockout. The lockout concept prevents the array from analyzing the same event more than once. The lockout signal is a digital pulse that is controlled by the signal duration above threshold.

2.2.1.4 Load Analyzer Data

The load analyzer board is controlled by an 8748 single chip microprocessor in conjunction with a 12-bit A/D. The seven parameters acquired by the load analyzer are:

1. Load Position
2. Load at Load Position
3. Maximum Load
4. Minimum Load
5. Load Frequency
6. Load Position at Maximum Load
7. Cycle Count (65,535 maximum capacity).

The principle for finding maximum and minimum loads is to digitize the load cycle and let the processor use comparitor algorithms to find the peak and valley. The valley is used as the zero value for load position and also resets the load frequency counter. Prior to resetting, the load frequency counter value is stored. The load position is the value of the cycle counter at the time the AE waveform occurs. Position at maximum load is the value of the counter at the time maximum load occurs. Load position, load position at maximum load, and load frequency are thus always counter values varying between 0 and 255. At readout, this is scaled from 0 to 100. Cycle count is based on counting valleys. The load analyzer board is interrupt driven by the Z-80 and handshaking is used to exchange the data.

To prevent noise transients from injecting false peaks or valleys, an averaging technique is employed. Sixteen data points are averaged together. This averaged value is then

compared to upper and lower range limits which are set by adding and subtracting a decimal value of ten to the previous valid averaged data point. If the newly averaged value falls within the range limits, then the value is considered valid. If not, the value is discarded and sixteen new data points are averaged.

2.2.1.5 Peak Time/Pulse Height/Duration

The peak time and pulse height (PT/PH) module employs a unique approach which offers precision and resolution. The RF AE signal from the signal processor is input to a peak follower circuit. The peak follower output is followed by a high speed analog-to-digital (A/D) converter. The peak follower approach is used so that the digitizing clock of the A/D can be made slower since no negative excursions occur. A 1 MHz clock is used in conjunction with the RAM storage to furnish a reading every microsecond. The RAM memory is next scanned by a single chip microcomputer (Intel 8748) to determine the peak height (PH) and the time it takes to reach the peak value (PT).

Signal duration is measured by gating a 1 MHz clock with the detected envelope. The number of counts over this time period furnishes a duration reading in microseconds.

2.2.1.6 Digital Counters

Each sensor channel has associated with it a counter for keeping track of sensor activity. This can be useful for judging sensor performance and array performance on large test vessels. If specific sensors have lower hit totals, this may be due to sensor degradation or travel path attenuation and test geometry effects.

2.2.1.7 Parametrics

The system has the capability to acquire eight external parametrics such as strain, temperature, etc. Resolution is 12 bits (1 part in 4096 of 5 volts). The number of parametrics acquired is set by the operator for each test.

2.2.1.8 Tag Count

Tag count is a concept for utilizing System-81 with a separate waveform recording instrument. Since the data acquisition rates will not be the same, a means to correlate the two data bases is required. A signal called tag count is generated by System-81 for each signal processed and recorded by the waveform recording instrument for every event it records. It is thus possible to relate the waveforms to other parameters determined by the System 81 for that signal. The origin of the signal can be from any of the 12 channels.

2.2.1.9 Cartridge Recorder

A high priority feature considered in the ZB-1 test was to preserve all raw data for subsequent re-analysis in improving AE/flaw relationships. A 3M cartridge recorder was chosen for this role. The cartridge unit is a 16-track digital device with a recording capacity of 67 MBytes for each cartridge. Data is passed to the recorder on a parallel buss. Data is recorded in 1 KByte blocks with each track having 4K blocks. Recording is on a serpantine principle. The unit has its own processor and communicates with the user through a command set and defined protocol. It also features a self startup routine for calibrating and checking itself.

2.2.1.10 Real-Time Display

The 5-inch display can be controlled by one of three processors. During pre-run and post-run, the master Z-80 type controller is in command. During the actual running of a test, one of the two 8085-type processors is controlling. One of the 8085s is for the zoned displays; the other is for an itemized listing. Selection of display type is from the front panel.

2.2.2 Source Location

The source location subsystem is a standard PDP 11/23 computer. Raw data including delta-time is transferred directly from the System 81 to the source location unit. Point source location for each signal is calculated and displayed on a video screen. The information can then be printed out on a facsimile recorder. An extensive calibration of the source location results achieved using Pentel pencil lead breaks as input signals at various locations on the vessel is discussed in Appendix C.

2.2.3 Waveform Recorder

The key elements of the waveform recorder are a Biomation 8100 transient analyzer which digitizes an incoming analog signal and a Kennedy 9800 9-track digital tape recorder to store the digitized waveforms. The waveform recorder receives signals from a special broadband waveguide sensor (Figure 2.18). The waveform subsystem can operate in one of two modes. Recording of a signal can be made contingent on verification of the signal by four array sensors or it can be free running wherein it records any signal that exceeds the threshold setting. In either case, it associates a "tag number" with the signal (Section 2.2.1.8). This permits a correlation of the waveform with source location information and other parameters measured in the System 81.

2.2.4 Waveform Analyzer

The waveform analyzer is a standard PDP 11/03 computer operating in conjunction with a Kennedy 9800 9-track tape playback instrument. Tapes containing recorded waveforms are installed on the Kennedy playback where they are processed by the PDP 11/03 computer according to the algorithms programmed into the computer.

This approach to waveform pattern recognition analysis is obviously cumbersome; however, the intent was to assemble a special-purpose "breadboard" system to test a function. It is not intended to represent a prototype system for general application.

2.3 AE SENSOR INSTALLATION

The philosophy used in determining sensor installation was to achieve two conditions:

1. Apply at least one array which optimized detection of AE from the flaws in the A533B insert.

2. Apply one array wherein reactor monitoring constraints were observed - i.e., pressure coupling and maximum distance from the AE source.

Ideally, the first array should give a measure of the maximum AE data detectable from the flaws under optimum conditions. This then would provide a base reference to determine the efficiency of the second array operating under the constraints of reactor monitoring.

All PNL AE sensors used in the ZB-1 test were metal waveguides with the exception of one special "hydro-test" array which will be described later. Waveguide sensors were chosen to accommodate the high temperature test conditions. Similar waveguides have also been selected for reactor monitoring. The waveguides are stainless steel welding rod 3.3 mm (0.125 in.) in diameter. The length used on ZB-1 was 605 mm (23.8 in.); however, the length is not critical.

The choice of 3.3 mm (0.125 in.) diameter for the waveguides is based on an experimental investigation. The propagation of elastic waves through cylinders is a complicated phenomenon, which depends strongly upon the cylinder dimensions, ultrasonic frequency, and especially the mode of propagation. Knowing this information allows a theoretical formulation of the effect to be generated. For the particular geometry and operating conditions of these sensors, however, it was not clear how to apply this

theory because the modes of propagation and excitation of the waveguides are not well understood. As a result, it was decided to proceed with an experimental evaluation for choosing the proper waveguide.

The major effect to be dealt with in waveguide design is acoustic dispersion; i.e., different ultrasonic frequencies travel at different speeds. Dispersion causes short ultrasonic pulses (composed of many different frequencies) to be spread out in time. To quantify the effect of dispersion, a series of measurements of pulse spreading was performed on rods of different diameters. In all cases the rods were 915 mm (36 in.) in length. A broadband pulse (center frequency of 500 kHz and bandwidth approximately 60%) approximately 2 microseconds long was transmitted down the rods and the received pulse after one transit through the rods was recorded. Table 2.1 shows the results of this experiment.

Table 2.1. Affect of Waveguide Diameter on Internal Dispersion of Pulse Energy

Diameter (millimeters)	Received Pulse Length (microsec)
8.0	300
4.8	300
3.9	150
3.3	50
2.4	20

From this simple experiment, it was determined that the thinnest rod was the most useful for faithfully transmitting pulses in the 300-500 kHz frequency range. The thin rods are also the least thermally conductive, and therefore, provide the best thermal isolation for piezoelectric crystals and electronics. The 3.3 mm (0.125 in.) rod was chosen as a compromise between the acoustical incentive to keep the waveguide very small and the need for sufficient mechanical strength to support the sensor/microamp combination.

A thickness poled, 2 MHz cut PZT-5 piezoelectric crystal together with a 20 dB gain preamplifier was mounted on one end of the waveguide. The other end (mounted against the surface being monitored) was machined to a 1.25 mm (0.05 in.) radius tip.

Layout of the AE sensor arrays is shown in Figures 2.9, 2.10, 2.11, and 2.12. The term "Quad Array" denotes one of the AE monitoring sensor arrangements devised some time ago by a U.S.

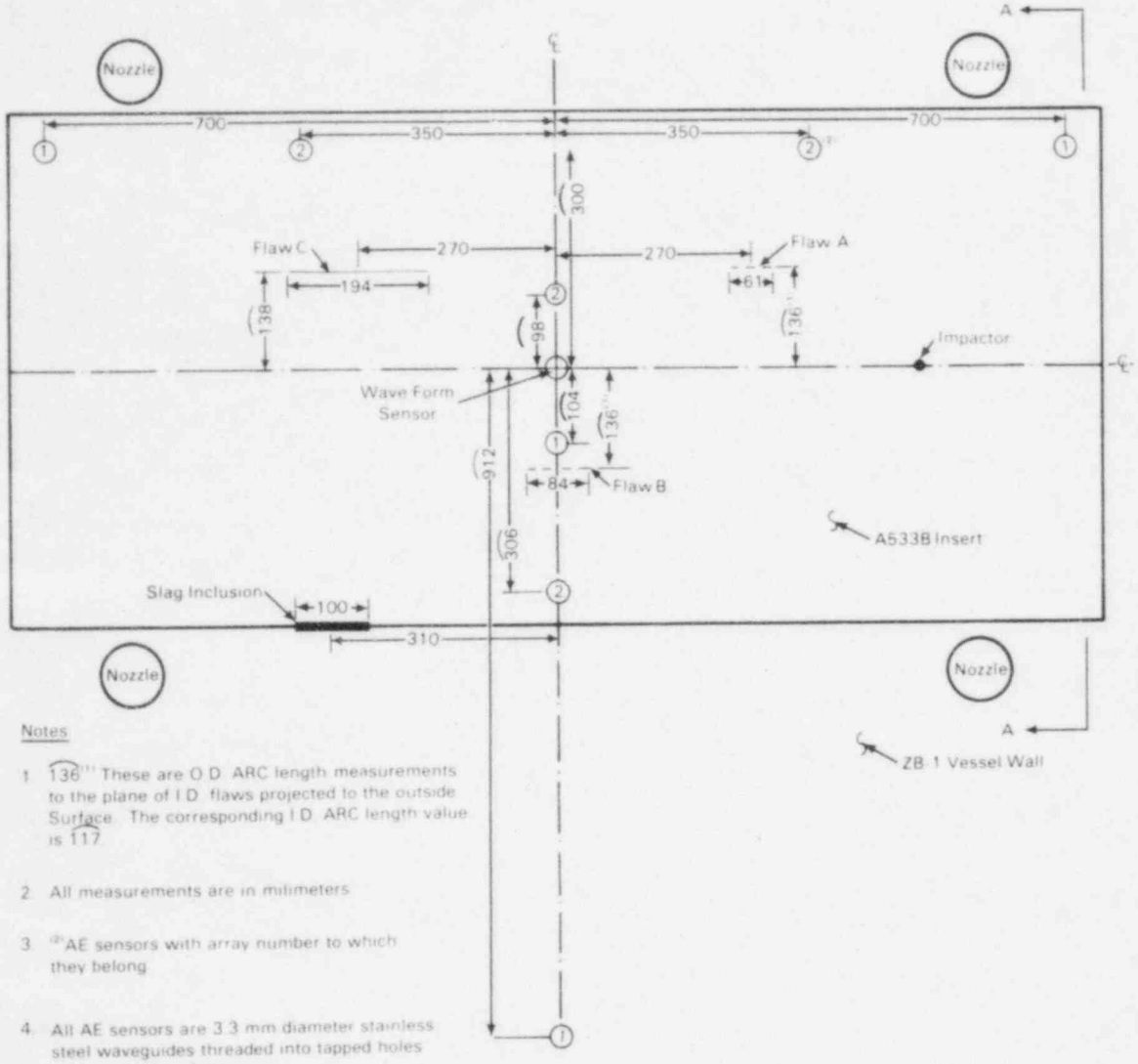

Notes

1. $\overset{\frown}{136}^{(1)}$ These are O.D. ARC length measurements to the plane of I.D. flaws projected to the outside Surface. The corresponding I.D. ARC length value is $\overset{\frown}{117}$.

2. All measurements are in milimeters.

3. (2) AE sensors with array number to which they belong.

4. All AE sensors are 3.3 mm diameter stainless steel waveguides threaded into tapped holes in the vessel surface.

5. Flaw lengths shown are for start of the test. Values for the end of the test are:
   A-151 mm
   B-206 mm
   C-194 mm

(see Figure 2.12 for Section A-A)

Figure 2.9. Layout of Quad AE Sensor Arrays in the Vicinity of Machined Flaws in the ZB-1 Vessel.

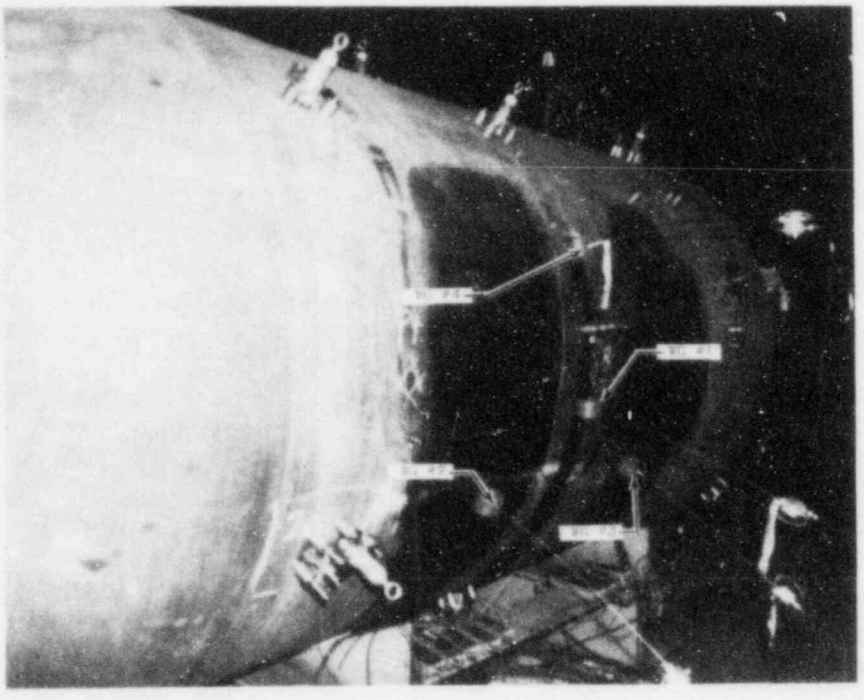

Figure 2.10. PNL Waveguide Sensors Installed on the KS07 Insert, ZB-1 Test.

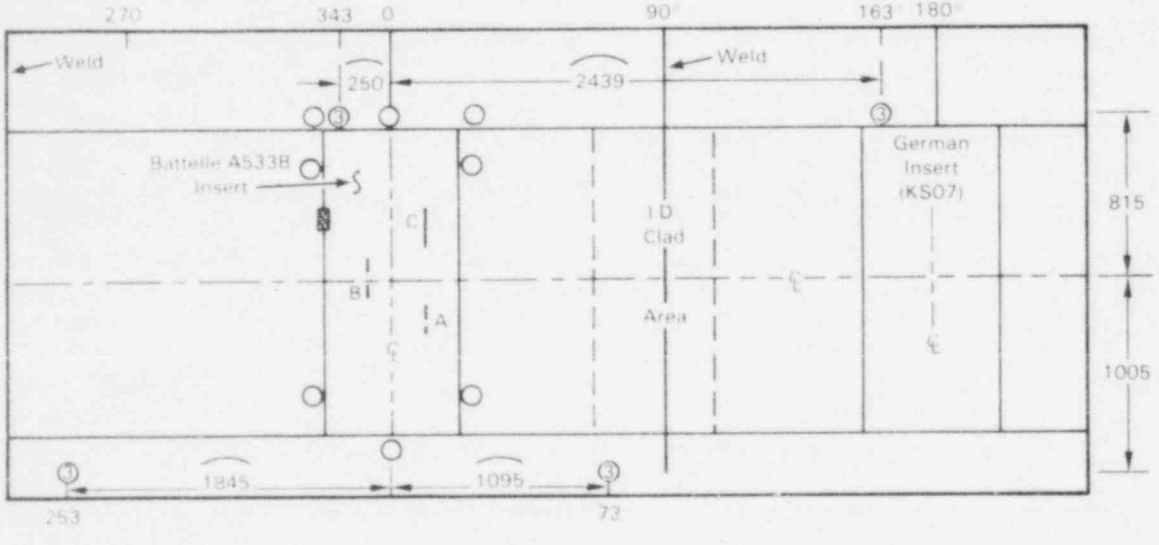

Note

1. 3 AE Sensors with array number to which they belong
2. All dimensions in millimeters
3. (Typ.) 250 ARC length on or for surface of vessel
4. All AE sensors are 3.3 mm diameter stainless steel wave guides pressure coupled to the surface of the vessel

Figure 2.11. Layout of Cylindrical AE Sensor Array on the ZB-1 Vessel.

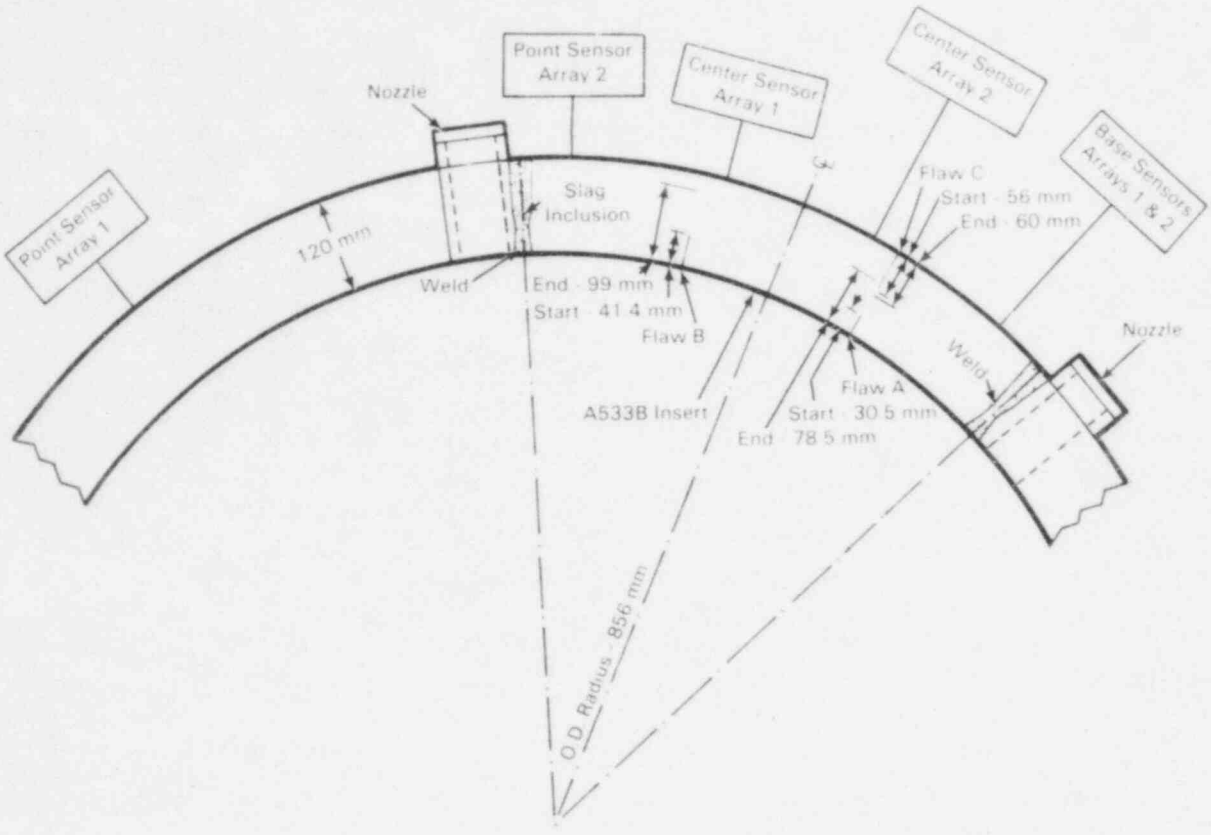

Figure 2.12. Section A-A Showing Through-Wall Relation of Quad Array AE Sensors to Machined Flaws.

commercial AE company (Dunegan/Endevco). It consists of a four sensor arrangement in the pattern of an equilateral triangle with one sensor at the center of the triangle. PNL has used this array very effectively in earlier vessel tests in the U.S. where a single flaw location was known and could be encompassed by the array.[6]

In Figure 2.9, the quad sensing arrays used in the vicinity of the machined flaws are shown. The quad array designated 2 was installed at the start of the test. Flaws A, B, and half of C are enclosed by the array. A similar quad sensing array was installed on the KS07 insert also. These are shown in Figure 2.10. The array designated 1 in Figure 2.11 was not installed until later in the test. This will be discussed further.

Array 2 waveguides and those on the KS07 patch were all mounted by threading into holes drilled and tapped about 7 mm (0.276 in.) deep into the surface of the vessel. The waveguides were bottomed in these holes.

Figure 2.11 gives the arrangement of an array installed to monitor the full vessel cylinder. This was designated as Array 3. Array 3 is representative of the sensors and application methodology that would be used for reactor monitoring. These sensors were again metal waveguides as described above; however, they were pressure coupled to the vessel surface. The interface pressure required between the sensing device and the surface being monitored for effective acoustic coupling in the 300-500 kHz frequency range has been evaluated experimentally. The results indicate that about 103 MPa (15,000 psi) is optimum; i.e., no sensitivity improvement is observed above that and sensitivity diminishes below that. With these waveguides having a 1.25 mm (0.05 in.) diameter tip, 133N (30 pounds force) produces 105 Mpa (15,300 psi) pressure at the waveguide/structure interface. Initially, these sensors were mounted using four magnets on a fixture for each sensor. The waveguide pressure was applied by a spring between the fixture and the waveguide. This approach was not fully satisfactory to supply the waveguide coupling force required. During Step 5 of the test, the fixtures were secured in place with stainless steel bands running around the vessel. This proved to be a more suitable method and resulted in improved sensitivity of the sensors.

A special set of sensors was used for one monitoring array during the hydrostatic test steps. The reasoning behind this was that with the metal waveguide sensors tuned to a peak response at about 400 kHz and with a very sharp low frequency roll-off (15-20 dB/100 kHz) to discriminate against background noise, they were not necessarily optimum for hydro test monitoring. Sensors with a much lower peak frequency response (100-200 kHz) are generally used in hydro test monitoring. The background noise level is much less than during reactor operation, hence, the improved sensitivity at lower frequency can be utilized. With this in mind, PNL felt it was necessary to use the lower frequency sensors to properly represent what might be achieved in flaw detection during periodic inservice hydro tests.

The special hydro test sensors were installed adjacent to Array 2 sensors. These were included in the monitoring during hydrostatic test steps. They were placed beside each Array 2 sensor using magnets to hold them in place and ultrasonic couplant to acoustically couple them to the vessel surface. The sensors were purchased from a U.S. firm (AE International) having extensive experience in AE monitoring of industrial vessels during hydrostatic testing. The sensors were AEI Type 8A1.1VA with a 110 kHz peak response and rated for service up to 204°C (400°F).

During the low temperature portion of the test, a potential problem with Array 2 was recognized. Referring to Figure 2.9, Flaw C intercepts the direct signal propagation path from Flaw B to the Array 2 sensor in the upper left corner. If we refer now to Figure 2.12 which is Section A-A from Figure 2.9 and examine the path from the bottom of Flaw B to the plane of the Base Sensors, Arrays 1 and 2 at the outer surface, it becomes evident that this is not a problem in the beginning. It does, however, appear to become a definite problem as Flaw B grows in depth. The direct line path is then intercepted by Flaw C. In order to overcome this problem, a larger quad array was installed during Step 5 of the test. This is designated Array 1 in Figure 2.9. The Array 1 waveguide sensors are mounted in drilled and tapped holes in the vessel surface the same as Array 2.

A waveguide sensor was installed at the center of the A533B insert for the purpose of measuring acoustic signal waveforms to be recorded in digitized form on tape. This information was used as input to the AE signal pattern recognition system. The waveguide, which is designated Waveform Sensor in Figure 2.9, was mounted in a drilled and tapped hole.

2.4 AE SENSOR CHARACTERIZATION

Characterization of the response of the AE sensors was performed on the ZB-1 vessel using a helium gas jet as an excitation source. The helium jet, when applied in a consistent manner, provides a reproducible broadband excitation source. One major feature is that it can be applied to any structure being monitored to characterize sensors after installation without damage to the structure surface. Figure 2.13 gives the frequency profile of the helium jet as measured by a U.S. National Bureau of Standards (NBS) conical sensor. This is an extremely flat response sensor from 100 kHz to well beyond 1 MHz. Figure 2.13 was produced with the NBS sensor mounted on a 300 x 300 x 120 mm carbon steel block and the helium jet from a 210 Pa (30 psi) source, through a #18 hypodermic needle was impinged on the block at a 3 mm (0.11 in.) standoff distance, 38 mm (1.5 in.) from the sensor.

All of the sensors were characterized after they were mounted on the ZB-1 vessel. The helium jet was used numerous times during the test to evaluate sensitivity of a particular sensor or to reassess the response of a full array. It is not useful to include the results from all of these. Typical results are shown in Figures 2.14 through 2.18.

A Tektronix Model 7L5 spectrum analyzer was used to produce the spectral traces. The spectral traces are taken at the output of preamplifiers. Differences in gain are accounted for so that

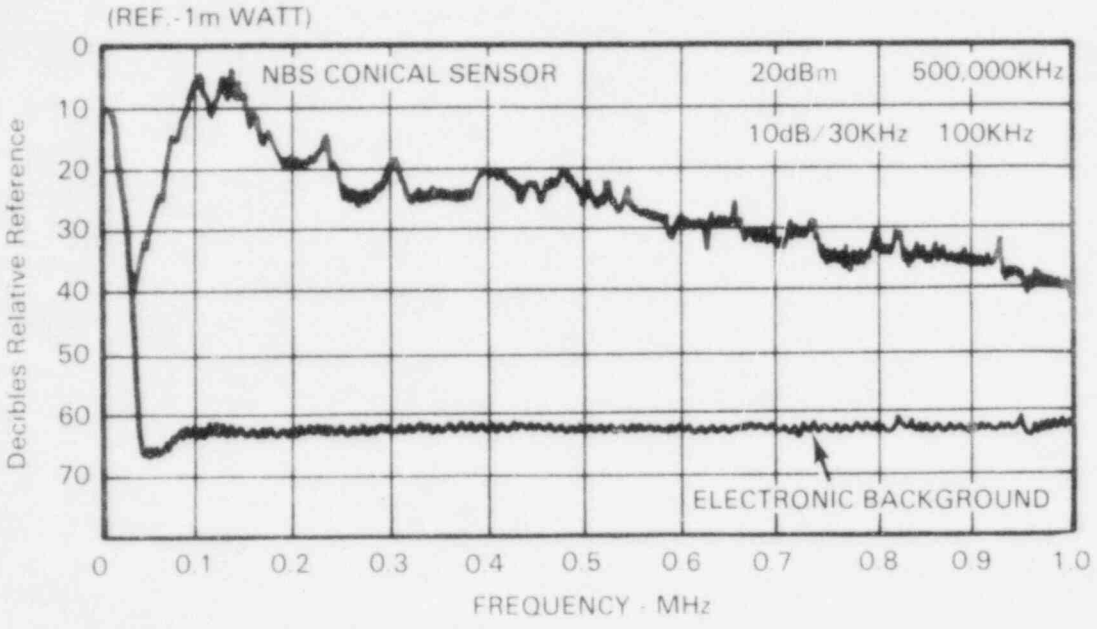

Figure 2.13. Helium Jet Excitation Profile with NBS Conical Sensor.

the traces can be compared directly. The waveguide sensors are tuned to a selected frequency response using inductive tuning coils at the microamplifier.

The spectral responses shown are a logarithmic measure. The reference point is the top of the grid which corresponds to 0 dB on the logarithmic scale. Working from the top down, the logarithmic scale is in dB below reference (10 dB/division). The analyzer reference value is 1 milliwatt when a 50 ohm input is used. The corresponding voltage values can be determined by:

$$V_{peak} = \frac{0.224}{\log^{-} (\frac{dBm}{20}) \times 0.707}$$

Thus, on a voltage scale, the reference corresponds to 317 millivolts peak.

Response of the Quad 2 (small quad) and the Cylindrical (monitors full vessel cylinder) arrays are shown in Figures 2.14 and 2.15. These measurements were taken at the output of the combined microamplifier at the sensor and a midamplifier following it in the circuit. The two amplifiers constitute the total preamplification. A feature to note is that the sensors have been tuned to yield a peak response at about 400 kHz with a sharp roll-off at the lower frequencies.

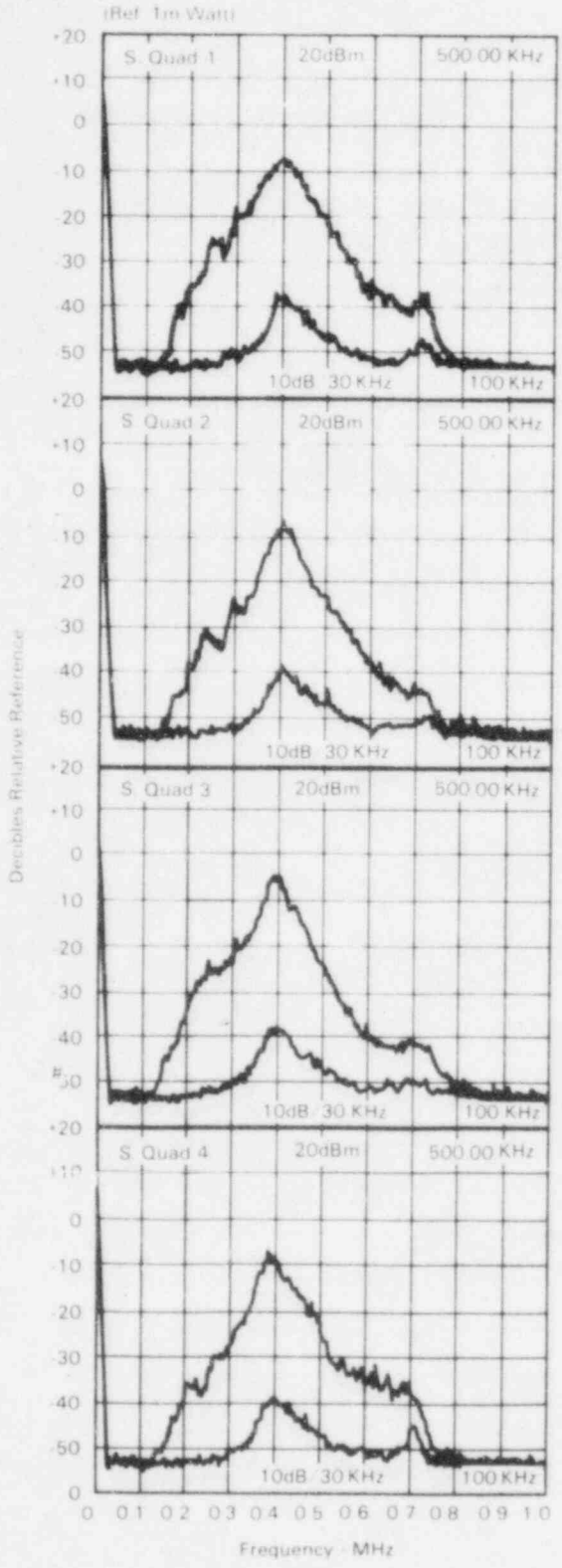

Figure 2.14. Response Characteristics of Array 2 (Small Quad).

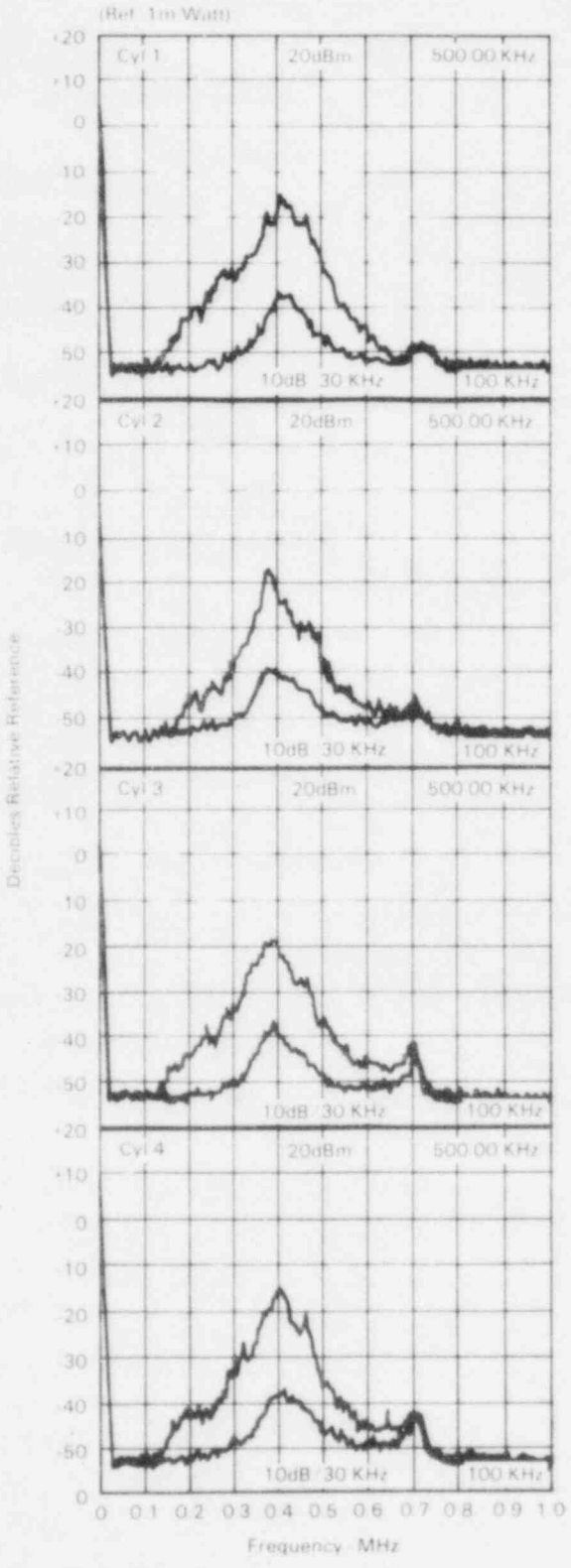

Figure 2.15. Response Characteristics of Cylindrical Array 3.

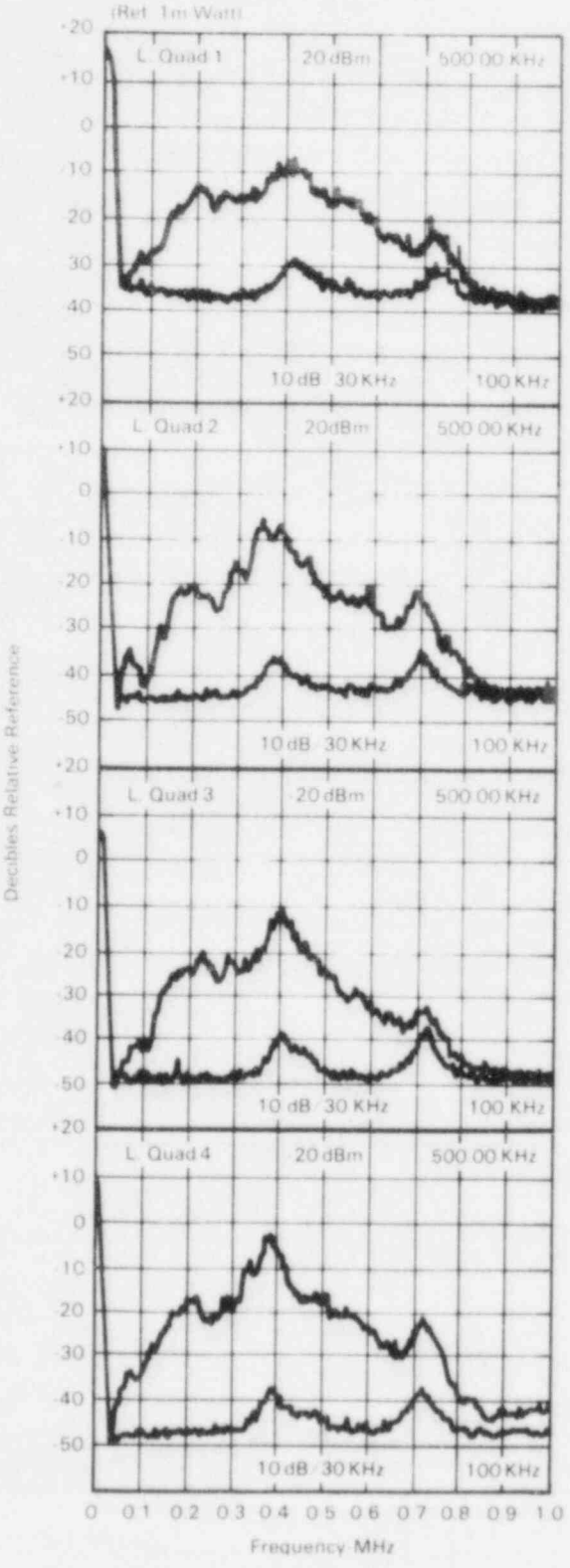

Figure 2.16. Response Characteristics of Quad Array 1.

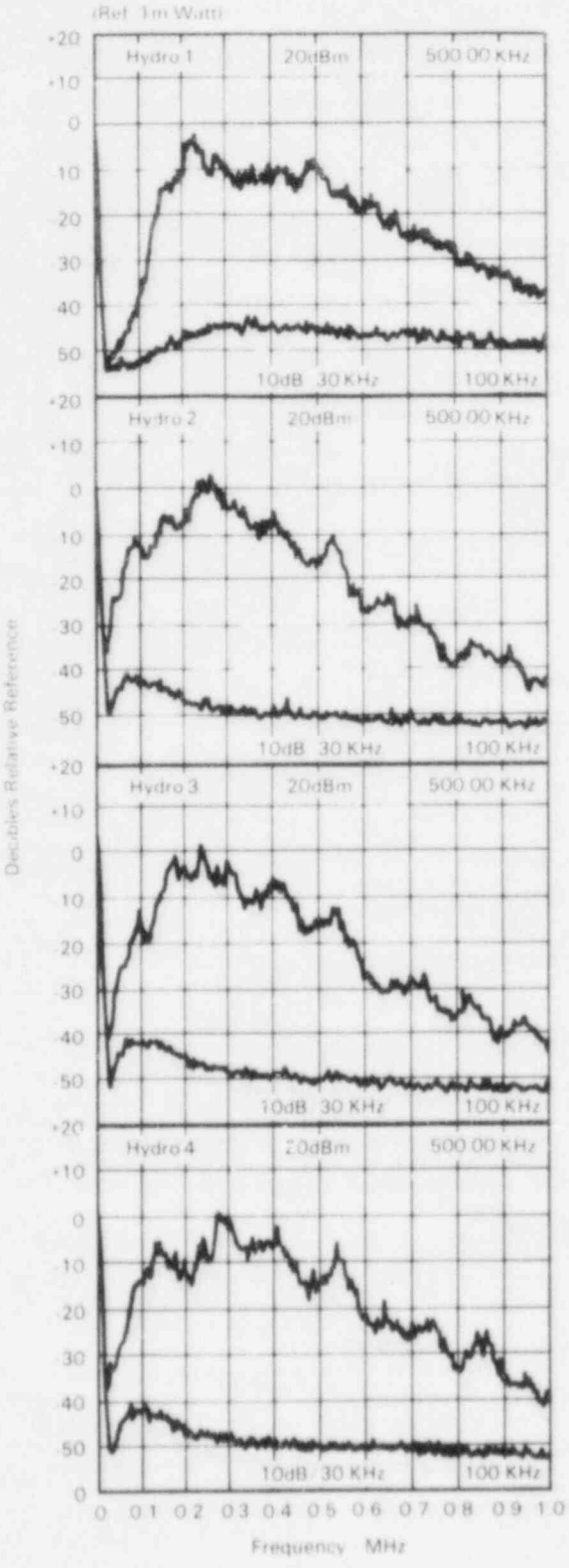

Figure 2.17. Response Characteristics of Hydro-Test Array.

Response of Quad 1 (large quad) array shown in Figure 2.16 was taken out of the microamplifier. This does not show the total low frequency roll-off that is finally achieved in the mid-amplifier. It does again show the tuning concentration at 400 kHz, however.

The hydro-test array which is characterized in Figure 2.17 is taken at the output of the two preamplifiers - i.e., the true character of frequency information presented to the AE instrument. It is evident that this array was much more sensitive at lower frequencies.

The waveguide arrays were tuned to 400 kHz response with sharp discrimination against lower frequencies based on separate studies of nuclear reactor background noise.[7-9] The studies showed a very strong noise field below about 250 kHz produced by coolant flow.

The waveform sensor was constructed to have relatively broad frequency response (Figure 2.18). The intent was to provide broadband frequency information but avoid background noise dominating the information.

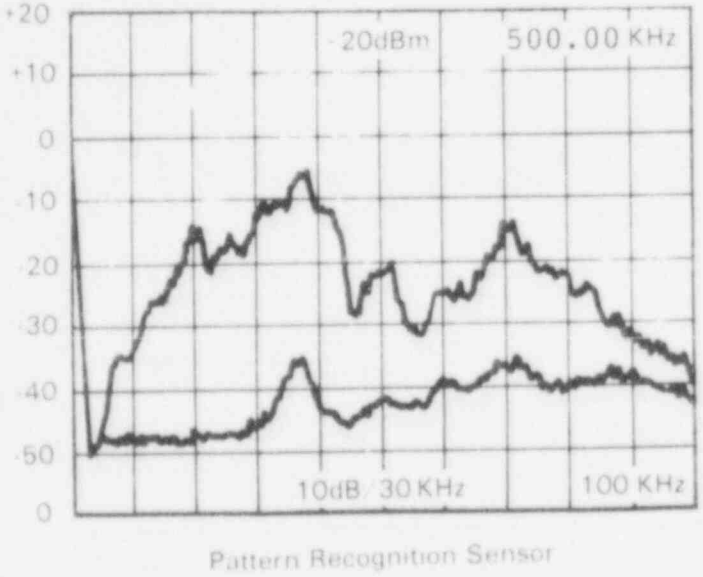

Figure 2.18. Response Characteristics of Waveform Sensor.

2.5 ACCESSORY INSTRUMENTATION

Several accessory instruments and/or devices were installed on the vessel in addition to the AE monitoring instruments. These included:

- Crack-opening-displacement (COD) gauges.
- Reactor coolant flow noise simulator.
- A mechanical impactor to provide a reference signal input.

Figure 2.19 illustrates the COD gauges and the flow noise simulator installed on the inside of the vessel. The COD gauges used on the vessel I.D. are MTS water immersible, high temperature gauges. These gauges are MTS Model 632.10B-01, Serial #132-134, Option 005 for service -18 to +288°C (0-550°F). They are

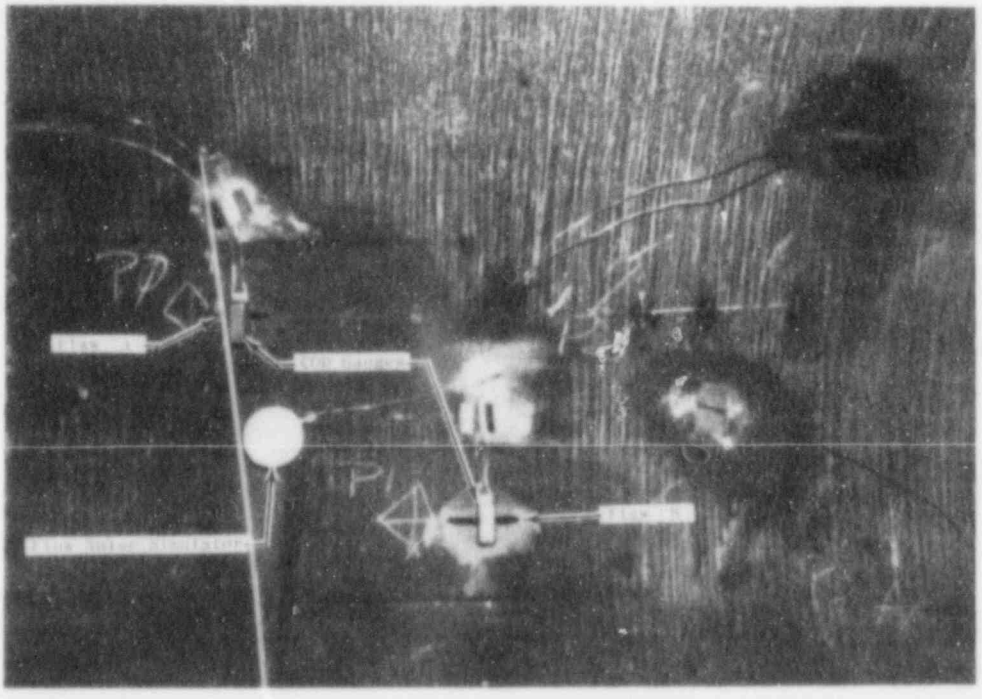

Figure 2.19. COD Gauges and Flow Noise Simulator Installed on the Inside of the ZB-1 Vessel.

rated for pressure from vacuum to 17.2 MPa (2500 psi) and have a COD measurement range of 0-3.8 mm (0-0.15 inches). The gauges were connected to a Vishay Model 2310 excitation/amplifier which

output to a digital voltmeter and the System 81 data acquisition system. The leads from these gauges passed through the vessel wall via high pressure compression fittings (Conax SP100-062-A2-G split seal fittings) installed in the closure cap on the nozzles. The COD gauge on the vessel O.D. was a Schaevitz LVDT Model 100XS-ZT with a temperature range of -195 to +593°C (-320 to +1100°F) and a capacity of ±2.5 mm (±0.1 inches). It was read out using a Schaevitz Model DTR400 digital readout. Calibration of the gauges is given in Figures 2.20, 2.21, 2.22, and 2.23.

The flow noise simulator shown in Figure 2.19 was fabricated at PNL. It is an electronically driven transducer designed for operation in a high temperature, high pressure water environment. It was mounted on an integral stud threaded into the vessel surface. The frequency characteristics of the acoustic output from the flow noise simulator is given in Figure 2.24. This was measured with the waveform sensor mounted on the outside of the vessel. The frequency profile was adjusted to provide a simulation of flow noise measured on operating reactors.

A mechanical impactor (identified in Figure 2.9) was installed to provide an input signal for checking the AE system functionally during the test. Particularly during the high temperature portion of the test, the vessel could not be accessed to inject signals to verify AE system operation. The mechanical impactor which was a solenoid driven plunger device could be actuated remotely.

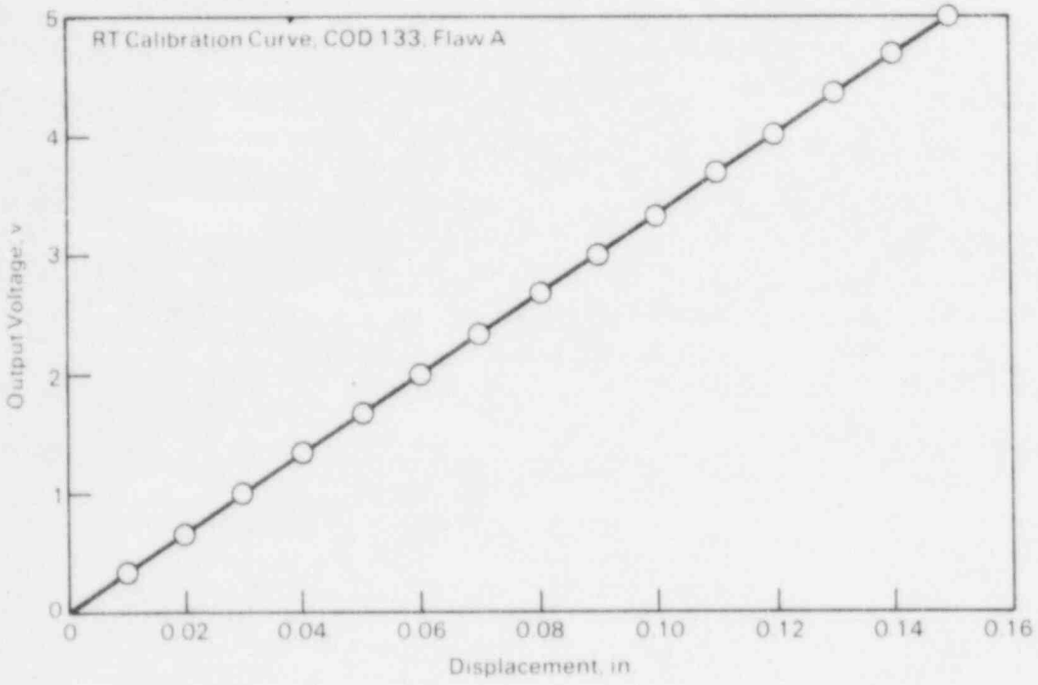

Figure 2.20. RT Calibration Curve, COD 133, Flaw A.

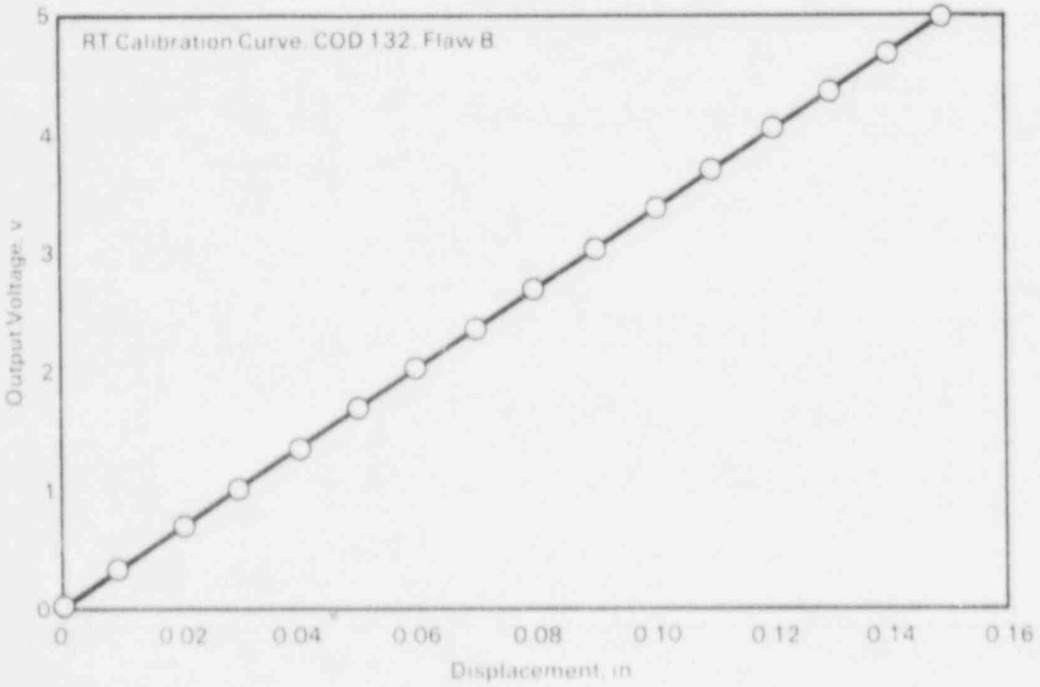

Figure 2.21. RT Calibration Curve, COD 132, Flaw B.

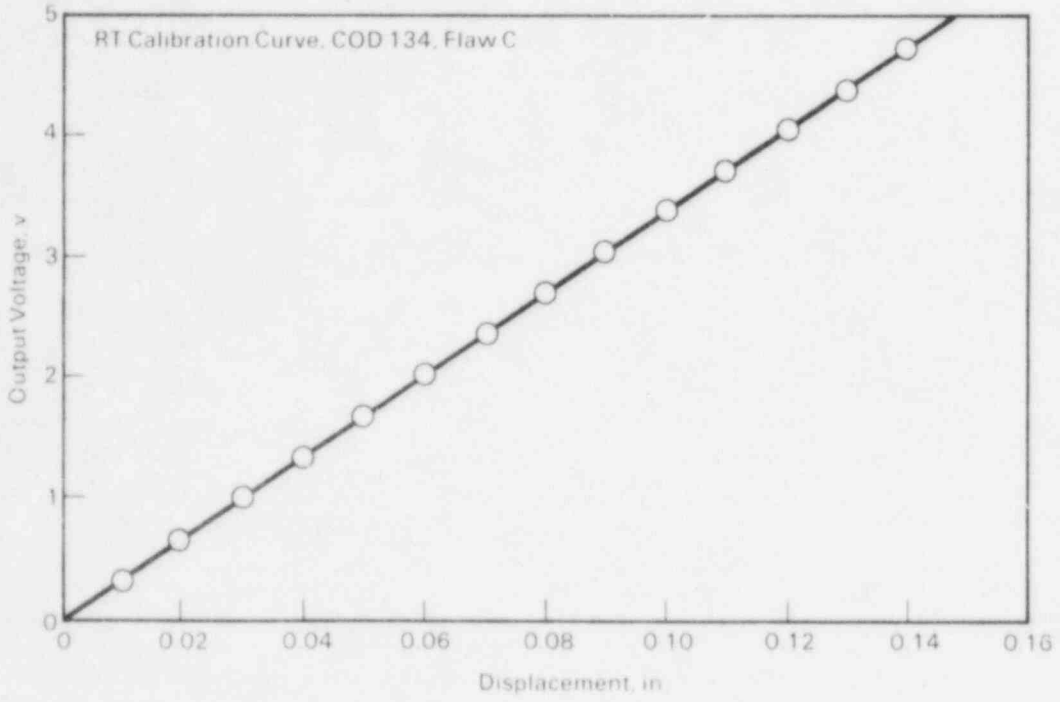

Figure 2.22. RT Calibration Curve, COD 134, Flaw C.

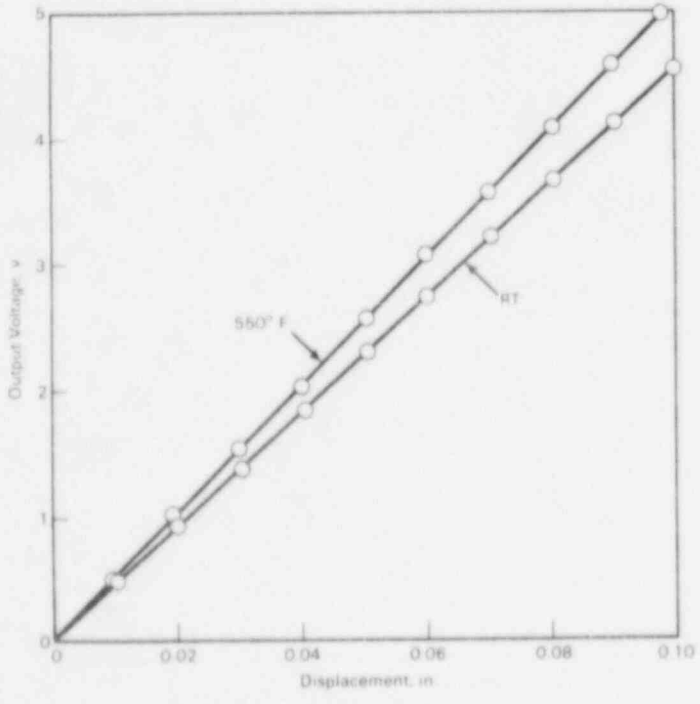

Figure 2.23. RT and 550°F Calibration Curves, COD 148, Flaw C.

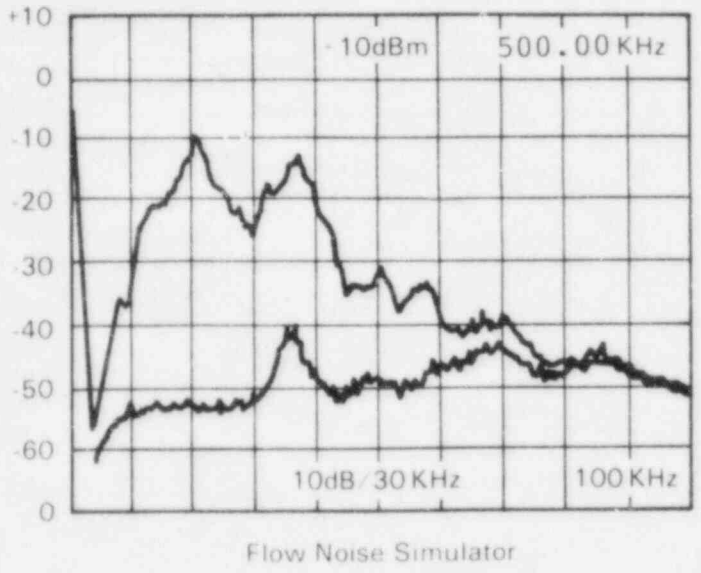

Figure 2.24. Frequency Profile of the Acoustic Output from the Flow Noise Simulator.

3.0 TEST CONDITIONS

The ZB-1 test was designed to provide a variety of test conditions (loading, temperature, R-ratio, noise sources, etc.). A flow diagram of the vessel pressurizing system is presented in Figure 3.1. Although problems were experienced with the physical integrity of the system during the course of the test, it performed the required function. Figure 3.2 shows the actual test sequence followed. As discussed in Section 1.2, this is a deviation from the original test plan.

The internal pressure levels applied to the vessel were designed to produce a nominal stress level in the vessel wall that is similar to that for a reactor pressure vessel (approximately 158 MPa or 23,000 psi). A tension-tension ramp pressure

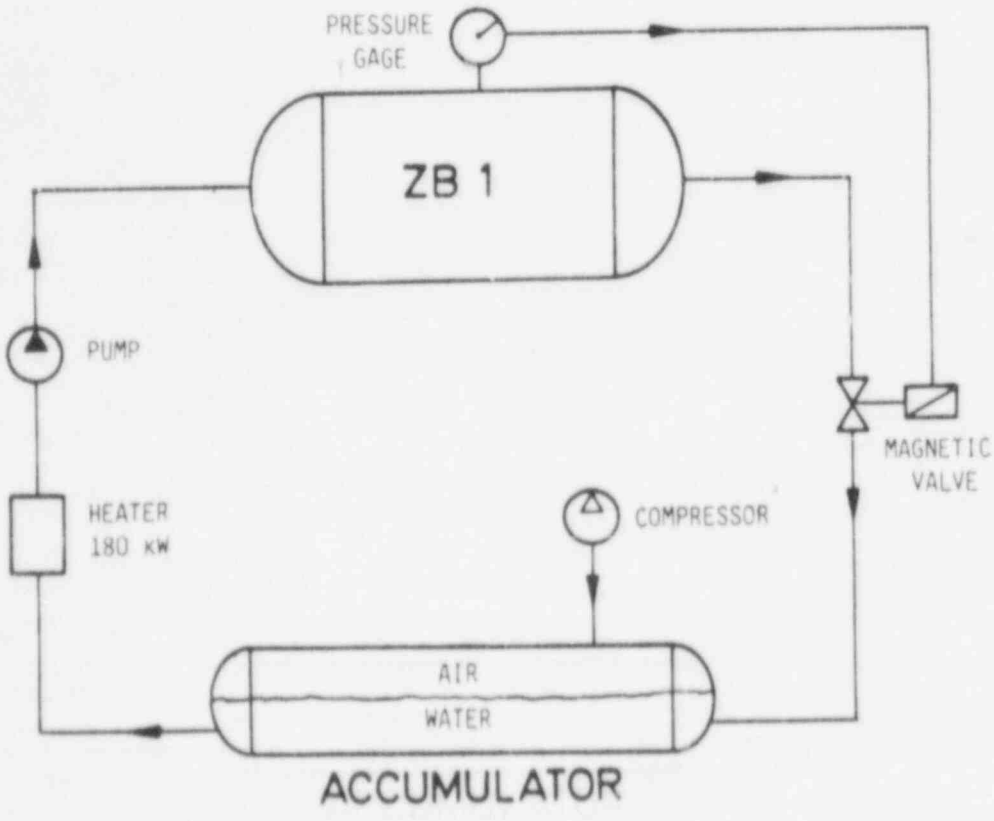

Figure 3.1. Flow Diagram of ZB-1 Vessel Pressure Cycling System.

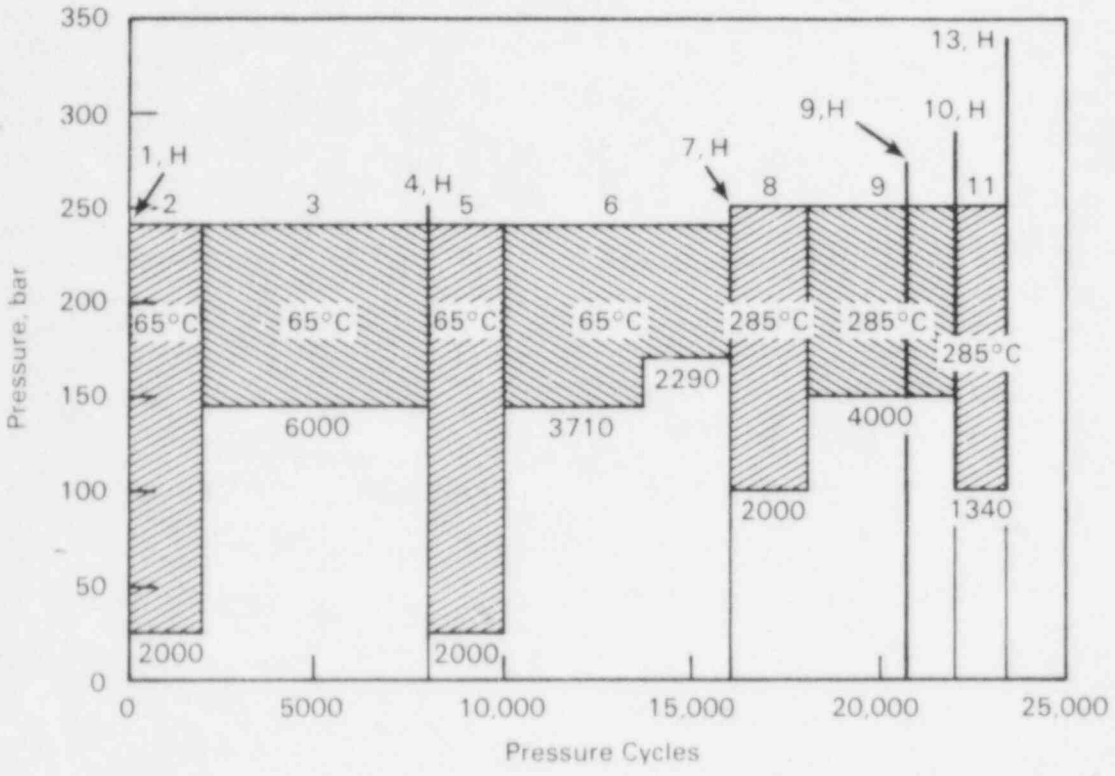

Figure 3.2. Test Sequence for the ZB-1 Vessel Test.

cycle was applied to the vessel at a rate of 78 seconds/cycle for Steps 2 and 5, 36 seconds/cycle for Steps 3 and 6, 160 seconds/cycle for Steps 8 and 11, and 120 seconds/cycle for Step 9. The pressure increasing portion of the cycle occupied about 75% of the total time per cycle.

No insulation was used on the vessel during the low temperature (65°C) portion of the test. During high temperature (285°C) testing, a wire reinforced glass fiber blanket insulation was used. Provision was made to install a 300 mm (12 inch) wide section of stainless steel reflective insulation representative of that used on modern nuclear reactors. The purpose was to evaluate the potential noise produced by the material from thermal and relative movement effects. Since the test ran longer than expected, it was never installed because AE monitoring had been performed in the meantime on a U.S. reactor (Watts Bar Unit 1) with reflective insulation in place. This was considered to be a more relevant test of insulation effects (there was no evidence of a problem), so the installation on ZB-1 was cancelled. Also, installation of the reflective insulation on ZB-1 imposed significant problems of interference with nozzles and AE sensors.

4.0 TEST RESULTS

The test results are discussed by topics rather than test chronology. This appears to be a more meaningful and useful approach.

4.1 HYDROSTATIC TEST RESULTS

As shown in Figure 3.2, there were six hydrostatic tests performed. The objective was to evaluate the effectiveness of AE monitoring during inservice hydrostatic tests to detect flaws. Flaw size and amount of over-pressure (maximum hydro pressure vs. operating pressure) are key variables. The hydro tests performed were:

Step	Overpressure, %	Temperature, °C
1	0	65
4	2	65
7	4	65
9*	10	240
10	15	65
13	36	65

*Not planned as a part of the original test matrix.

Table 4.1 gives the depth of the flaws in the vessel at the time the various hydrotests were performed. Figure 4.1 shows a graph of the stress intensity factor levels that the flaws reached during the hydrotests. Flaw C is not shown in Steps 9 and 10 due to unreliable COD data. Also shown in Figure 4.1 are the maximum cyclic stress intensity levels each flaw experienced prior to the hydrotest. For Step 1, the precracking K-levels are given to document the pretest loading history. The amount of over-stressing of each flaw (in terms of K-levels) is given as the difference between the hydro-test and prior-cyclic stress intensity factors.

Significant over-stressing occurred in Steps 1, 9, 10, and 13. The prior cyclic stress intensity levels for Steps 10 and 13 did not exceed the hydrotest stress intensity levels for the previous hydrotest. Thus, some fatigue crack growth retardation may have occurred during the last 1000 cycles of Step 9 and during Step 11. No evidence of this effect was noted by AE or fractography. Figure 4.2 shows a graph of prior cyclic and hydrotest plastic zone radii for each flaw. Note that the Step 9 and 10 hydros had very similar plastic zone radii. This was caused by the higher test temperature (i.e., lower yield strength) for the Step 9 hydro. Probably very little fatigue crack growth occurred between Step 9 and Step 10 hydrotests, thus

Table 4.1. Estimated Flaw Depths at Time of Hydro Test

Step	A	B	C	KS07R Weld Crack
1	1.20	1.63	2.20	0.20*
4	1.46	1.97	2.26	?
7	1.95	2.58	2.31	?
9	2.45	3.30	?	?
10	2.63	3.41	?	?
13	3.09**	3.90**	2.37**	0.39-1.57***

Except as noted, flaw depths were estimated from COD measurements. All measurements in inches.

*Original depth of crack in the KS07R weld crack is a very rough estimate from examination of trepans cut from points along the weld after the test.

**Depth measurements were made on the fracture surface of the flaws removed after the test.

***This is the range of crack depth around the insert estimated by NDE and from trepan samples.

producing a small "effective" over-pressure for the Step 10 hydro.

4.1.1 Step 1 - Phase 1

The Step 1 hydro was made up of two phases - before and after replacement of the KS07 degraded material insert. Step 1 was a 1.0 operating pressure (240 bar) hydro test performed at about 65°C. The first phase was performed at the outset of the test in early October 1982 and represented a preservice hydro. The principal AE sensor arrays used were waveguide quad arrays mounted in tapped holes on the A533B insert and the KS07 insert. Vessel pressure was raised to 140 bar at the outset where pressure system problems required a delay. At this point, the KS07 insert was starting to produce high amplitude AE (10 volts and above) that clustered along a circumferential weld in the middle of the insert. After reviewing the data, the test was resumed with the precaution that pressurization would be in increments with a pressure hold between increments to determine the AE response characteristics. The test was terminated at 232 bar due to concern over possible failure of the KS07 insert. Figure 4.3 summarizes the final part of the test. It is evident in Figure 4.3 that the KS07 insert was producing a large amount of AE

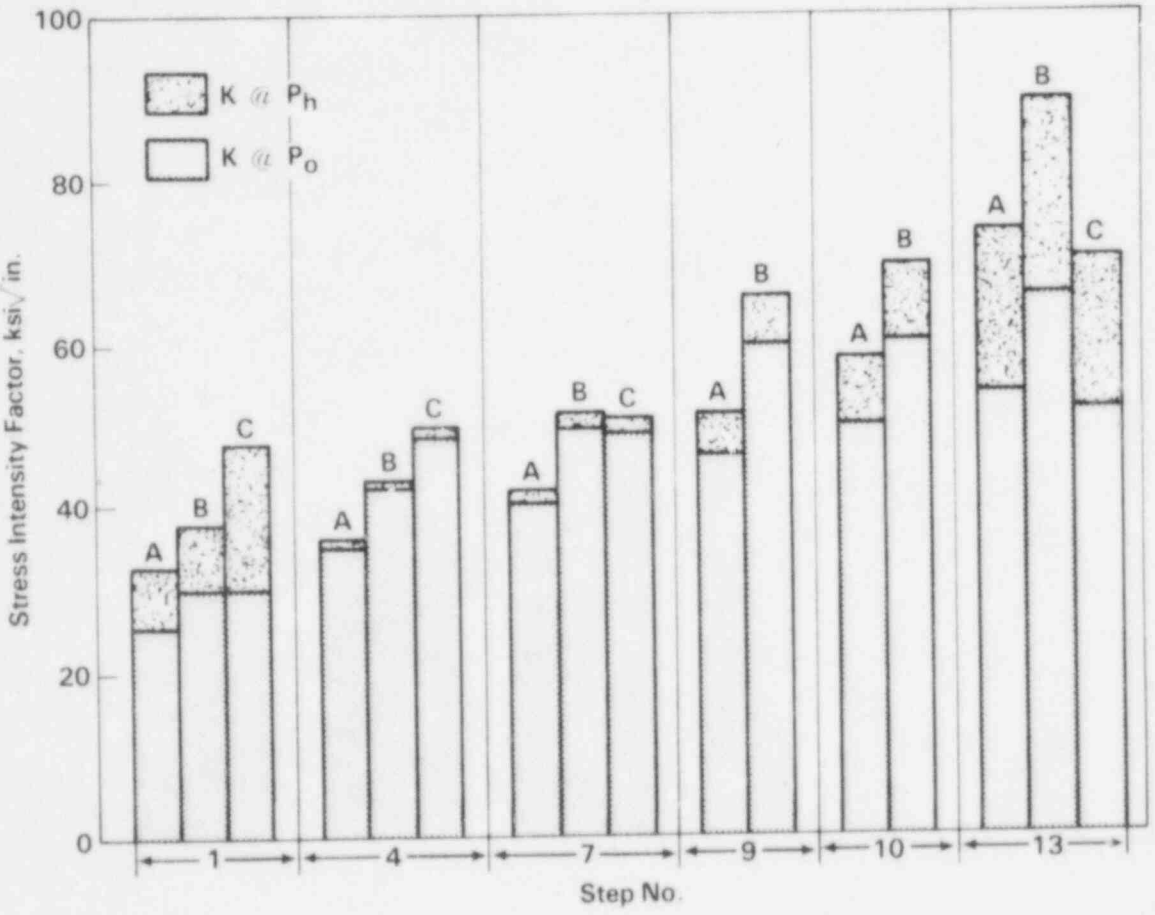

Figure 4.1. Hydrotest and Prior Cyclic Loading Stress Intensity Factor Levels for Flaws A, B, and C.

compared to the A533B insert. Note also, the Kaiser effect. The vessel had been previously tested to 163 bar and the AE in Figure 4.3 does not start until the pressure exceeds 163 bar. The major reason for concern is shown in Figure 4.4. At 230 bar, AE was detected from the KS07 insert at constant or decreasing pressure. By 232 bar, this characteristic was quite pronounced indicating that crack growth was occurring at static pressure. In addition, there were audible "bangs" from the vessel which were picked up by a microphone placed near the KS07 insert. AE signal amplitude distribution (Figure 4.5) showed a marked contrast between the KS07 and the A533B inserts. AE from the KS07 insert was high amplitude ($\geq$10 volts) while that from the A533B insert was mostly below 4 volts. AE source location information in Figure 4.6 again shows a sharp contrast between the A533B insert and the KS07 insert. Source indications are well distributed on the A533B while there is a cluster of indications along the circumferential weld in the KS07.

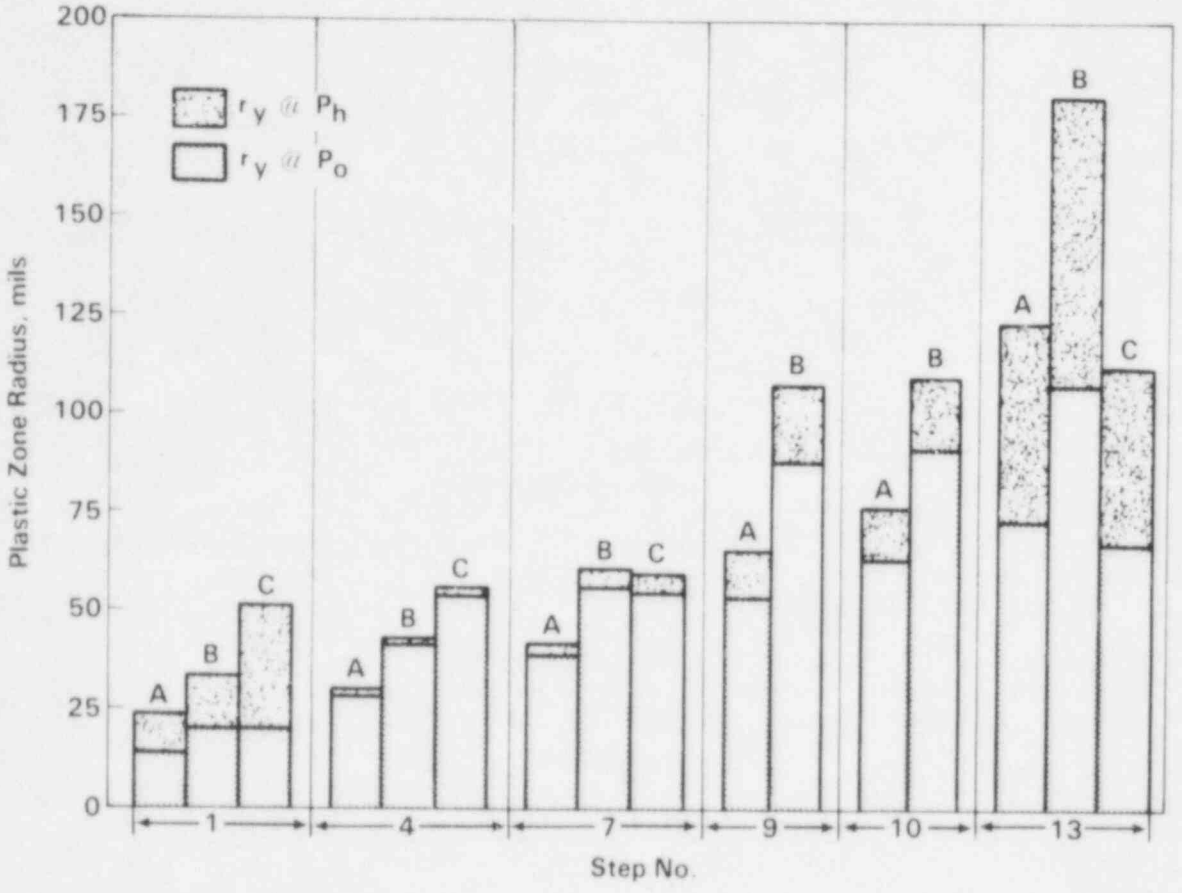

Figure 4.2. Hydrotest and Prior Cyclic Loading Plastic Zone Radii for Flaws A, B, and C.

The key information from Phase 1 of Step 1 which raised a serious question concerning the integrity of the KS07 insert included:

- The early onset of high amplitude AE (140 bar).
- Predominance of high amplitude signals from KS07.
- Clustering of AE source indications along a weld across the middle of KS07.
- Large quantity of AE signals.
- Continuation of AE at static pressure starting at 230 bar.
- Audible "bangs" heard which appeared to emanate from KS07 during the 230 to 232 bar pressure range.

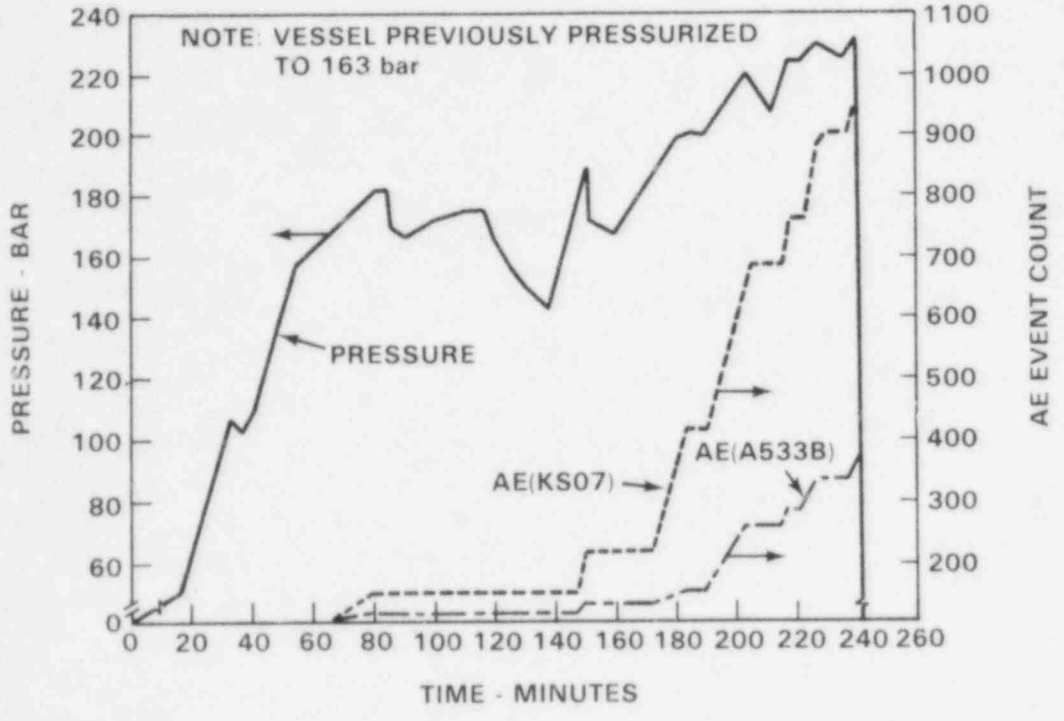

Figure 4.3. AE and Pressure Versus Time for the First Phase of Step 1.

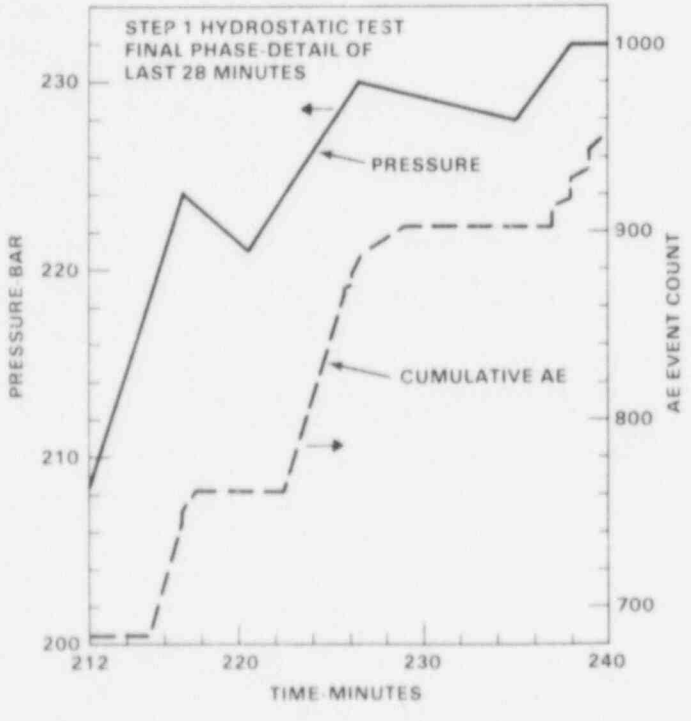

Figure 4.4. AE (KS07 Insert) and Pressure Versus Time, Last 28 Minutes of the First Phase of Step 1.

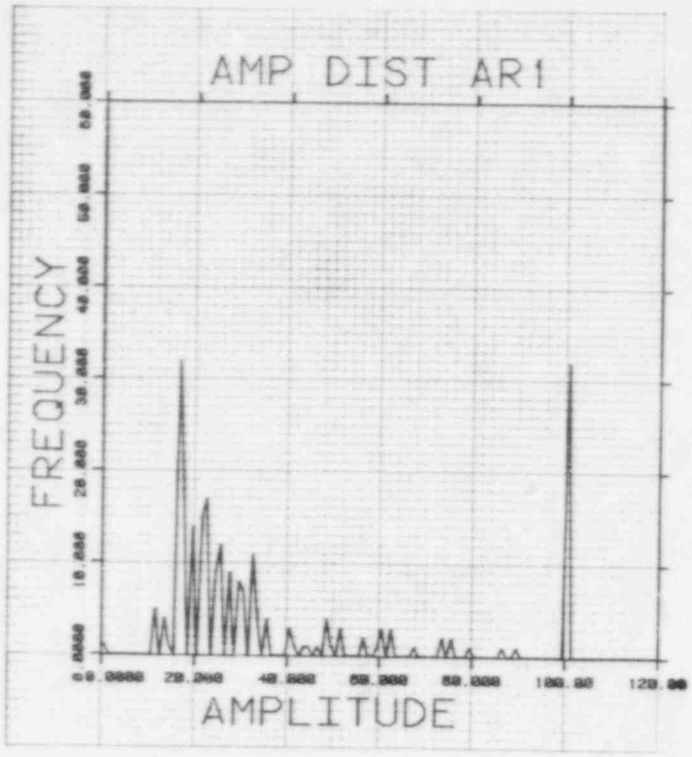

A533B Insert

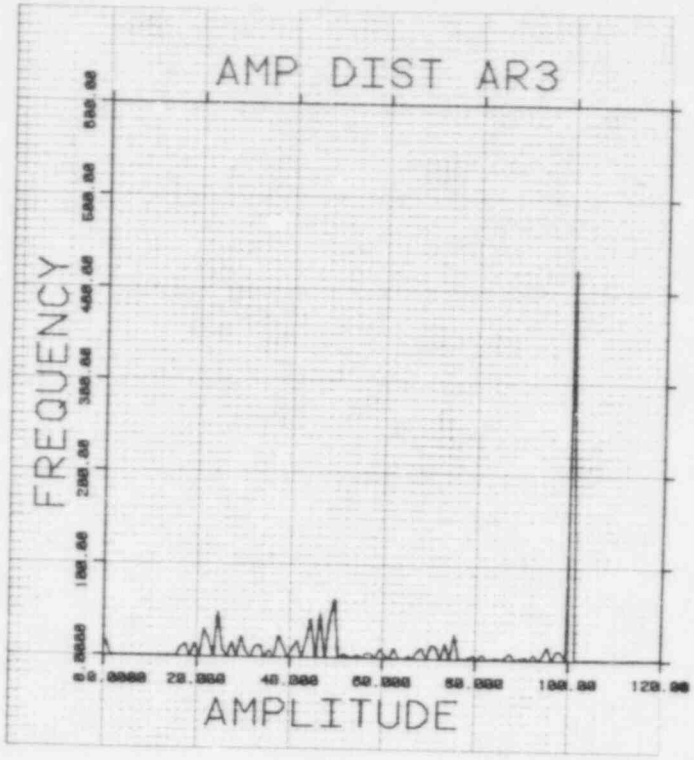

KS07 Insert

NOTE: Amplitude Scales are in Volts x 10.

Figure 4.5. AE Signal Amplitude Distribution for Both Inserts During the First Phase of Step 1.

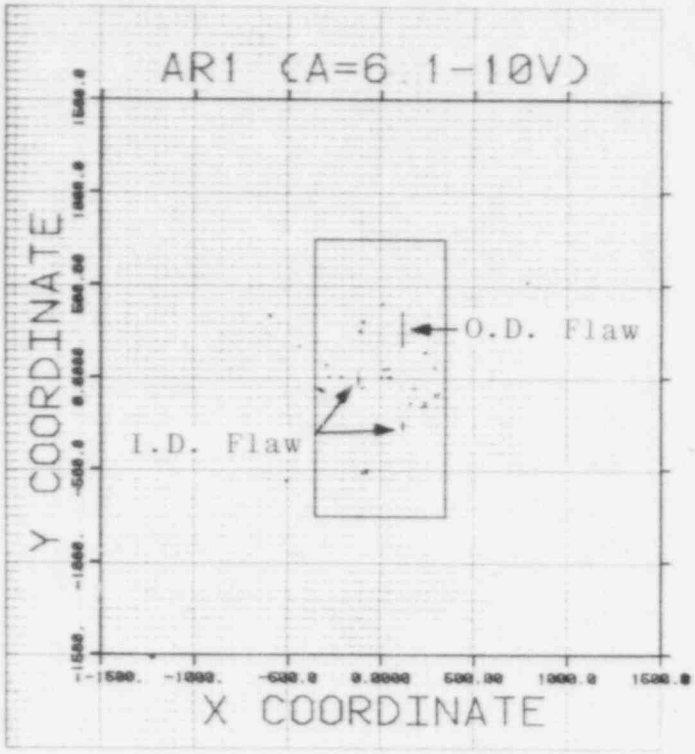

AE Data in 6.1 to 10.0 Volt Amplitude Range Only

A533B Insert

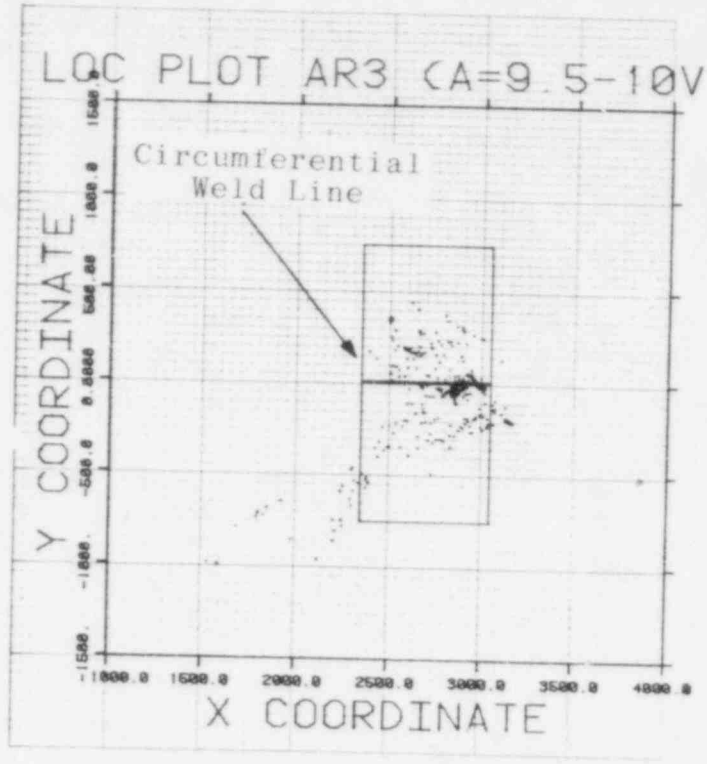

AE Data in 9.5 to 10.0 Volt Amplitude Range Only

KS07 Insert

Figure 4.6. AE Source Locations for First Phase of Step 1.

Based on the above points, the decision was made to replace the KS07 insert with sound material. This was accomplished by the end of December 1982. A533 steel was used for the new insert.

After the KS07 insert was removed from the vessel, destructive tests were performed to estimate the level of damage caused by the hydrotest. Three tensile specimens were machined from the KS07 insert (see Figure 4.7). Each specimen conformed to the curvature of the insert and had the same thickness. The

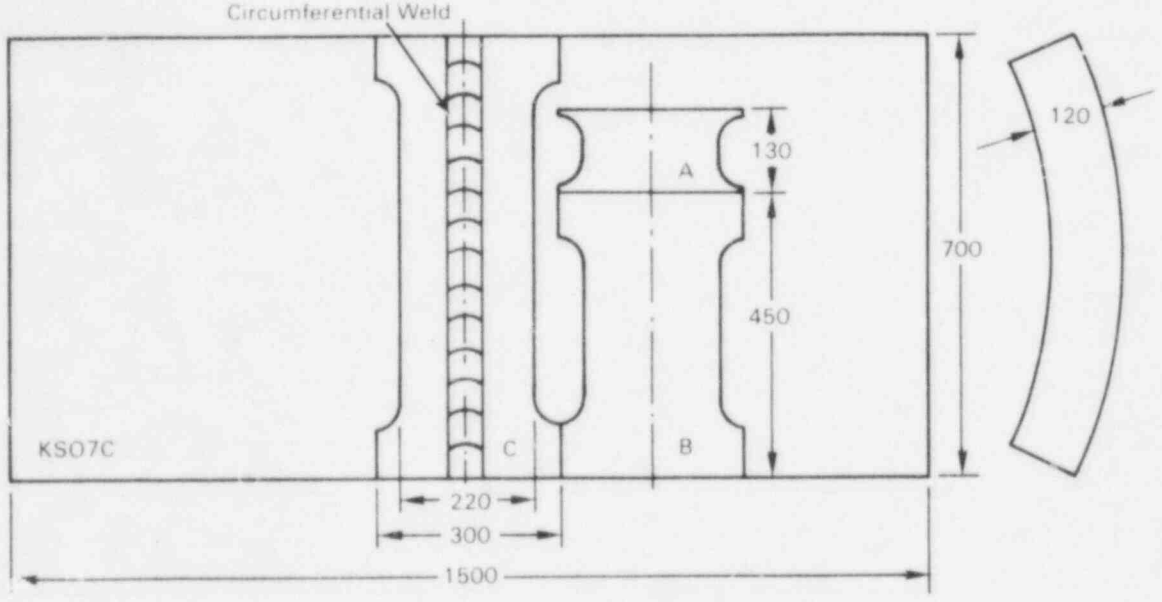

Figure 4.7. Cutting Plan for Curved Tensile Specimens Taken from KS07 Insert.

specimens were pulled to failure at 60°C. Different levels of bending moment were produced in each specimen owing to variable specimen lengths (Figure 4.7). Test results are given in Table 4.2. Also shown in Table 4.2 are maximum stress and stress intensity factors for the tensile specimens and KS07 insert. For the tensile specimens, nominal (i.e., remote from cracks) tensile and bending stresses at the inner surface of the specimens which was the vessel inside surface are given. These numbers are compared to the nominal loop stress for the insert during the hydrotest. Specimens A and B failed at about the same stress level, whereas specimen C failed at a much higher stress. Fracture surface examinations showed that specimens A and B had initial flaw sizes approximately the same. This accounts for the similar failure levels. The specimen C initial flaw size was somewhat smaller than A or B but not enough smaller to account

Table 4.2. Tensile Test Results for Specimens A, B, and C from KS07 Insert.

Specimen	Specimen Failure Load, lb. (x 10^6)	Maximum Inner Surface Stress, ksi (specimen)	Maximum Inner Surface Hoop Stress, ksi (vessel)	Maximum Inner Intensity Factor, ksi$\sqrt{in.}$ (specimen)	Maximum Inner Intensity Factor, ksi$\sqrt{in.}$ (vessel)
A	1.45	40.9	22.5	110	50-60
B	0.79	44.6	22.5	100	50-60
C	0.67	71.0	22.5	-	50-60

for the increased failure stress. Specimen C failed at the higher stress principally because the weldment was much stronger than the surrounding KS07 material. Stress intensity factors at failure were estimated for specimens A and B by approximating the loading and flaw geometry as a superposition of tensile and bending K-solutions for single-edge-notch specimens. These calculations indicated that the critical stress intensity factor at failure was about 100 ksi$\sqrt{in}$. In comparison, the stress intensity factor of a 30% through-wall flaw extending one-half the insert in length was estimated at between 50-60 ksi$\sqrt{in}$. at maximum hydrotest pressure. These calculations, thus, indicate that the KS07 insert was not as near failure during the hydrotest as suspected. Of course, the flaws were severe enough to justify stopping the test and replacing the insert, since very little fatigue damage could have been tolerated.

4.1.2 Step 1 - Phase 2

Step 1 - Phase 2 was performed prior to restarting the test after the KS07 insert was replaced. The vessel was pressurized to 240 bar (1.0 x planned operating pressure). Figures 4.8 and 4.9 give the pressure curve and total AE response versus time. Some important items to consider here are:

- The vessel was pressurized to 232 bar in Step 1 - Phase 1.
- Array 3 (cylindrical array) had not been strapped down at this point so the sensitivity is marginal.

For all AE arrays, about half of the total AE detected occurred in the final pressure rise from 232 to 240 bar.

Turning now to Figure 4.10, there were some indications from the region where the KS07R (replacement) weld first showed AE from crack growth during the cyclic part of the test. Of the total AE detected, about half originated from the KS07R weld

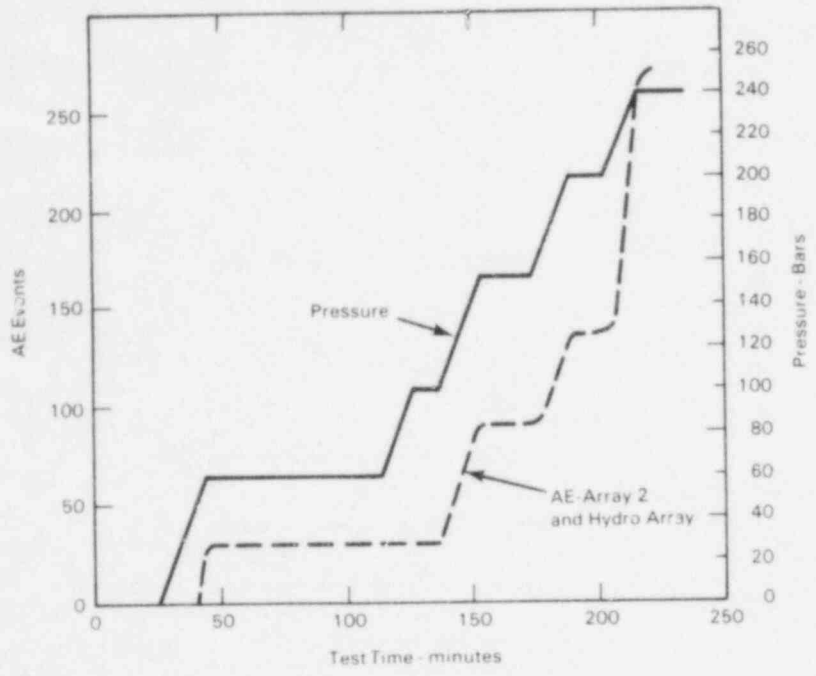

Figure 4.8. Pressure and AE from Waveguide Array 2 and Hydro Array - Step 1, Phase 2, ZB-1 Vessel.

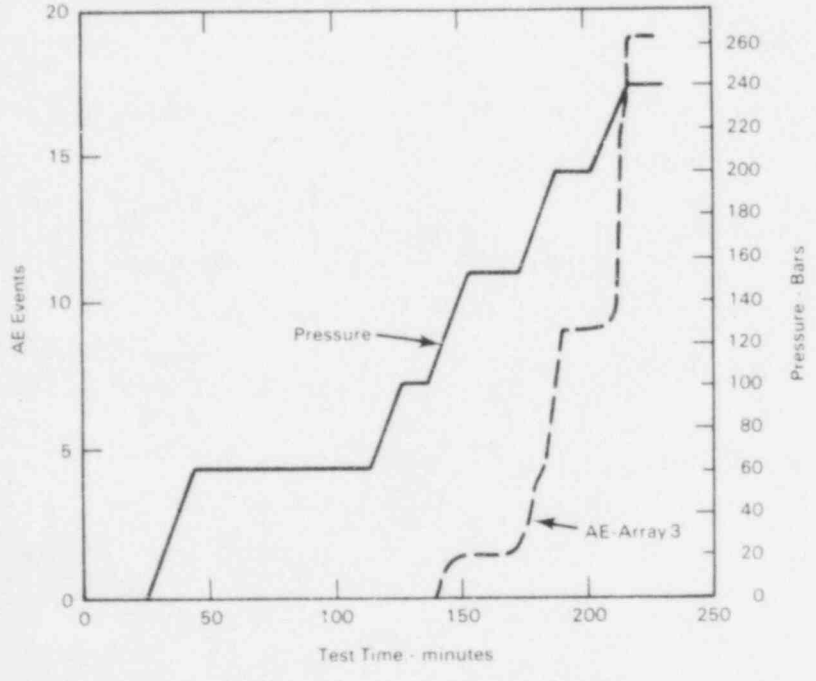

Figure 4.9. Pressure and AE from Waveguide Array 3 - Step 1, Phase 2, ZB-1 Vessel.

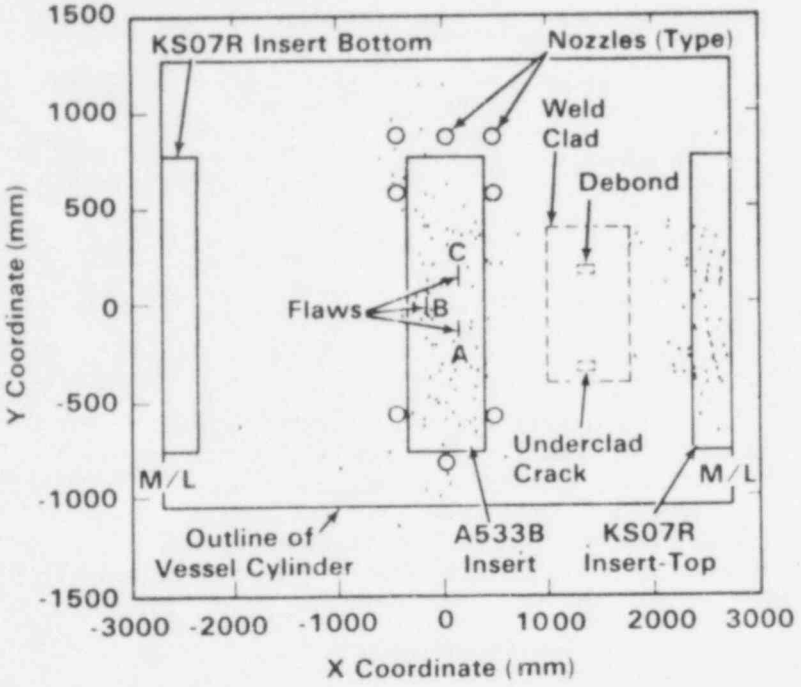

Figure 4.10. AE Source Indications - Array 2, Step 1, Phase 2 Hydro, ZB-1 Vessel.

region between 210 and 240 bar. At the time, these were not noted as being significant, which was a human error under the pressure of starting up the test; but nonetheless, it does demonstrate that in the context of a preservice hydro, the AE was sensitive to the apparent presence of a crack in the weld region. This also lends credence to the hypothesis that the KS07 weld crack formed at the time of welding.

AE indications from the A533 insert were scattered with no concentration at any of the flaws. This is not surprising since these flaws had been stressed to a similar level during the Phase 1 hydrotest.

The results from Array 3 in Figure 4.11 were similar but the amount of AE was much less due to the lower sensitivity of Array 3 at that time. There was one notable difference in that Array 3 showed a few indications from the bottom part of the KS07R weld region. Generally, Array 3 was found to be more effective in source location on the total vessel which may explain this.

The most important result from Step 1 - Phase 2 hydro is that it showed evidence that AE can detect a natural flaw even during a low-pressure-level hydrotest in the preservice test context. The KS07R insert weld had not experienced service stresses at this point.

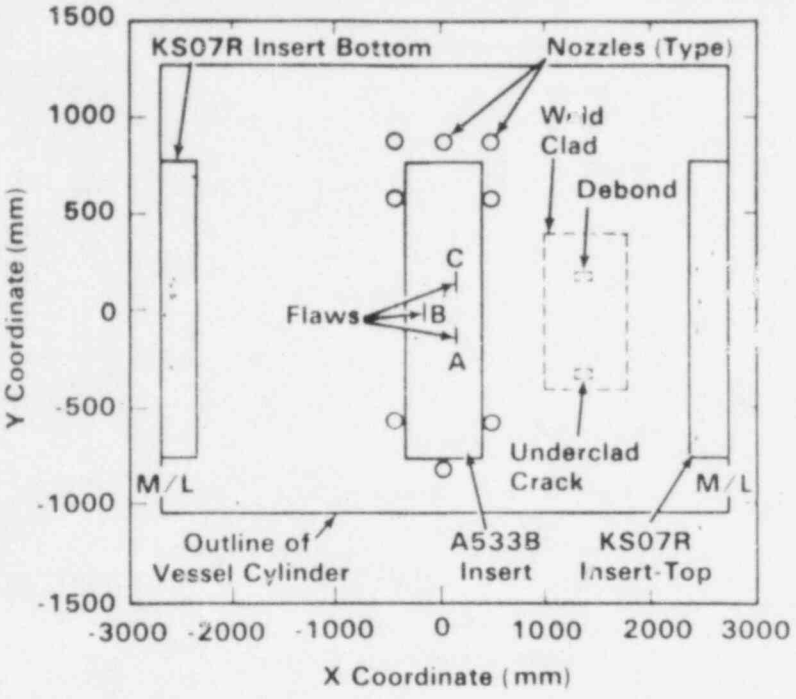

Figure 4.11. AE Source Indications - Array 3, Step 1, Phase 2 Hydro, ZB-1 Vessel.

4.1.3 Step 4

The Step 4 hydro was 1.02 x operating pressure or 245 bar. This was performed after 2000 load cycles between 24 and 240 bar plus 6000 cycles between 144 and 240 bar; all at 65°C.

AE monitoring concentrated on the A533 insert. There were only six events detected with three coming from the region of Flaw B. These results are illustrated in Figures 4.12 and 4.13.

Step 4 begins to raise a question concerning the effectiveness of AE for detecting flaws during inservice hydros at least at very low overpressures.

4.1.4 Step 7

In Step 7, the pressure was raised to 1.04 x operating pressure or 250 bar. The total cyclic loading by this time was 4000 cycles between 24 and 240 bar, 9710 cycles between 144 and 240 bar, and 2290 cycles between 168 and 240 bar; all at 65°C. Again, there was very little AE detected from the A533 insert flaws as shown in Figures 4.14 and 4.15. These are the results from the hydro array next to waveguide Array 1 and Array 3. By this point, Array 3 had been strapped down to increase it's sensitivity.

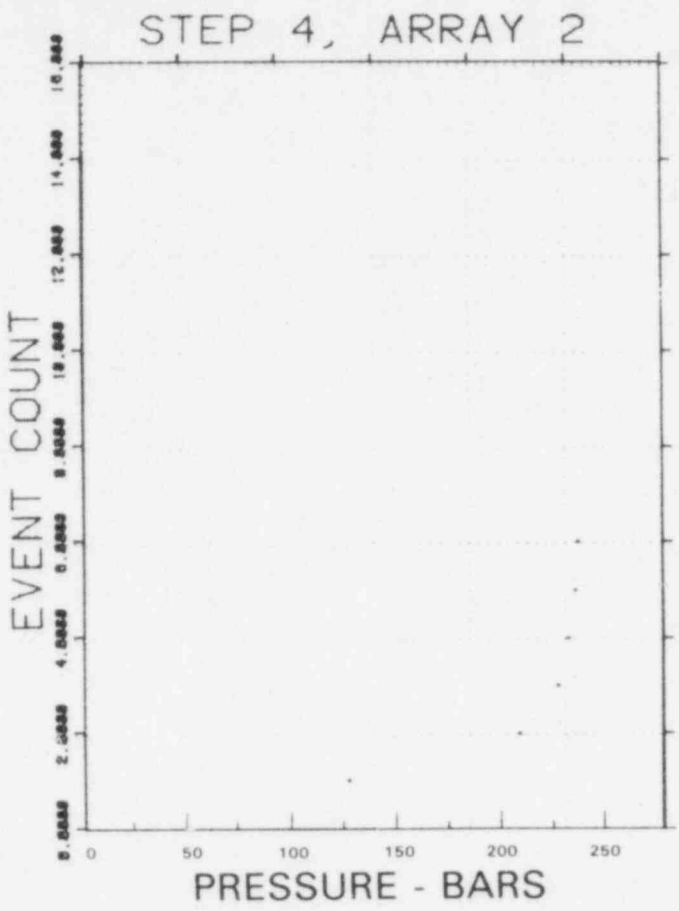

Figure 4.12. AE Versus Pressure - Step 4, ZB-1 Vessel.

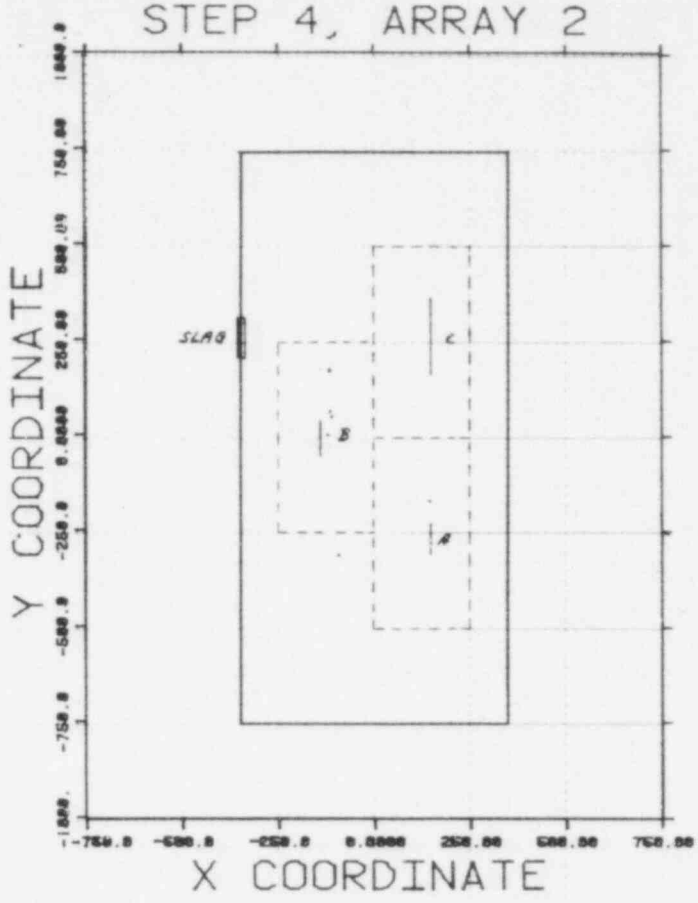

Figure 4.13. Source Indications - Step 4 Hydro, ZB-1 Vessel.

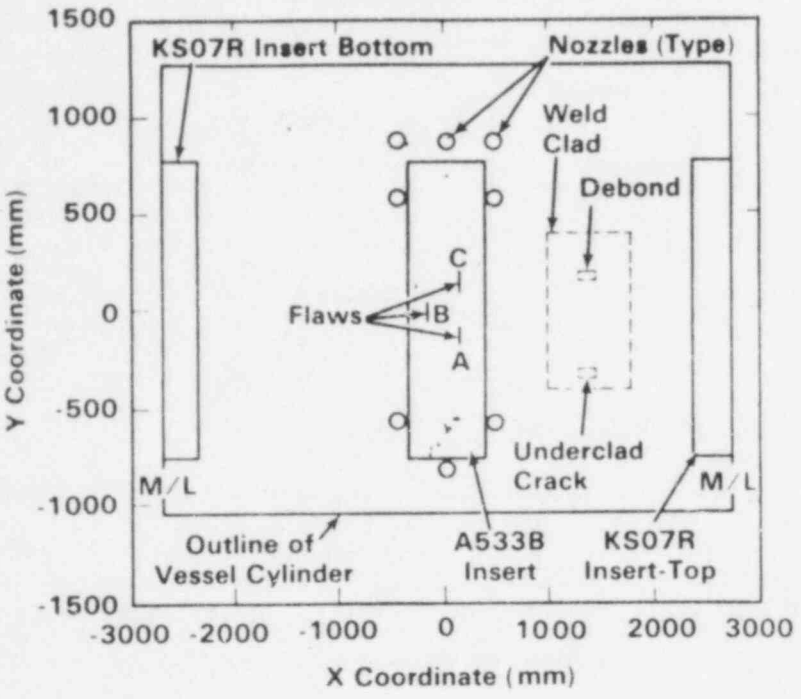

Figure 4.14. AE Source Locations from Hydro Array During Step 7 Hydro, ZB-1 Vessel.

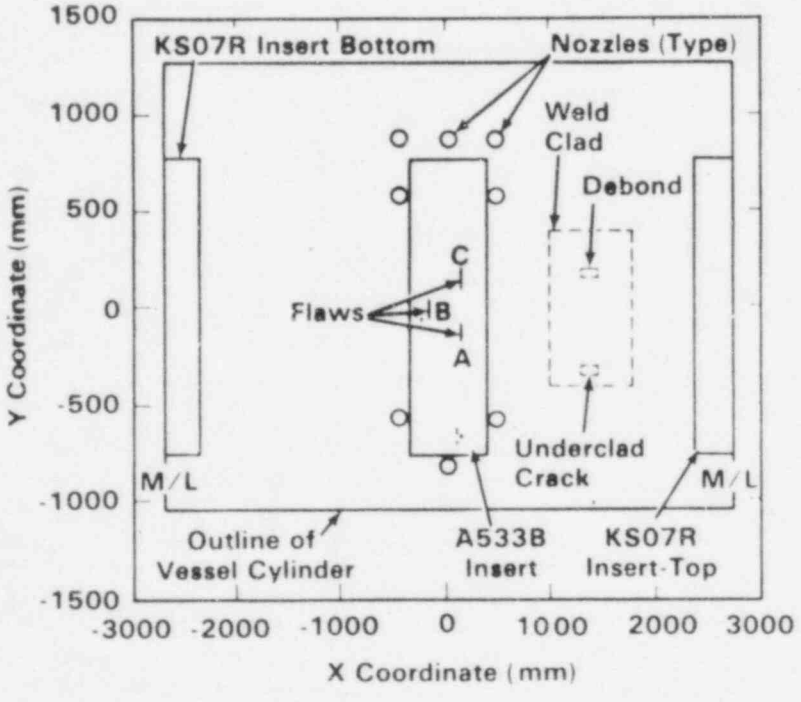

Figure 4.15. AE Source Indications from Array 3 During Step 7 Hydro, ZB-1 Vessel.

4.1.5 Step 9

This was an unplanned hydrotest that was performed after 2900 cycles of Step 9 cyclic loading were completed. This test was conducted because of concern over vessel integrity. The pressure level for this hydro was 1.10 x operating pressure or 275 bar. The test temperature was 240°C which was in contrast to the other hydros performed at 65°C. Since the yield strength of A533B steel decreases with increasing temperature, the plastic zone size expansion caused by the overpressure was greater than if the test had been run at 65°C. Figures 4.16 and 4.17 give the AE source location information for Arrays 2 and 3, respectively. Most of the indications were scattered about regions where flaws were known to exist. The located events were not tightly grouped. Figures 4.18 and 4.19 give the amplitude filtered AE events detected when the test pressure exceeded operating pressure. Many of the scattered indications were eliminated by filtering the data in this fashion. The remaining events are largely associated with Flaws A, B and C in the case of Array 2. Array 3 detected Flaw B and perhaps the KS07R weld flaw but not Flaws A or C. This hydrotest may have also influenced the Step 10 hydro by reducing the effective overpressure due to the larger plastic zone volume expansion (see Figure 4.2).

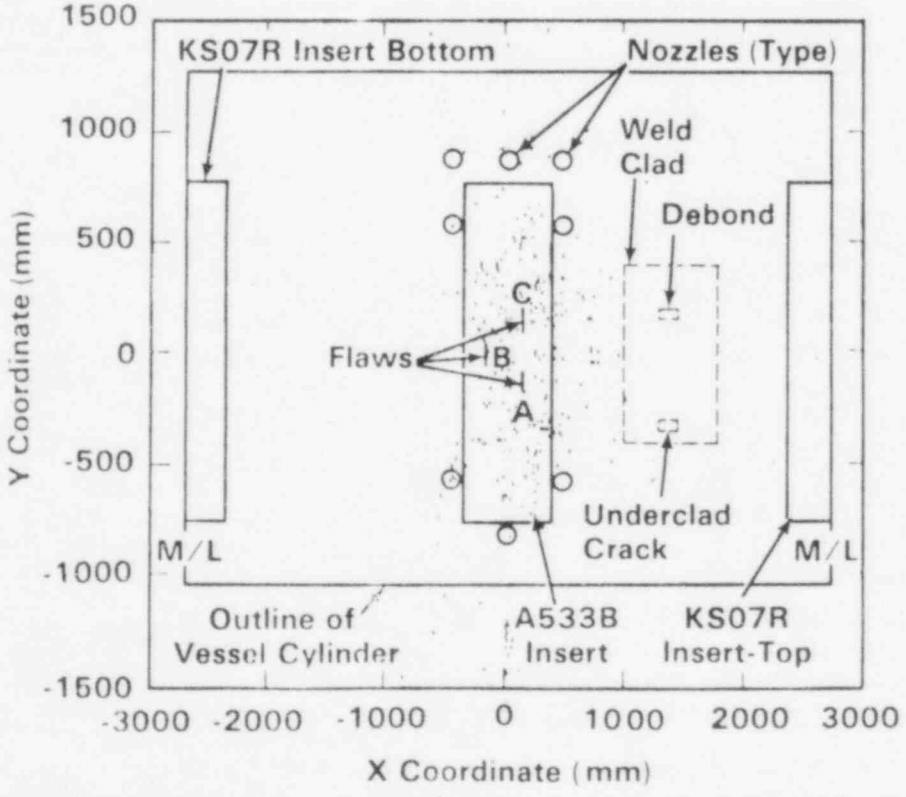

Figure 4.16. AE Source Locations, Array 2 - Step 9 Hydro Test, ZB-1 Vessel.

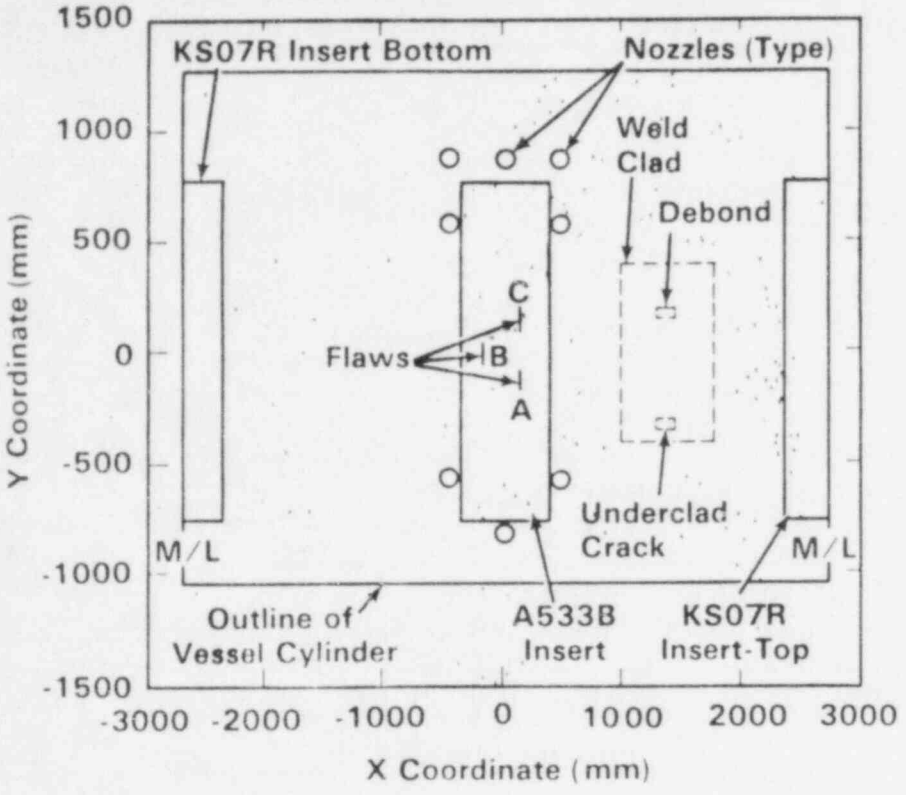

Figure 4.17. AE Source Locations, Array 3 - Step 9 Hydro Test, ZB-1 Vessel.

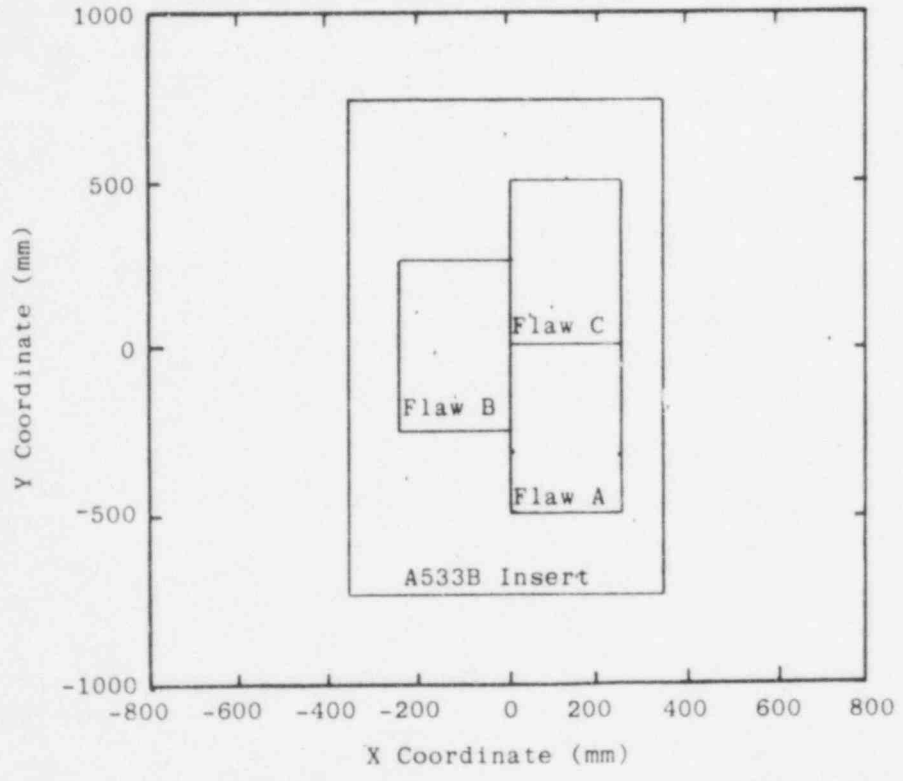

Figure 4.18. AE Source Locations on the A533B Insert, Array 2 - Step 9 Hydro Test, Filtered to Events Detected above 250 Bar with Amplitudes between 8-10 Volts.

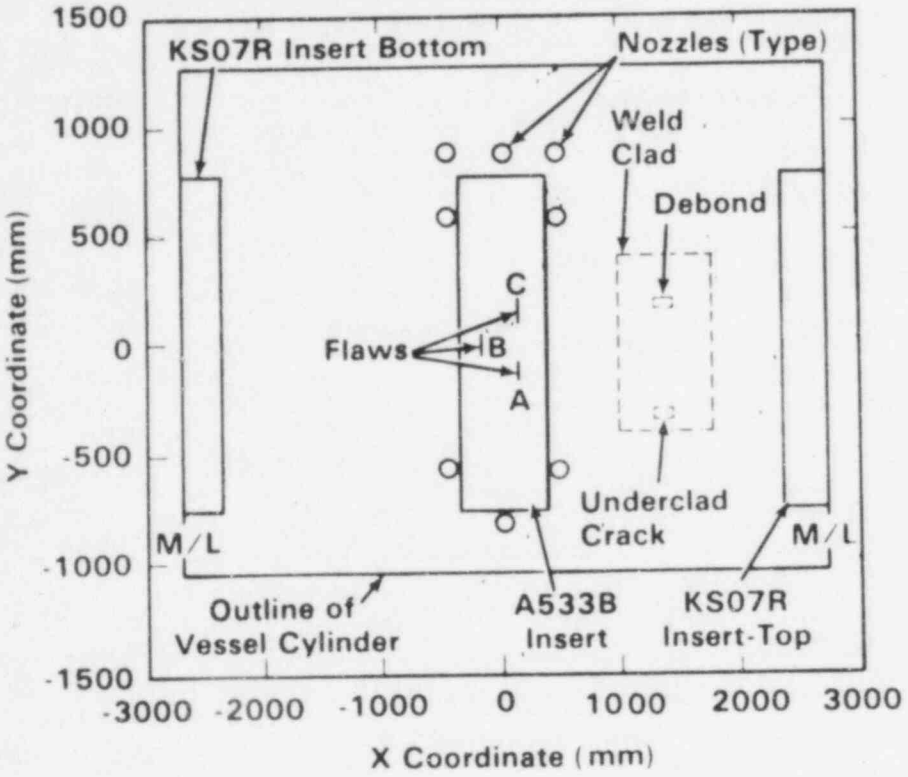

Figure 4.19. AE Source Locations on ZB-1 Vessel, Array 3 - Step 9 Hydro Test, Filtered to Events Detected Above 250 Bar with Amplitudes Between 8-10 Volts.

4.1.6 Step 10

Step 10, which involved an overpressure 1.15 x operating pressure or 288 bar, was performed twice. The vessel was opened for inspection at the end of Step 9. When the Step 10, Part 1 hydro was subsequently performed, it was evident that the inside surface was heavily oxidized and cracking of newly formed oxide was producing a large amount of scattered AE. The vessel was cycled ten times between 25 and 250 bar to fracture the oxide coating and then Step 10, Part 2 hydro was performed.

At Step 10, the total cyclic loading history was 4000 cycles between 24 and 240 bar, 9710 cycles between 144 and 240 bar, 2290 cycles between 168 and 240 bar, all at 65°C; plus 2000 cycles between 100 and 250 bar and 4000 cycles between 150 and 250 bar, the latter at 285°C.

Figures 4.20 and 4.21 illustrate the large amount of AE detected during the first pressurization and show the scattered sources. Figure 4.20 focuses on the A533 insert while Figure 4.21 covers the whole vessel. Figures 4.22 and 4.23 show that there were no identifiable concentrations of AE associated with Flaws A, B, or C.

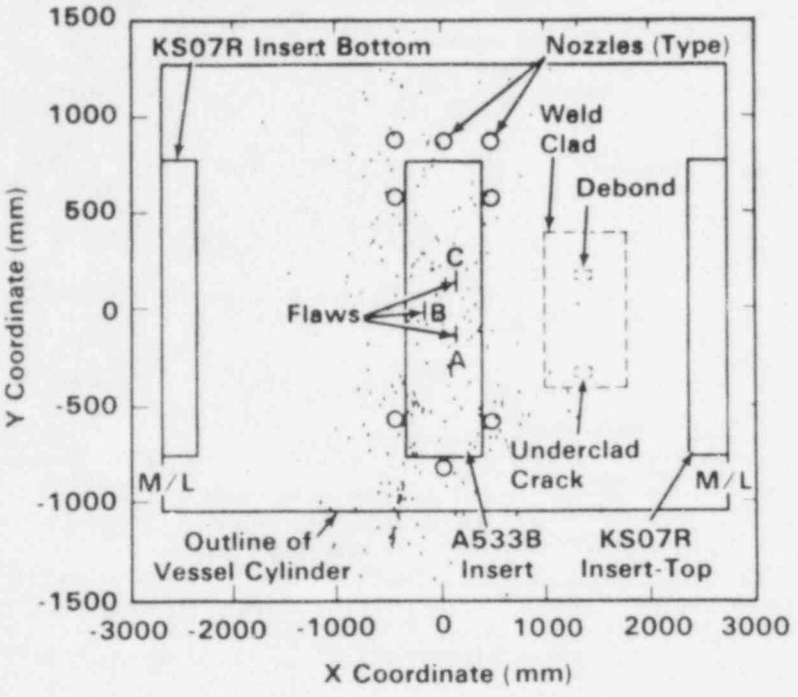

Figure 4.20. Source Locations, Array 1 and Hydro Array - Step 10, First Part, ZB-1 Vessel.

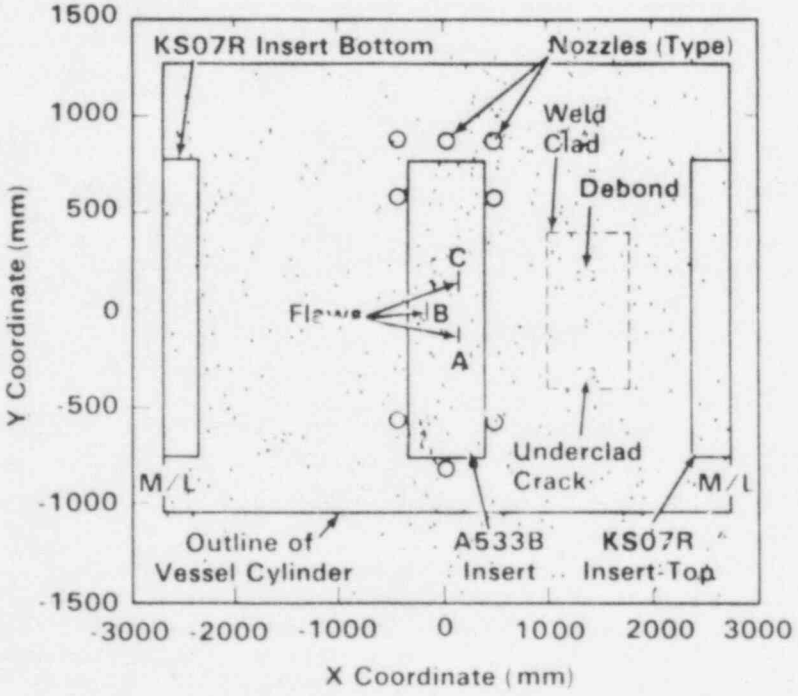

Figure 4.21. Source Locations, Array 3 - Step 10, First Part, ZB-1 Vessel.

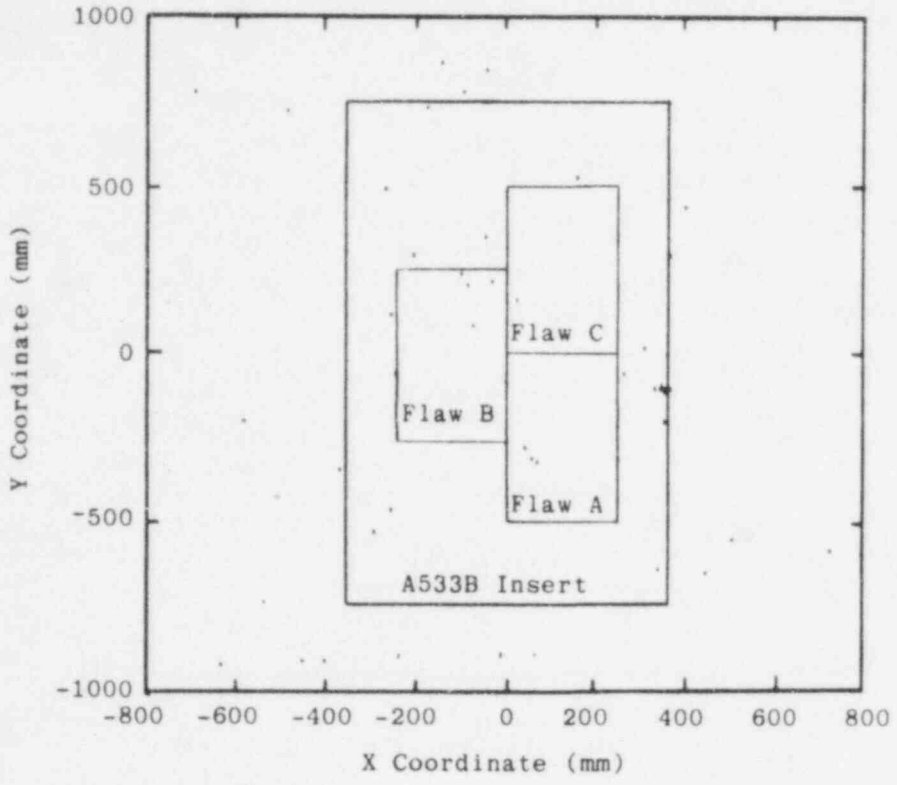

Figure 4.22. AE Source Locations on the A533B Insert, Array 1 - Step 10, First Part, Filtered to Events Detected Above 250 Bar with Amplitudes Between 8-10 Volts.

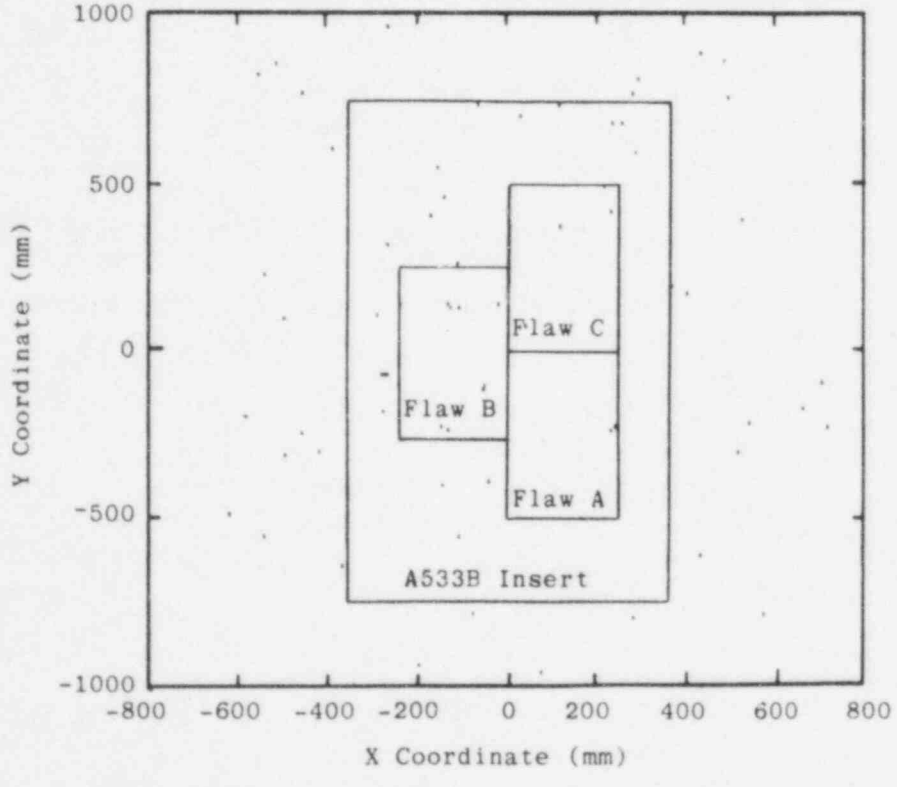

Figure 4.23. AE Source Locations on the A533B Insert, Array 3 - Step 10, First Part, Filtered to Events Detected Above 250 Bar with Amplitudes Between 2-10 Volts.

Detected AE for Step 10, Part 2 hydro (Figures 4.24 and 4.25) was substantially less than in Part 1. The vessel was cycled ten times from 25 to 250 bar between Parts 1 and 2 to attempt to eliminate noise from oxide film rupture. The concentration at the bottom center in Figure 4.24 may have been noise from the banding holding Array 3 sensors. Figures 4.26 and 4.27 show that there were no concentrations of source locations associated with any of the flaws.

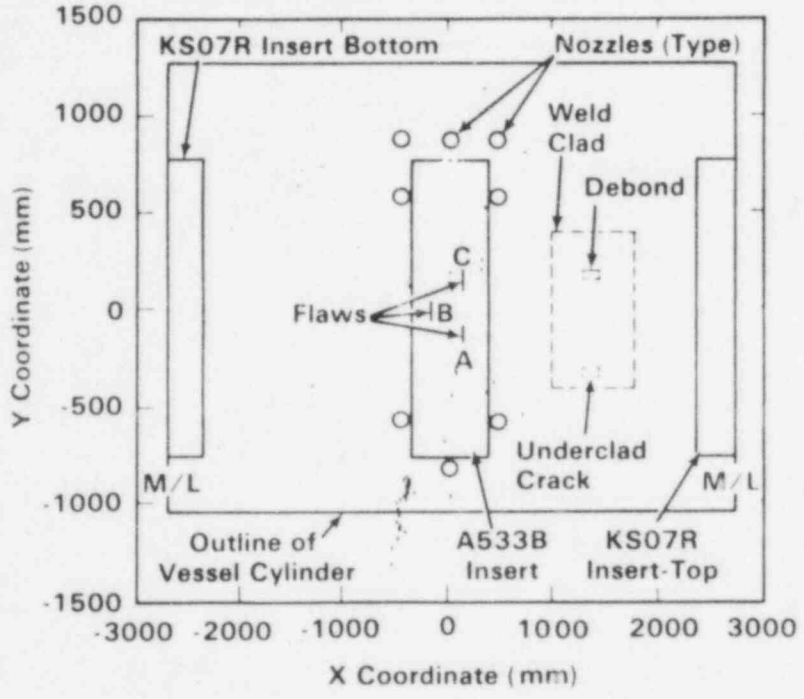

Figure 4.24. Source Locations, Array 1 and Hydro Array - Step 10, Part 2, ZB-1 Vessel.

4.1.7 Step 13

The final part of the test was the Step 13 hydrotest. At this point, there was concern over the integrity of the vessel primarily due to the crack in the KS07R weld. To guard against unexpected crack growth, Step 13 was performed in increments as given in Figure 4.28.

For Step 13, the Hydro Array was placed parallel to Array 3 (circumferential array) in an effort to obtain improved source location from the low frequency Hydro Array for the full vessel cylinder. In practice, the waveguide circumferential array

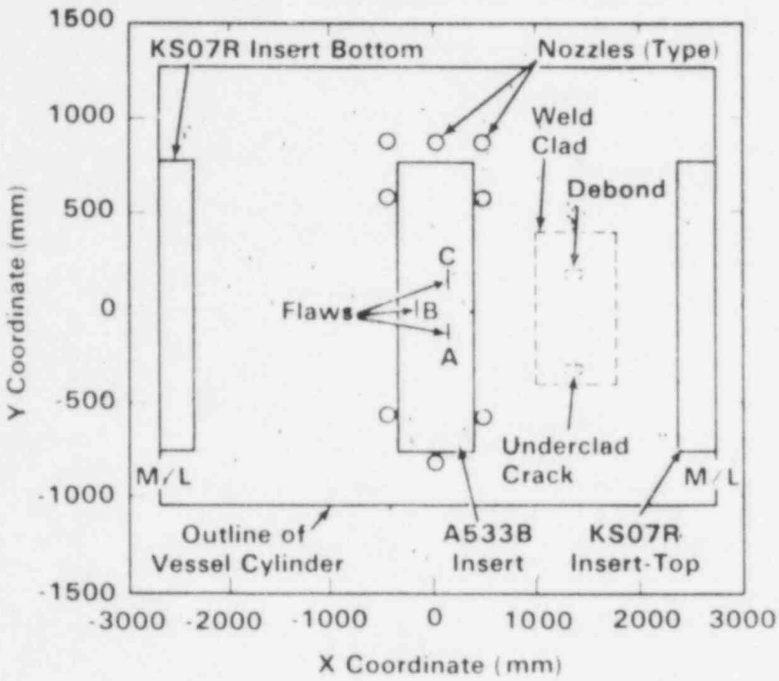

Figure 4.25. Source Locations, Array 3 - Step 10, Part 2, ZB-1 Vessel.

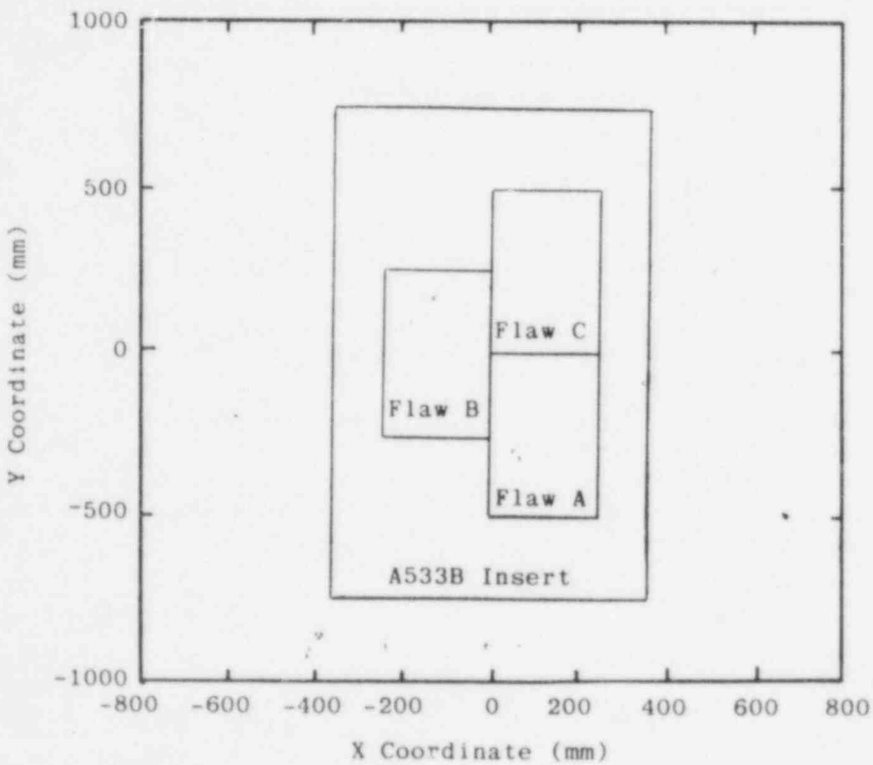

Figure 4.26. AE Source Locations on the A533B Insert, Array 1 - Step 10, Part 2, Filtered to Events Detected Above 250 Bar with Amplitudes Between 8-10 Volts.

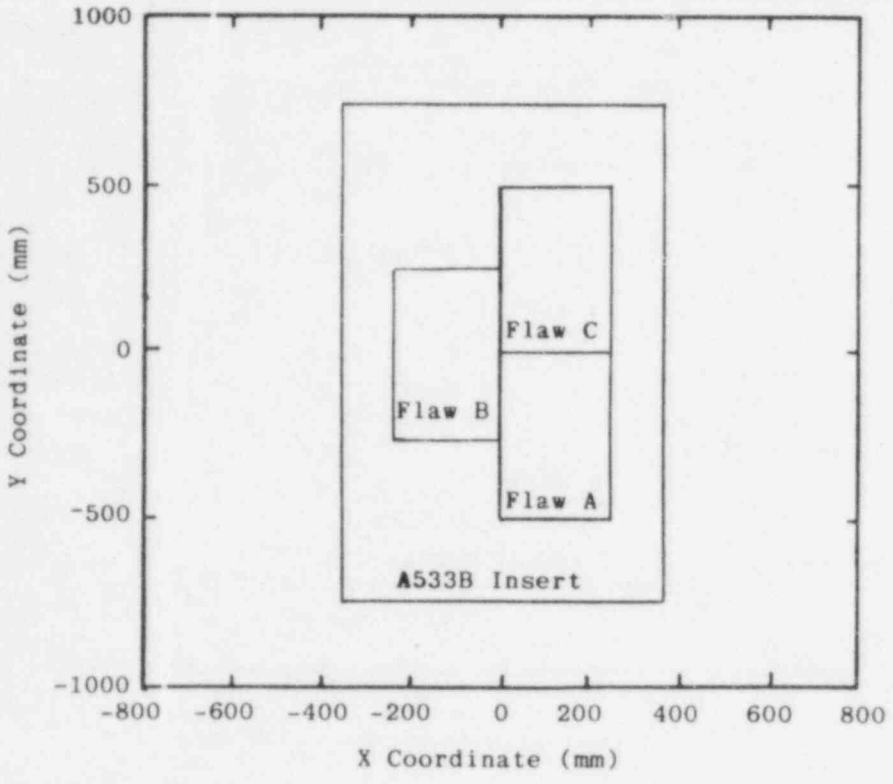

Figure 4.27. AE Source Locations on the A533B Insert, Array 3 - Step 10, Part 2, Filtered to Events Detected Above 250 Bar with Amplitudes Between 2-10 Volts.

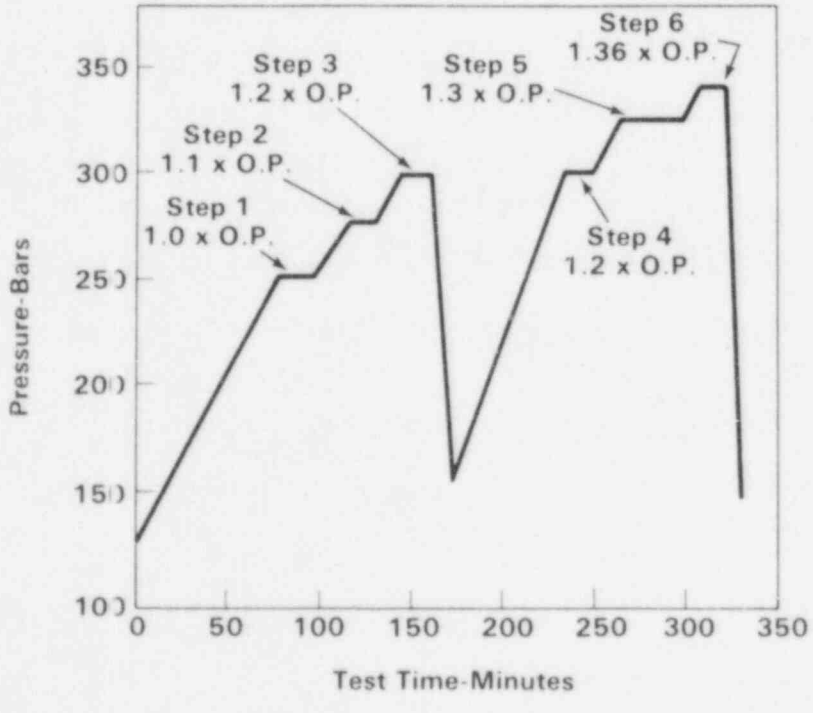

Figure 4.28. Pressure Versus Time Curve, Step 13, ZB-1 Vessel Test.

(Array 3) was the more effective for source location. Figures 4.29 and 4.30 give source location results for the total Step 13 hydro as produced by the two arrays. Both show generally similar groupings (1-5) but the Array 3 groups are better defined and more closely associated with known potential sources. Groups #1 and #5 in both figures are associated with the straps around the vessel to secure Array 3 sensors. Groups #3 and #4 are associated with the KS07R weld crack. Group #2 is associated primarily with Flaw B. The rest of the AE source indications in Figures 4.29 and 4.30 are scattered and do not appear to relate to any known defect.

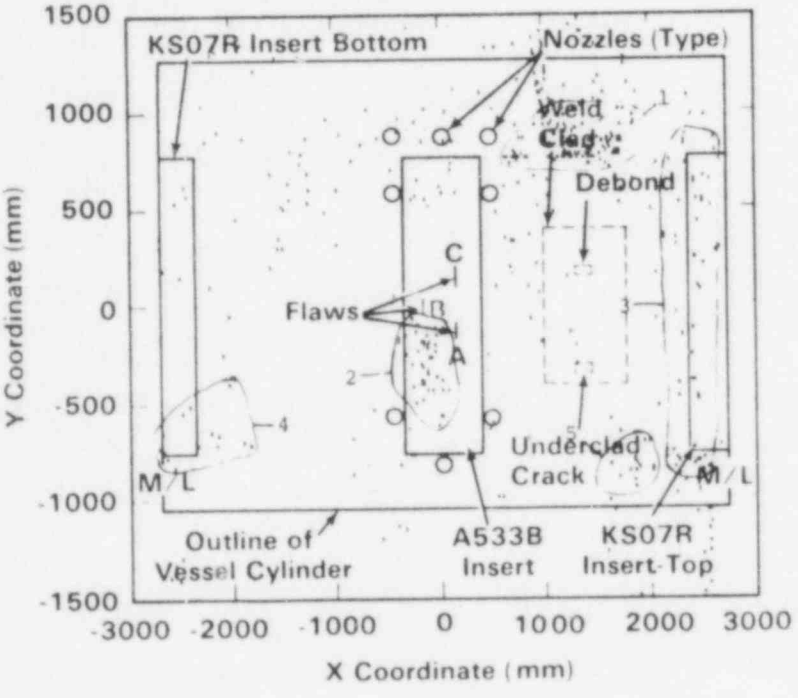

Figure 4.29. AE Source Location, Hydro Array - Step 13, Total, ZB-1 Vessel.

The development of the AE data by each part of the Step 13 hydro is given in Figures 4.31 through 4.42. Also Figures 4.43 and 4.44 show source location plots for AE events detected above 250 bar pressure in the vicinity of the A533B insert. Observations from these figures are:

- Data from Flaw B appears early in the hydro (250 to 300 bar pressure).
- The KS07R weld crack does not appear to produce AE until Part 5 (325 bar).

Flaws A and C did not produce any notable AE indications during Step 13.

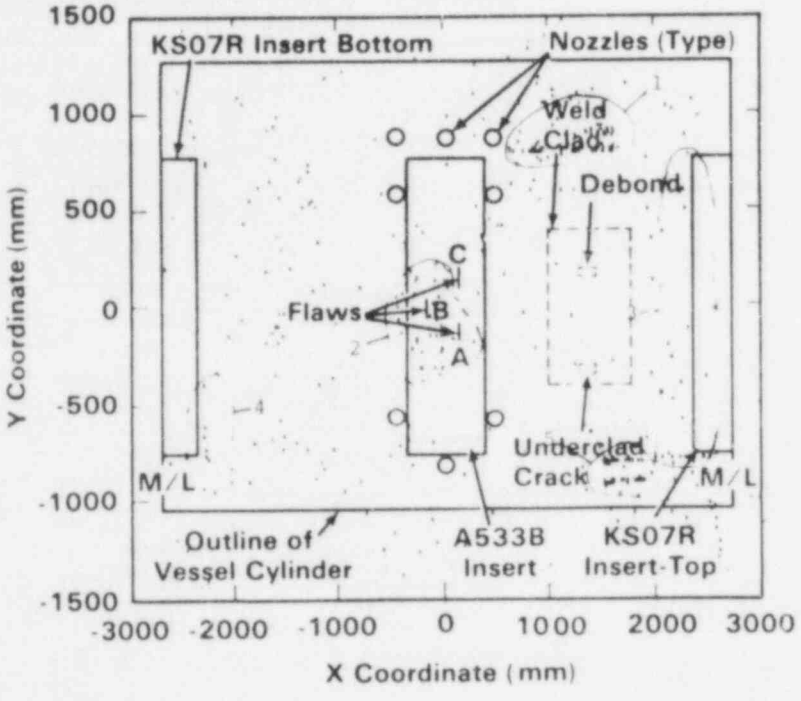

Figure 4.30. AE Source Location, Array 3 - Step 13, Total, ZB-1 Vessel.

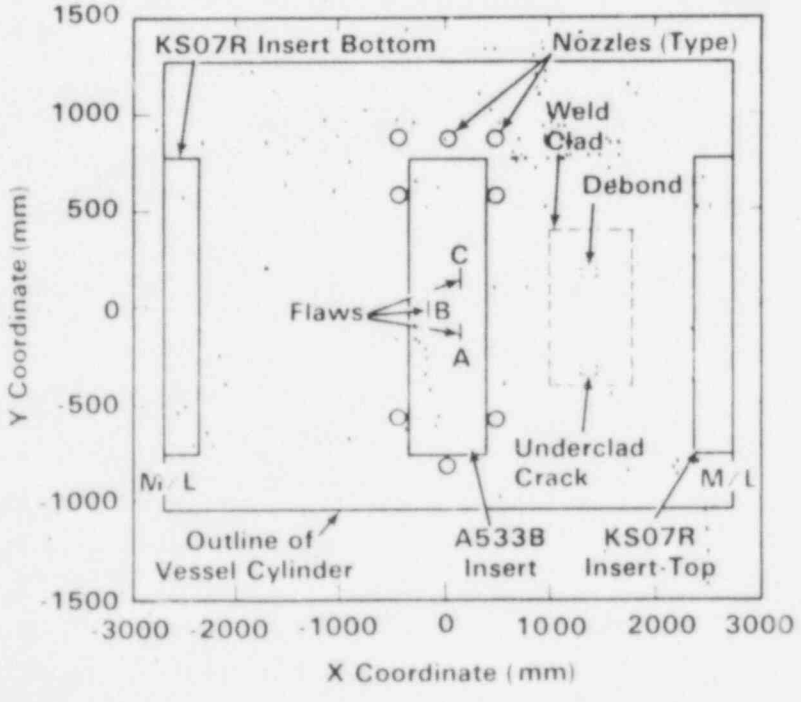

Figure 4.31. AE Source Location, Hydro Array - Step 13, Part 1, ZB-1 Vessel.

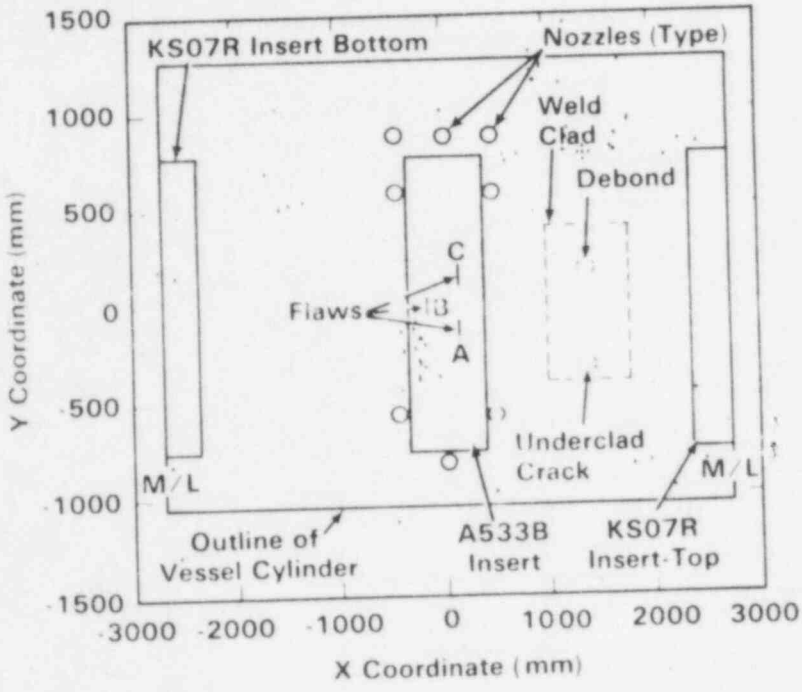

Figure 4.32. AE Source Location, Hydro Array - Step 13, Part 2, ZB-1 Vessel.

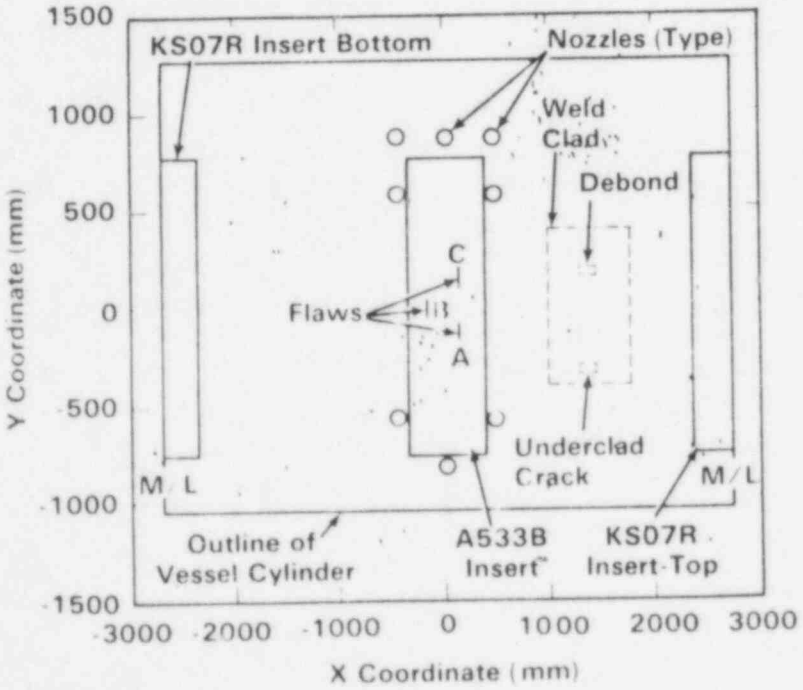

igure 4.33. AE Source Location, Hydro Array - Step 13, Part 3, ZB-1 Vessel.

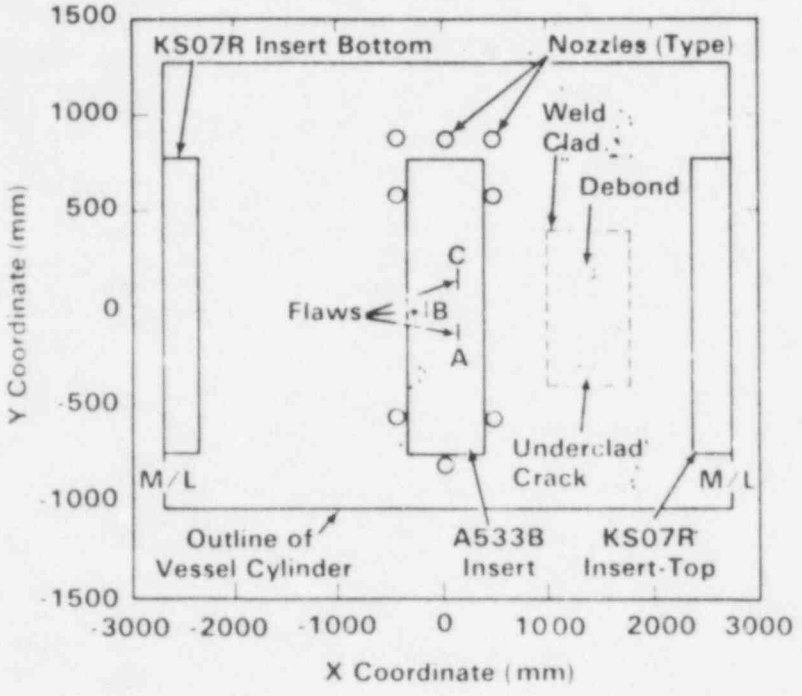

Figure 4.34. AE Source Location, Hydro Array - Step 13, Part 4, ZB-1 Vessel.

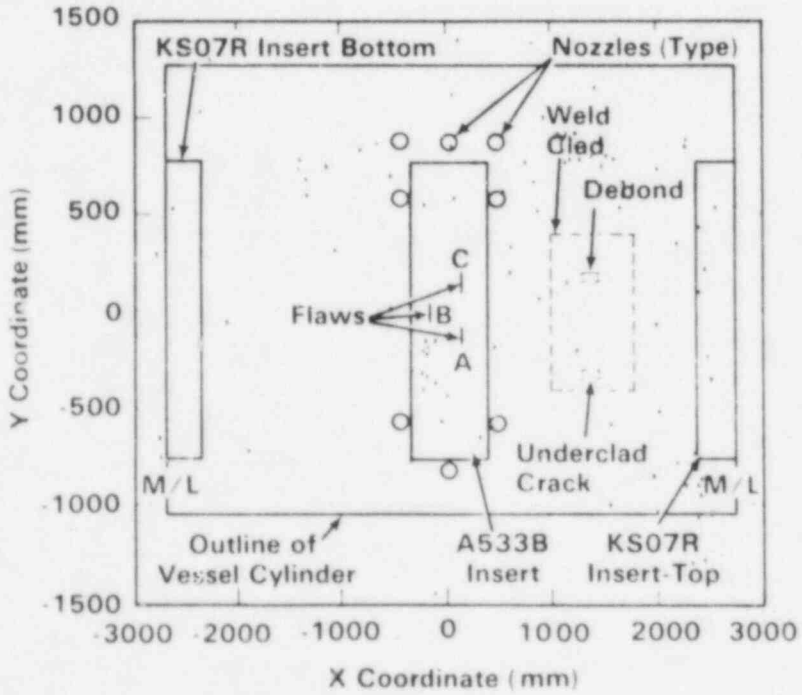

Figure 4.35. AE Source Location, Hydro Array - Step 13, Part 5, ZB-1 Vessel.

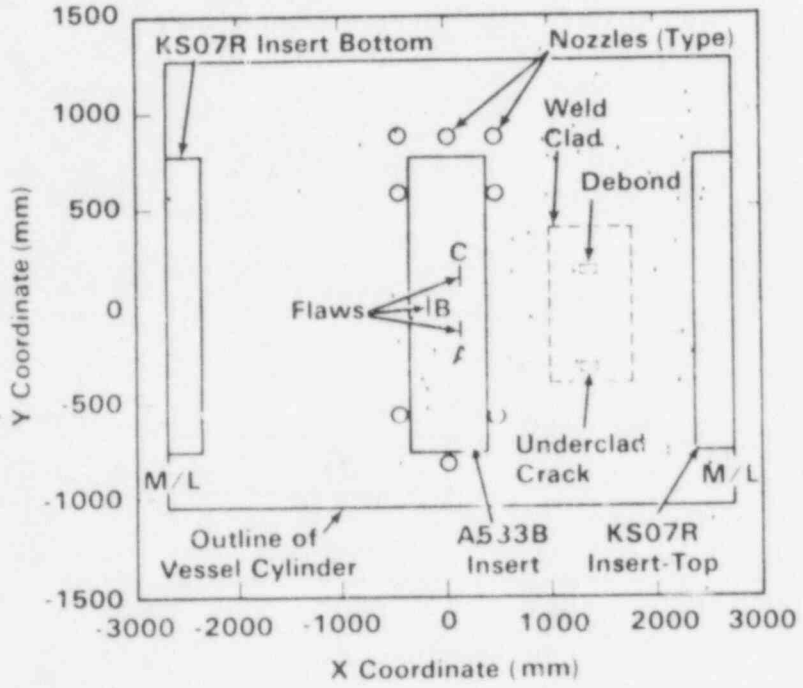

Figure 4.36. AE Source Location, Hydro Array, Step 13, Part 6, ZB-1 Vessel.

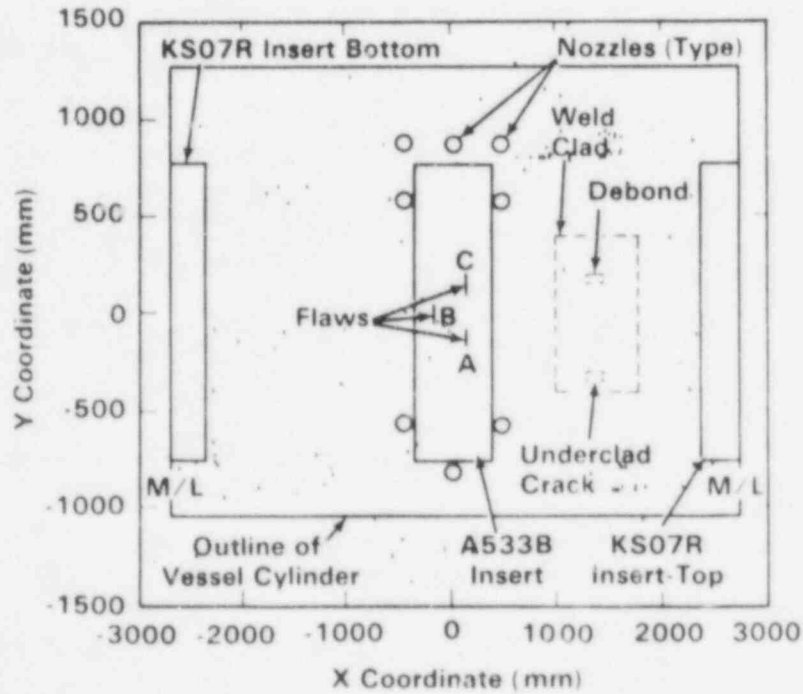

Figure 4.37. AE Source Location, Array 3 - Step 13, Part 1, ZB-1 Vessel.

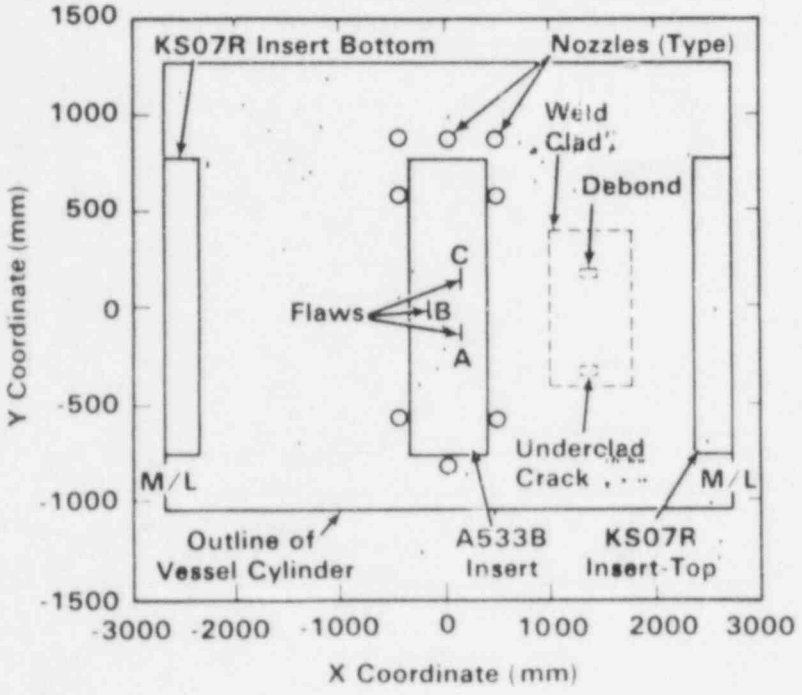

Figure 4.38. AE Source Location, Array 3 - Step 13, Part 2, ZB-1 Vessel.

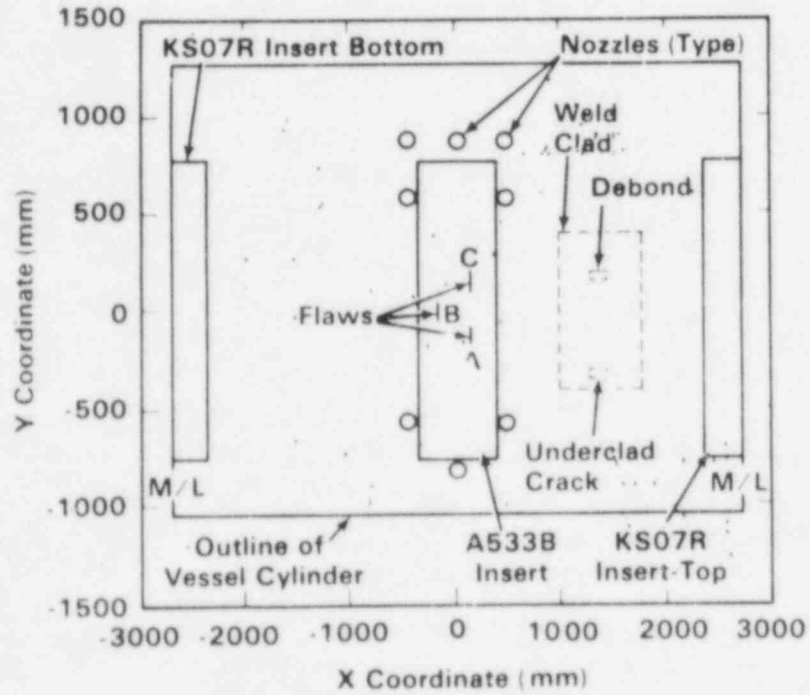

Figure 4.39. AE Source Location, Array 3 - Step 13, Part 3, ZB-1 Vessel.

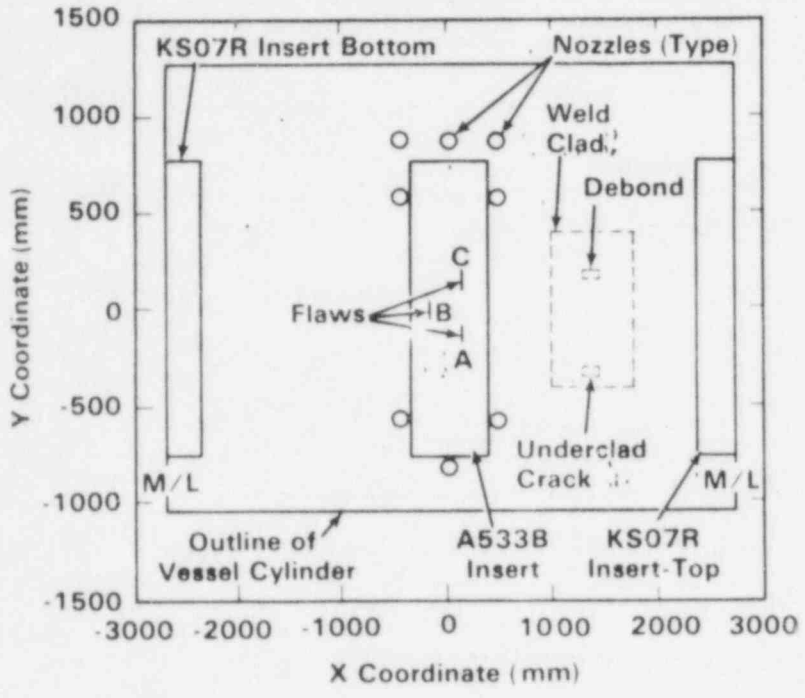

Figure 4.40. AE Source Locations, Array 3 - Step 13, Part 4, ZB-1 Vessel.

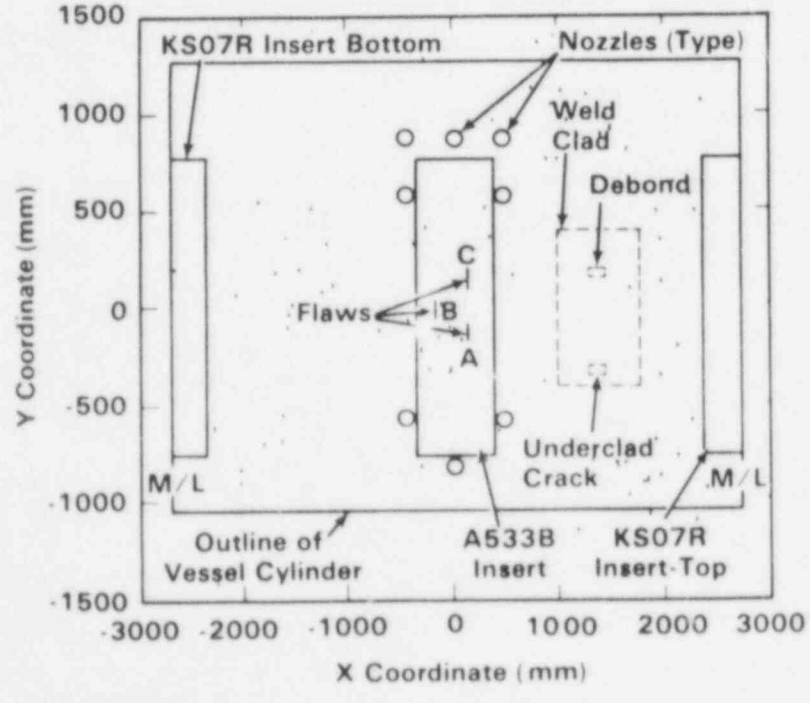

Figure 4.41. AE Source Location, Array 3 - Step 13, Part 5, ZB-1 Vessel.

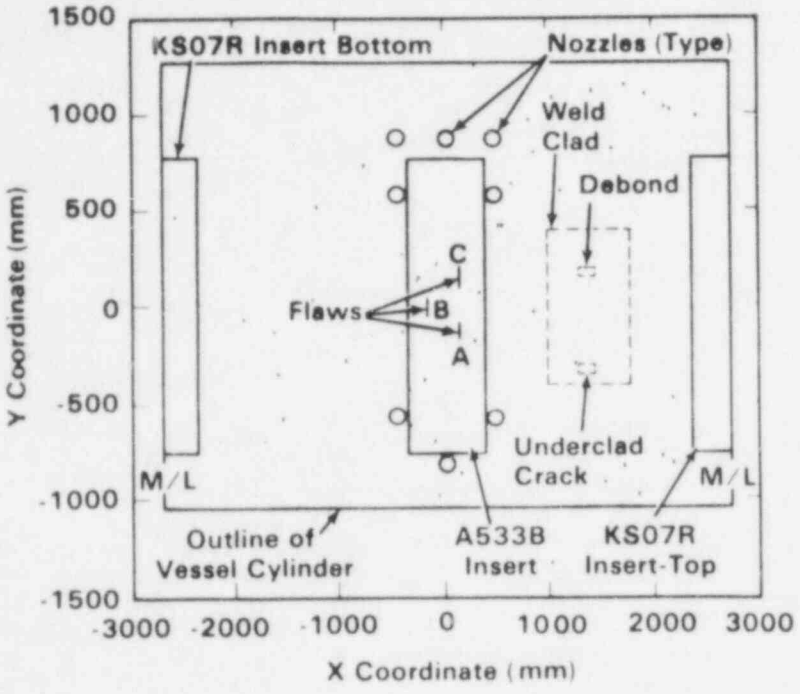

Figure 4.42. AE Source Location, Array 3 - Step 13, Part 6, ZB-1 Vessel.

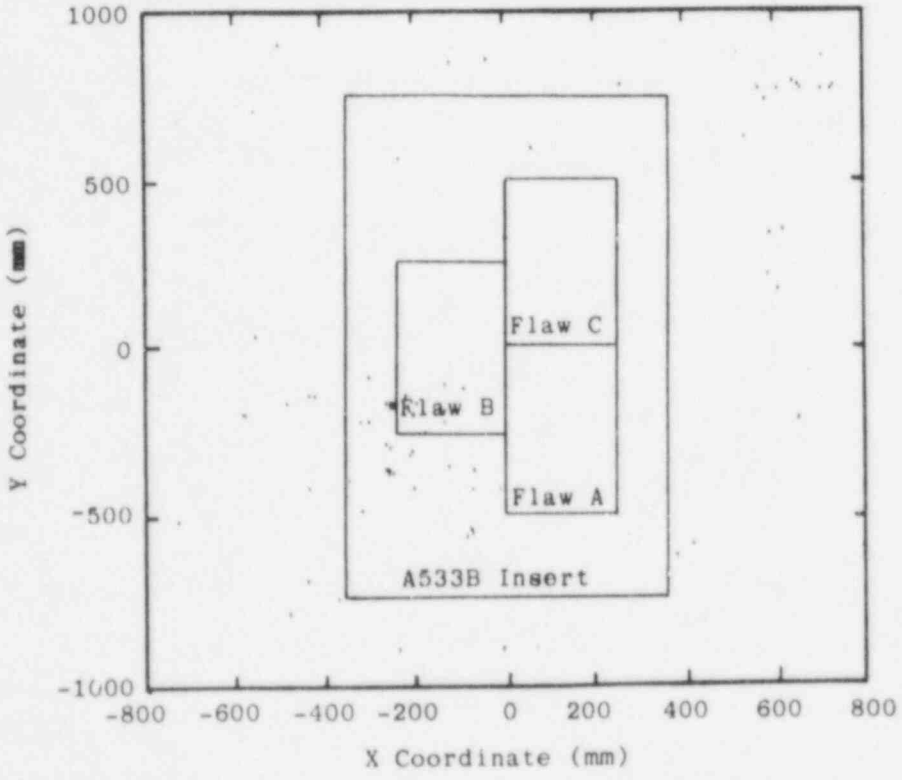

Figure 4.43. AE Source Location Near the A533B Insert, Hydro Array - Step 13, Filtered to Events Detected Above 250 Bar with Amplitudes Between 2-10 Volts.

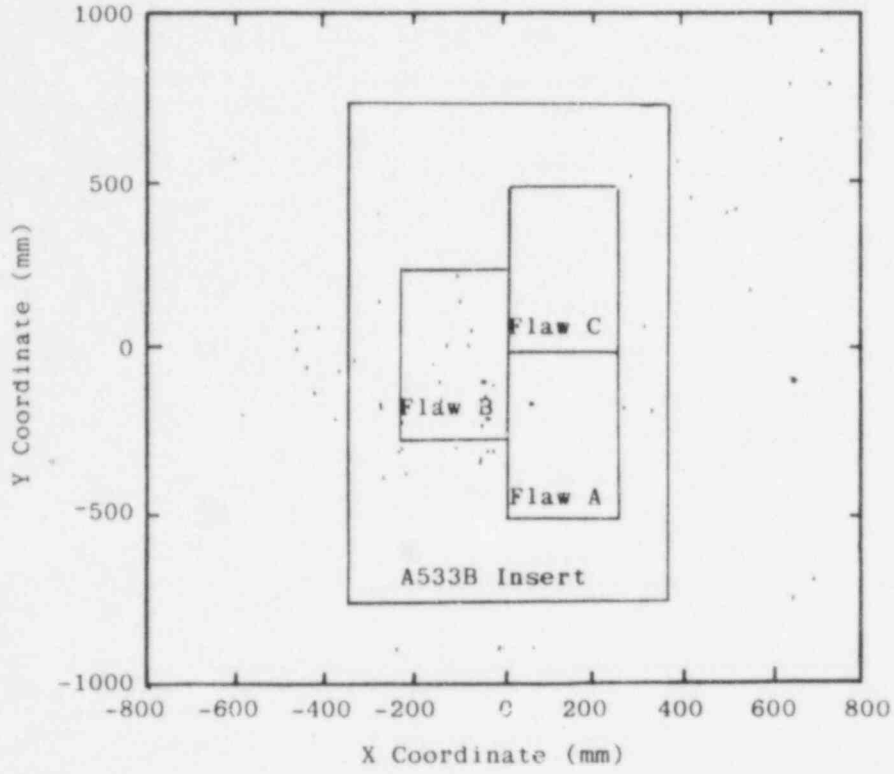

Figure 4.44. AE Source Locations Near the A533B Insert, Array 3 - Step 13, Filtered to Events Detected Above 250 Bar with Amplitudes Between 2-10 Volts.

4.1.8 Summary

The AE results from the six hydro tests performed in the course of the ZB-1 test lead to the following conclusions:

- AE appeared to be sensitive to the KS07R weld crack in the second part of Step 1. The flaw was estimated to have been about 5 mm deep at that time, yet the AE from the 1.0 x operating pressure hydro showed indications of the crack. Also in the first part of Step 1, the KS07 degraded material produced an abundance of AE even before reaching the 1.0 x operating pressure level. The machined defects did not produce AE in Part 2 of Step 1 because they were previously stressed in Part 1 of Step 1 (some flaw indications noted at that time).

- The hydro results raise a serious question about the effectiveness of AE monitoring during inservice hydrostatic testing to 1.15 x operating pressure. Steps 4, 7 and 10 produced no notable indications from the

known flaws. In Step 13, AE was identified with Flaw B at about 1.0 x operating pressure; however, it was 83% through-wall at this point. The stress intensity level required to activate Flaw B was about 70 ksi$\sqrt{in.}$ Flaws A and C barely exceeded this level during the Step 13 hydrotest. Since no notable AE was detected for any of the flaws below this stress intensity level, small flaws do not appear to be detectable at low overpressure levels during an inservice hydrotest.

4.2 SPECIAL TEST FEATURES

There were several special features of the test which can best be treated under a collective section of the report. These features include:

- flow noise simulation
- slag inclusion
- weld cladding
- nozzle cracks
- blind test.

4.2.1 Flow Noise Simulator

As discussed under Section 2.5, an electronically driven transducer was installed on the inside of the vessel to evaluate the effect of reactor coolant flow noise on detection of AE from crack growth. The noise simulator was operated for 1000 cycles during Step 6 testing. The low frequency hydro array sensor channels were completely saturated by the noise simulator input. The tuned 400 kHz waveguide sensors were, however, only moderately affected. Figure 4.45 gives AE versus load cycles for the total Step 6. When the flow noise simulator was operated, it was necessary to raise the detection threshold from 1.5 volts to 2.0 volts to avoid triggering on the noise. This adjustment did not have any evident affect on the slope of the AE versus cycles. The observed effect of the noise simulator on the low frequency and high frequency sensor response is consistent with expectations based on studies of reactor flow noise.

Further tests with the flow noise simulator were planned for the high temperature testing; however, before an appropriate point in the test sequence was reached, the simulator failed. Since actual on-reactor evaluation of the flow noise had been achieved at Watts Bar Unit 1 at this point[4] which showed the noise problem was manageable, the decision was made to not replace the noise simulator. Viewed from the vantage of on-reactor experience, the noise simulator was successful and was representative of real conditions.

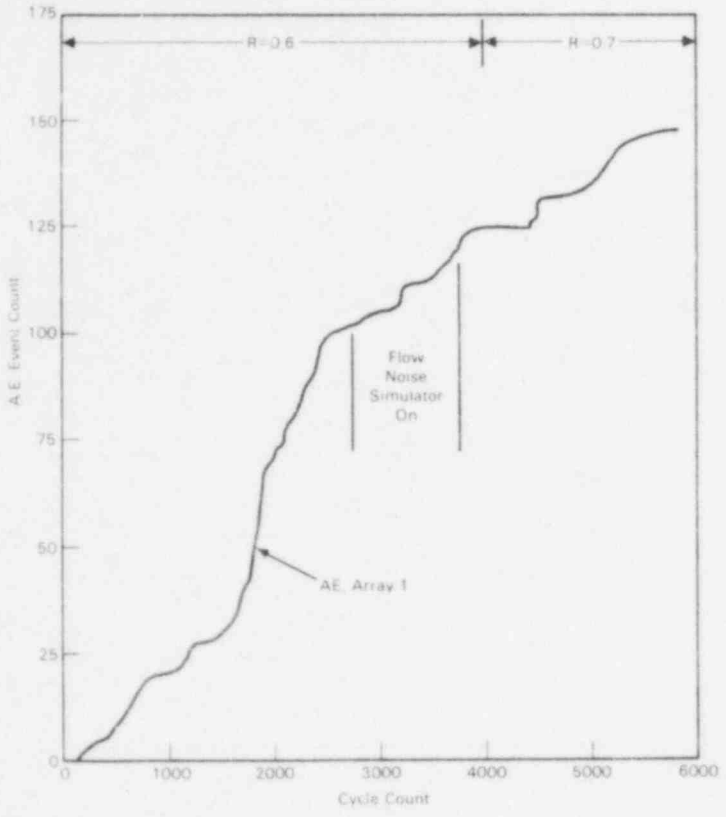

Figure 4.45. AE Versus Load Cycles, Array 2, Step 6, with Flow Noise Simulator and "R" Change.

4.2.2 Slag Inclusion

A slag inclusion was intentionally placed in the installation weld of the A533B steel insert (Section 2.1). The purpose was to provide data on noise that could be generated during cyclic loading from a slag inclusion that might confuse AE detection of crack growth. Although the slag inclusion was intended to be large (100 x 10-15 mm), post test destructive examination confirmed that the actual inclusion was 110 mm by about 3 mm. Figure 4.46 shows the profile of the slag inclusion as estimated from destructive examination. The area containing the slag was sectioned at three locations (A, B, and C) with similar results. Section C-C was examined in greater detail to provide representative information. Figure 4.47 gives the cross-section of the slag and the weld structure surrounding it. There is evidence of the slag being cracked but no indication of cracking in the surrounding weld metal (Figure 4.48).

Only very limited acoustic data was detected from the area of the slag inclusion and this occurred during Step 5. This

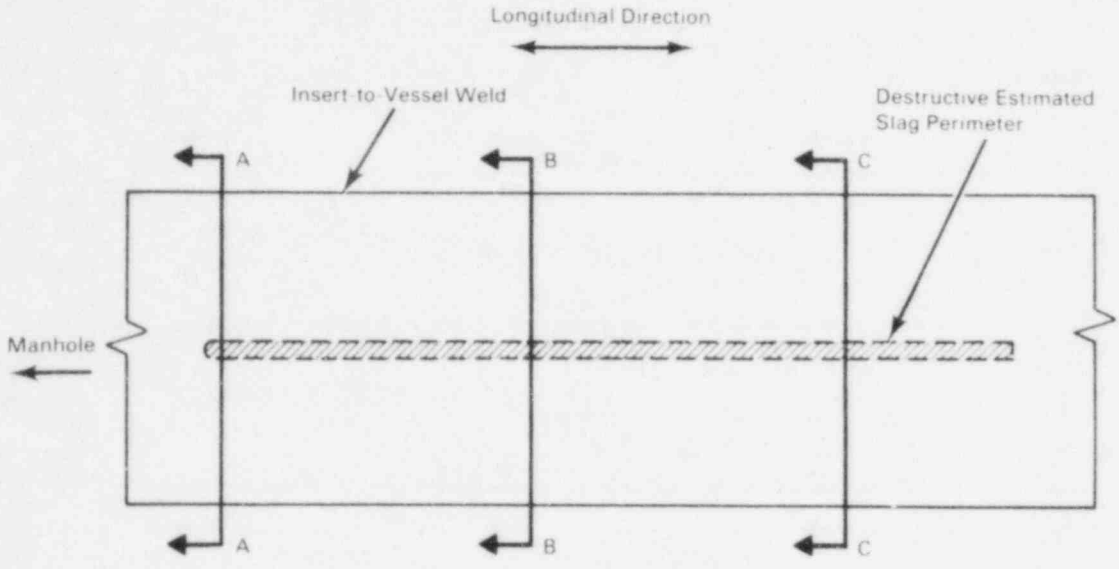

Figure 4.46. Slag Inclusion Perimeter (110 x 3 x 2 mm) Showing Location of Sections.

suggests that slag inclusions of the size involved in the test would have a very low probability of creating a problem with AE monitoring.

4.2.3 Weld Cladding

An area of stainless steel weld cladding was installed on the inside, top center of the vessel midway between the A533B and the KS07 inserts (see Figure 2.2). The purpose of the cladding was to establish areas of underclad cracking and poor weld-to-base metal bond to determine if they produced misleading acoustic information and if cracks did grow, were they detected by AE.

The clad area is described in detail in Figure 4.49. No notable AE was detected from the clad area. In fact, during the high temperature portion of the test when testing was resumed after the vessel was open to air, the clad area served a unique purpose. There were large quantities of scattered acoustic data which were felt to be the result of cracking the oxide formed when the vessel was open. The lack of AE from the clad area helped confirm that the source was associated with oxide formed on the exposed carbon steel surfaces.

A trepan sample was removed from the underclad cracking area following the test. Sectioning of this sample revealed a single, very small underclad crack (Figure 4.50). Since the stresses transverse to the defect would be very low, it is not surprising that there was no evidence of crack growth. A second

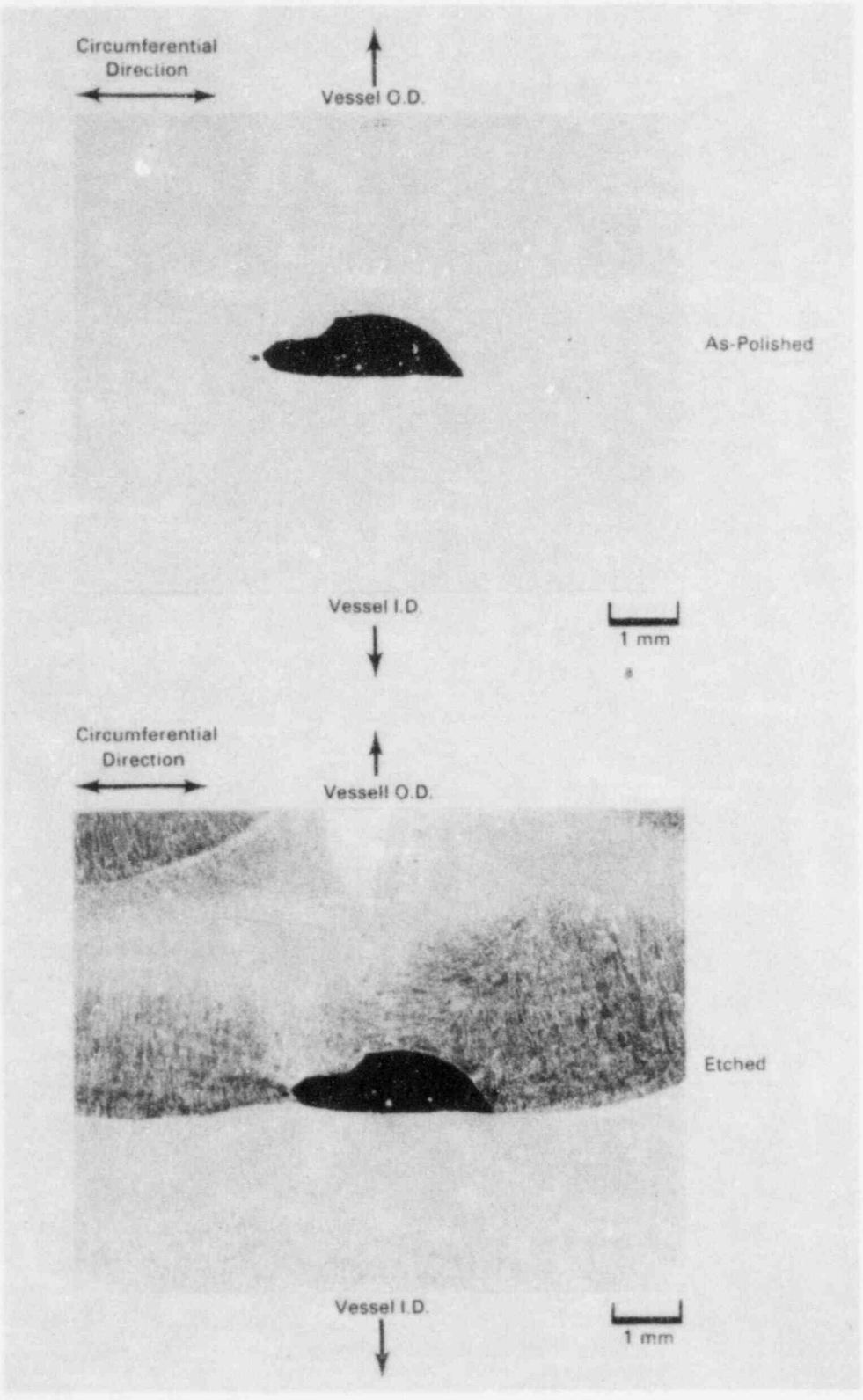

Figure 4.47. Slag Inclusion Section C-C.

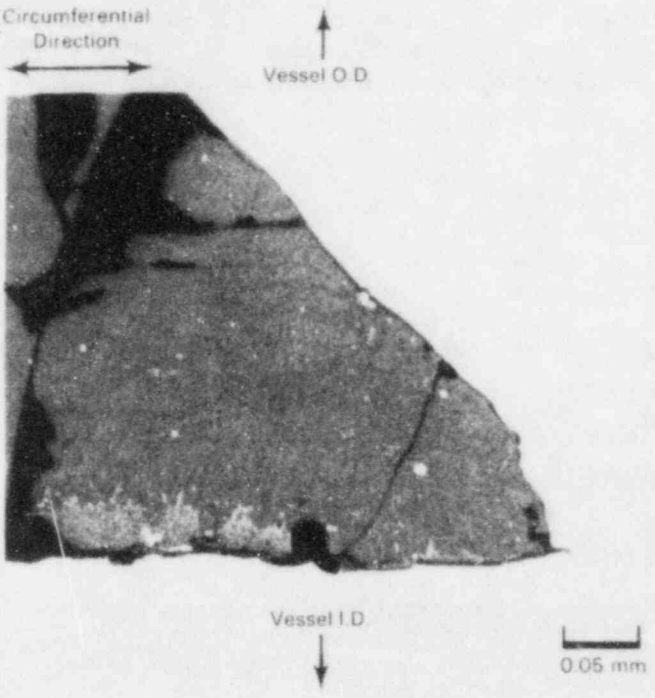

Figure 4.48. Magnified View of Right Corner of Slag, Section C-C.

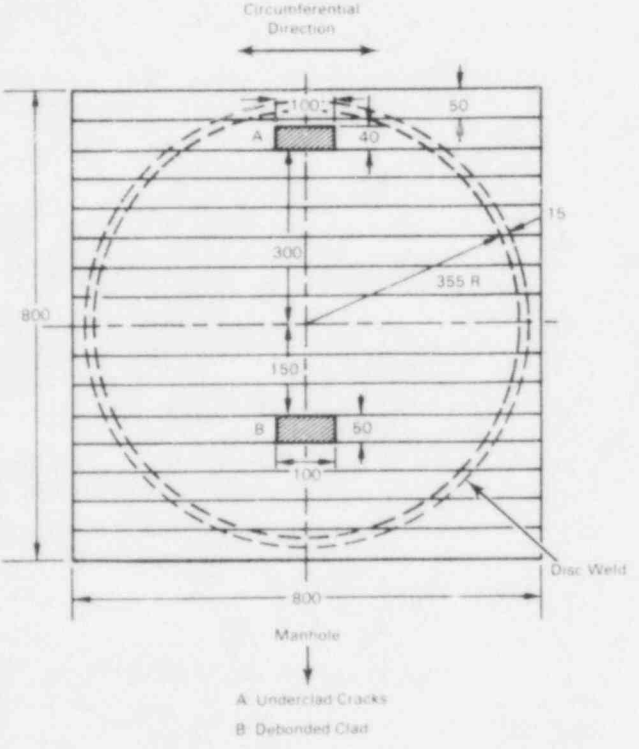

Figure 4.49. Details of Weld Cladding with Defects.

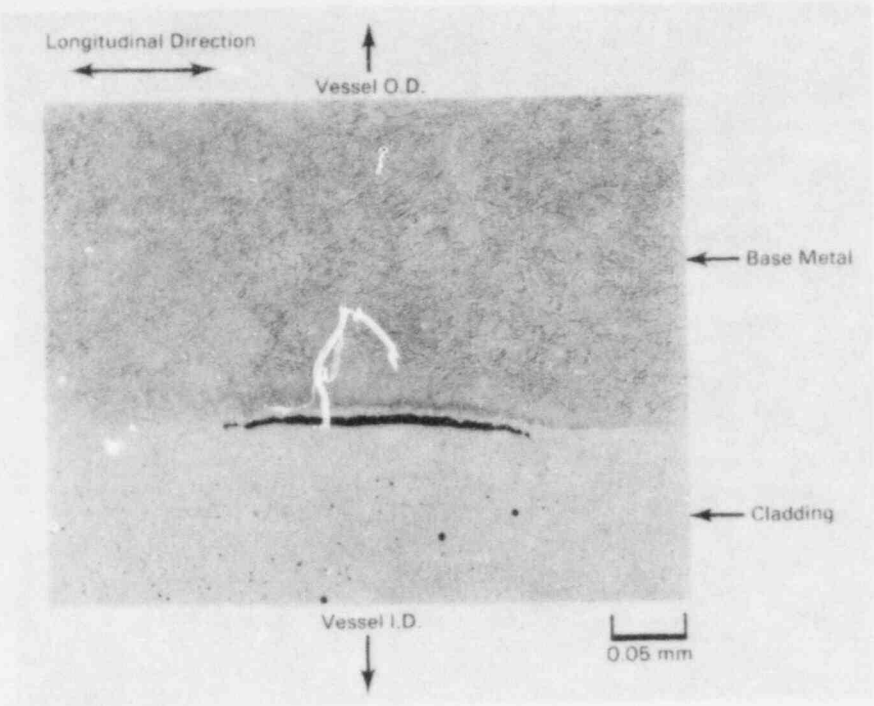

Figure 4.50. Photomicrograph of Section Perpendicular to Weld Deposition Direction, Underclad Cracking Area.

trepan was removed which was intended to sample the debonded area; however, it was removed from the wrong location.

Due to the lack of intended flaws, the weld cladding did not fulfill the objective planned.

4.2.4 Blind Test

One of the aspects of the test which was recognized early in the planning was the fact that the location of the machined flaws was known and COD information would be measured routinely. Obviously, detection and evaluation of these flaws during the test could be considered nonrepresentative of reactor monitoring conditions. To offset this, various methods of creating an unknown or blind monitoring situation such as changing the load unknown to the AE monitoring team were considered.

In reality, a far more meaningful "blind" circumstance evolved during the test. There is strong circumstantial evidence that the installation weld for the KS07 replacement insert cracked on the I.D. at the time of insert installation unknown to anyone. The crack began to grow extensively during the high temperature phase of the test. AE gave positive indications of this early in the high temperature testing. Figures 4.51, 4.52,

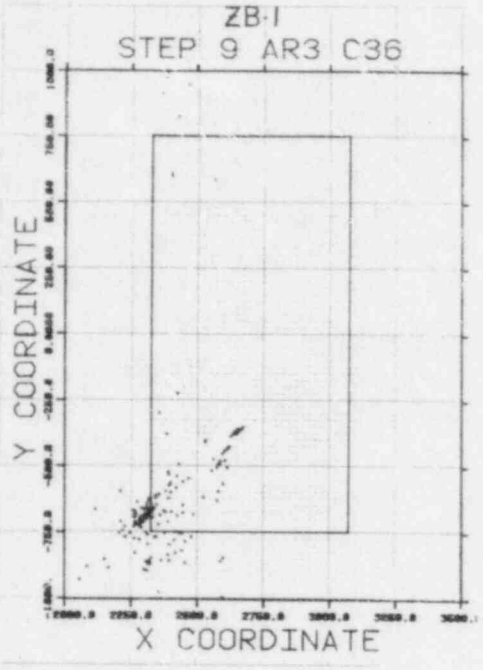

Figure 4.51. AE Indications of KS07R Weld Crack Growth, Step 9, 0-400 Load Cycles.

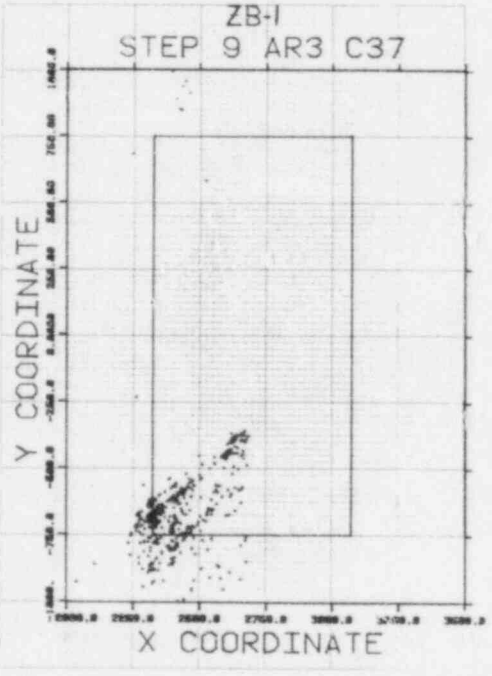

Figure 4.52. AE Indications of KS07R Weld Crack Growth, Step 9, 401-692 Load Cycles.

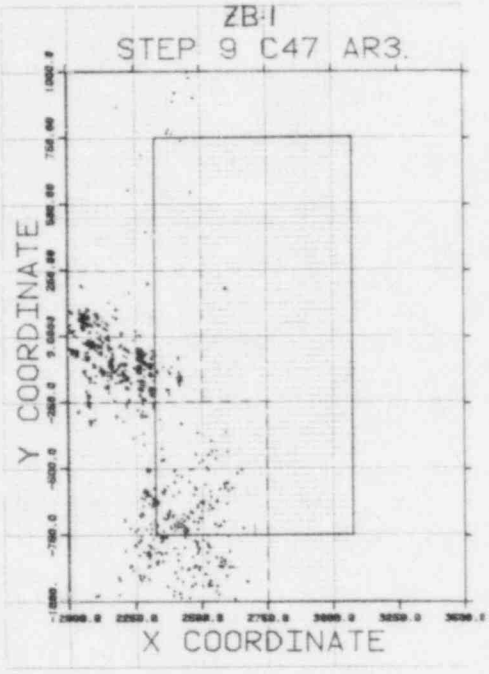

Figure 4.53. AE Indications of KS07R Weld Crack Growth, Step 9, 1526-1800 Load Cycles.

and 4.53 show the nature of the AE indications early in Step 9. Based on these indications, ultrasonic inspection of the area was called for three different times to verify a crack. It was not until the third inspection that the crack was verified. By that point, the crack was estimated to be about 20 mm deep in the region shown in Figures 4.51, 4.52, and 4.53. By the end of the test, the crack, which extended the full length of the KS07R weld, reached a depth of about 40 mm in the region described above ranging down to 10-20 mm in the bottom longitudinal weld. The original crack in the circumferential portions of the weld appeared to have grown little, if any, which is reasonable since the nominal stresses from internal pressurization would be half that on the longitudinal welds. AE from the lower longitudinal weld was identified later during the high temperature testing, but no notable AE was seen from the circumferential portions of the weld.

Initial quantitative evaluation of the crack using AE data and the AE/flaw growth relationship developed for A533B steel was not satisfactory. This appears to be a function of the extremely high amount of AE produced by the growing crack. The reason for the abundance of AE is not yet fully understood. This is discussed further in Section 4.5.

4.2.5 Nozzle Cracks

There were eight small nozzles (100 mm O.D. and 100 mm long with a 70 mm bore that penetrated the vessel wall) located in the near vicinity of the A533B insert (see Figure 2.2). All of these nozzles developed cracks starting at the inner corner running into the vessel wall. The cracks were oriented parallel to the longitudinal axis of the vessel, perpendicular to the direction of maximum stress. It is suspected that most of this cracking occurred during the high temperature phase of testing.

These cracks were not positively indicated by AE. In retrospect, there are some periods where source location showed data that may have been relatable to nozzle cracking but it was not sufficiently clear to identify in advance that cracking was in process. This obviously is a point of concern.

Examination of the geometry of the nozzles and location of the AE sensors, however, appears to offer an explanation. The AE sensors were located to detect cracking in the vessel wall with an unobstructed signal propagation path. The bore of the nozzle acts as a discontinuity in direct signal propagation to one or more of the AE sensors. The effect of this type of discontinuity has been studied by others.[10] AE may well have been detected but with the propagation path to one sensor distorted by the nozzle bore, the result would be an unlocated signal due to an abnormal propagation time to the one sensor. The raw data is on record and further analysis may permit verification of the explanation by modifying the source location algorithm to locate on information from any three of the four sensors. This is a unique circumstance because on a reactor, for example, sensors would be located on the barrel of the nozzle where it now assumes a configuration analagous to the vessel cylinder. The fact that the KS07 replacement weld cracking in the vessel wall was so readily detected by AE supports the concept that the nozzles in ZB-1, oriented as they were to the sensors, represent a unique geometric influence on AE detection.

4.2.6 Summary

The flow noise simulator was effective in testing the influence of reactor coolant flow noise on detection of AE from crack growth. The results were consistent with subsequent data obtained during hot functional testing at Watts Bar, Unit 1 nuclear reactor in indicating that the flow noise is a manageable problem.

A slag inclusion placed in the A533B insert weld partially accomplished its purpose. It indicated that a small slag inclusion (100 x 3 mm) should not interfere with AE detection.

Due to the small size, however, essentially no AE was detected which precluded assessing the similarity between AE which might be produced by a major slag inclusion and that from crack growth.

Weld cladding did not fulfill its intended purpose of evaluating AE detection of possible noise from defective cladding areas and detection of underclad crack growth due to the lack of intended flaws. Detection of underclad cracking should not be a problem, however, since the AE signals would not traverse the defective area to reach AE sensors on the vessel O.D.

Unplanned cracking in the KS07R weld provided an effective "blind" test of AE detection of crack growth which gave very positive results. Evaluation of the flaw by AE currently produces exaggerated results due to the very large amount of AE.

Cracking in the bore of blind nozzles on the vessel was not clearly indicated by AE. This, however, appears to be due to a unique geometry effect wherein the discontinuity of the nozzle bore interfered with propagation of signals to some of the AE sensors installed to monitor the vessel cylinder.

4.3 AE MONITORING DATA AT 65°C (150°F)

The first part of the ZB-1 vessel cyclic loading test was performed at 65°C (150°F). As illustrated in Figure 3.2, this consisted of four elements - test steps 2, 3, 5, and 6. The cyclic loading steps were alternately low and high R-ratio to produce crack front marking between steps as a result of the different crack growth rates. This is discussed further under Section 4.5.1. The maximum pressure for all low temperature cyclic loading was 240 bar (3530 psig). Growth of the machined flaws during the 65°C test is given in Section 4.5.1.

4.3.1 Step 2, R=0.1 Loading Condition

During the early part of the test, Array 2 was the most sensitive to growth of the machined flaws. The data provided in Figures 4.54 and 4.55 are total, unfiltered data detected during Step 2. Figure 4.54 shows most of the AE sources confined to the A533B insert but scattered. In Figure 4.55, the data is distributed over the entire test step but note the increased slope starting at about 1400 load cycles. Figure 4.56 begins to bring out a feature that was characteristic of the Array 2 AE data from flaw growth during the low temperature testing. There is a prominent amount of high amplitude data ($\geq$10 volts). In Figures 4.57 and 4.58, the data has been filtered to peak load and 8 to 10 volts amplitude. The remaining AE sources are now clustered primarily around Flaw B. The AE versus load cycles

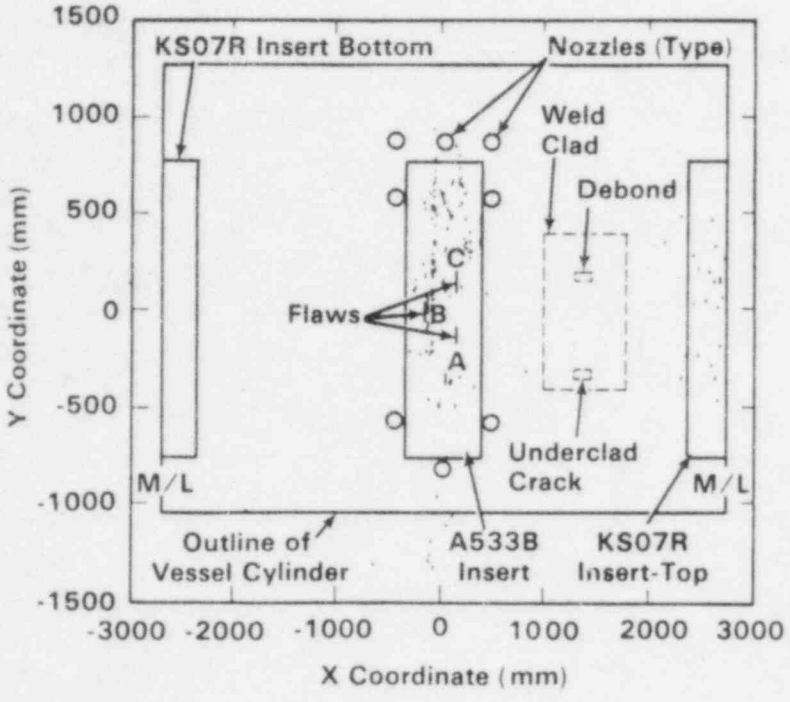

Figure 4.54. AE Source Locations - Step 2, Array 2, Unfiltered.

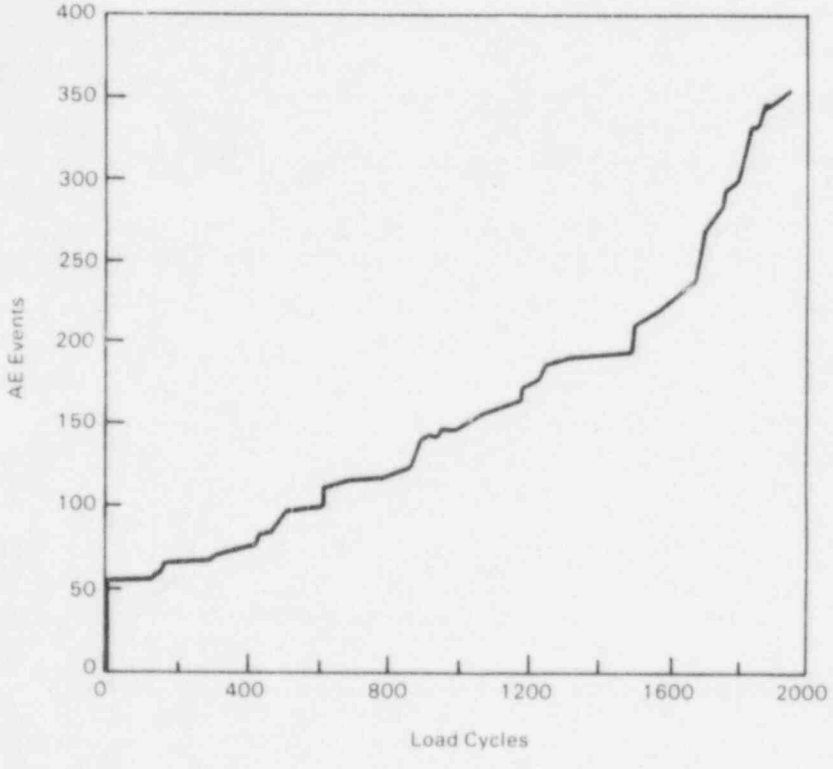

Figure 4.55. AE Versus Load Cycles - Step 2, Array 2, Unfiltered.

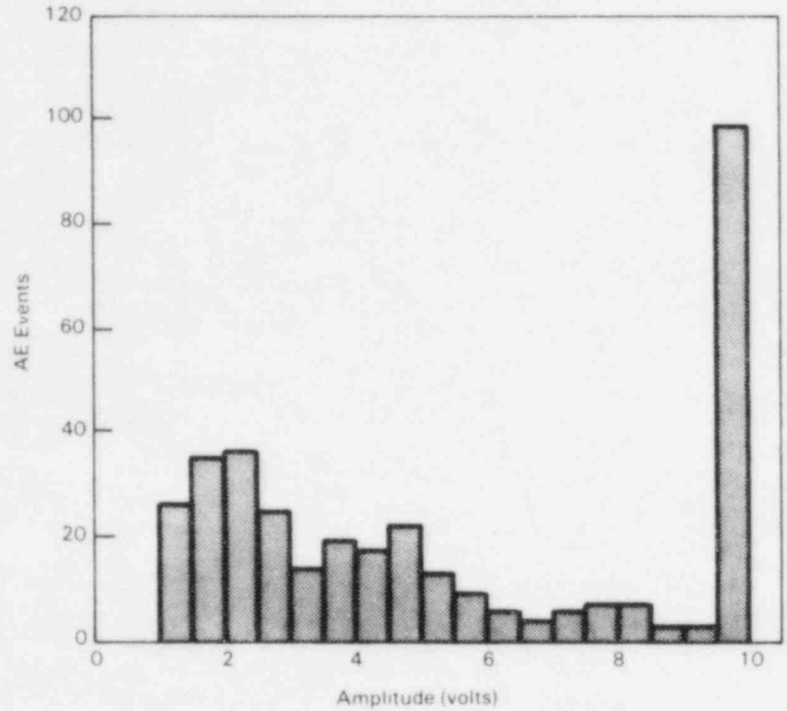

Figure 5.56. AE Amplitude Distribution - Step 2, Array 2, Unfiltered.

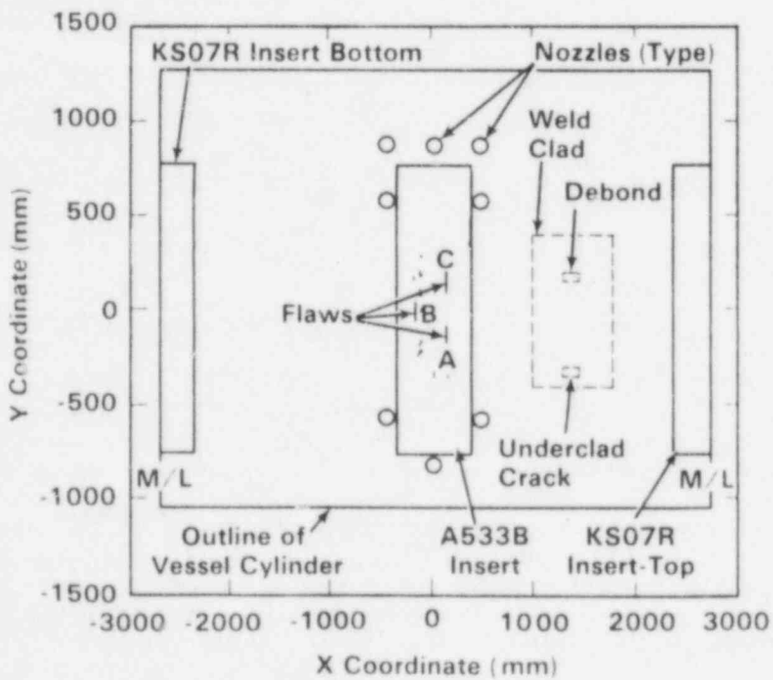

Figure 5.57. AE Source Location - Step 2, Array 2, Filtered to Peak Load and 8-10 Volts Amplitude.

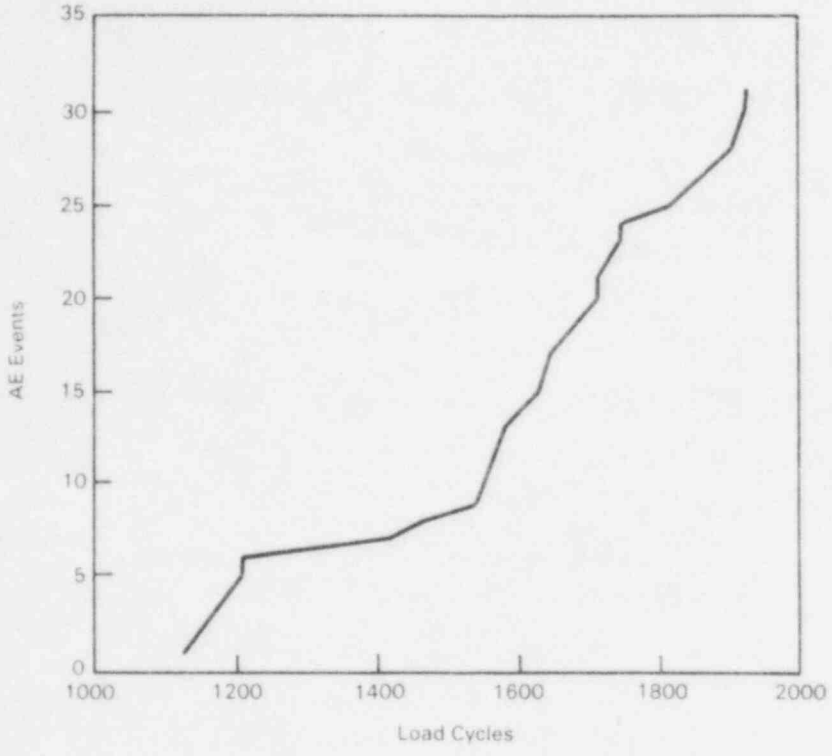

Figure 5.58. AE Versus Load Cycles - Step 2, Array 2, Filtered to Peak Load and 8-10 Volts Amplitude.

also shows a more rational relation with the AE starting at about 1200 load cycles.

The sensitivity of Array 3 (cylindrical) was poor at this stage of the test and as a result, it was not locating AE sources properly. The pattern of the detected AE filtered to peak load (Figure 4.59) is very similar to the filtered data from Array 2, but the source location is quite poor (Figure 4.60). This is not surprising with low sensitivity.

4.3.2 Step 3, R=0.6 Loading Condition

Step 3 produced relatively limited crack growth being a high R-ratio step. A problem with noise from the manhole gasket evolved in Step 3 which is evident in Figure 4.61. This also illustrates a problem with the quad array. It tends to show the location of sources outside the array as being on a line between the source and the quad array, particularly when the data rate is relatively high. Much of the source information streaming in from the top of Figure 4.61 is produced by signals from the manhole area. The AE versus load cycle curve in Figure 4.62 also suggests the intrusion of an outside noise source by the non-linearity of the curve. In the signal amplitude distribution (Figure 4.63), there is a large population of signals in the

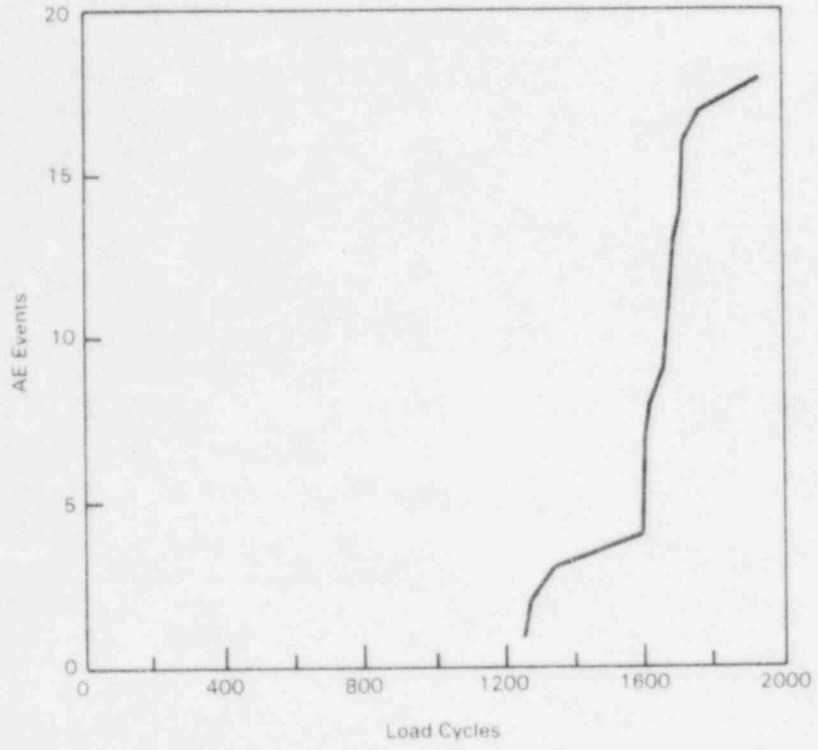

Figure 4.59. AE Versus Load Cycles - Step 2, Array 3, Filtered to Peak Load.

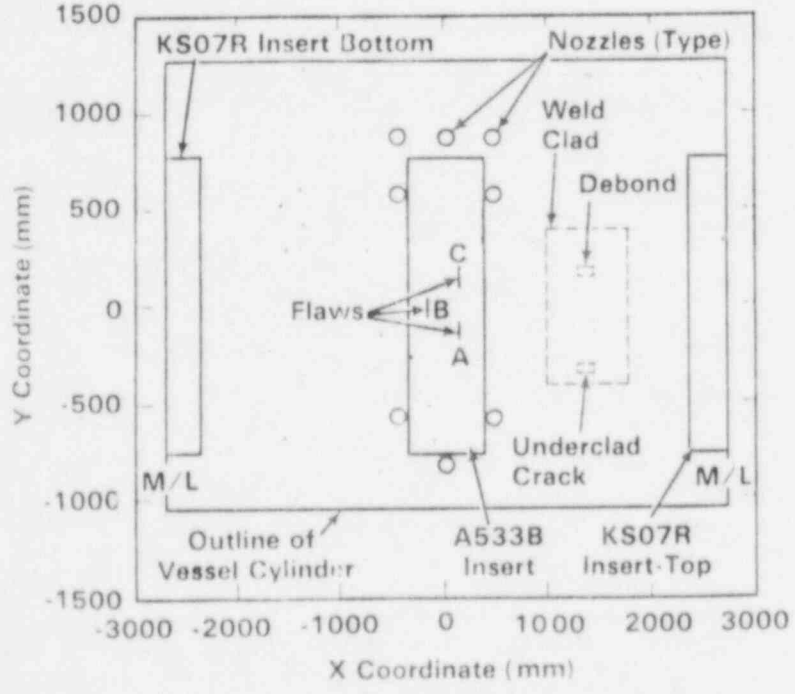

Figure 4.60. AE Source Locations - Step 2, Array 3, Filtered to Peak Load.

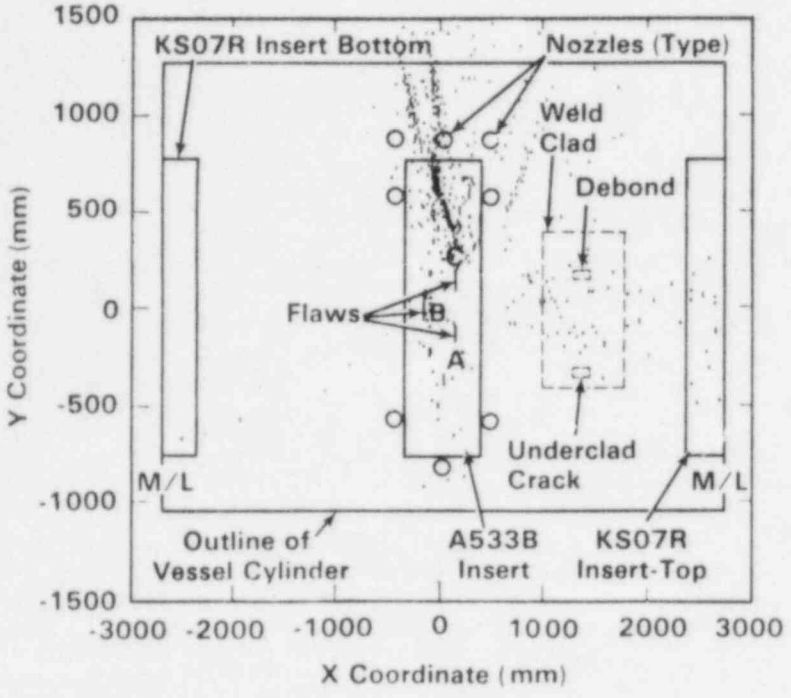

Figure 4.61. AE Source Locations - Step 3, Array 2, Unfiltered.

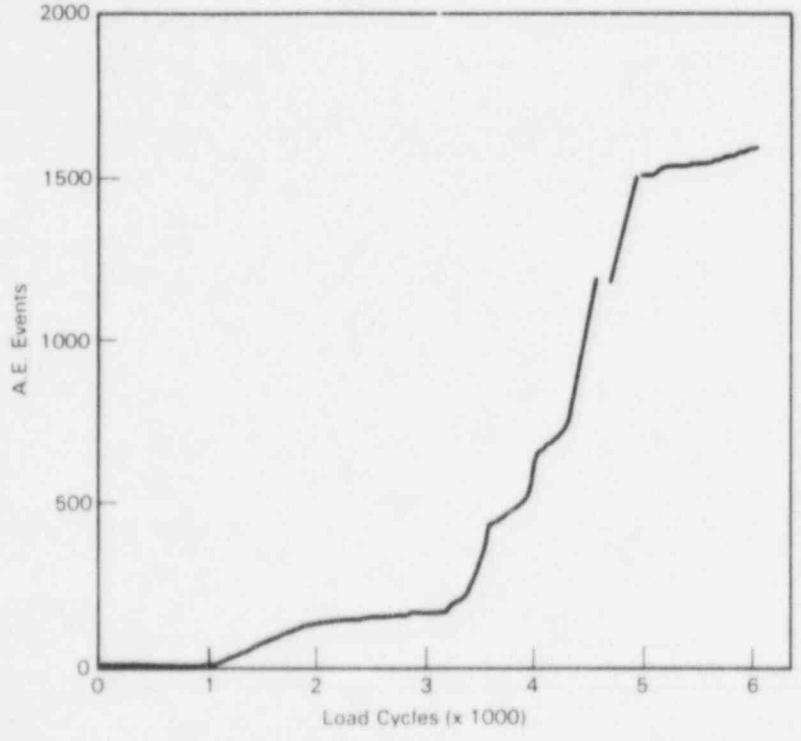

Figure 4.62. AE Versus Load Cycles - Step 3, Array 2, Unfiltered.

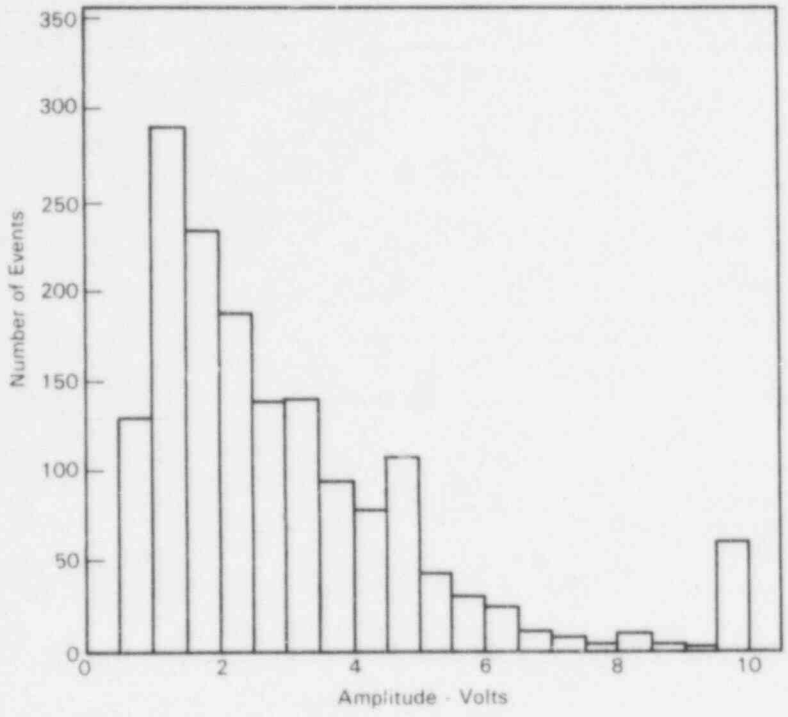

Figure 4.63. AE Amplitude Distribution - Step 3, Array 2, Unfiltered.

under 6 volt region with a single prominent indication in the $\geq$10 volt area. The earlier indications from Array 2 suggested that the crack growth signals were in the high amplitude range. If the total data is filtered by peak load and 8-10 volts amplitude, all of the extraneous data is eliminated leaving only the indications from the region of the machined defects (Figure 4.64). The associated AE versus load cycles is now reasonably linear as seen in Figure 4.65.

Array 3 appears to be indicating that the manhole noise is coming from the bottom part of the manhole in Figure 4.66, but it is mislocating the information. This is probably due to the fact that a source location algorithm for location on the hemispherical end caps was not used. Data from Flaws A and B is located quite well. The AE versus load cycles curve (Figure 4.67) is again nonlinear suggesting a discontinuous noise source.

The data shown in Figure 4.66 is a good illustration of the need for a real-time pattern recognition filter to separate crack growth AE from noise signals such as the manhole gasket noise. The parametric filter used (peak load) was effective, but it does not appear to be able to fully isolate the crack growth AE from manhole noise. Also, it does not appear that a peak load parameter would be available for use as a filter in reactor monitoring.

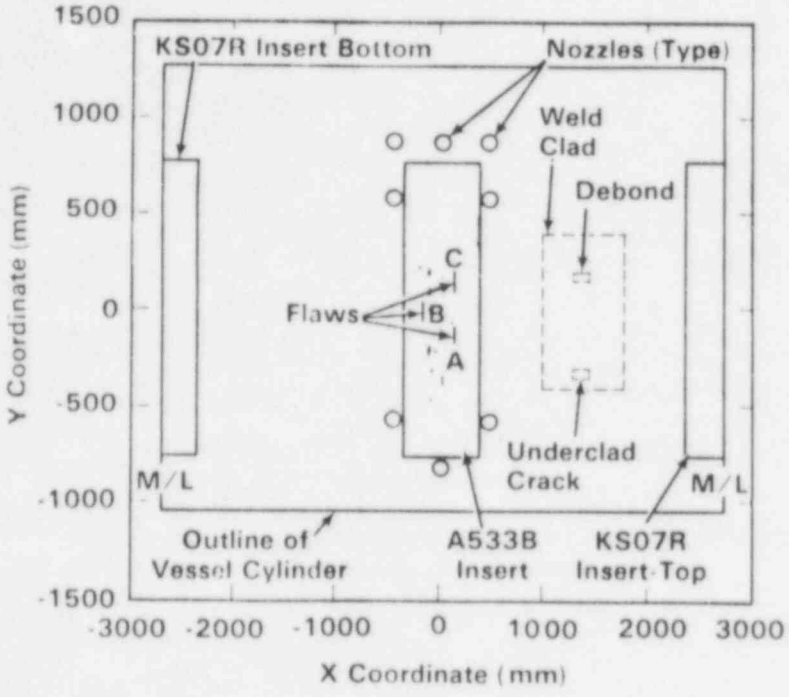

Figure 4.64. AE Source Locations - Step 3, Array 2, Filtered to Peak Load and 8-10 Volts Amplitude.

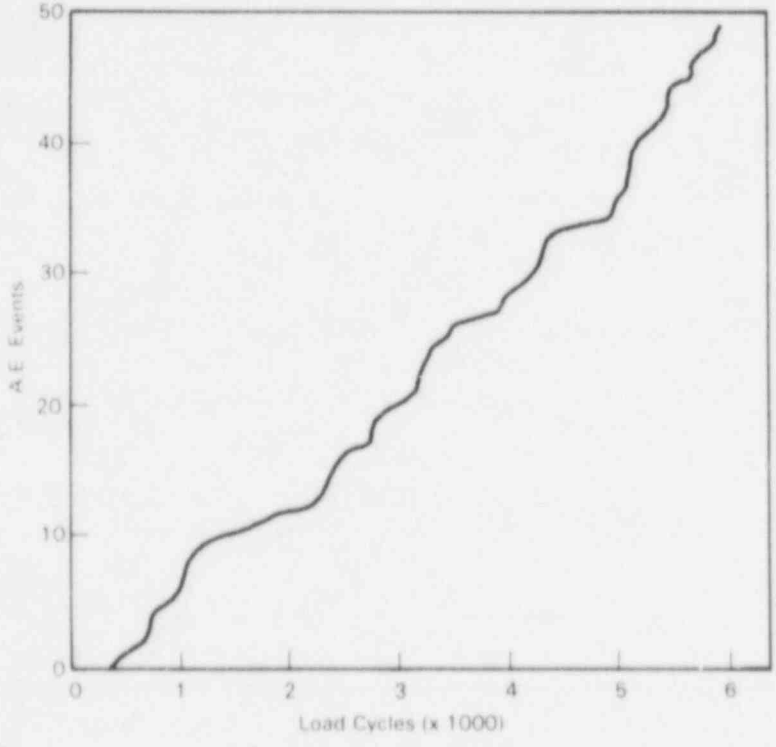

Figure 4.65. AE Versus Load Cycles - Step 3, Array 2, Filtered to Peak Load and 8-10 Volts Amplitude.

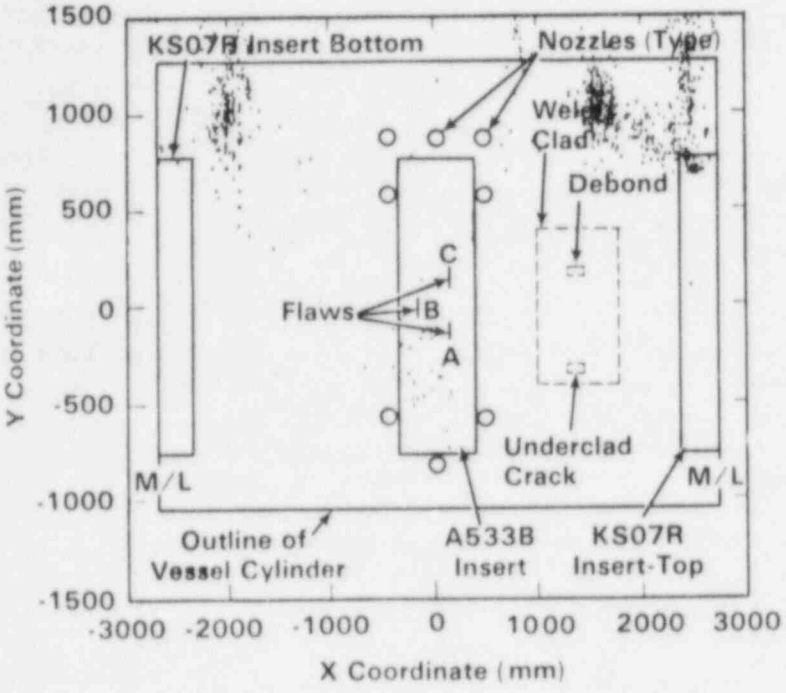

Figure 4.66. AE Source Locations - Step 3, Array 3, Filtered to Peak Load.

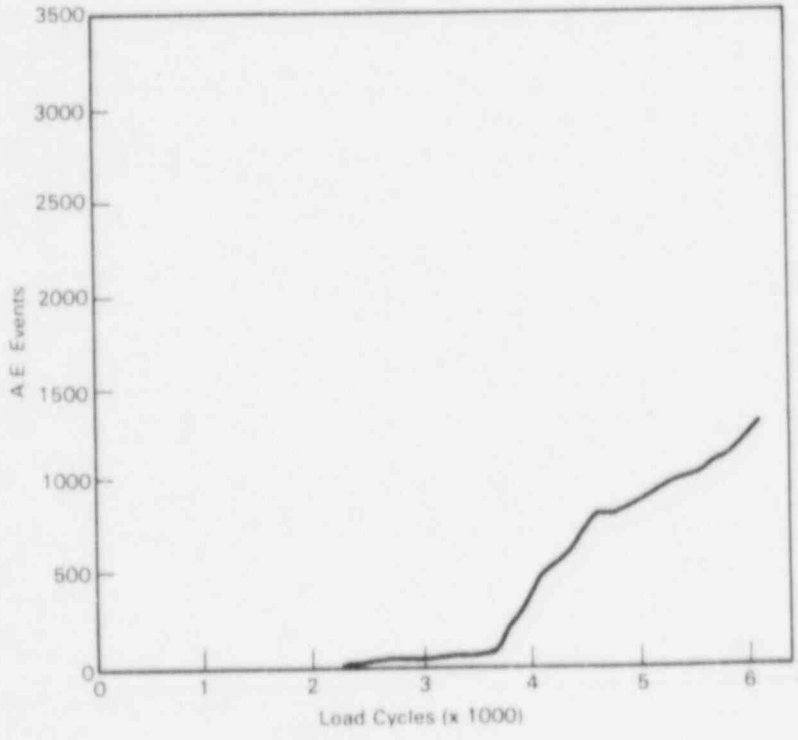

Figure 4.67. AE Versus Load Cycles - Step 3, Array 3, Filtered to Peak Load.

4.3.3 Step 5, R=0.1 Loading Condition

Step 5 was a major crack growth step and was relatively free of manhole cover noise. The unfiltered data from Array 2 in Figure 4.68 is reasonably concise, focusing largely on Flaws A and B. The AE versus load cycles for the unfiltered data (Figure 4.69) is also quite linear.

Figures 4.70 and 4.71 illustrate the characteristics of crack growth data observed with Array 2 during low temperature testing - i.e., high amplitude and concentrated around the peak load. Using these two parameters as a filter results in the data in Figures 4.72 and 4.73 which is associated exclusively with flaw growth.

Array 3 performed more effectively in Step 5 after some adjustment of the sensors. Figure 4.74 gives the profile of AE versus load cycles for the unfiltered data. There is a distinct change in slope between about 300 and 600 cycles. This appears to be due to noise from the manhole cover gasket. Figure 4.75 shows a number of signals being located in the vicinity of the manhole (top of the figure). There is also a notable cluster of AE sources showing near Flaws A and B. Figure 4.76 shows a large portion of the data occurring near peak load. If the data is

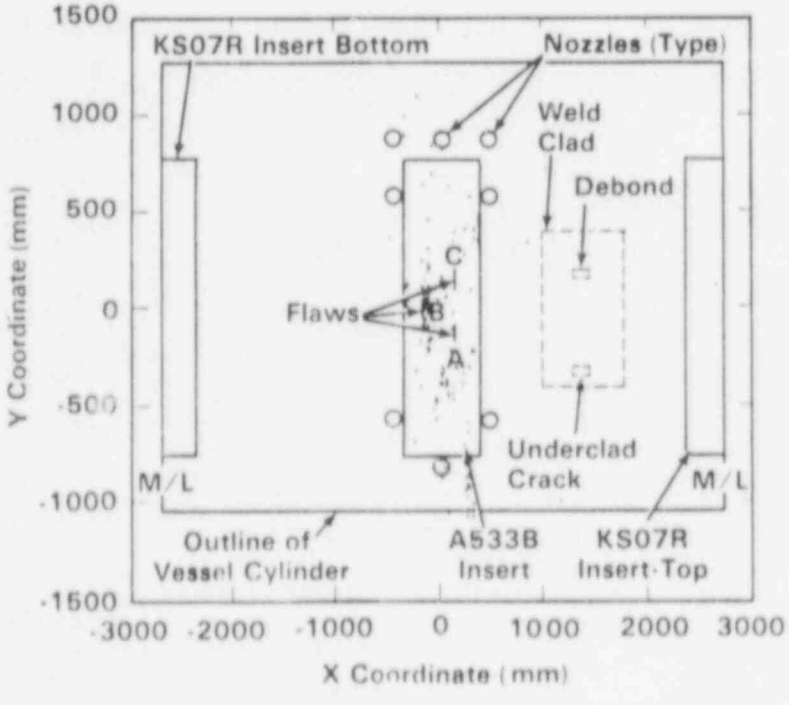

Figure 4.68. AE Source Locations - Step 5, Array 2, Unfiltered.

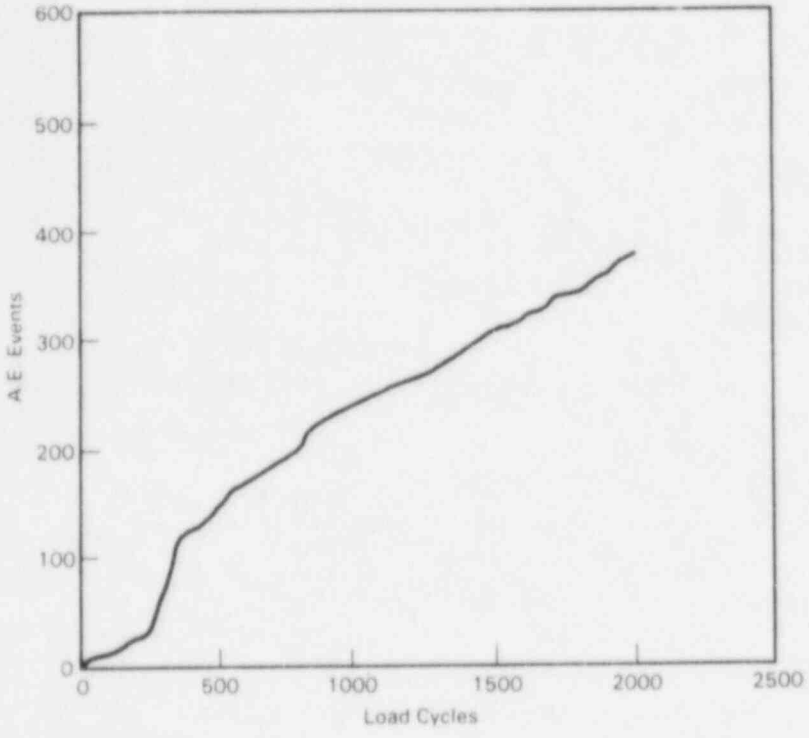

Figure 4.69. AE Versus Load Cycles - Step 5, Array 2, Unfiltered.

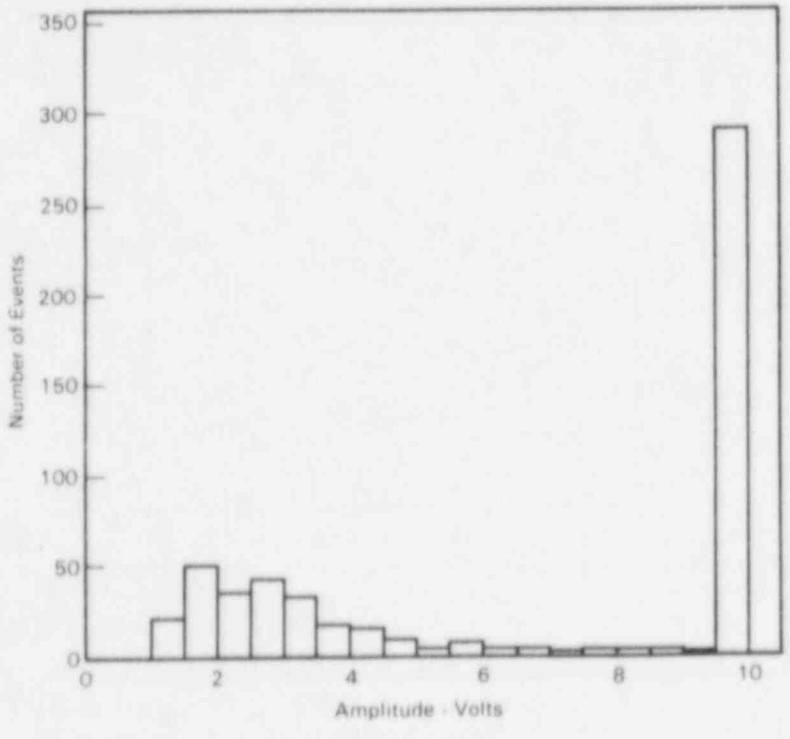

Figure 4.70. AE Amplitude Distribution - Step 5, Array 2.

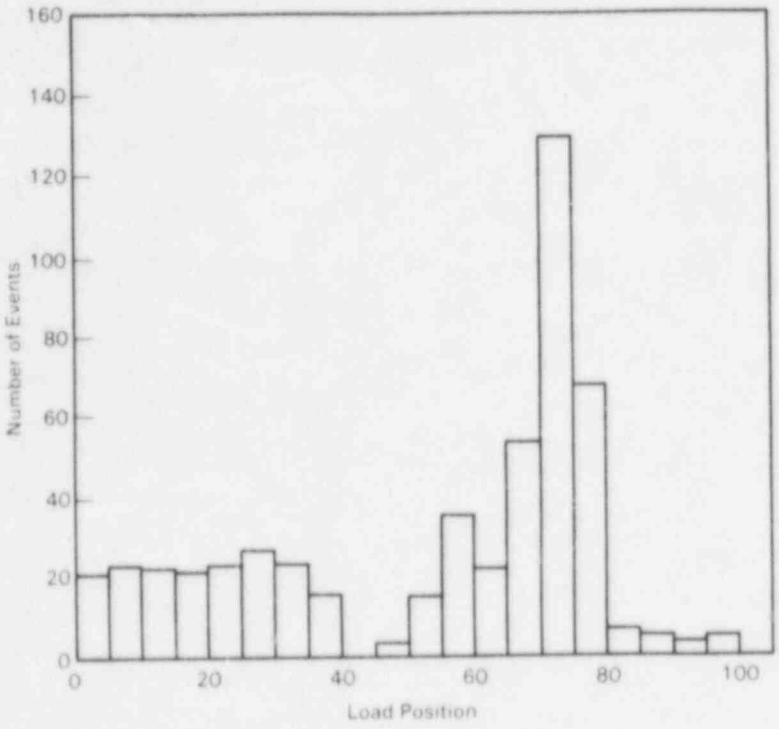

Figure 4.71. AE Relative to Position on the Load Cycle Profile - Step 5, Array 2.

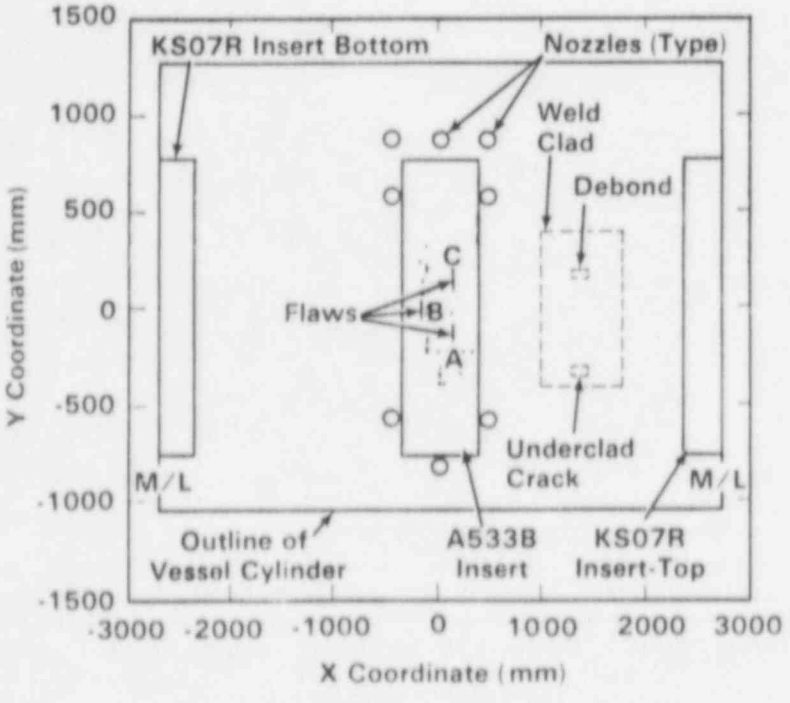

Figure 4.72. AE Source Locations - Step 5, Array 2, Filtered to Peak Load (65-80) and 8-10 Volts Amplitude.

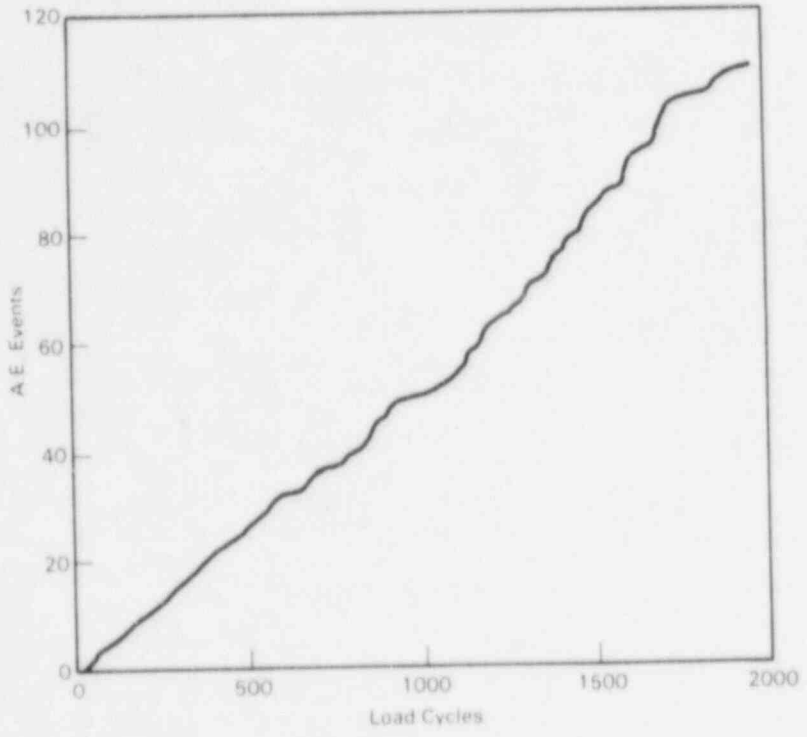

Figure 4.73. AE Versus Load Cycles - Step 5, Array 2, Filtered to Peak Load (65-80) and 8-10 Volts Amplitude.

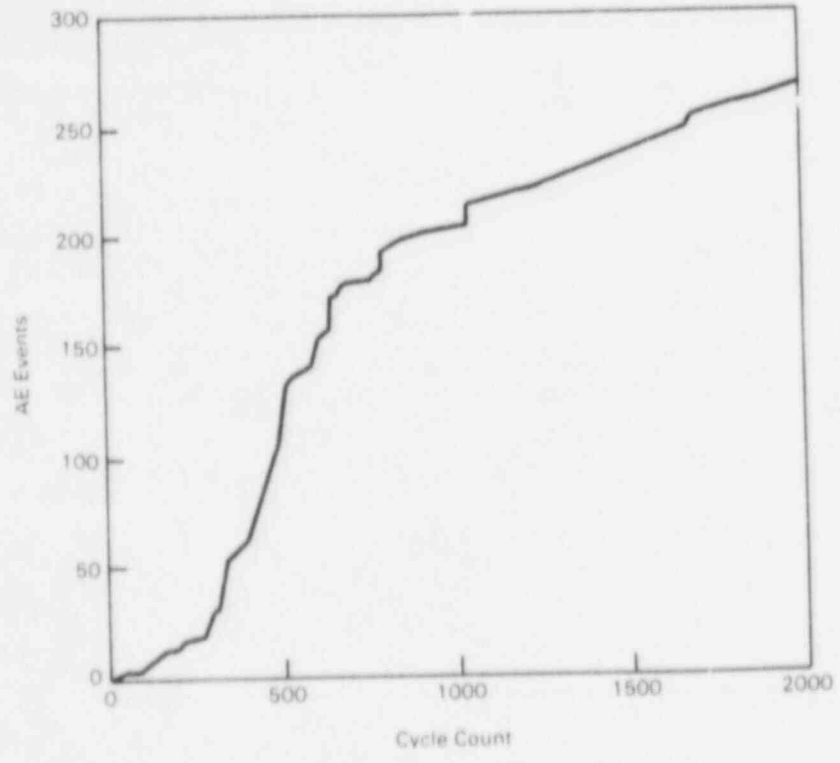

Figure 4.74. AE Versus Load Cycles - Step 5, Array 3, Unfiltered.

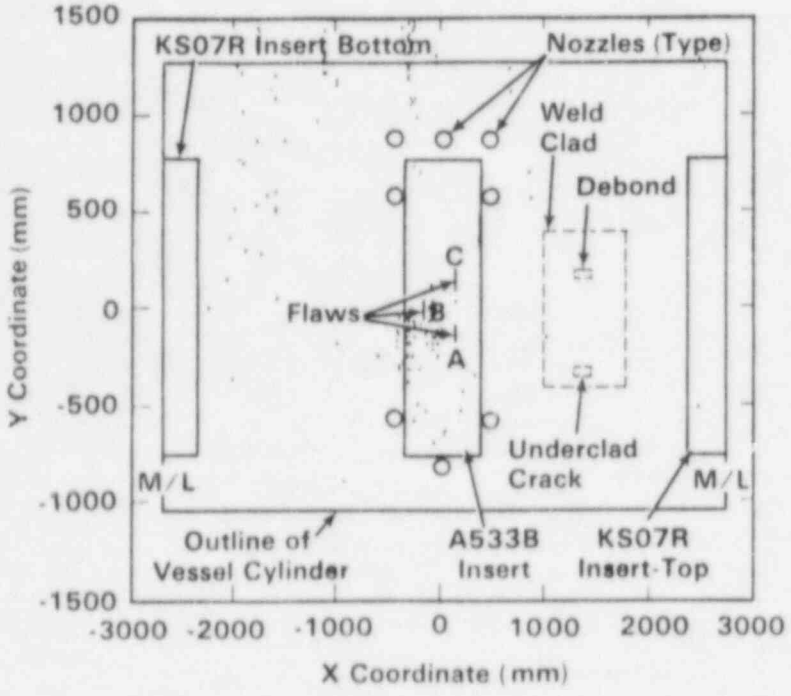

Figure 4.75. AE Source Locations - Step 5, Array 3, Unfiltered.

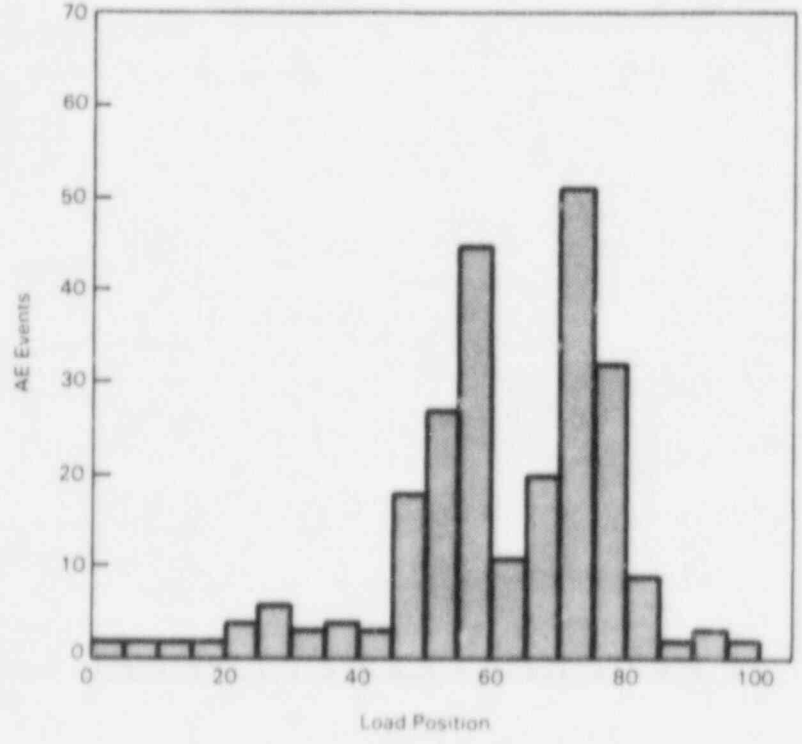

Figure 4.76. AE Distribution by Load Position.

filtered to the load position range of 65 to 80, the data in Figures 4.77 and 4.78 results. This shows a more linear distribution of AE versus cycles and most of the data from the manhole cover has been eliminated.

4.3.4 Step 6, R=0.6 and 0.7 Loading Conditions

Step 6 contained some special features. The flow noise simulator was operated between 2750 and 3710 load cycles. Starting at 3710 load cycles, the R-ratio was increased to 0.7 for the balance of the step. There was also intermittent periods of noise from the manhole cover.

Array 2 shows evidence of the manhole cover noise in Figure 4.79 which is the data points streaming in from the top of the figure. It also shows Flaws A and B activity. Figure 4.80 shows the effect of intermittent manhole cover noise with the sharp increases in event count at three locations. It also shows that the flow noise simulator had no evident effect on the detection of AE data. The slope of the AE curve reduces when the R-ratio is increased to 0.7 which is reasonable.

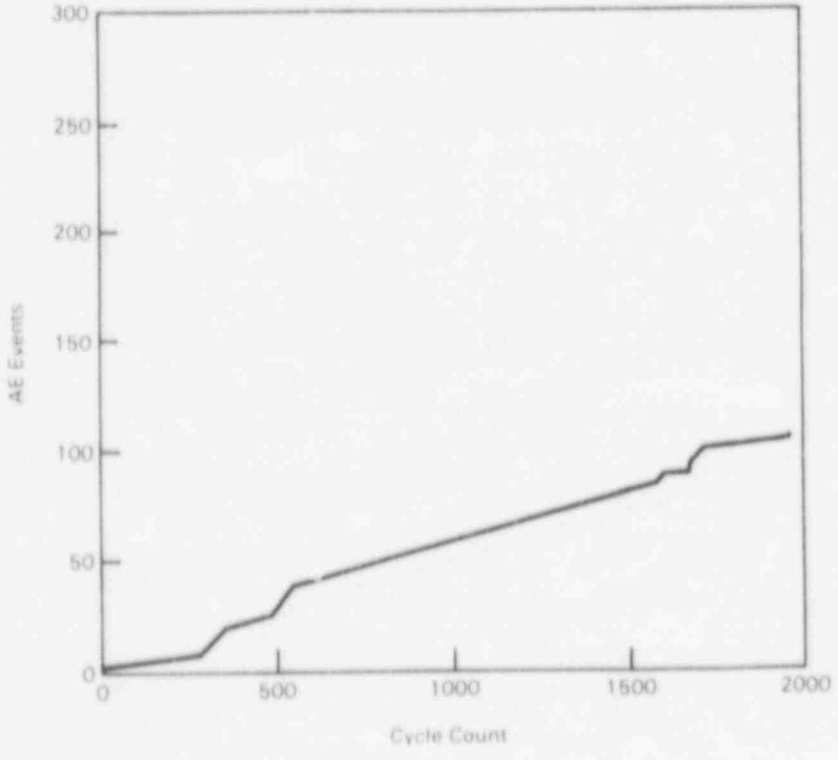

Figure 4.77. AE Versus Load Cycles - Step 5, Array 3, Filtered to 65-80 Load Position.

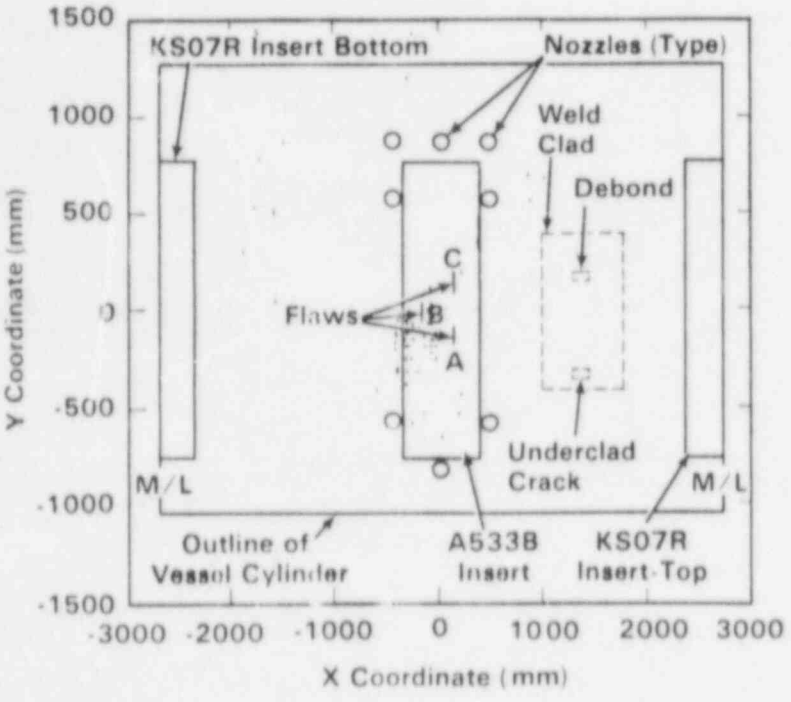

Figure 4.78. AE Source Locations - Step 5, Array 3, Filtered to 65-80 Load Position.

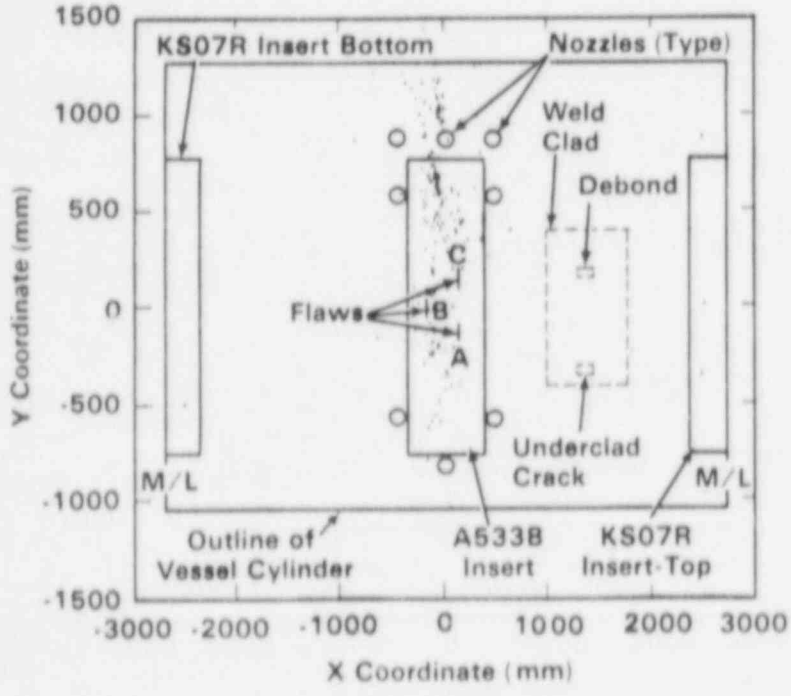

Figure 4.79. AE Source Locations - Step 6, Array 2, Unfiltered.

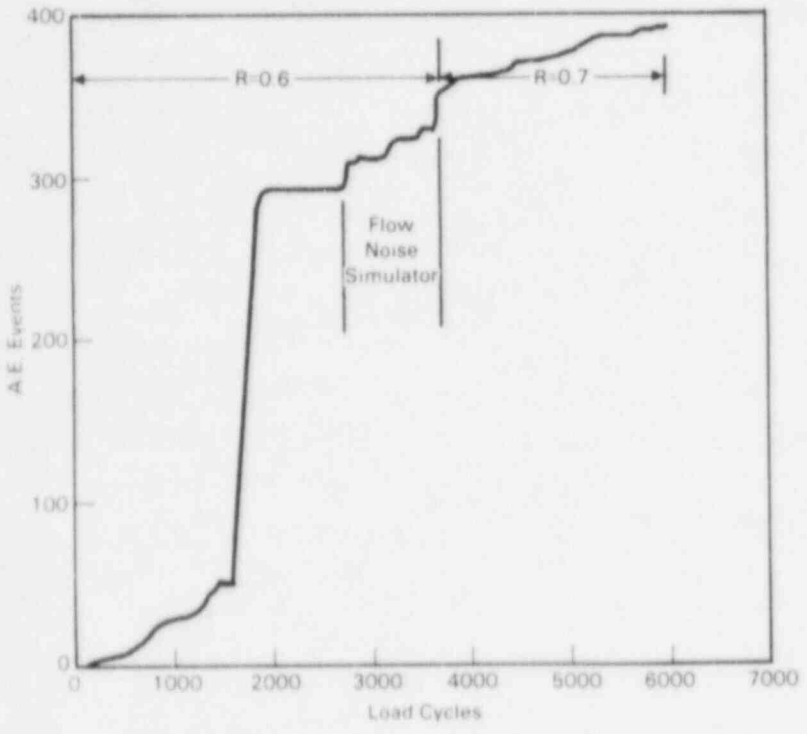

Figure 4.80. AE Versus Load Cycles - Step 6, Array 2, Unfiltered.

The distribution of gross data by load position in Figure 4.81 shows an abnormal profile for crack growth data with much data appearing slightly above the midpoint (37-1/2) of the increasing pressure ramp. This was suspected to be a result of manhole cover noise. The amplitude distribution (Figure 4.82), however, is normal compared to earlier test data. Analysis of the 8-10 volt amplitude data relative to load position (Figure 4.83) shows a typical distribution for crack growth data and the source location of the filtered data (Figure 4.84) shows that most of the high amplitude signals originate with the flaws. The AE versus load cycles curve in Figure 4.85 shows a smoother increase in AE activity.

If the data is further restricted to 8 to 10 volts and 65-80 load position, it is now refined to only AE from the flaws (Figure 4.86) with AE versus load cycles as shown in Figure 4.87. There is evidence here that the flow noise simulator did add some to the data.

Array 3 (cylindrical array) was strapped down for most of Step 6 which improved the sensitivity. The characteristics of data from Array 3 is similar to Array 2 in amplitude distribution and distribution by load position.

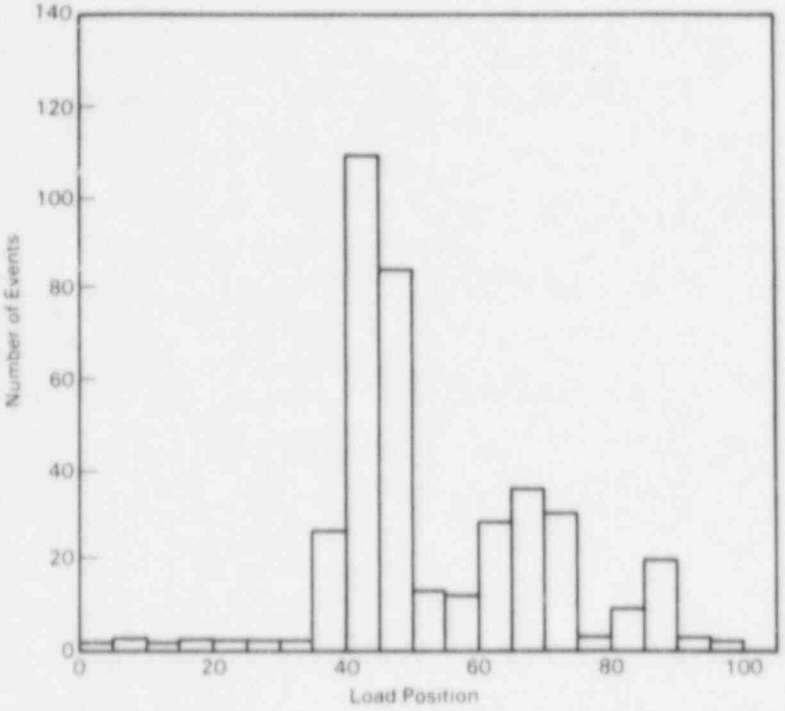

Figure 4.81. AE Distribution by Load Position - Step 6, Array 2, Unfiltered.

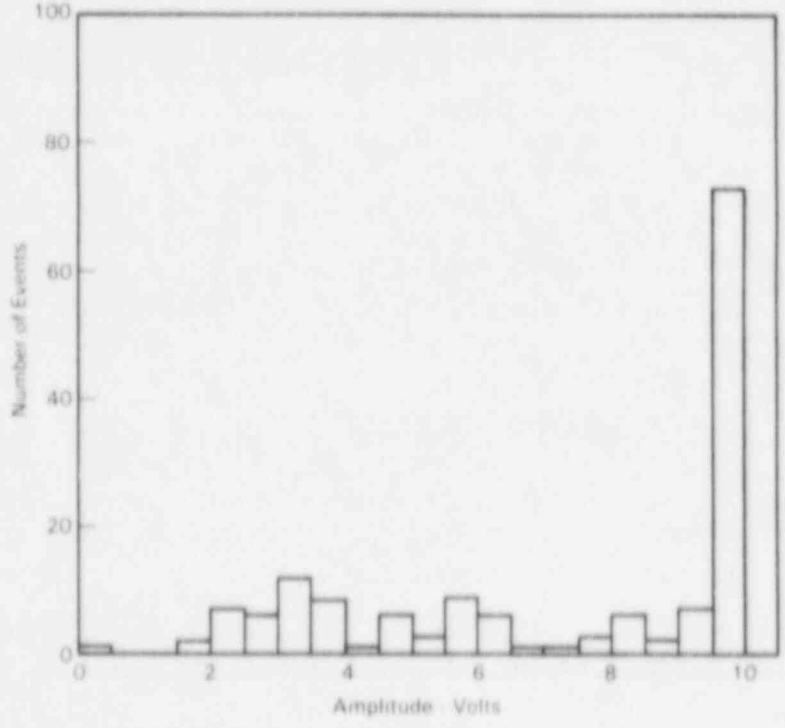

Figure 4.82. AE Amplitude Distribution - Step 6, Array 2, Unfiltered.

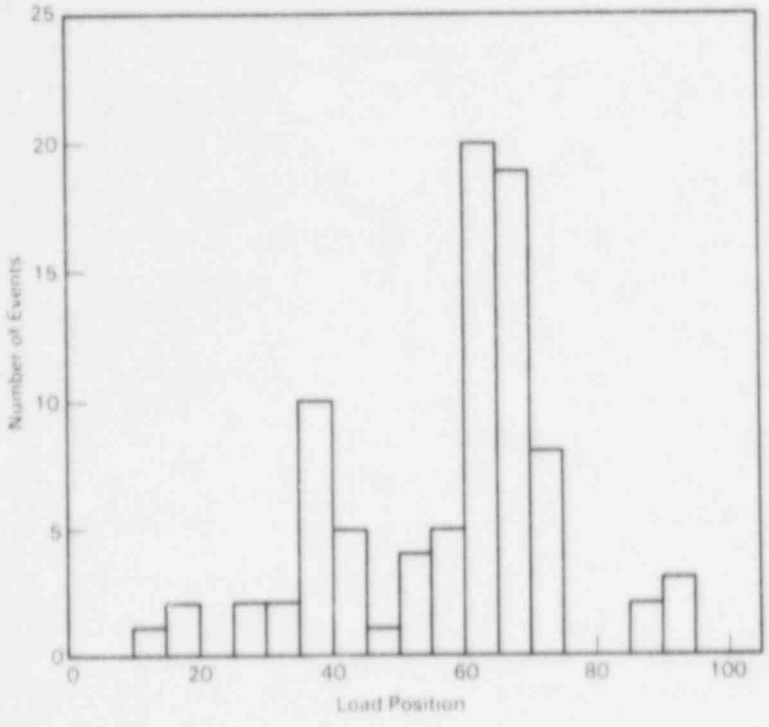

Figure 4.83. Distribution of AE in the 8-10 Volt Range by Load Position - Step 6, Array 2.

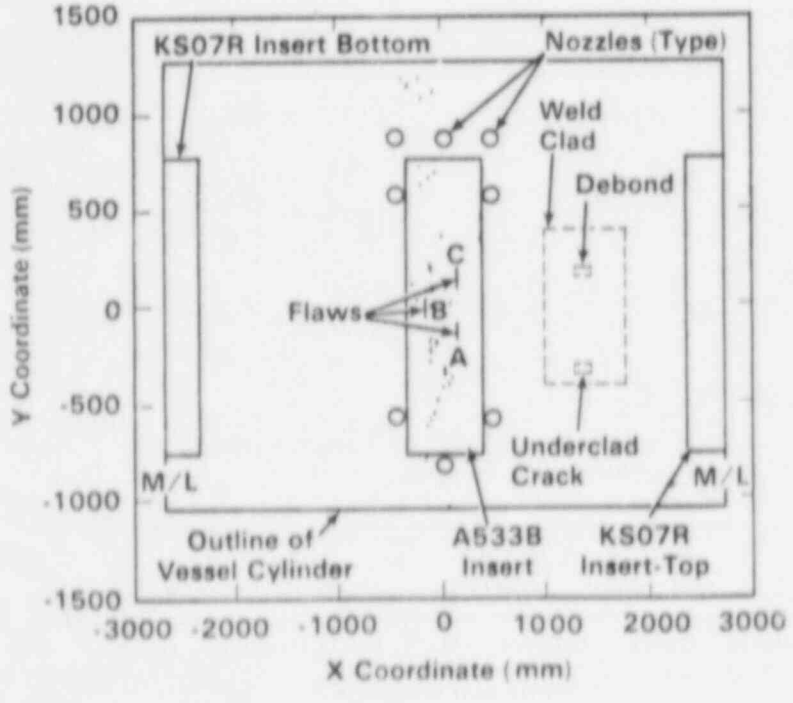

Figure 4.84. AE Source Locations - Step 6, Array 2, Filtered to 8-10 Volts Amplitude.

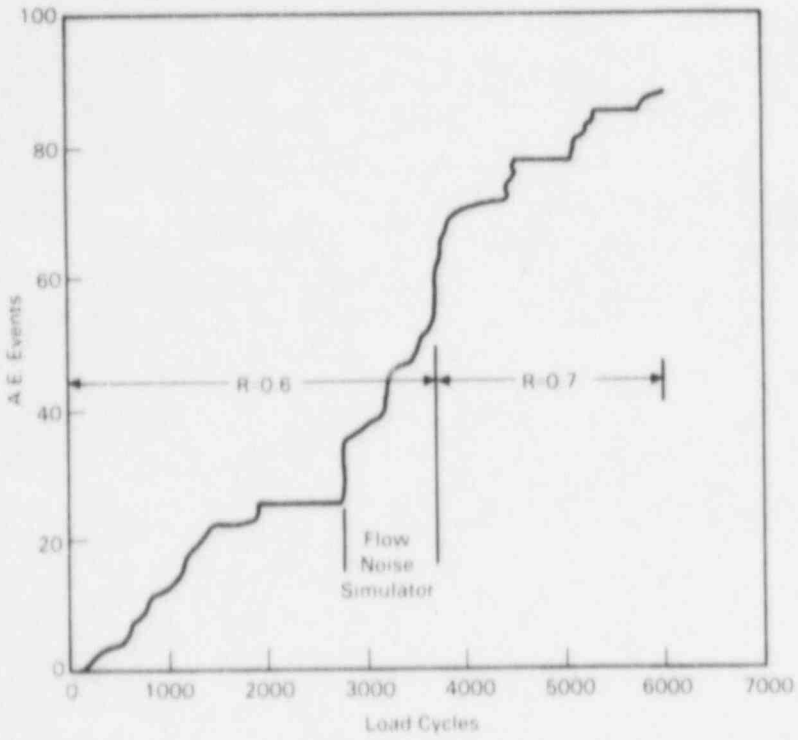

Figure 4.85. AE Versus Load Cycles - Step 6, Array 2, Filtered to 8-10 Volts Amplitude.

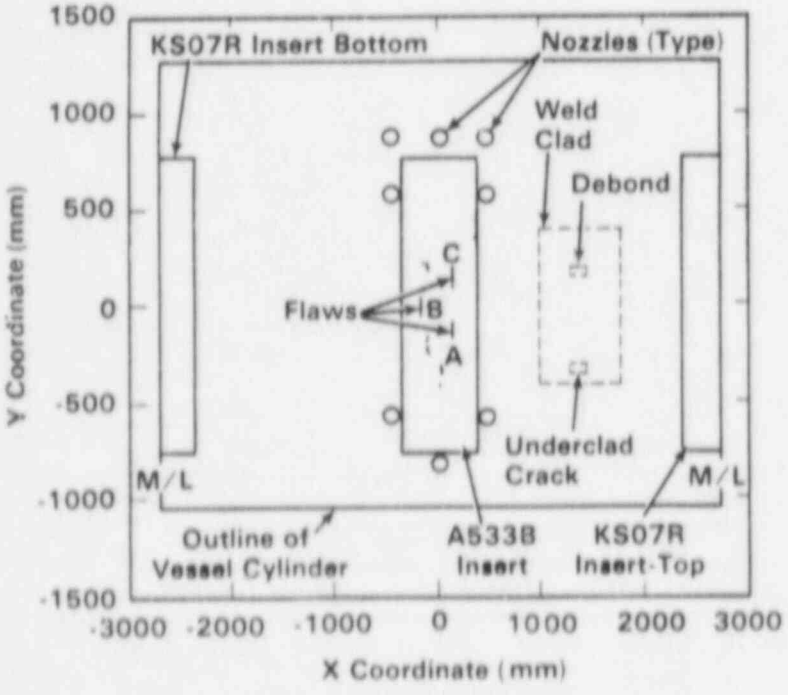

Figure 4.86. AE Source Locations - Step 6, Array 2, Filtered to 8-10 Volts Amplitude and 65-80 Load Position.

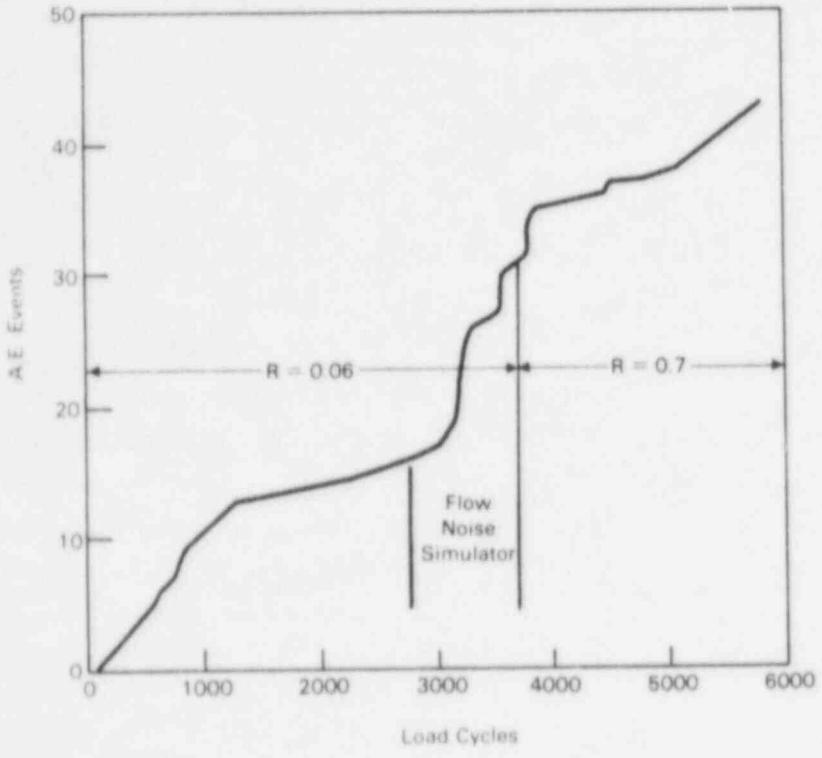

Figure 4.87. AE Versus Load Cycles - Step 6, Array 2, Filtered to 8-10 Volts Amplitude and 65-80 Load Position.

In Figure 4.88, source location for the unfiltered data shows noise data from the manhole cover, as well as data from the flaws. There is also some data starting to appear from the KS07R weld area. As with Array 2, the Array 3 data relative to load cycles (Figure 4.89) shows evidence of the intermittent noise from the manhole cover. When the data is filtered to peak load position (Figure 4.90), it removes much of the manhole cover noise but the data from the flaws and from the KS07R remains. The AE versus load cycles for Array 3 filtered in Figure 4.91 is consistent with Array 2.

4.3.5 Summary

AE from growth of Flaws A and B was detected by both the quad array (Array 2) on the A533 insert and the cylindrical array (Array 3) monitoring the vessel cylinder. The crack growth AE assumed consistent characteristics of high amplitude and of occurring at or near peak load.

The flow noise simulator had little affect on AE detection with sensors tuned to about 400 kHz, however, low frequency (150 kHz) sensors were completely saturated. These results are consistent with results obtained on a nuclear reactor.

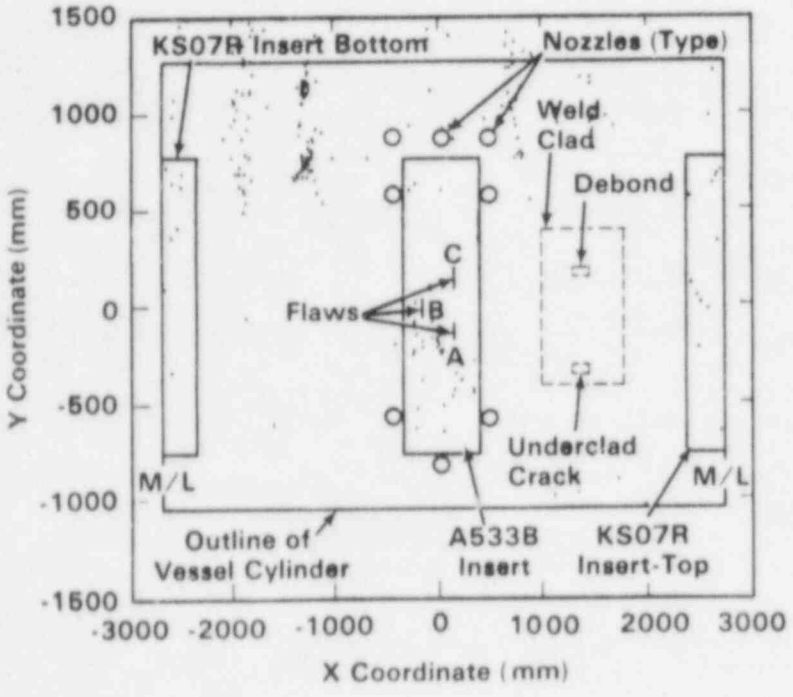

Figure 4.88. AE Source Locations - Step 6, Array 3, Unfiltered.

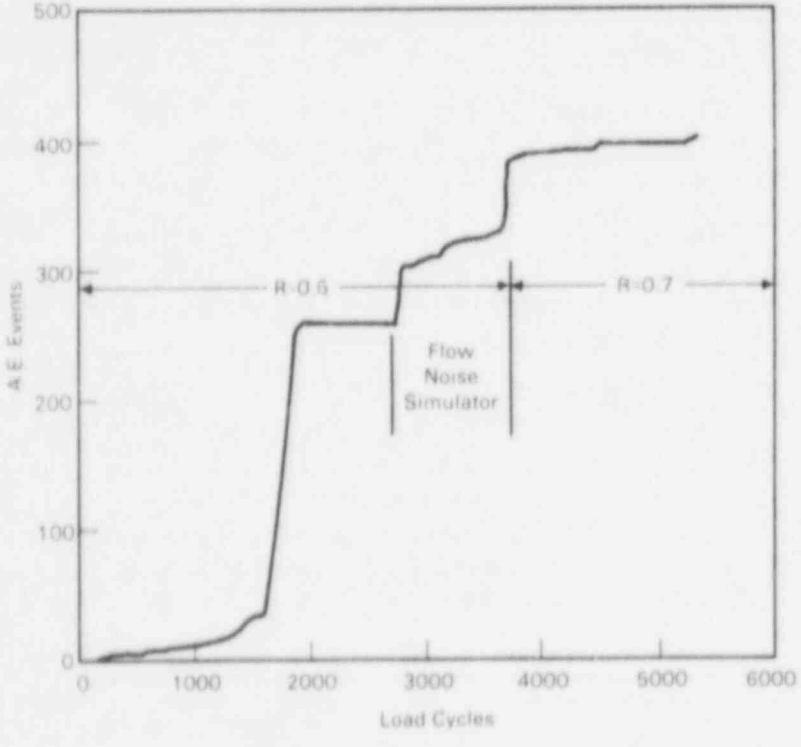

Figure 4.89. AE Versus Load Cycles - Step 6, Array 3, Unfiltered.

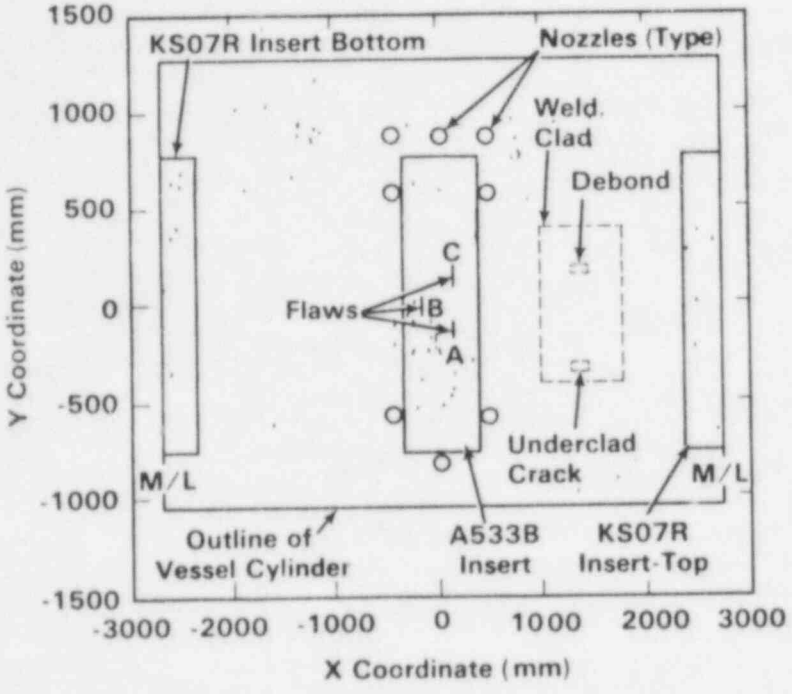

Figure 4.90. AE Source Locations - Step 6, Array 3, Filtered to 65-80 Load Position.

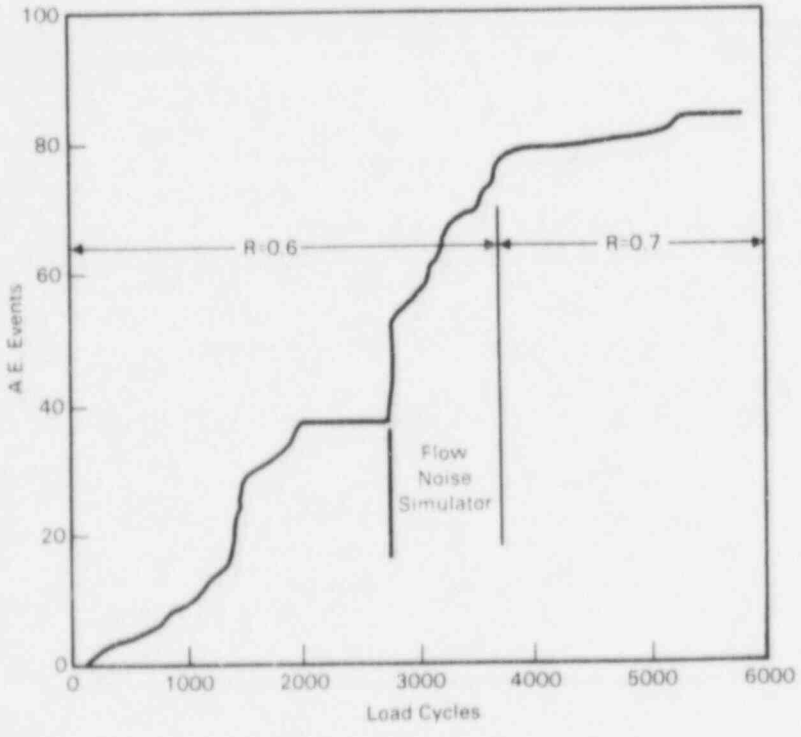

Figure 4.91. AE Versus Load Cycles - Step 6, Array 3, Filtered to 65-80 Load Position.

Noise from a manhole cover assembly was an intermittent problem throughout the low temperature testing. Generally, this noise could be handled by filtering with parametrics (load position and signal amplitude). This, however, underscores the need for real time AE identification by pattern recognition to isolate crack growth AE. Generally, parametrics such as load position in particular will be of little use in a general reactor monitoring situation.

The amount of AE detected in Step 2 was somewhat low. Array 3 data did not follow a consistent pattern in Steps 2 and 3 but when the sensor mounting was improved, the AE information was comparable to Array 2 in Steps 5 and 6.

There was some evidence of the KS07R weld crack becoming active during Step 6. The indications were not sufficiently prominent to draw attention at the time, however.

Point location of AE sources was not always as concise as desired. Point source location using a two dimensional concept on a heavy section, complex structure is a significant challenge. This is an aspect of established AE technology that needs to be reassessed and upgraded.

4.4 AE MONITORING DATA AT 285°C (550°F)

4.4.1 Step 8, R=0.4 Loading Conditions

The acoustic source which dominated the AE data in Step 8 was noise originating from the manhole pressure seal. The first 1200 cycles of this step were performed with a manhole gasket material that produced a large amount of acoustic noise. Figures 4.92-4.94 give the unfiltered source location plots for Arrays 1-3, respectively. Figure 4.93 shows the large amount of manhole noise that was detected by Array 2.

Amplitude distributions (Figures 4.95-4.97) for these data show that the vast majority of the signals had relatively low amplitudes ($\leq$5.0 volts). Load position histograms for Arrays 1-3 are given in Figures 4.99-4.100. The data from Arrays 2 and 3 show that most of the events occurred during the descending portion of the load cycle. The load position distribution for Array 1 (Figure 4.98) does not show the same trend as Arrays 2 and 3, but this array recorded fewer events (note scales in Figures 4.98-4.100). With a greater amount of noise, these unfiltered amplitude and load position histograms contrast sharply with the AE data obtained during the 65°C (150°F) portion of the test. The crack growth AE signals had high amplitudes mostly in the range of 8 to 10 volts and load position numbers generally between 65 and 80 when measured by Array 2 sensors.

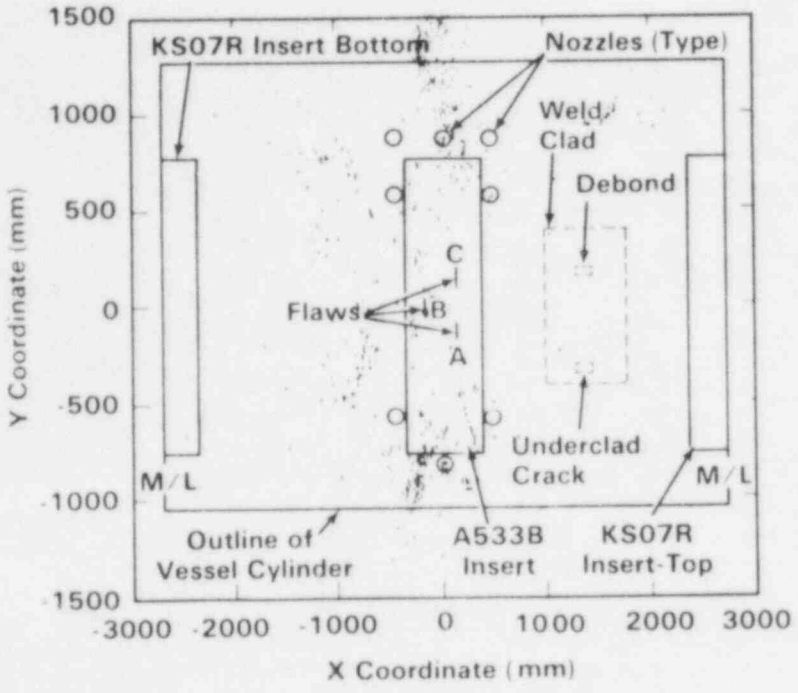

Figure 4.92. AE Source Locations - Array 1, Step 8, Unfiltered.

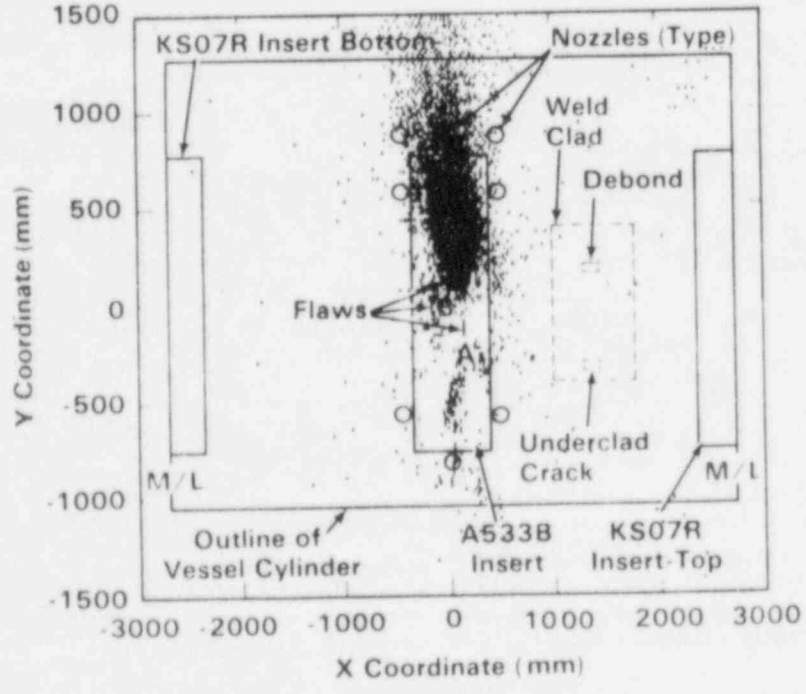

Figure 4.93. AE Source Locations - Array 2, Step 8, Unfiltered.

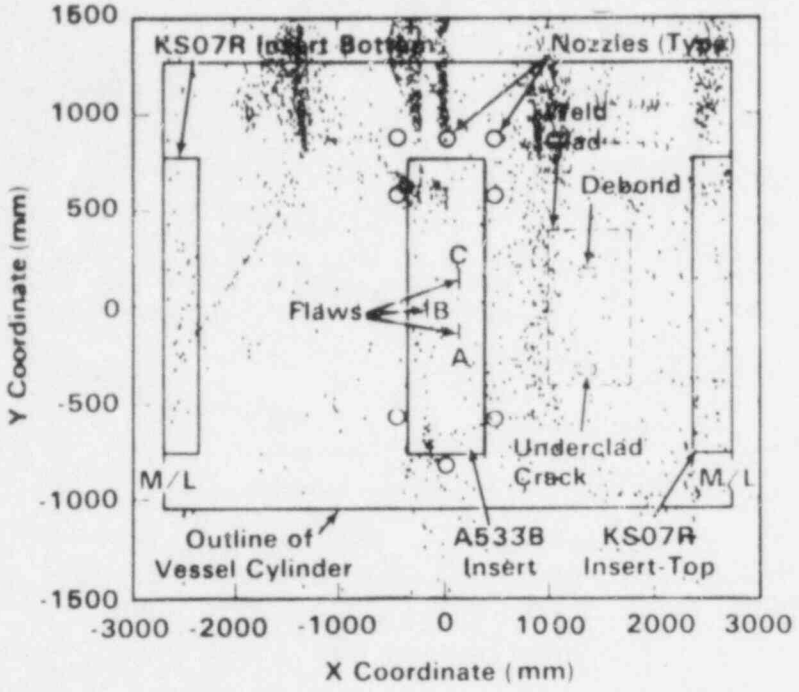

Figure 4.94. AE Source Locations - Array 3, Step 8, Unfiltered.

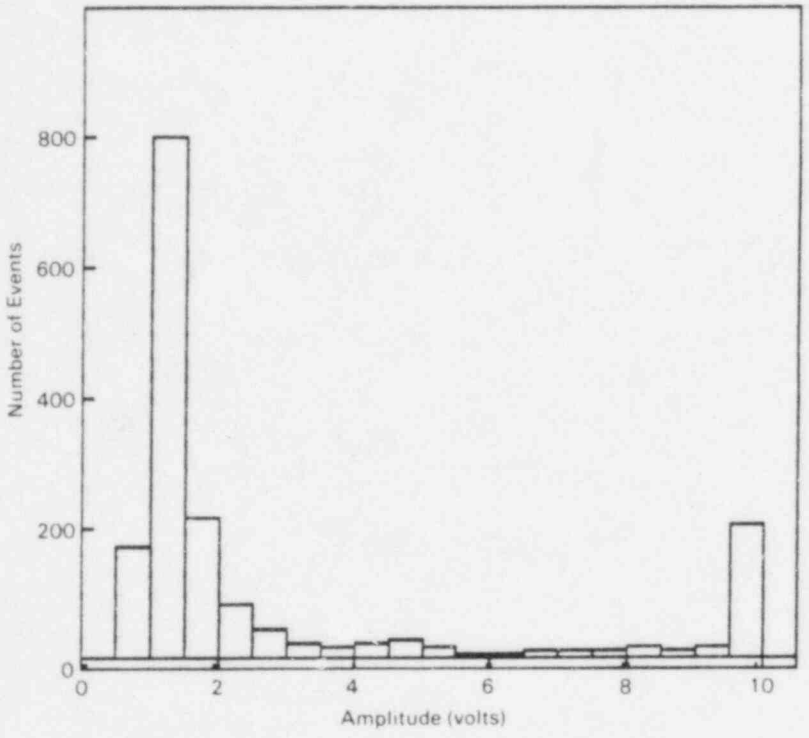

Figure 4.95. Amplitude Distribution - Array 1, Step 8, Unfiltered.

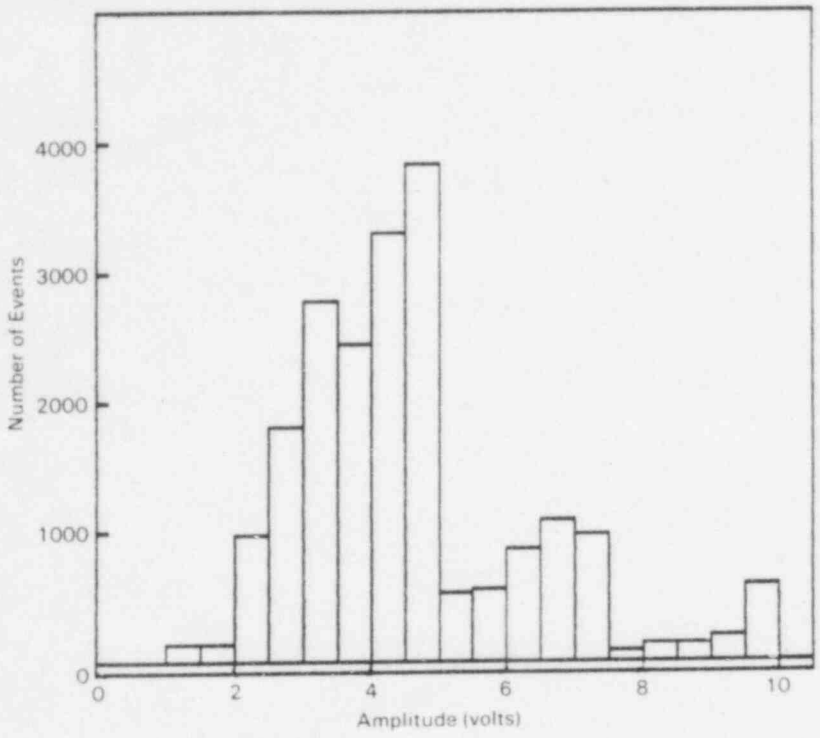

Figure 4.96. Amplitude Distribution - Array 2, Step 8, Unfiltered.

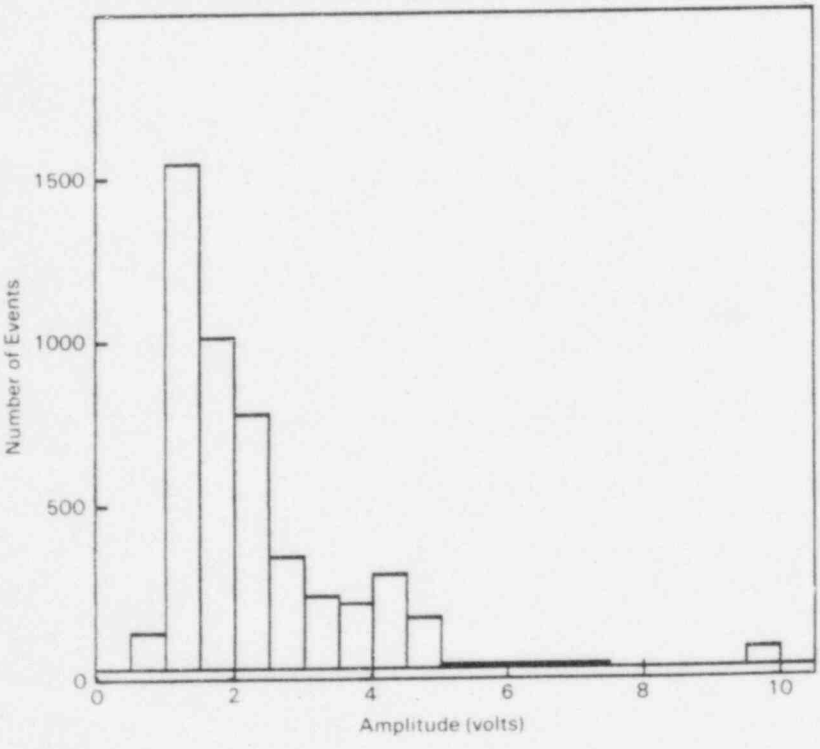

Figure 4.97. Amplitude Distribution - Array 3, Step 8, Unfiltered.

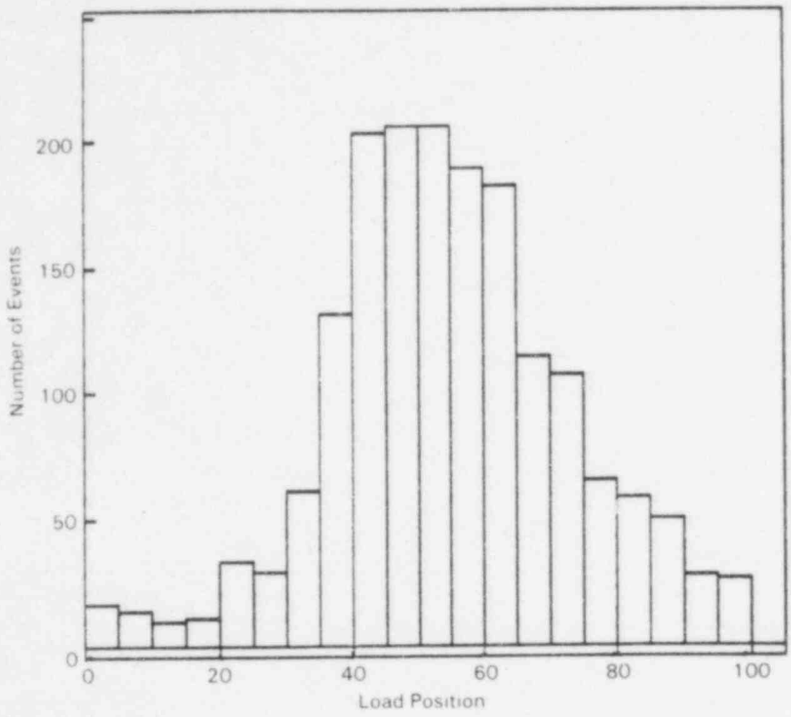

Figure 4.98. Load Position Distribution - Array 1, Step 8, Unfiltered.

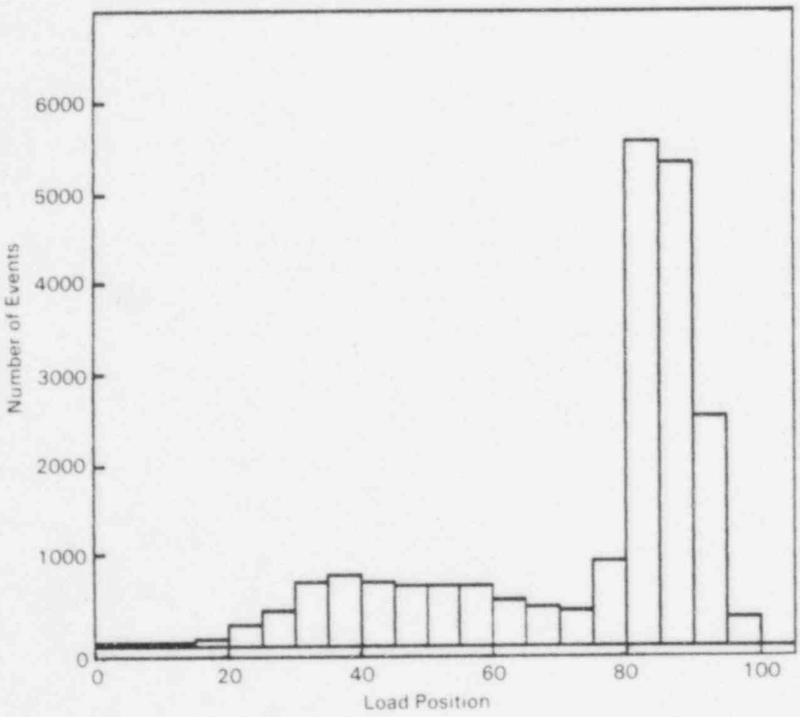

Figure 4.99. Load Position Distribution - Array 2, Step 8, Unfiltered.

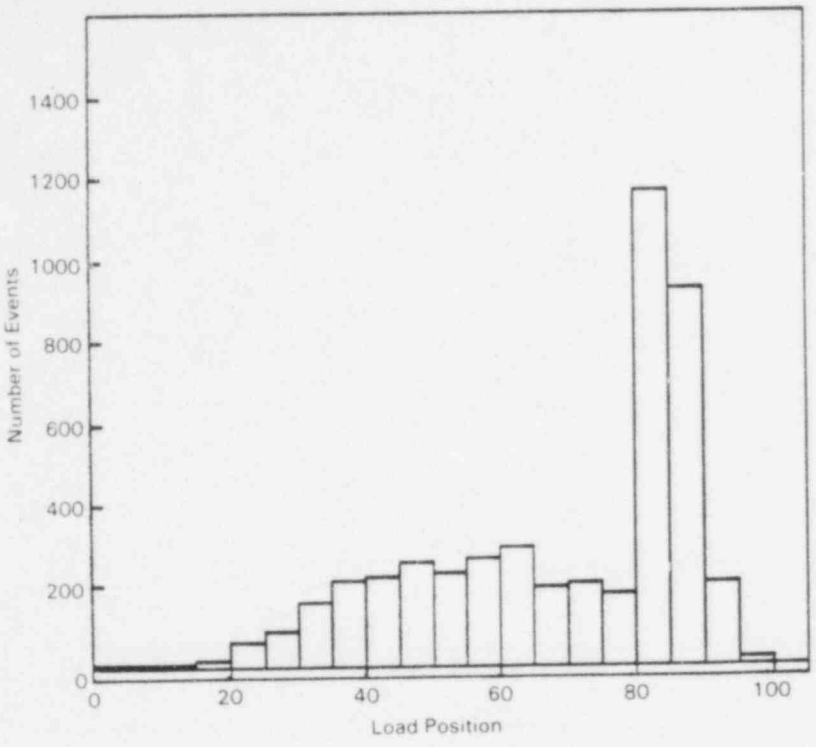

Figure 4.100. Load Position Distribution - Array 3, Step 3, Unfiltered.

For events detected by Array 3, the peak load (65-80) signal amplitudes were within a 2-10 volt range.

In order to separate the crack growth AE from manhole noise, filtered source location plots for each array were developed. AE events with the signal attributes given above are plotted in Figures 4.101-4.103 for Arrays 1-3, respectively. It is evident from these figures that AE detected from the machined defects at 285°C has signal characteristics similar to 65°C AE events. The grouping of signals located near the lower circumferential weld in Figure 4.101 were from the mechanical impactor.

Figures 4.104-4.106 give filtered plots of the AE event count versus pressure cycles for Flaw B during Step 8 for all arrays. Note that the shape of the curves are nearly the same indicating that each array responded similarly to AE from Flaw B but the further the array was located from Flaw B, fewer counts were detected. The form of these curves doesn't correspond to the form of the compliance versus cycles curve (see Figure 4.133) for Step 8. This result is not surprising given the normal variations in AE data that have been observed from laboratory test data.

Figure 4.107 gives the AE events versus cycles curve for the KS07R flaw. This curve was constructed by filtering about the

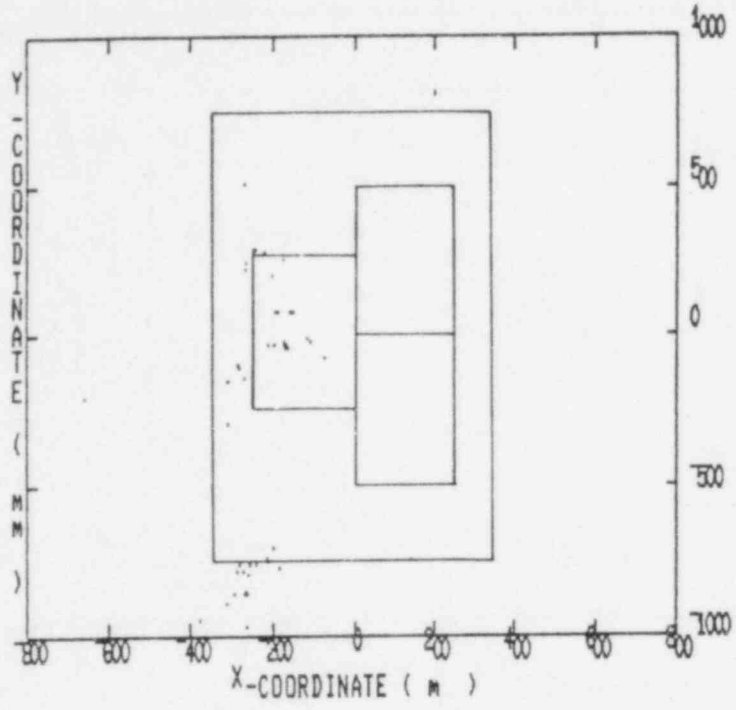

Figure 4.101. AE Source Locations - Array 1, Step 8, Filtered to Peak Load (65-80) and 8-10 Volts Amplitude.

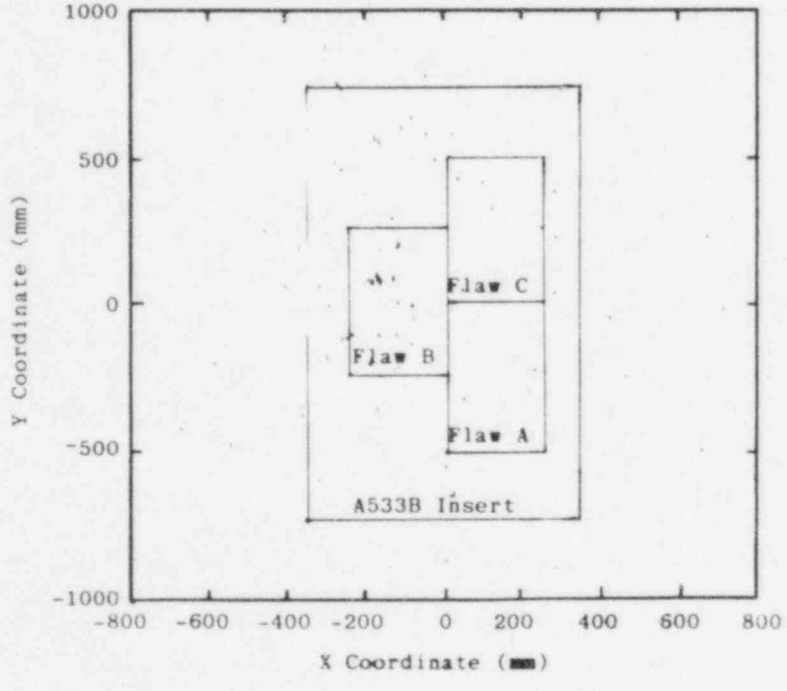

Figure 4.102. AE Source Locations - Array 2, Step 8, Filtered to Peak Load (65-80) and 8-10 Volts Amplitude.

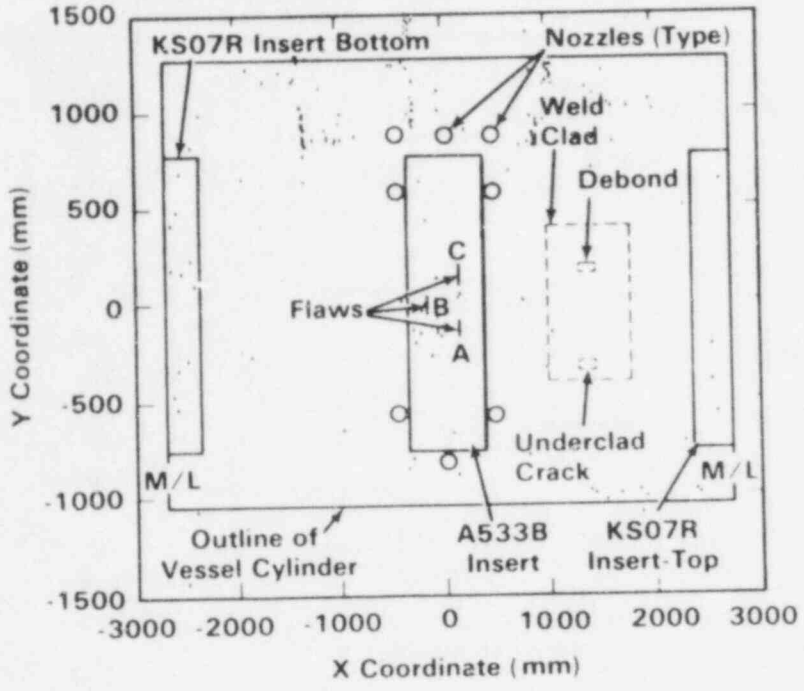

Figure 4.103. AE Source Locations - Array 3, Step 8, Filtered to Peak Load (65-80) and 2-10 Volts Amplitude.

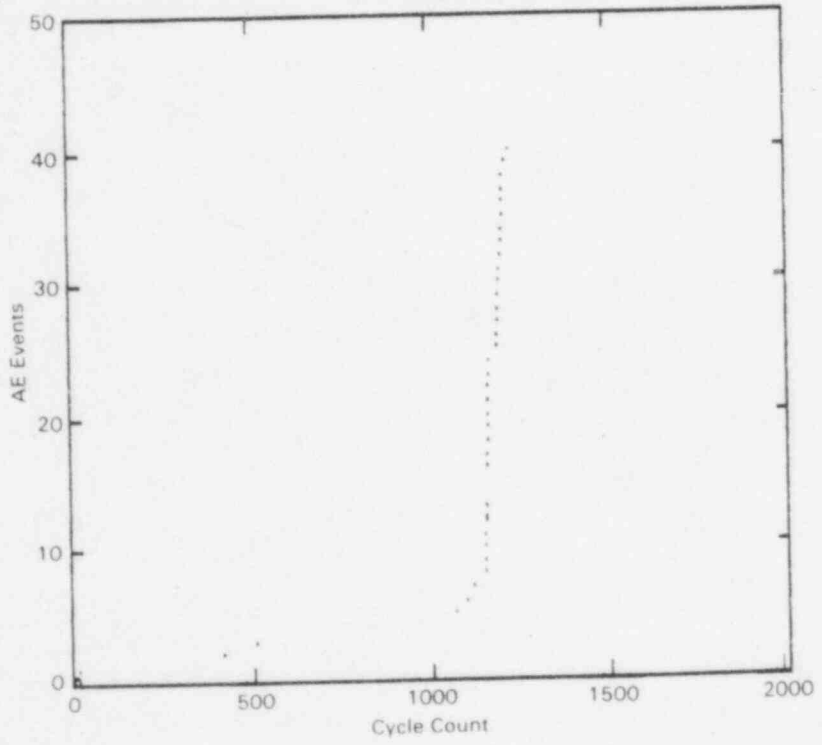

Figure 4.104. AE Event Count Versus Pressure Cycles - Array 1, Step 8, Filtered to Peak Load (65-80) and 8-10 Volts Amplitude, Flaw B.

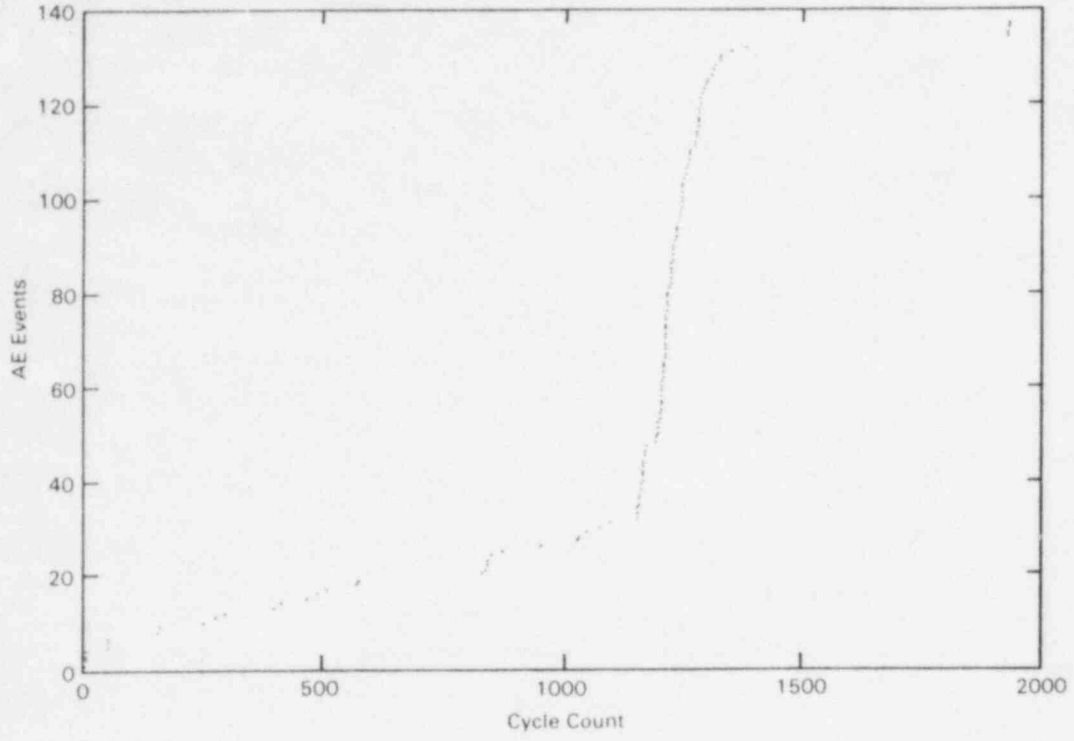

Figure 4.105. AE Event Count Versus Pressure Cycles - Array 2, Step 8, Filtered to Peak Load (65-80) and 8-10 Volts Amplitude, Flaw B.

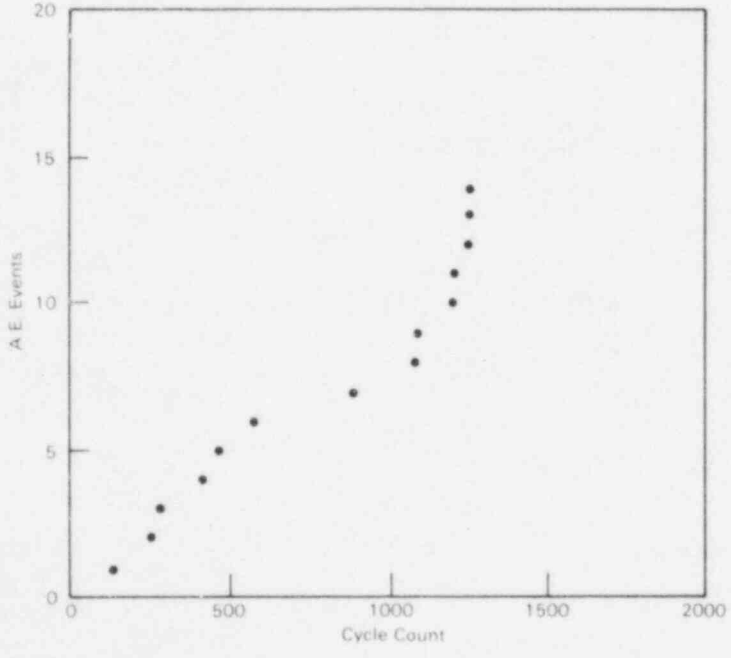

Figure 4.106. AE Event Count Versus Pressure Cycles - Array 3, Step 8, Filtered to Peak Load (65-80) and 2-10 Volts Amplitude, Flaw B.

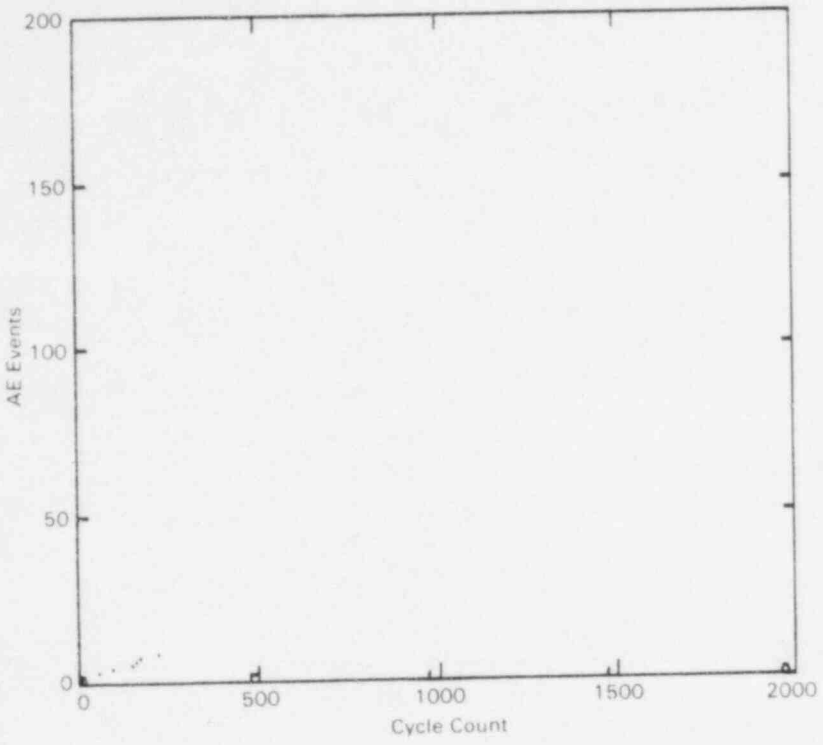

Figure 4.107. AE Event Count Versus Pressure Cycles - Array 3, Step 8, Filtered to Peak Load (65-80), KS07R Flaw.

upper longitudinal weld in the KS07R replacement patch. A 500 mm wide by 1600 mm long zone of acceptance was centered about this defect. Only events with load positions between 65 and 80 are plotted in Figure 4.107. The activity from this flaw was small at this point in the test compared to the activity rate that developed in Steps 9 and 11.

4.4.2 Step 9, R=0.6 Loading Condition

With the replacement of the manhole gasket material in Step 8, the manhole noise problem was greatly reduced. This source was still active during Step 9 but was overshadowed by the appearance of a new AE source. During this step the dominant source of activity was the upper longitudinal KS07R replacement patch weld. Figures 4.108-4.110 give the unfiltered source location plots for Arrays 1-3, respectively. Note that data from Arrays 2 and 3 clearly show the large amount of data coming from the KS07R flaw.

Amplitude distributions for Arrays 1-3 are given in Figures 4.111-4.113. Most of the emissions were low in amplitude. Flaw growth emissions from the KS07R weld had amplitudes that were generally lower than from Flaws A, B, and C; however, this result was probably influenced by the relatively long source to sensor distance for this flaw.

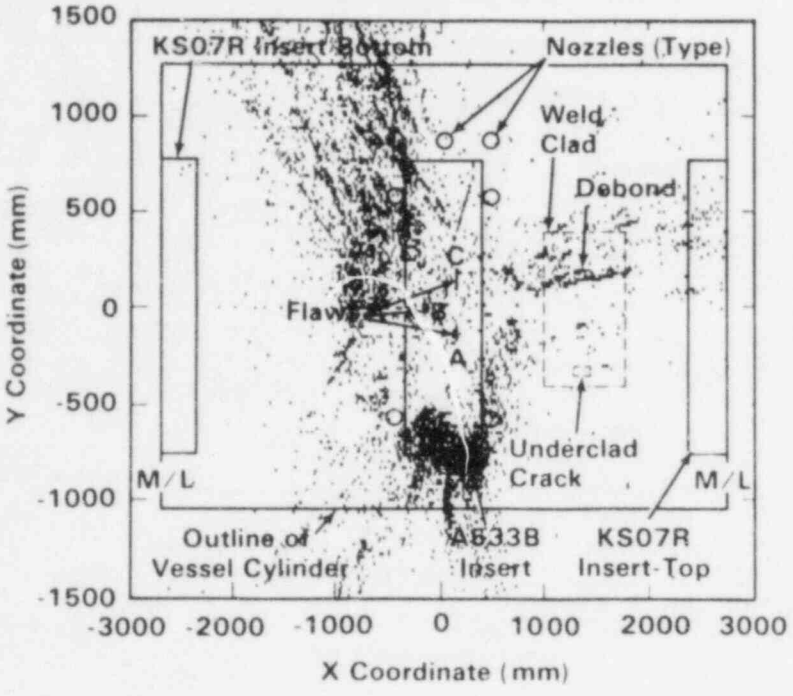

Figure 4.108. AE Source Locations - Array 1, Step 9, Unfiltered.

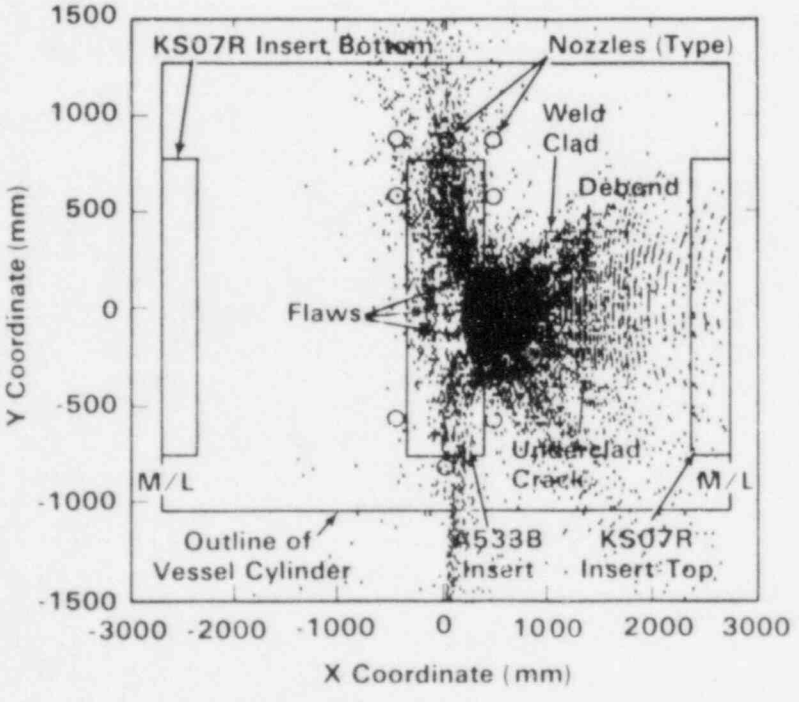

Figure 4.109. AE Source Locations - Array 2, Step 9, Unfiltered.

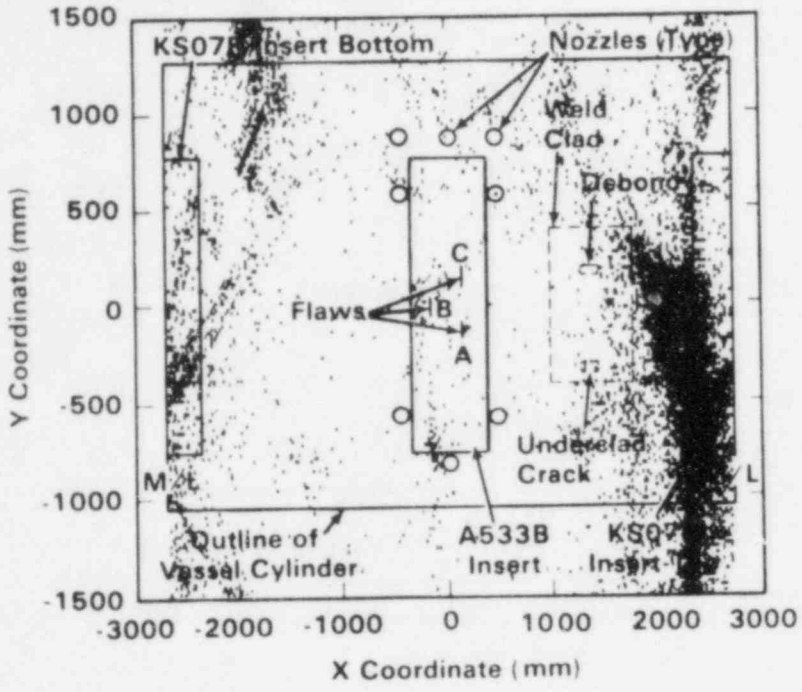

Figure 4.110. AE Source Locations - Array 3, Step 9, Unfiltered.

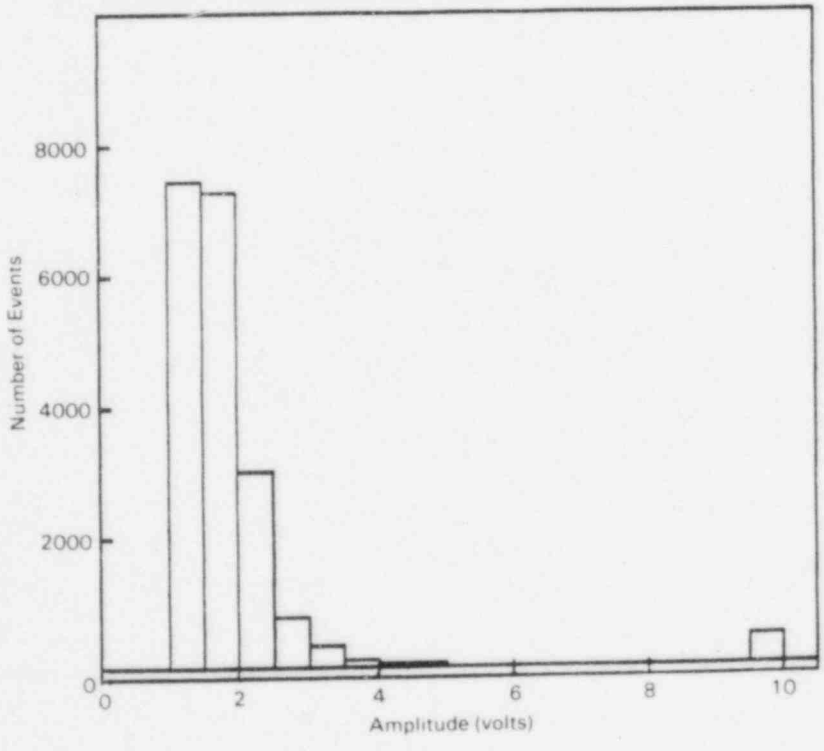

Figure 4.111. Amplitude Distribution - Array 1, Step 9, Unfiltered.

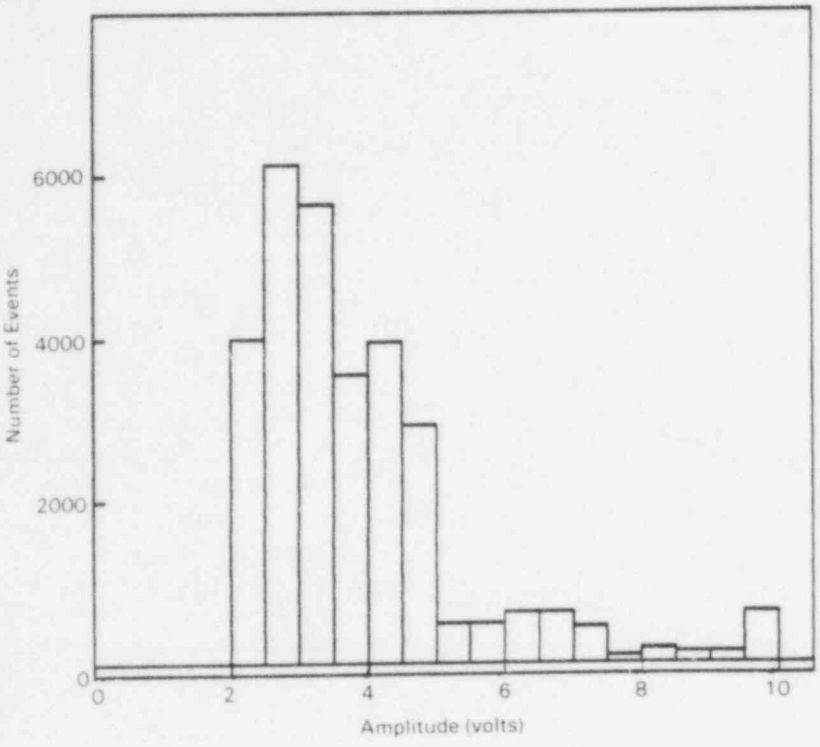

Figure 4.112. Amplitude Distribution - Array 2, Step 9, Unfiltered.

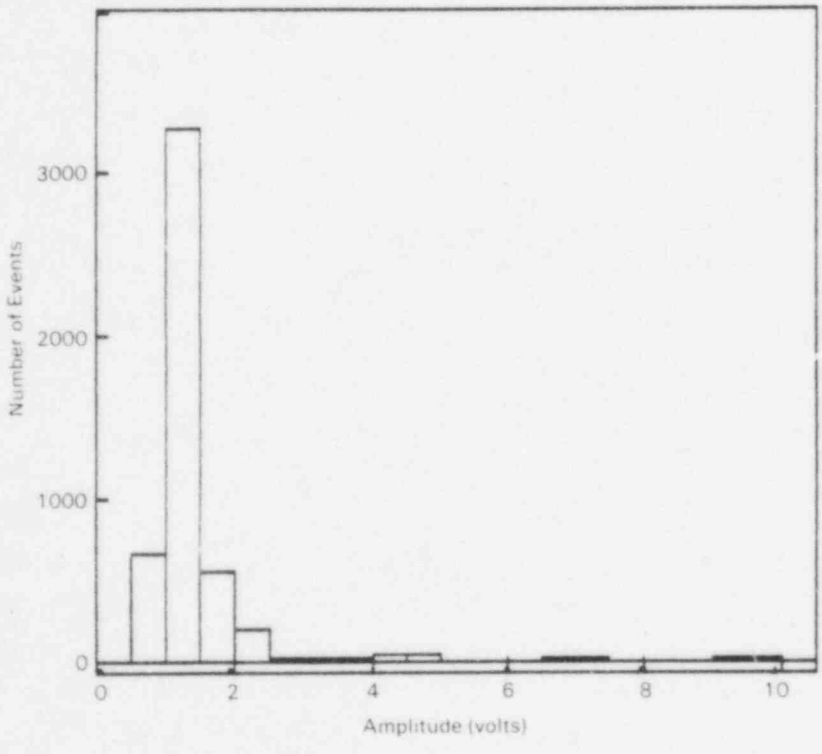

Figure 4.113. Amplitude Distribution - Array 3, Step 9, Unfiltered.

Load position histograms for Arrays 1-3 are shown in Figures 4.114-4.116. The major difference between these histograms and previous histograms is a marked increase in activity during the upramp of the pressure cycle. This was evidently caused by the large increase in AE activity from the KS07R flaw. This result contrasts with flaw growth signal attributes observed from Flaws A, B, and C.

Filtered source location plots for Arrays 1-3 are given in Figures 4.117-4.120. The same filtering parameters employed in Step 8 were utilized to create these plots. Note that all arrays were sensitive to events from Flaws A and B, but only Arrays 2 and 3 detected activity from Flaw C. The grouping of events near the upper left hand corner of the Flaw B zone of acceptance are thought to be incorrectly located Flaw B emissions. Pentel calibration data (Figure 4.121) taken during Step 9 suggests that Array 1 located some events in this vicinity.

Figures 4.122-4.124 show the AE events versus cycles curves for Flaw B filtered with respect to load position and amplitude for each array. The form of the curves show the same shape. The number of events detected by a particular array depended on its distance from the flaws.

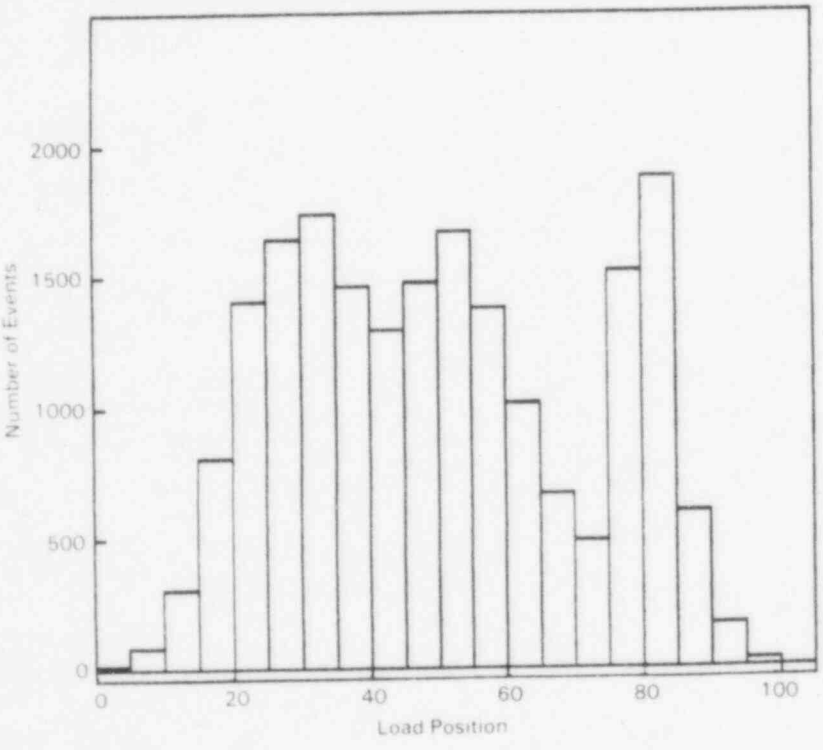

Figure 4.114. Load Position Distribution - Array 1, Step 9, Unfiltered.

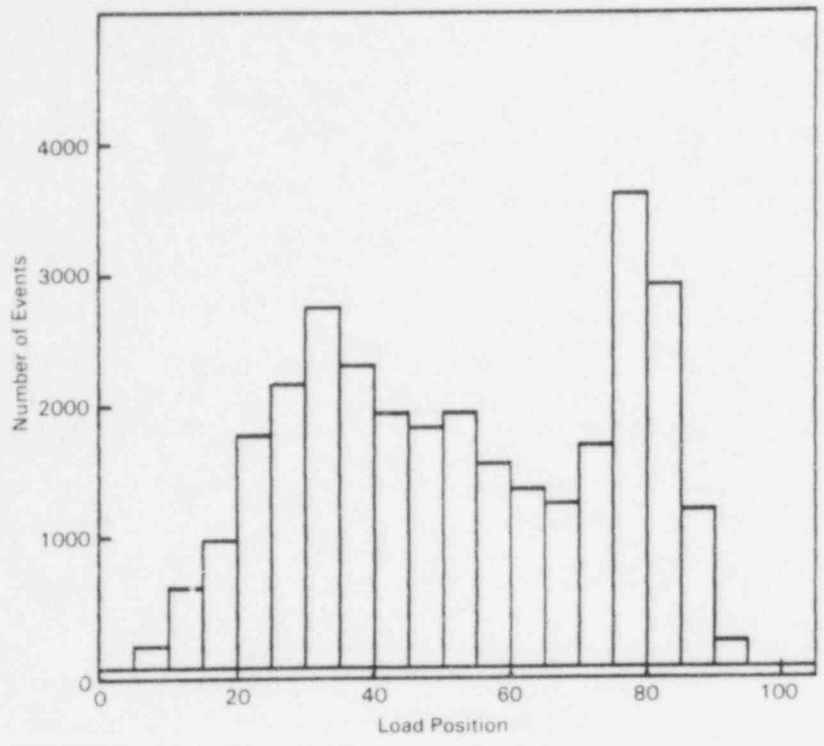

Figure 4.115. Load Position Distribution - Array 2, Step 9, Unfiltered.

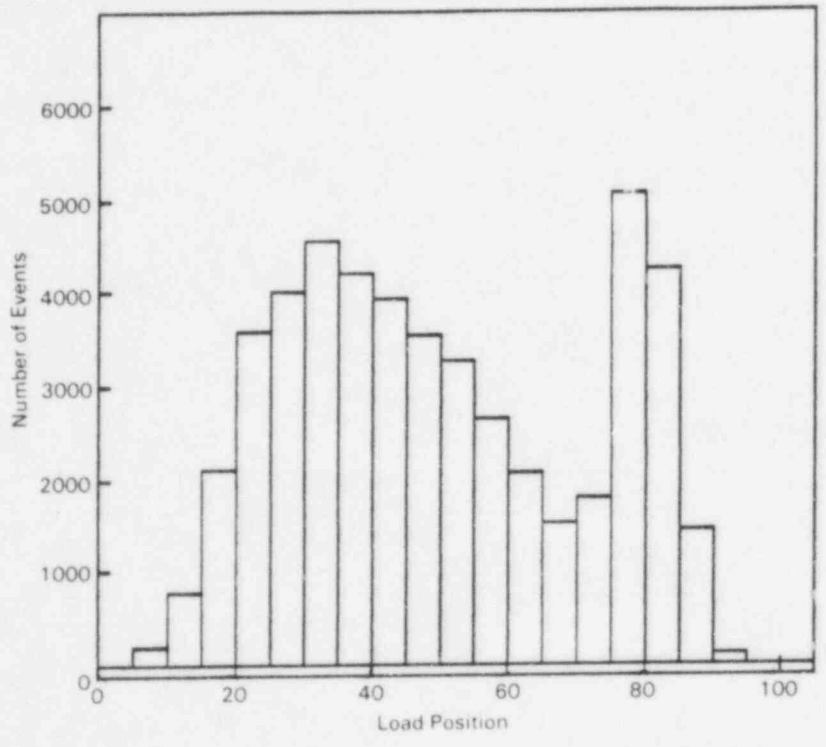

Figure 4.116. Load Position Distribution - Array 3, Step 9, Unfiltered.

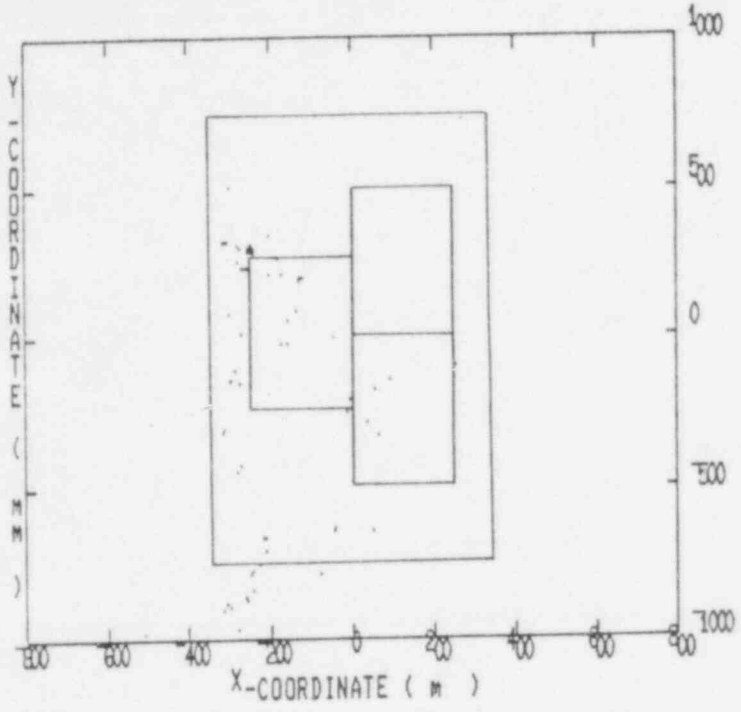

Figure 4.117. AE Source Locations - Array 1, Step 9, Filtered to Peak Load (65-80) and 8-10 Volts Amplitude.

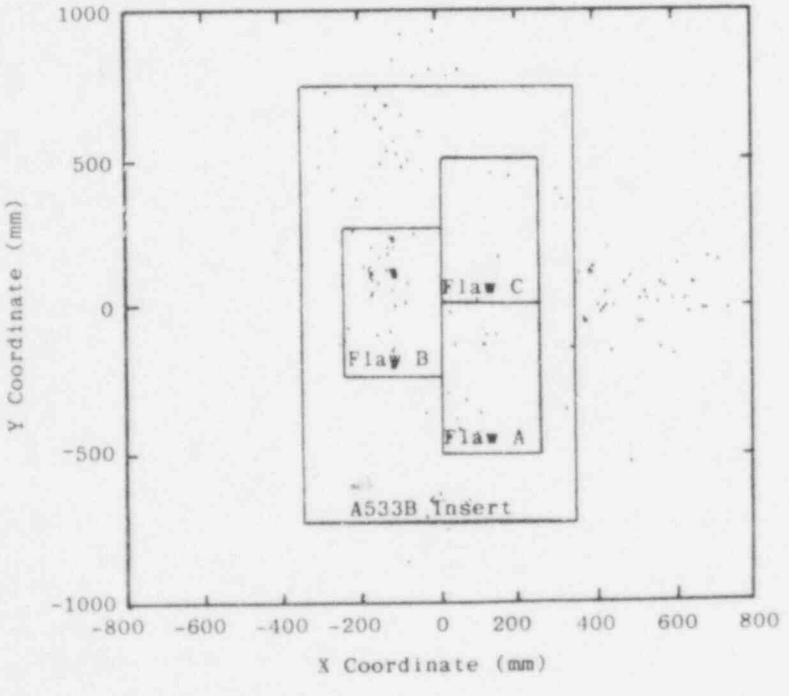

Figure 4.118. AE Source Locations - Array 2, Step 9, Filtered to Peak Load (65-80) and 8-10 Volts Amplitude.

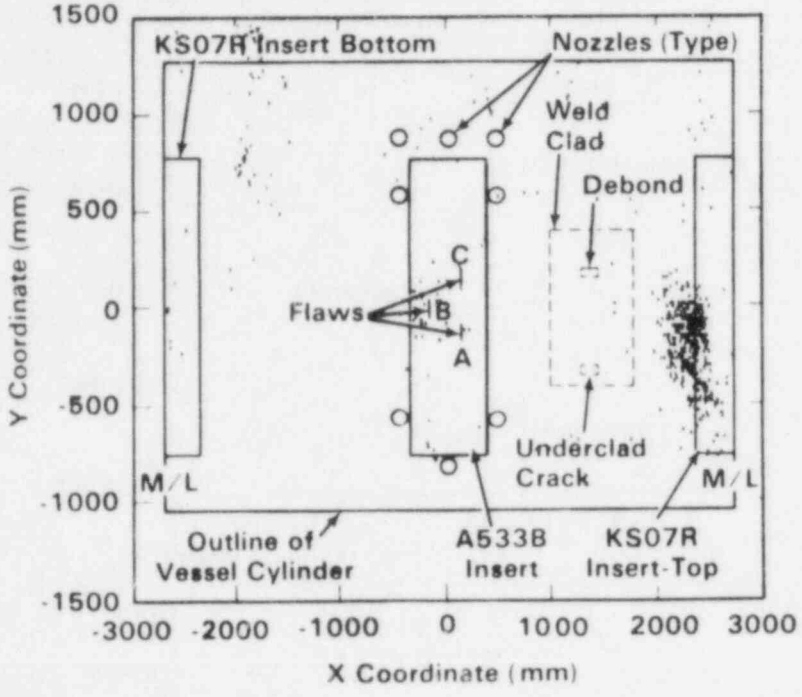

Figure 4.119. AE Source Locations - Array 3, Step 9, Filtered to Peak Load (65-80) and 2-10 Volts Amplitude.

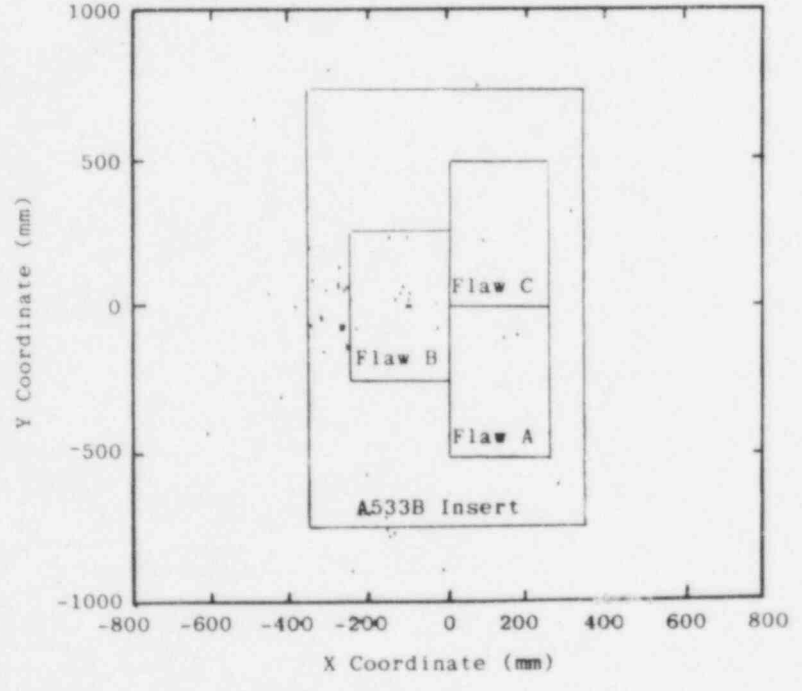

Figure 4.120. AE Source Locations Near A533B Insert - Array 3, Step 9, Filtered to Peak Load (65-80) and 2-10 Volts Amplitude.

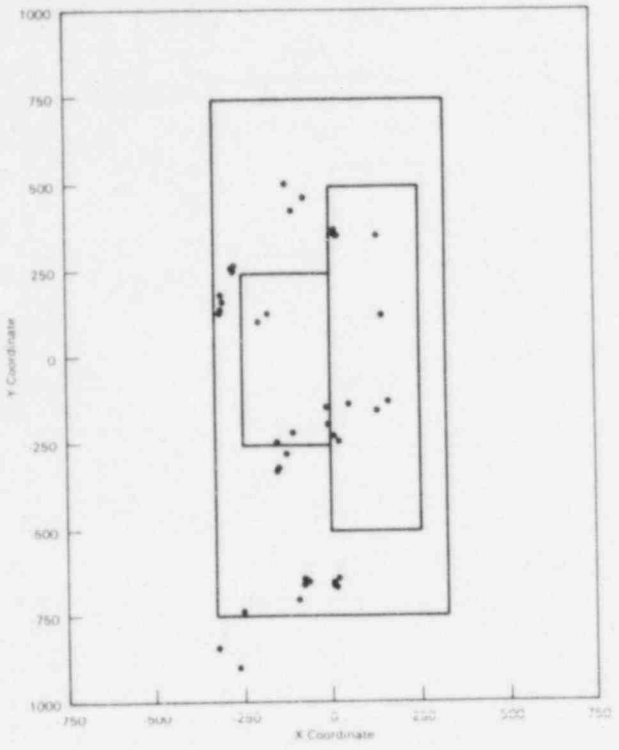

Figure 4.121. Internal Pentel Calibration - Array 1, Step 9.

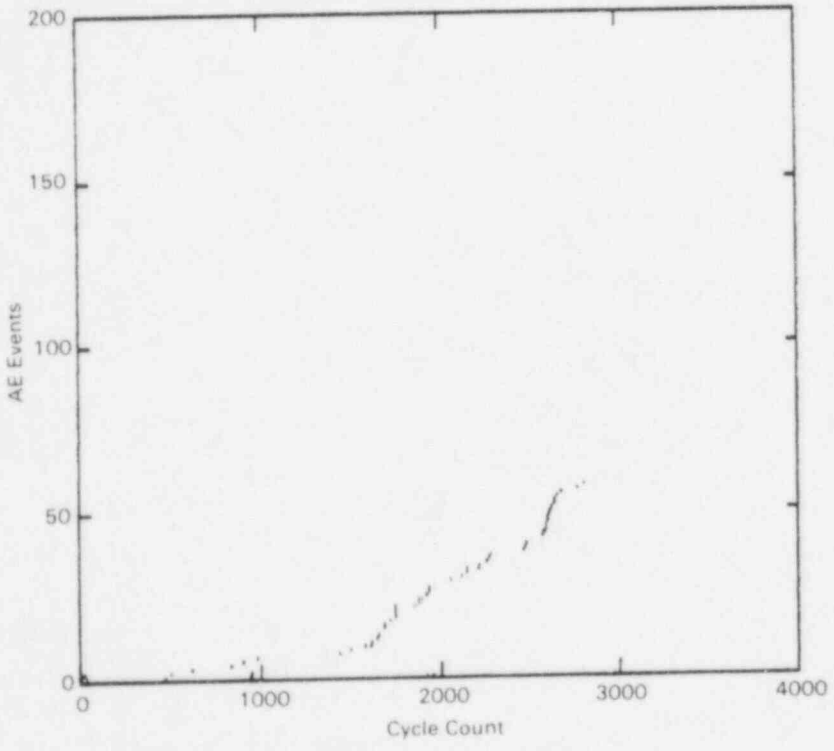

Figure 4.122. AE Event Count Versus Pressure Cycles - Array 1, Step 9, Filtered to Peak Load (65-80) and 8-10 Volts Amplitude, Flaw B.

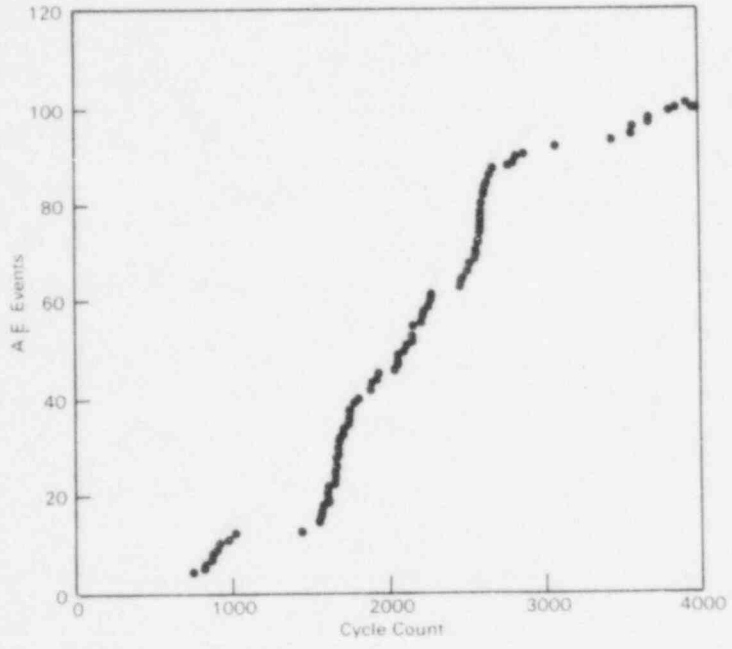

Figure 4.123. AE Event Count Versus Pressure Cycles - Array 2, Step 9, Filtered to Peak Load (65-80) and 8-10 Volts Amplitude, Flaw B.

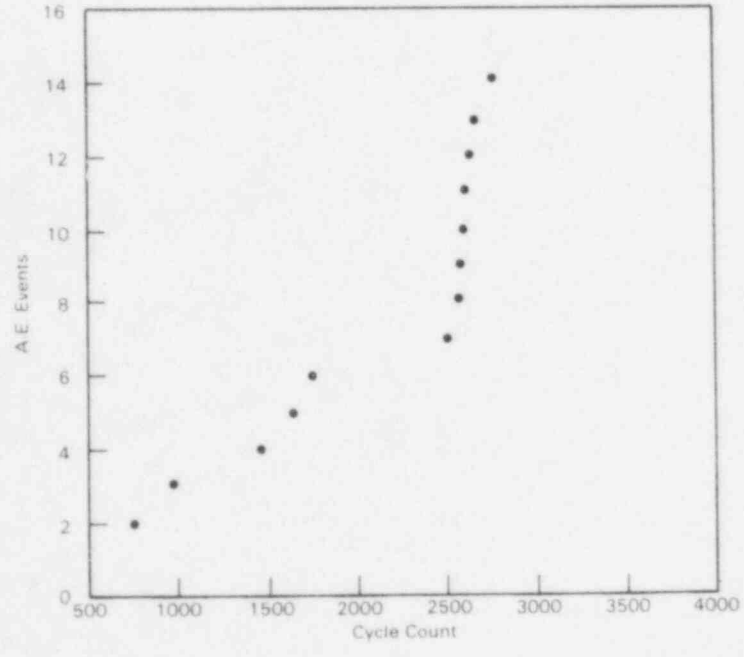

Figure 4.124. AE Event Count Versus Pressure Cycles - Array 3, Step 9, Filtered to Peak Load (65-80) and 2-10 Volts Amplitude, Flaw B.

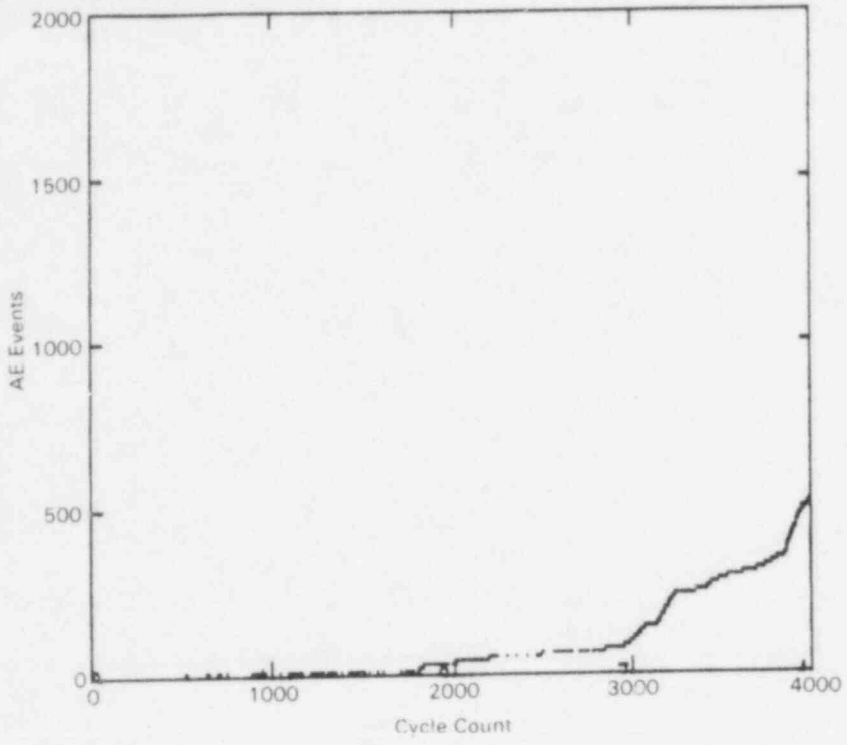

Figure 4.125. AE Event Count Versus Pressure Cycles - Array 3, Step 9, Filtered to Peak Load (65-80), KS07R Flaw.

Figure 4.125 gives the load position filtered event count versus cycles curve for the KS07R flaw. The activity of this flaw increased vastly from what was observed in Step 8. At the end of this step, an average of 12 events per cycle were detected.

4.4.3 Step 11, R=0.4 Loading Condition

The dominant source of AE activity during this step was the KS07R replacement patch weld. So much activity was detected from this weld that the AE monitoring system was not able to detect signals from the machined cracks. Figure 4.126 gives the unfiltered source location plot for Array 1 for a 72 cycle block of data during Step 11. All of this data was most likely KS07R flaw origin events that were "pulled in" by the array. Figure 4.127 gives the same source location plot but filtered this time to isolate any possible AE activity from Flaws A, B, or C. It is evident from Figure 4.127 that there weren't any events detected from these flaws during this part of Step 11.

Figure 4.128 shows the unfiltered source location plot for Array 3 near the end of Step 11. The vast majority of the emissions are associated with the KS07R flaw. These emissions were low amplitude that occurred during the load upramp with a large number at maximum load (see Figures 4.129 and 4.130).

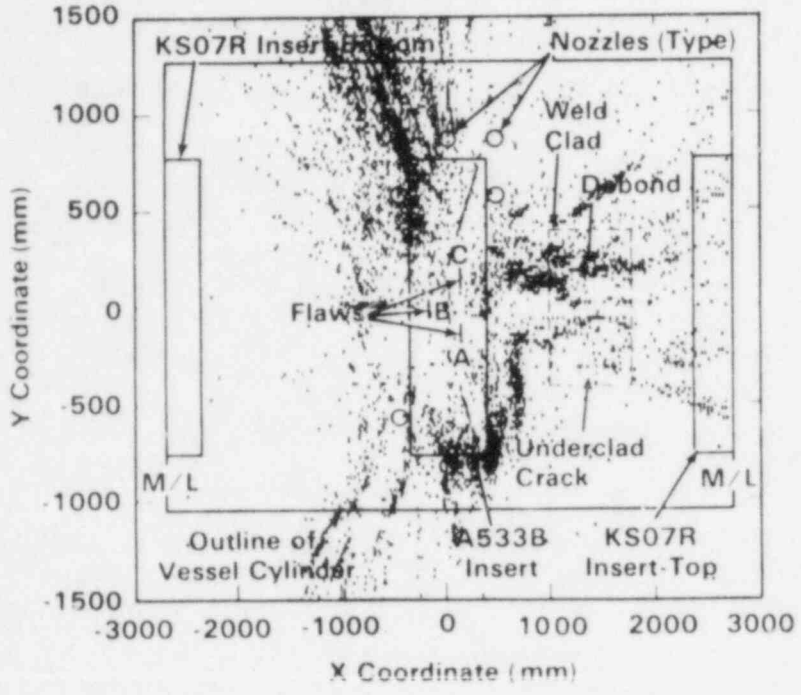

Figure 4.126. Step 11 (401-473 Cycles), Array 1.

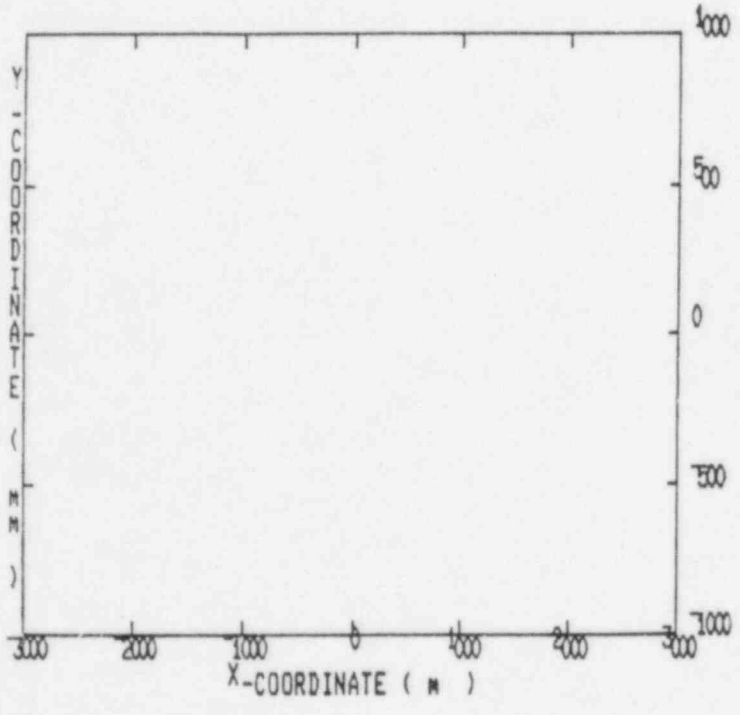

Figure 4.127. Step 11 (401-473 Cycles), Array 1, Filtered to Peak Load (65-80) and 8-10 Volts Amplitude.

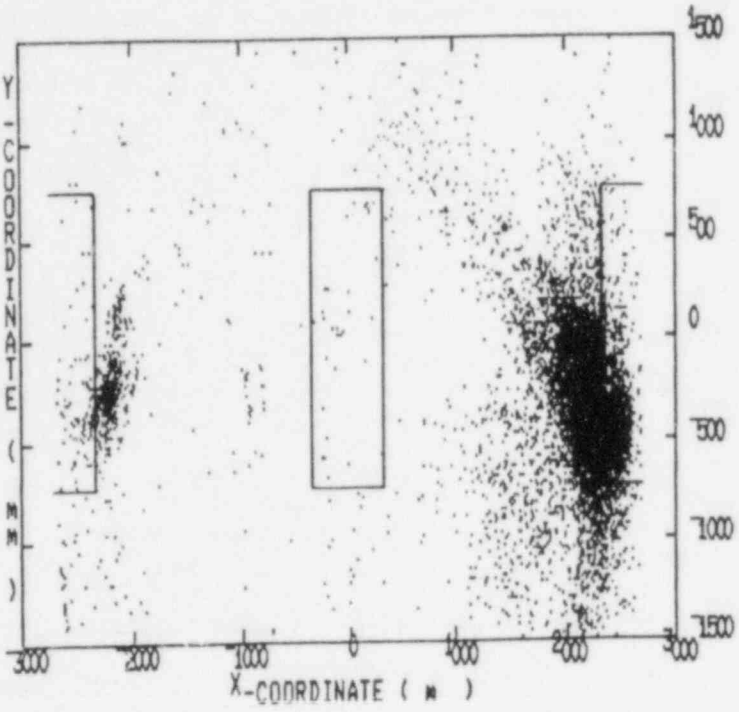

Figure 4.128. Step 11 (1271-1347 Cycles), Array 3.

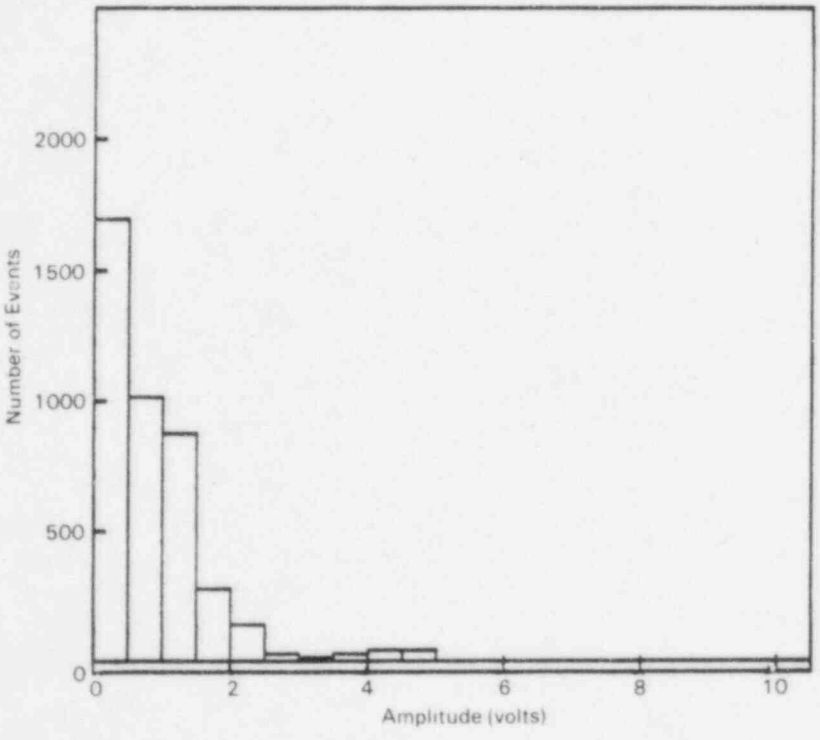

Figure 4.129. Step 11 (1271-1347 Cycles), Array 3.

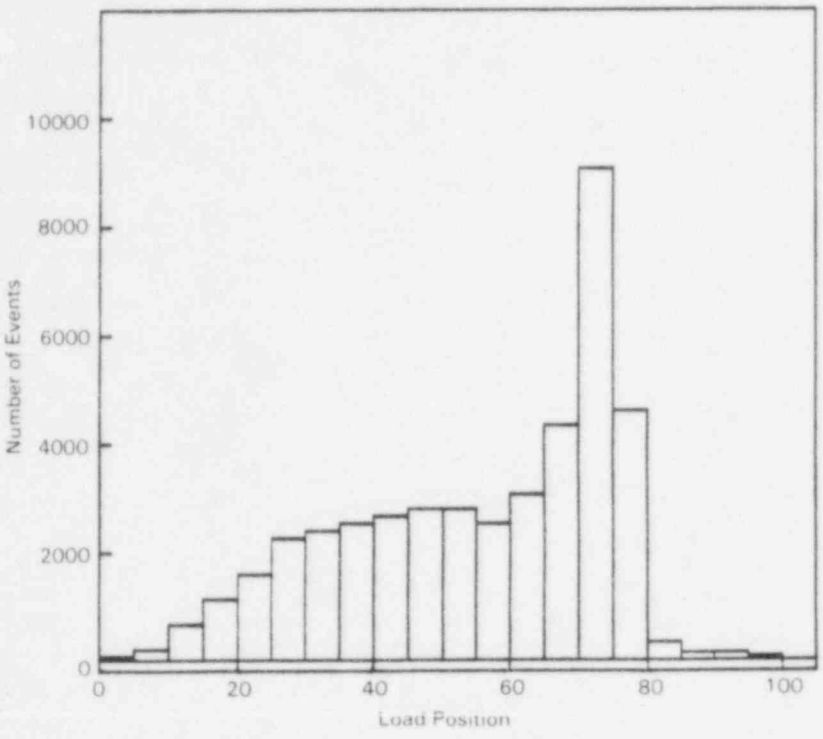

Figure 4.130. Step 11 (1271-1347 Cycles), Array 3.

Figure 4.131 plots the average AE event rate versus pressure cycles for the KS07R flaw during Step 11. The event rates increased dramatically from about 12 events/cycle at the end of Step 9 to about 232 events/cycle at the end of Step 11. This level of activity is much greater than event rates observed from laboratory specimens tested at similar stress intensity levels. Several reasons may have contributed to this very high activity level. First, the material chemistry of the KS07R weldment is undoubtedly different from A533B steel. Impurity levels appear to be largely responsible for the AE activity in high-strength-low-allow steels and so material chemistry may be an important factor in the production of AE from this weldment. Secondly, differences in heat treat conditions may be responsible for the emissiveness of this material. The cracking originated in the HAZ of an unstress relieved weldment. In this condition, the HAZ may exhibit lower toughness than fully stress relieved material, thereby giving rise to increased AE. Lastly, the flaw geometry in the KS07R weldment was extremely complex. Many surfaces were available to produce corrosion and rubbing types of AE. In addition, the accumulated length of the flaw provided many sites for AE production.

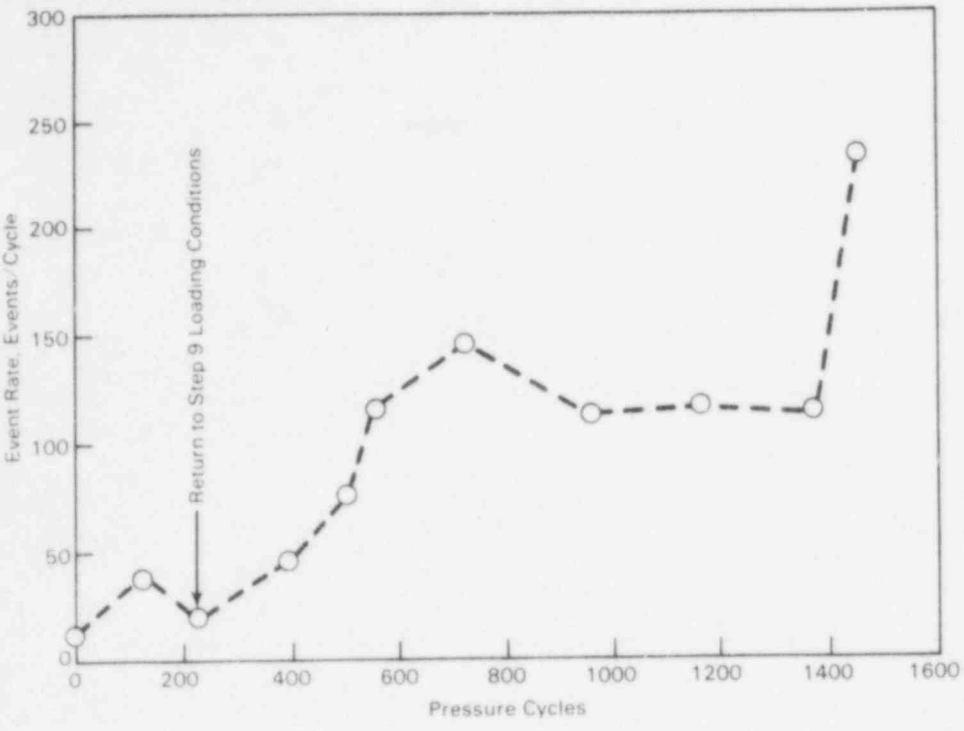

Figure 4.131. AE Event Rate Versus Pressure Cycles for KS07R Flaw, Step 11.

4.4.4 Summary

The dominant sources of acoustic emission during the high temperature portions of the test were manhole noise during Step 8, and KS07R weld cracking during Steps 9 and 11. Flaw growth activity from A, B, and C was detected by all arrays during Steps 8 and 9, but was overshadowed by the large amount of activity from the KS07R weldment during Step 11. In the hot phase of the test, Array 3 was most effective at detecting and locating activity from the KS07R weld cracking and least effective at detecting events from Flaws A, B, and C under the given circumstances. Overall, Array 3 (cylindrical array) performed better than Arrays 1 and 2 (quad arrays). The latter two showed a pronounced tendency to mislocate data originating outside of the array to show it inside the array. This was not the case with Array 3. The amplitude and load position characteristics of the AE signals from Flaws A, B, and C were similar to signals detected during 65°C testing. Signal attributes for events from the KS07R weld cracks were different than for Flaws A, B, and C. The difference in signal amplitudes was probably in part due to the large source-to-sensor distance. The substantially higher event rates from the KS07R weld cracks may have resulted from differences in material chemistry, heat treatment, and flaw geometry.

4.5 AE/FLAW GROWTH INTERPRETATION

4.5.1 Crack Growth of Flaws A, B, and C

The growth of the three machined defects was estimated during the test by several nondestructive inspection techniques. Ultrasonic and magnetic particle inspections were performed periodically to measure crack depth and surface length, respectively. In addition, crack-opening-displacement (COD) gauges were attached to each notch to measure crack-mouth-opening at the center of the notch. These measurements were taken primarily for correlation with post-test fractographic measurements of crack depth. Periodically during the test the "compliance" of each flaw was determined by measuring the slope of the COD versus pressure curve. Compliance values were obtained from the following relationship:

$$C = \frac{\delta}{P} \frac{E}{t}$$

where C is the dimensionless compliance, δ/P is the slope of the COD versus pressure curve, E is the elastic modulus (corrected for temperature variations), and t is the vessel wall thickness. The results of these measurements are plotted in Figures 4.132-4.134. An end of test compliance measurement was not obtained for Flaw A since its COD gauge was irrepairably damaged part way

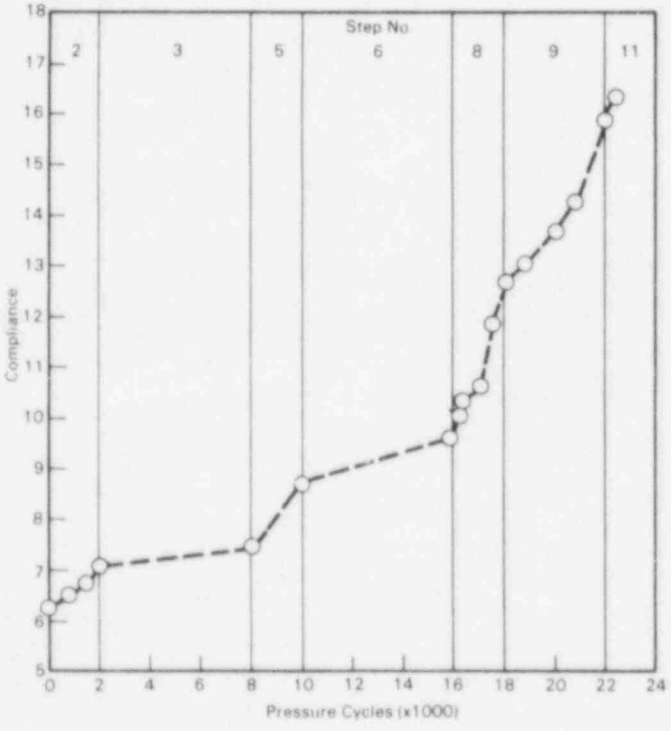

Figure 4.132. Flaw A Compliance Versus Pressure Cycles.

Figure 4.133. Flaw B Compliance Versus Pressure Cycles.

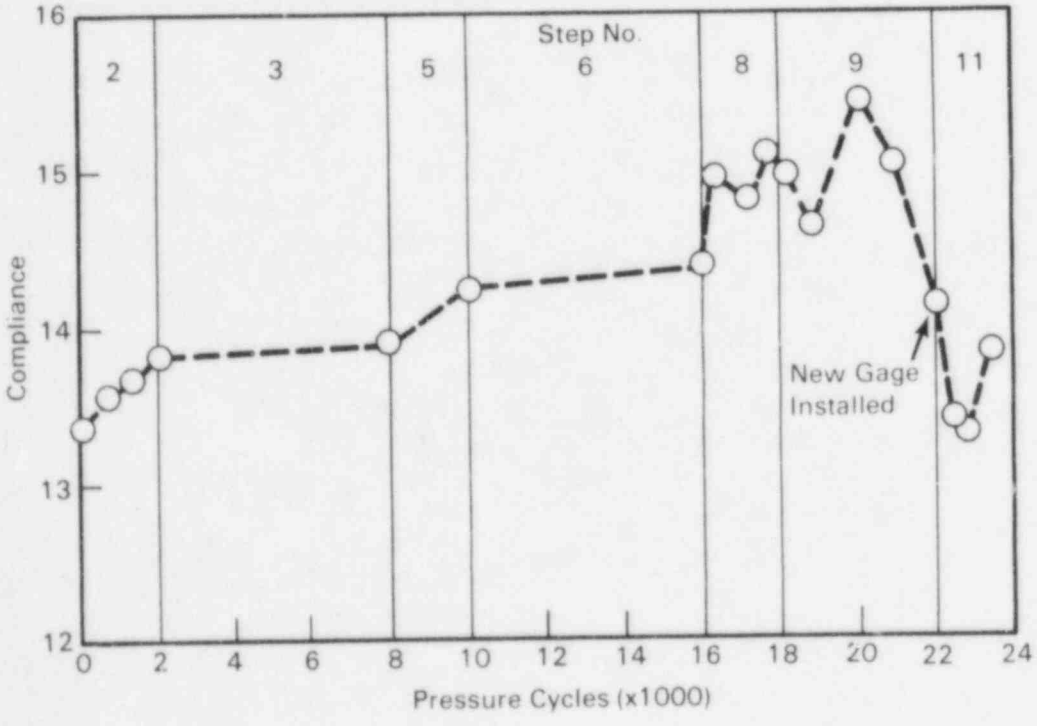

Figure 4.134. Flaw C Compliance Versus Pressure Cycles.

through Step 11. Compliance readings for Flaw C were erratic during Steps 8 and 9, so the gauge was replaced for Step 11. This change may account for the lower compliance values measured during Step 11.

To aid the fractographic determination of crack depth, the test sequence was designed to produce fracture surfaces consisting of alternating bands of low and high R-ratio fatigue crack growth. In principle, the different R-ratio bands should be optically distinguishable because of differing crack growth rates (thereby producing variable surface roughness) at each loading condition. Thus, post-test examination of the fracture surfaces should reveal the boundaries between different segments of the test.

Corrosion of the fracture surfaces from exposure to high temperature water obscured some of the fractographic detail (see Figures 4.135-4.137). Therefore, not all of the boundaries between loading blocks were readily distinguishable. Table 4.3 gives crack depth values at the end of each loading step for which measurements could be made. (Some of the fracture surface measurements were made by MPA, Stuttgart.)

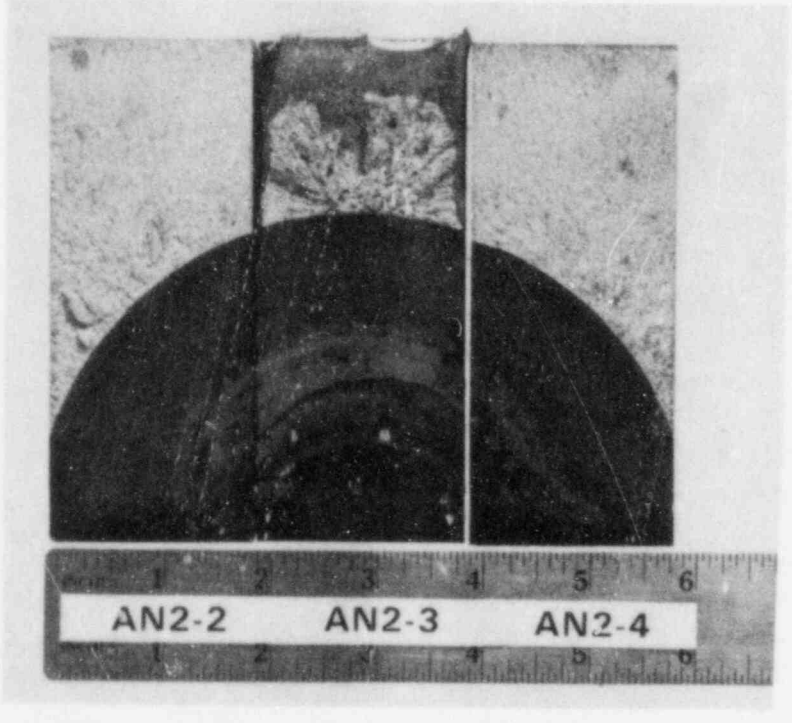

Figure 4.135. Fracture Surface for Flaw A.

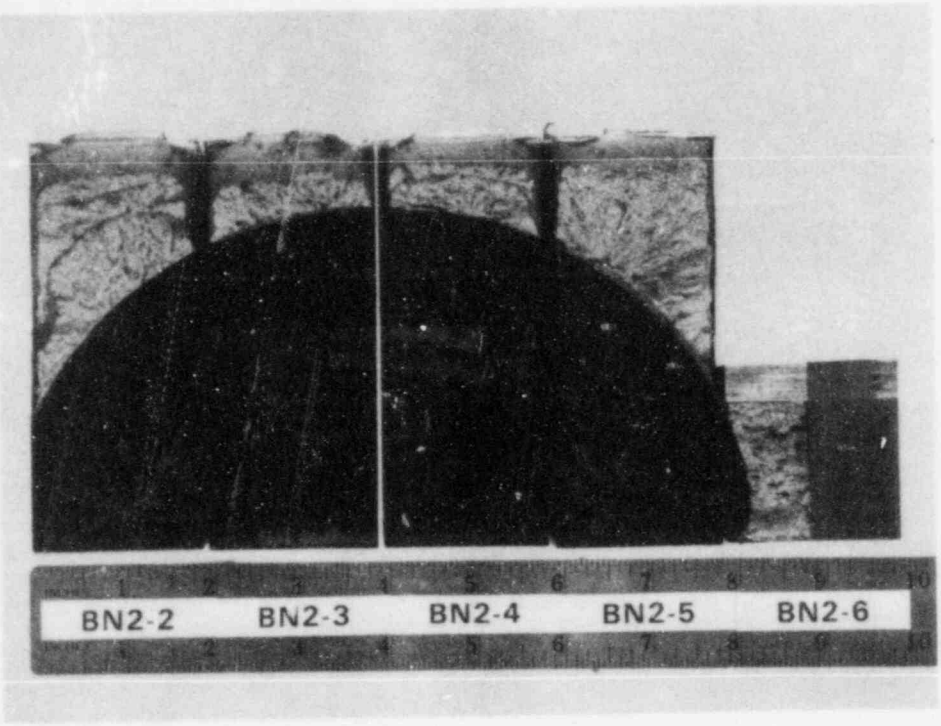

Figure 4.136. Fracture Surface for Flaw B.

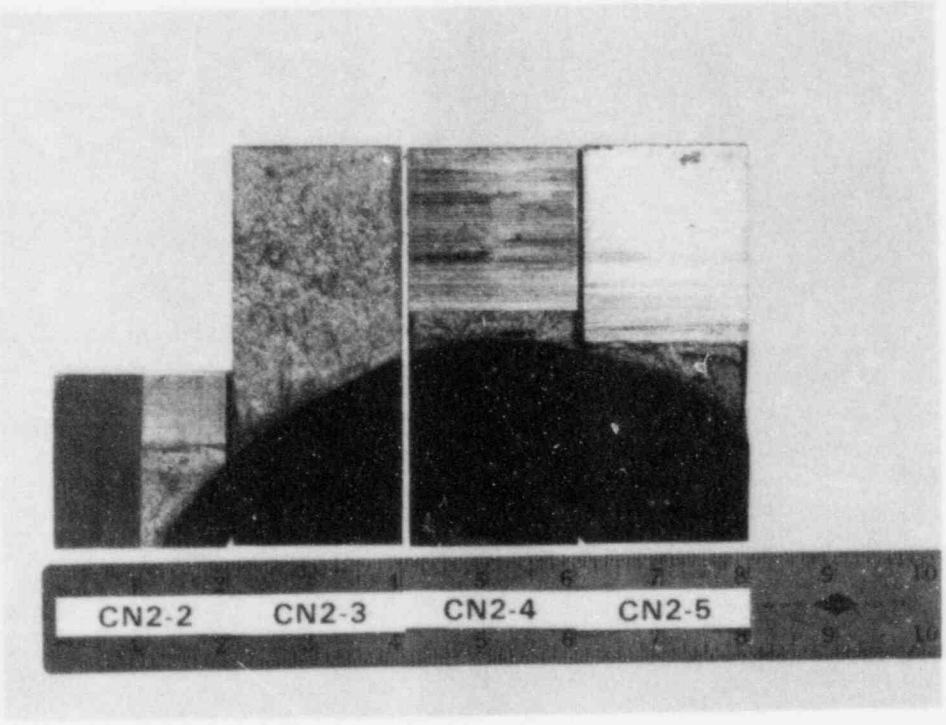

Figure 4.137. Fracture Surface for Flaw C.

Table 4.3. Crack Depth and Surface Length Estimates for Flaws A, B, and C.

Step No.	Pressure Cycles	FLAW A a FS	a NDE	a COD	2c NDE	FLAW B a FS	a NDE	a COD	2c NDE	FLAW C a FS	a NDE	a COD	2c NDE
1	0	1.20	1.20	1.20	2.40	1.63	1.63	1.63	3.32	2.20	2.20	2.20	7.48
2	2000	-	1.50	1.38	-	-	1.75	1.83	-	-	2.25	2.25	-
3	8000	-	-	1.46	-	-	-	1.97	-	-	-	2.26	-
5	10000	1.84	-	1.76	-	2.37	-	2.39	-	2.29	-	2.29	-
	11600	-	1.68	-	3.94	-	2.24	-	5.51	-	-	-	7.48
6	16000	1.95 1.90*	-	1.95	-	2.58 2.54*	-	2.58	-	2.31	-	2.31	-
	17200	-	2.03	2.06	5.04	-	2.45	2.86	7.24	-	2.28	-	7.48
8	18000	2.15*	-	2.28	-	2.83*	-	3.07	-	-	-	-	-
	21130	-	2.63	2.45	-	-	3.24	3.30	-	-	2.28	-	-
9	22000	2.77*	-	2.63	-	3.48*	-	3.41	-	-	-	-	-
	22400	-	-	-	5.47	-	-	-	7.76	-	-	-	7.48
11	23348	3.09 3.10*	2.91	-	5.95	3.90 3.87*	3.74	3.90	8.13	2.37 2.36*	2.15	-	7.48

NOTES: All dimensions are in inches.

a = Flaw depth
2c = Flaw surface length
FS = Fracture surface measurement
NDE = Ultrasonic or magnetic particle inspection measurement
COD = Crack-opening-displacement estimate
* = Measurements made by MPA, Stuttgart

COD measurements should also provide a measure of flaw depth if the crack aspect ratio remains nearly constant. For Flaws A and B this requirement was satisfied. An aspect ratio of about 0.5 was maintained throughout the test. The fracture surface measurements were used to "calibrate" the COD readings so that intermediate flaw depths could be determined by interpolation. These numbers were compared with the periodic ultrasonic inspection results as an additional check (see Table 4.3).

From the crack depth estimates the rate of crack growth was determined for each flaw. These numbers were used to test the flaw evaluation model (see Section 4.5.3). Crack growth rates plotted against the stress intensity factor range are given in Figure 4.138 for Flaws A and B. This information was used to estimate a crack growth versus pressure cycles curve for the KS07R flaw (see Section 4.5.2).

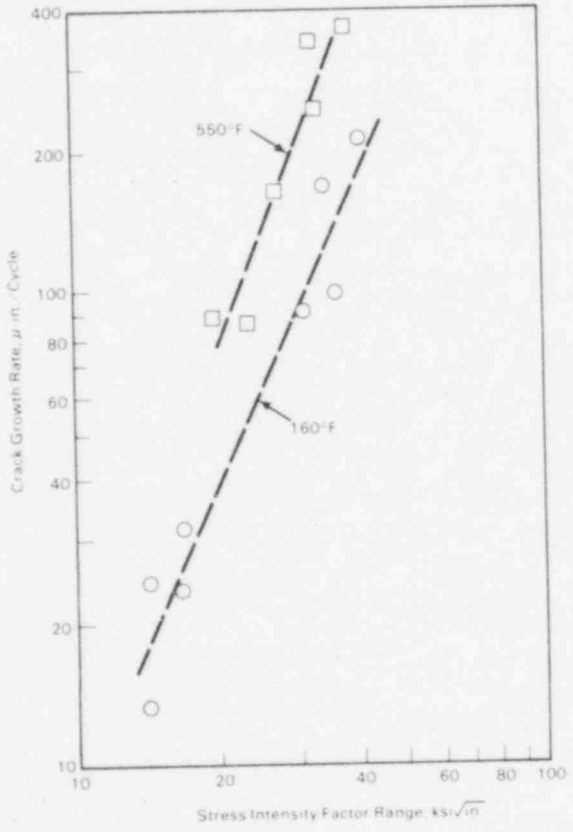

Figure 4.138. Crack Growth Rate Versus Stress Intensity Factor Range for Flaws A and B.

4.5.2 Crack Growth of KS07R Flaw

The presence of the flaw in the KS07R insert weld was first positively identified by AE during Step 9 of the test. It was subsequently determined by magnetic particle inspection that the flaw extended around the entire perimeter of the KS07R replacement patch. Figure 4.139 gives photographs of various regions of the cracked weldment after test completion. Figure 4.140 shows the locations where the photographs in Figure 4.139 were taken. Both sides of the longitudinal and circumferential weld heat-affected-zones were cracked. In addition, cracks transverse to the direction of weld metal deposition were also commonly found.

Attempts were made to characterize the depth of cracking using ultrasonic, potential drop, and drill-hole methods of measurement. Figure 4.141 summarizes the results from these measurements. The cracks were deepest on the upper longitudinal insert-to-vessel weld (viewed from inside the vessel). In this area, the cracks were typically between 0.8 in. (20 mm) and 1.6 in. (40 mm) deep. The cracks on the lower longitudinal and circumferential welds were between 0.4 in. (10 mm) and 0.8 in. (20 mm) deep. Core samples were removed in three locations (see Figure 4.142) to determine the nature of the cracking and verify the NDE measurements. Table 4.4 gives crack depths determined from both NDE and destructive measurements.

Table 4.4. Core Sample Crack Depth Measurements

Core Sample	Crack Depth, in.	
	NDE	Destructive
B1	0.98-1.20	1.15
B2	0.32-0.43	0.49
B3	0.39	0.29

Note that cracks parallel to the circumferential weld (core B3) were not as deep as cracks parallel to the longitudinal welds (cores B1 and B2).

Fracture surface examination of a crack in core B1 (see Figure 4.143) indicates that the crack was probably formed during patch-to-vessel welding and was about 0.2 inch (5.0 mm) deep before the test was begun. Cracks in the circumferential welds probably did not grow significantly by fatigue since they were parallel to the hoop stress. Metallographic sections from cores B2 and B3 indicated that the cracks originated in the weld heat-affected-zone (HAZ) or at surface defects and irregularities (see Figures 4.144-4.146). Knoop hardness measurements

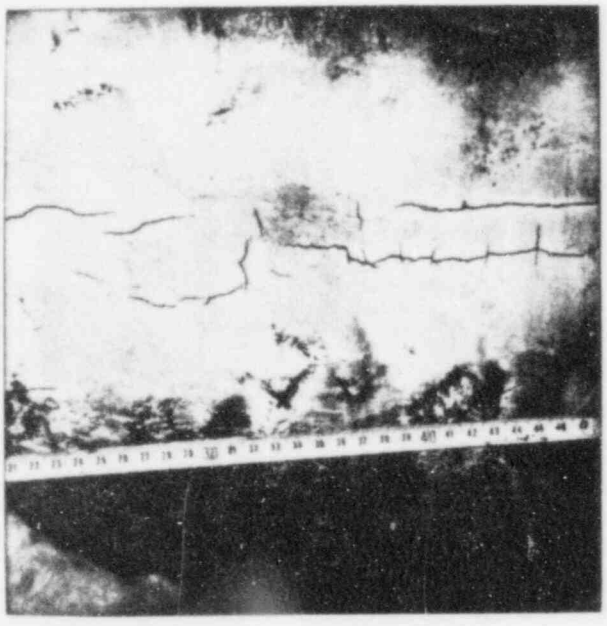

Foto 1

Foto 2

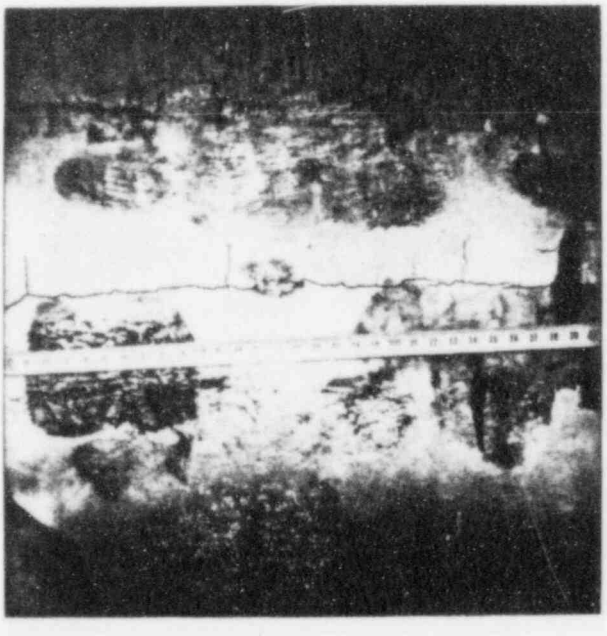

Foto 3

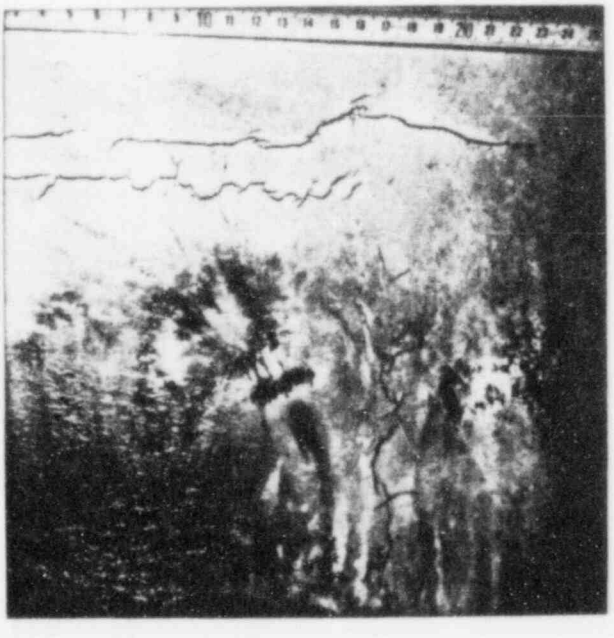

Foto 4

Figure 4.139. Cracks in KS07R Replacement Patch Welds.

Foto 5

Figure 4.139 (cont'd)

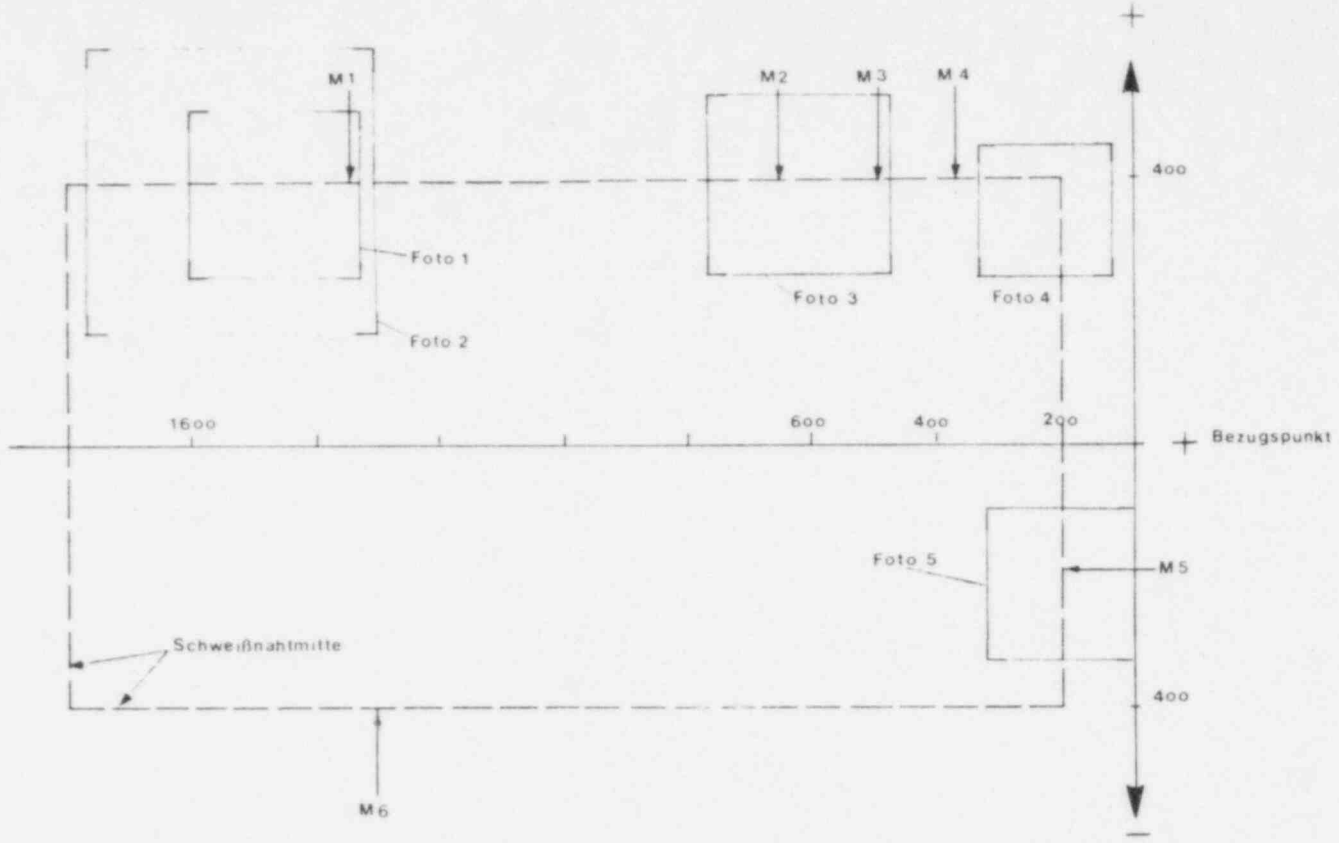

Rheinisch-Westfälischer TÜV
Zentralabteilung Zerstörungsfreie Prüfung

Rheinisch-Westfälischer Technischer Überwachungs-Verein e.V.
Anlage 4 zum Bericht vom 3.1083
Prüf.-Nr. 28/104220

M1 ... M6 = Meßpunkte

Lage der Meßpunkte an der Schweißnaht des Austauschsegmentes
Ansicht von innen

Werkstoff des Austauschsegmentes: 20 Mn Mo Ni 5 5

Figure 4.140. Location of Photographs Inside ZB-1 Vessel Showing KS07R Weld Cracking.

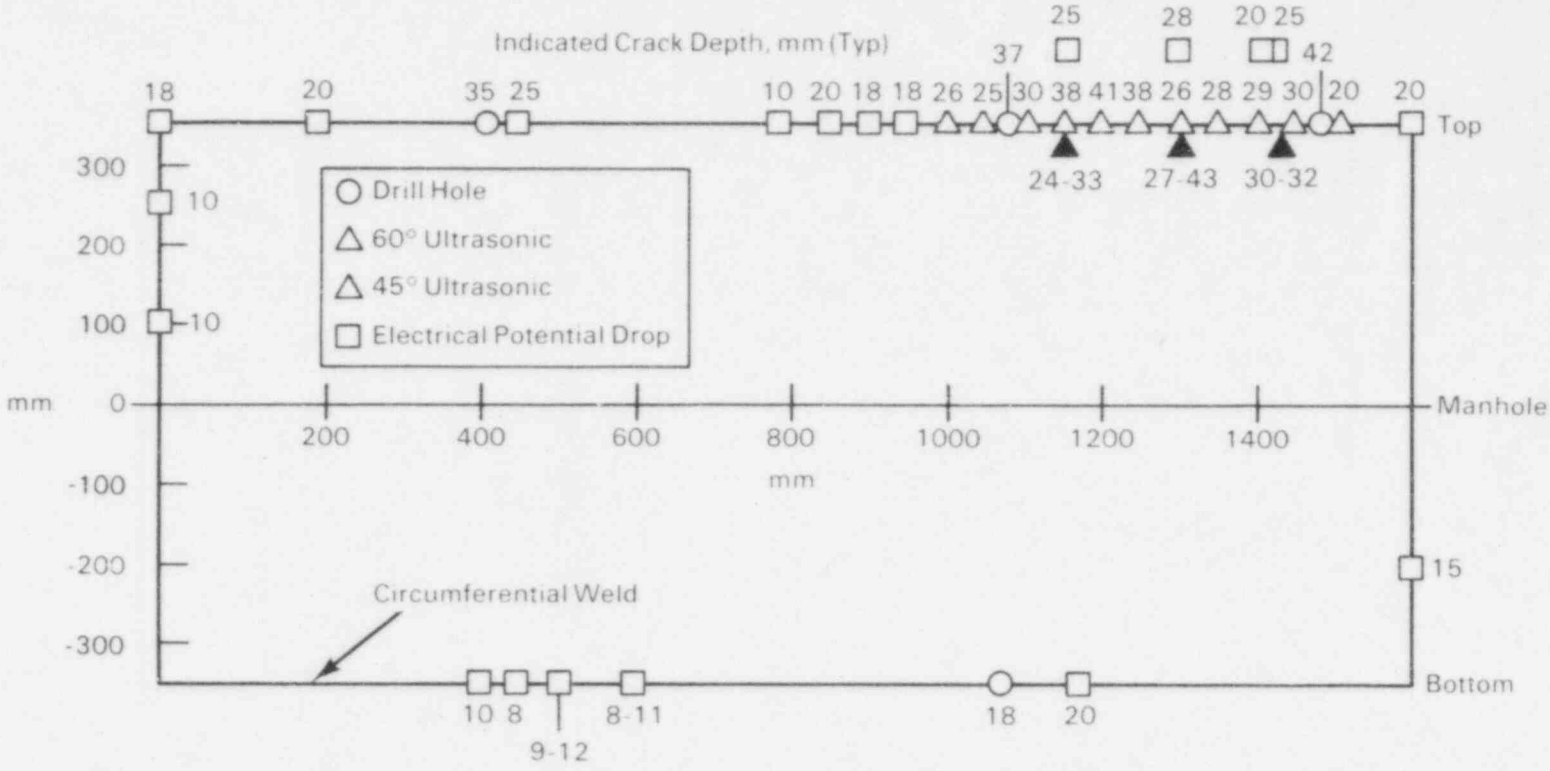

Figure 4.141. Crack Depth Measurements on Patch 53 After Step 11, Viewed from the Inside. Summary of all inspections done after Step 11 by different labs.

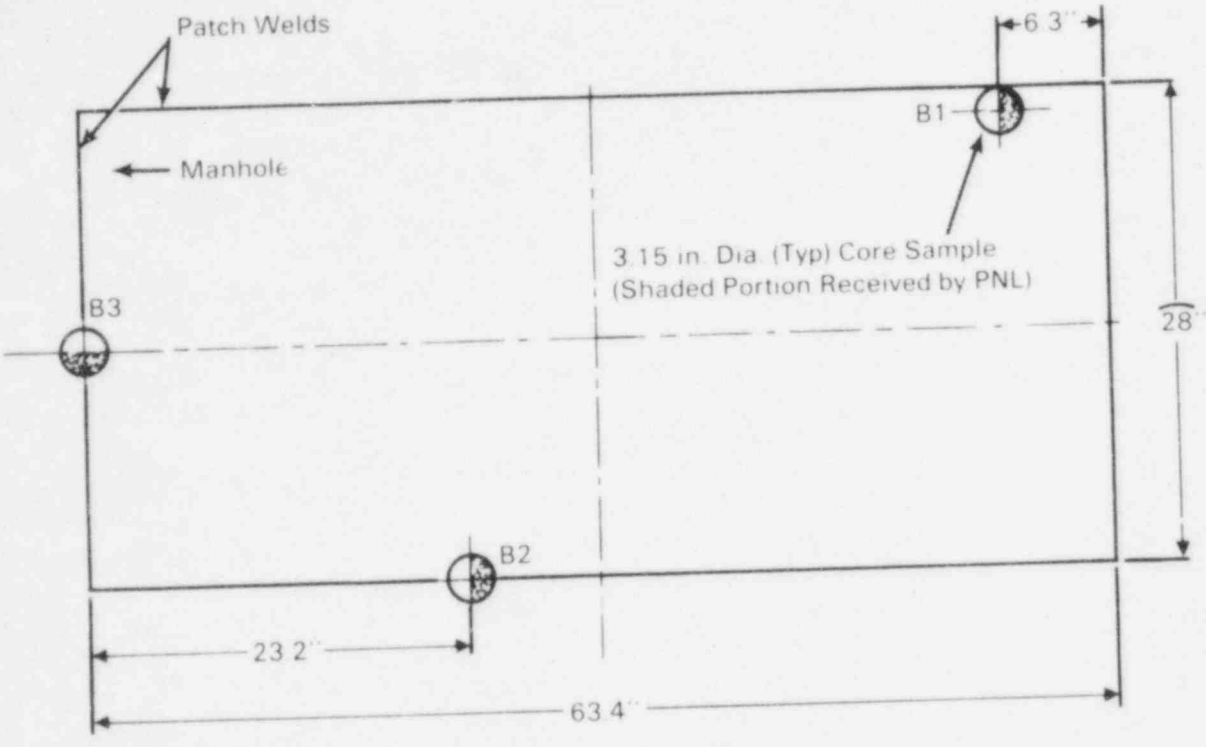

Figure 4.142. KS07 Replacement Patch Boundaries Viewed from Inside ZB-1 Vessel.

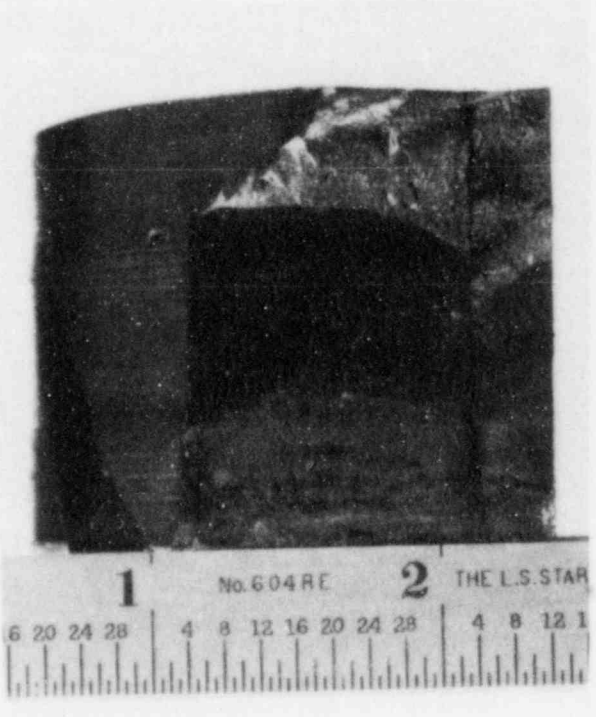

Figure 4.143. Fracture Surface of KS07R Weld Crack from Core B1.

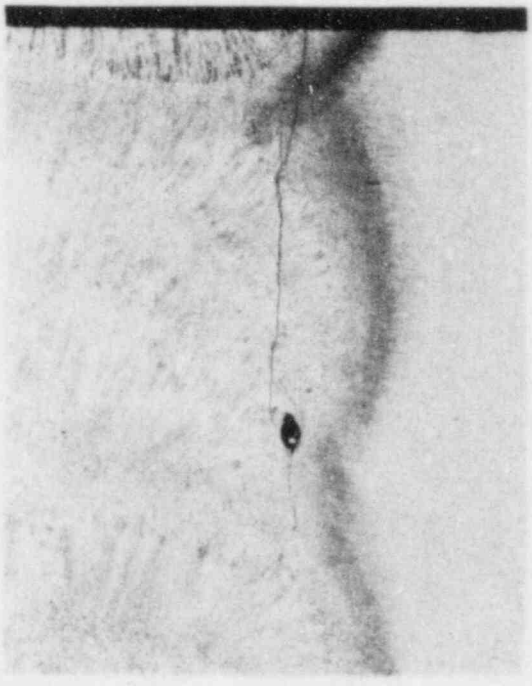

Figure 4.144. Metallographic Section from Core B2. Crack is parallel to the longitudinal weld and is about 0.49 in. deep.

Figure 4.145. Metallographic Section from Core B2. Crack is perpendicular to longitudinal weld and is about 0.22 in. deep.

Figure 4.146. Metallographic Section from Core B3. Crack is parallel to circumferential weld and is about 0.29 in. deep.

were made of the base metal, HAZ and weld metal for the cracks shown in Figures 4.144 and 4.146. The results indicated that the crack initiation sites were 10 to 20 percent harder than the surrounding material.

A fatigue crack growth analysis was performed for the deepest crack in the upper longitudinal weld. It was assumed that this flaw was a uniform depth of 0.16 in. (4 mm) and 63 in. (1600 mm) long at the beginning of the test. Crack growth rates at various stages in the test were calculated from the data given in Figure 4.138 for Flaws A and B. Figure 4.147 gives the crack depth versus pressure cycles curve for this hypothetical flaw. Along with the postulated crack depths shown in Figure 4.147 are fracture surface measurements of crack depth from specimen B1 (see Figure 4.143). Considering the approximate nature of the crack growth calculations and the nonstatistical fracture surface measurements, the two sets of numbers are in reasonable agreement.

4.5.3 Flaw Severity Evaluations

One of the principal objectives of this test was to evaluate the ability of a laboratory developed AE/flaw severity relationship to determine the crack growth rate of flaws in a large scale structure.

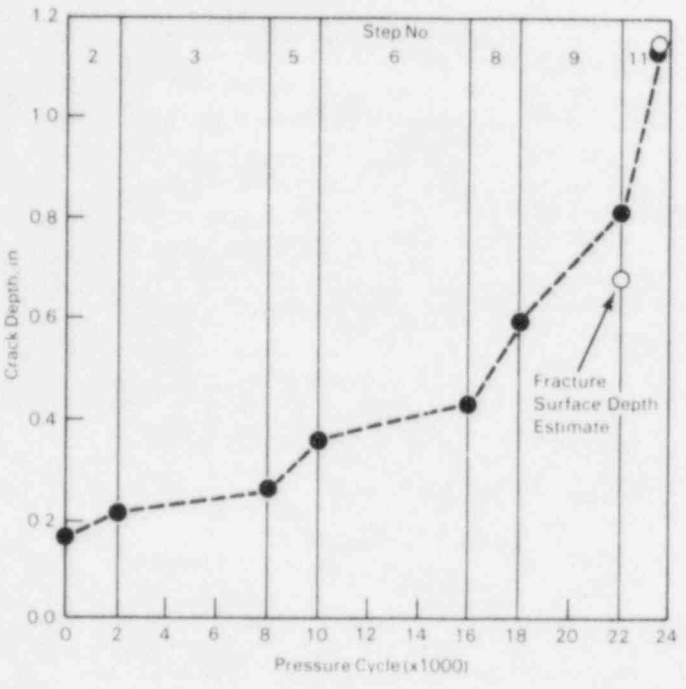

Figure 4.147. Postulated Crack Depth Versus Pressure Cycles for KS07R Weld Flaw.

To test the flaw severity relationship, AE data acquired by Arrays 2 and 3 were utilized. Array 2 consisted of sensors attached to metal waveguides that were threaded into small holes located near Flaws A, B, and C. Array 2 was intended to focus on Flaws A, B, and C. Array 3 consisted of the same type of sensors, pressure coupled and located to monitor the entire cylindrical portion of the vessel. Most of the Array 3 sensors were remote from Flaws A, B, and C. The AE data detected by each array was filtered with respect to source location, load position, and signal amplitude. Table 4.5 gives the load position and signal amplitude filters that were employed.

Table 4.5. Flaw Severity Filtering Parameters

Array	Amplitude Range, volts	Load Position Range
2	8-10	65-80
3	2-10	65-80

The number of AE events detected for each flaw during the various cyclic loading steps is given in Figure 4.148. In all instances, except one, the array nearest the flaws (Array 2) detected more

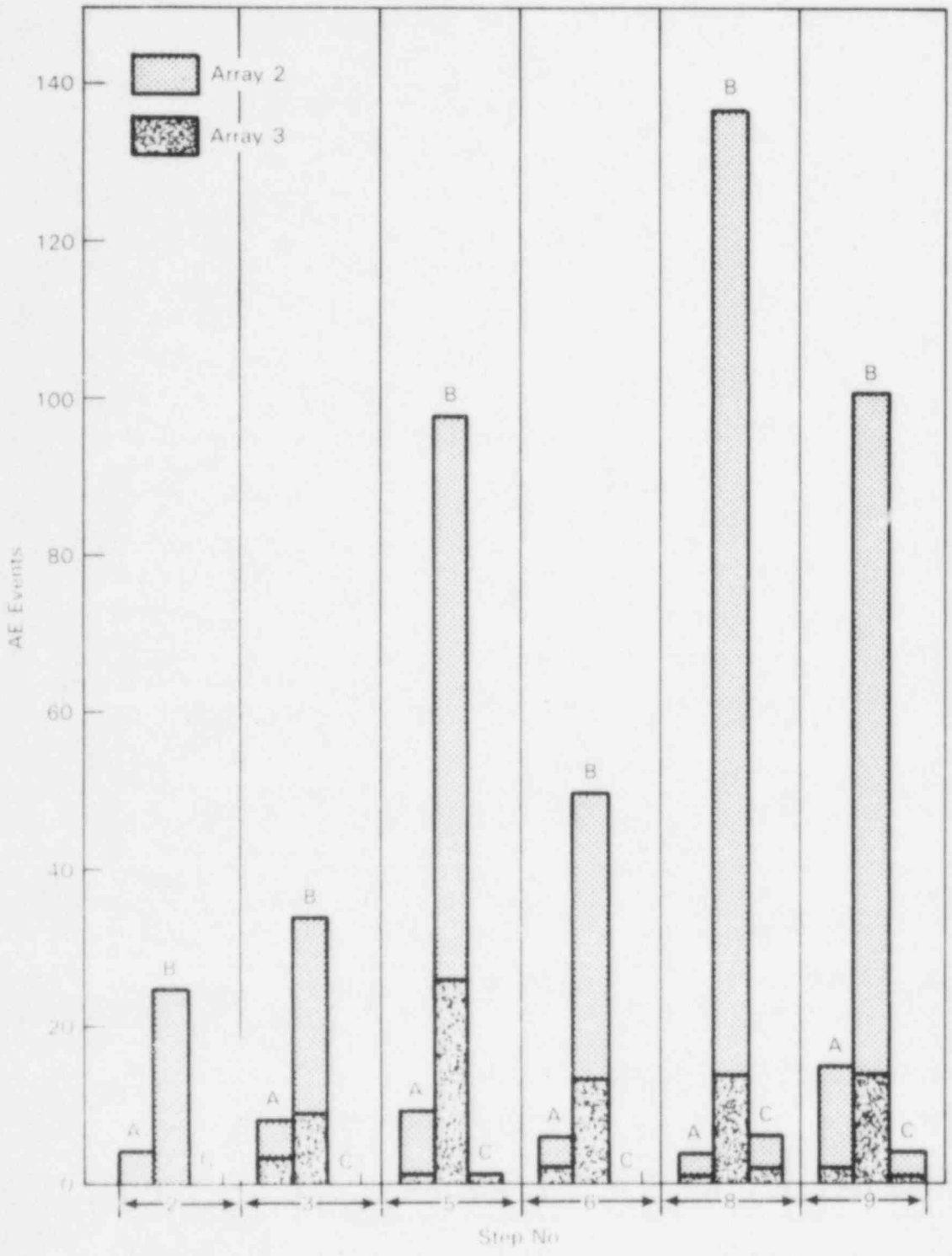

Figure 4.148. Number of AE Events Detected from Each Flaw Versus Cyclic Loading Step for Arrays 2 and 3, Filtered with Respect to Signal Amplitude and Load Position (see Table 4.5).

AE events than the array farther away (Array 3). It should be noted that Array 3 was not at peak sensitivity until loading Step 6 (Array 3 was strapped down at this point). Also, AE signals had to be detected at a distance of about 10 feet (3 meters) in order to be validated by Array 3. Both arrays detected many more events from Flaw B than from the other two flaws. No notable AE was detected by either array from Flaw C, but then this flaw grew very slowly throughout the test. This result suggests a threshold crack growth rate for reliable AE detection. Typically, less than 20 events were detected by Array 3 for each portion of the test. This underscores the need for an effective signal recognition algorithm during plant operation. Figure 4.149 gives two graphs showing the number of AE events detected from each flaw plotted against the approximate crack area increase for each loading step. These graphs show that the number of AE events produced doesn't consistently depend on the amount of crack area created. Data from both arrays shows that relatively large increases in cracked area sometimes produce substantial quantities of AE. Also small amounts of crack growth at low temperatures may be undetectable. Figure 4.150 clearly shows that the number of AE events detected per unit of crack area appears to be independent of the crack propagation rate. The primary source of AE in A533B steel during fatigue crack growth has been shown to be decohesion and fracture of nonmetallic inclusions within the plastic zone ahead of the advancing crack. This suggests that the number of AE events detected during each loading step should be related to the volume of material that the plastic zone sweeps out. Plots of AE versus plastic zone volume swept out for Flaws A and B are given in Figure 4.151. The number of events detected tended to increase with an increase in volume of deformed material. The low and high temperature data increase at roughly the same rate, but there appears to be a threshold for detection of AE at high temperature. These results are similar to the data given in Figure 4.149 in that small quantities of crack growth are difficult to detect. Based on the results given in Figure 4.152, there does not appear to be a relationship between AE per unit of plastic zone volume and the crack growth rate.

By taking the filtered AE information for each flaw, AE rate values in events/second were calculated for each of the cyclic loading steps. These data were compared with extrapolations of the laboratory developed flaw severity relationships given in Figure 4.153. The results of these comparisons are shown in Figure 4.154 for Arrays 2 and 3. The plots given in this figure show that the 65^{o}C data for both arrays generally resides below the line representing the RT laboratory data. This result is surprising and may be partially due to the difference in test temperatures, the extrapolation of the flaw severity relationship to low crack growth rates, and a possible dependency of the

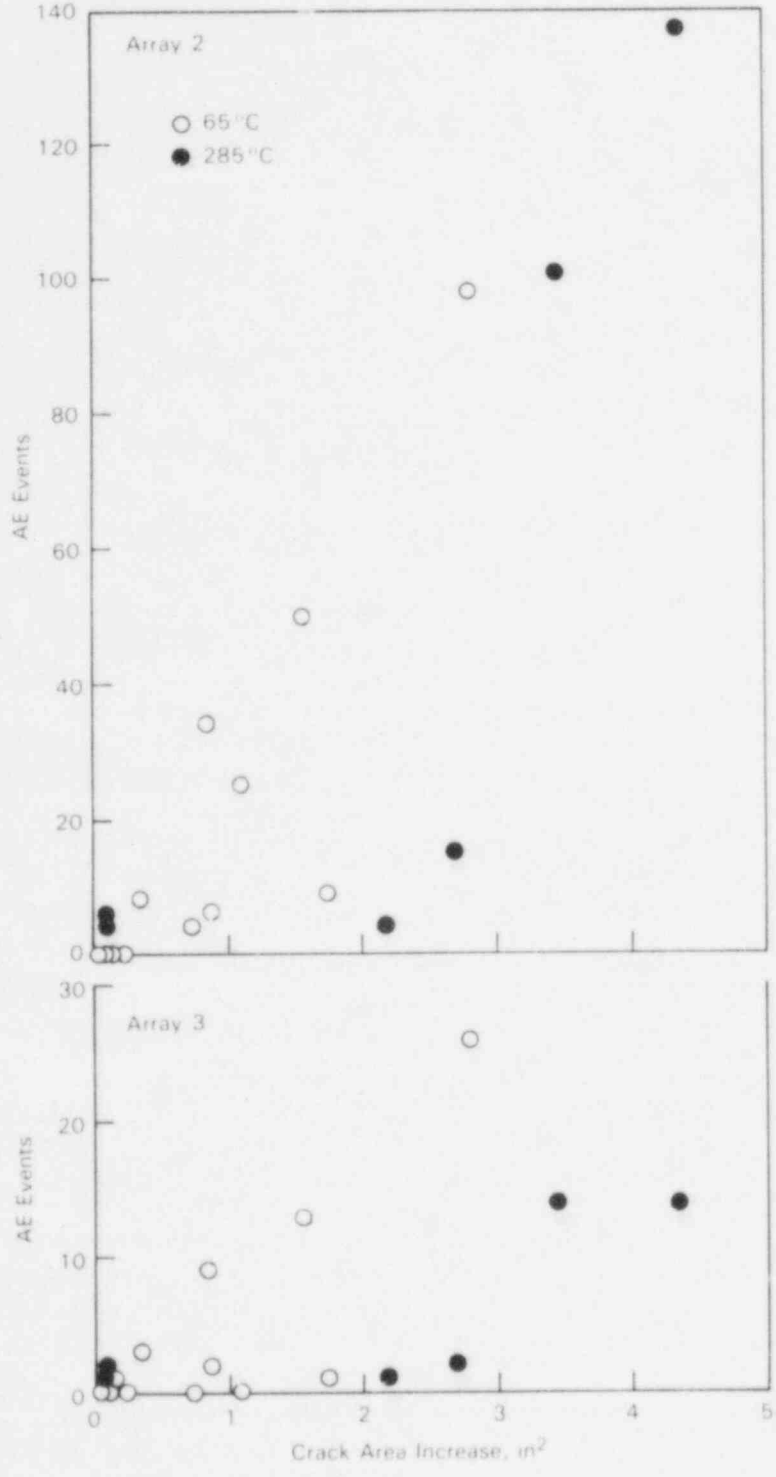

Figure 4.149. Number of AE Events Versus Crack Area Increase for Arrays 2 and 3.

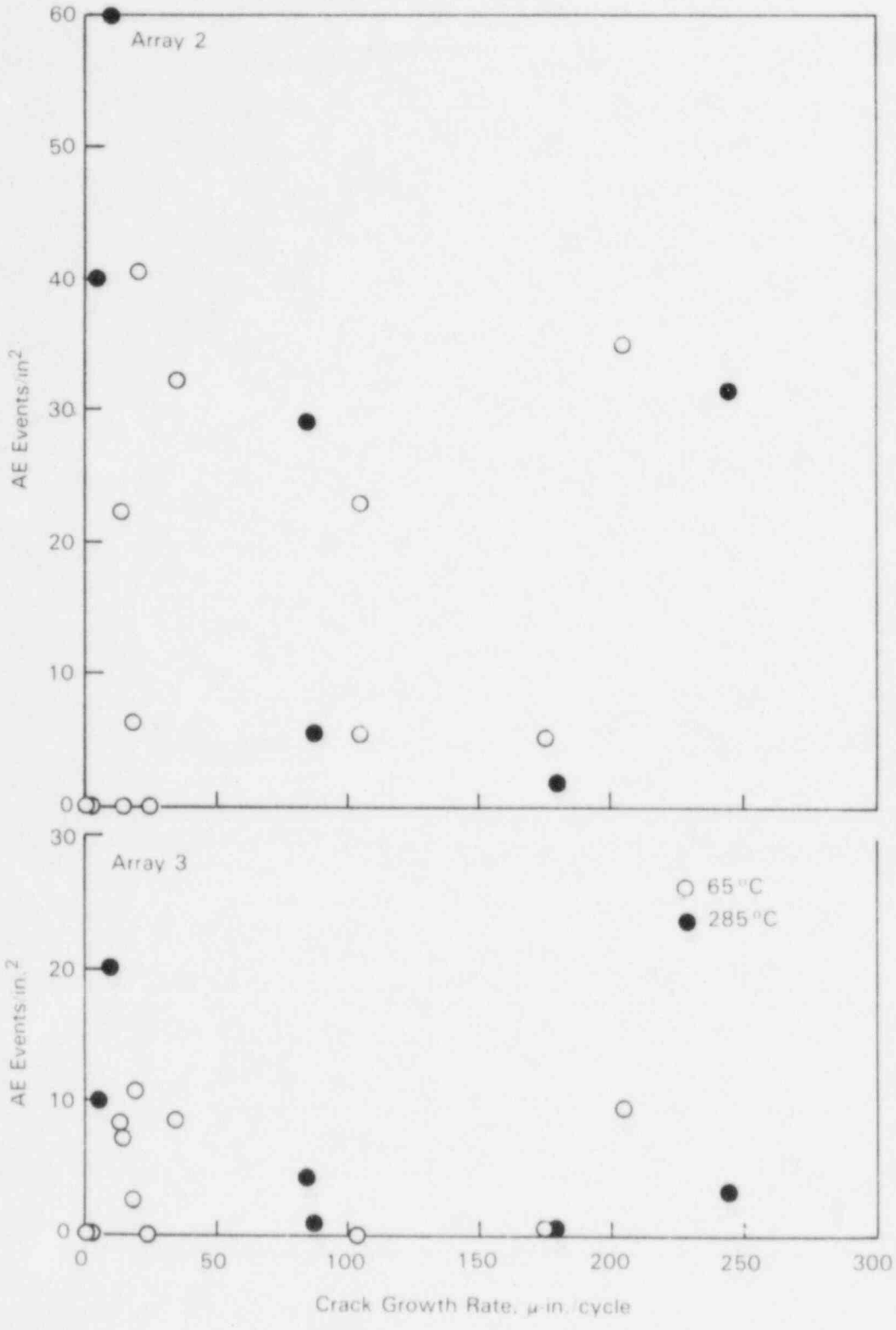

Figure 4.150. Number of AE Events/Crack Area Increase Versus Crack Growth Rate for Arrays 2 and 3.

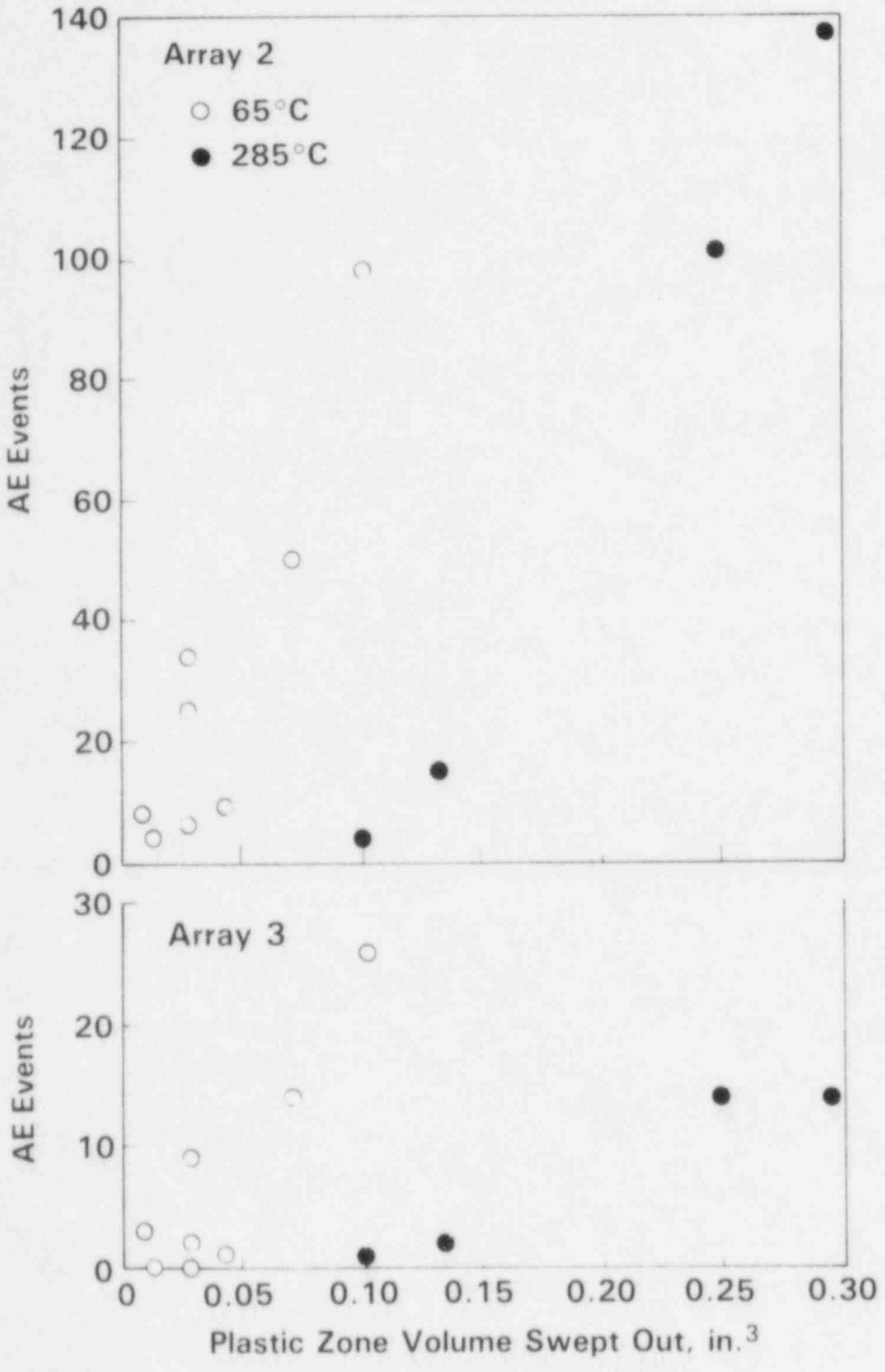

Figure 4.151. Number of AE Events Versus Plastic Zone Volume Swept Out for Arrays 2 and 3 (Flaws A and B Only).

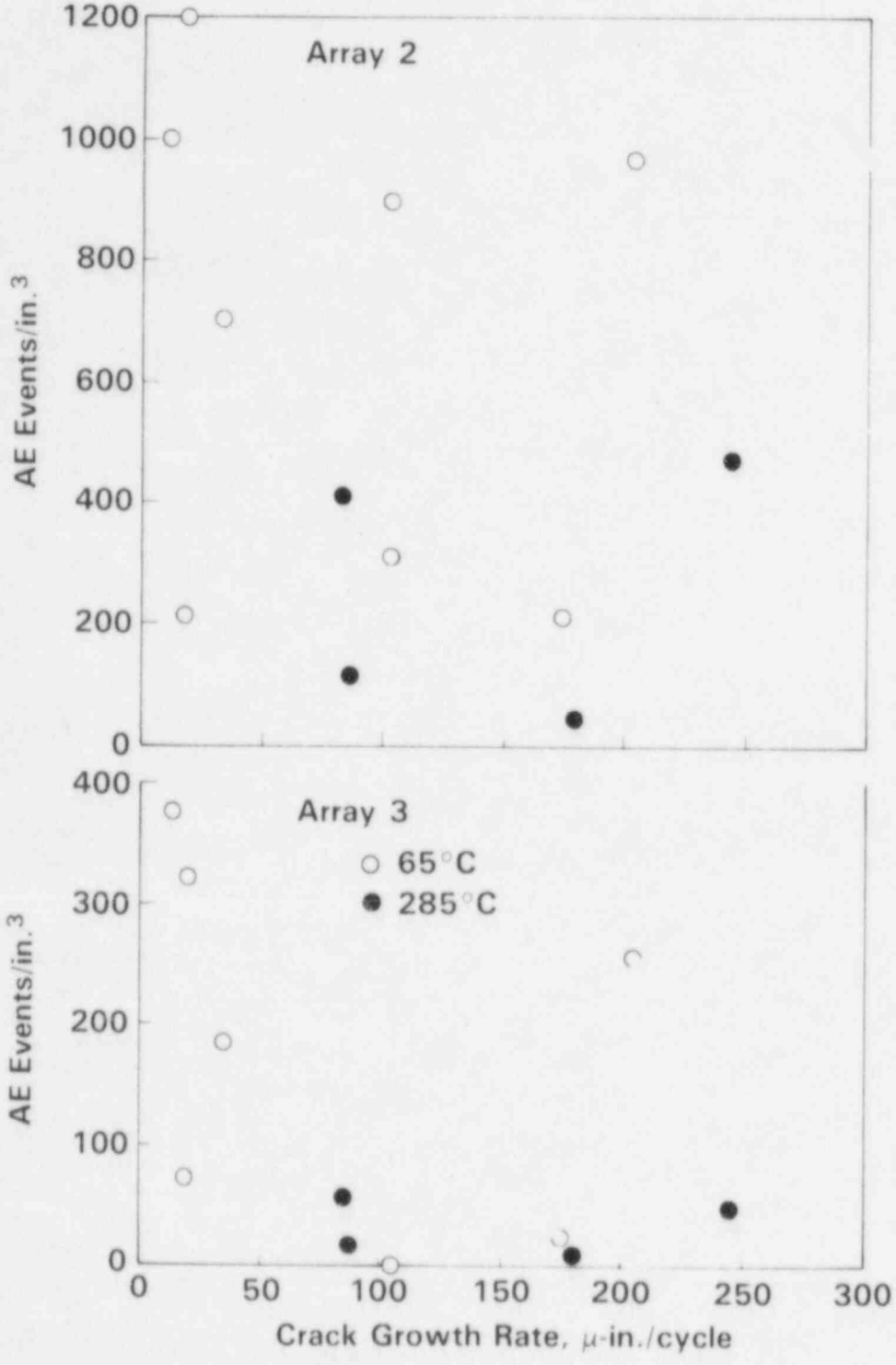

Figure 4.152. Number of AE Events/Plastic Zone Volume Swept Out Versus Crack Growth Rate for Arrays 2 and 3 (Flaws A and B Only).

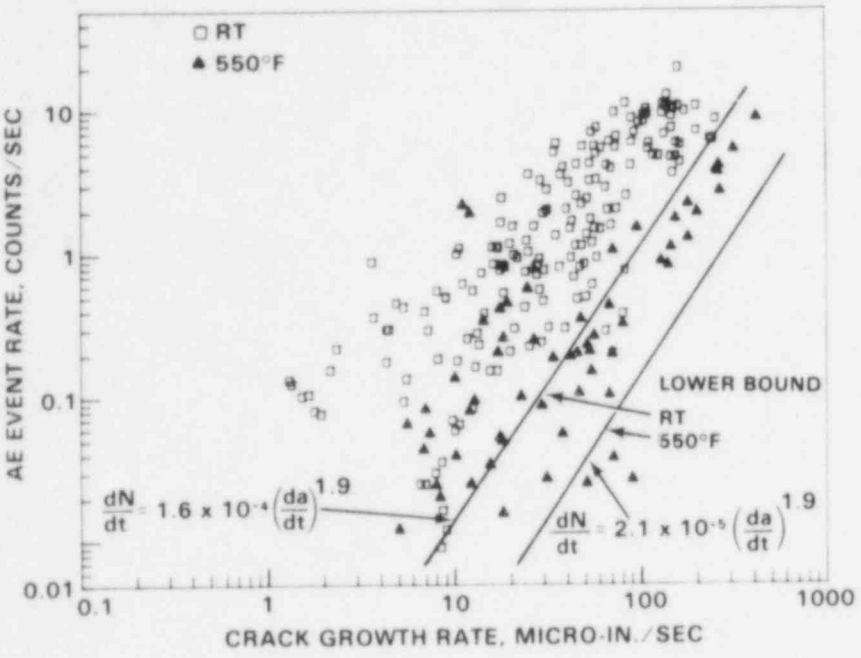

Figure 4.153. Experimental Fatigue Crack Growth/AE Data.

AE data on a cycle rate at low K-levels in a water environment. The data points on the abscissa are instances when no events were detected. These instances were associated with low crack growth rate (Flaw C) or inadequate Array 3 sensitivity. On the other hand, the Array 2 high temperature data resides above its corresponding extrapolated line, as expected. The data from Array 3 was distributed both above (4 points) and below (2 points) the 285°C lower bound line.

Another way to present the same information is to use the AE data in conjunction with the extrapolated flaw severity relationships to calculate crack growth rates. Figures 4.155 and 4.156 show graphs of crack growth rates determined from AE data plotted against crack growth rates taken from COD and fracture surface measurements. The diagonal line in the figure shows where the two crack growth rates are equivalent. The results from both arrays clearly indicate underpredicted crack growth rates for low temperature test conditions. The results for high temperature testing were mixed. When Array 2 data was used to calculate crack growth rate, a consistent overprediction was obtained (Figure 4.155). Crack growth rate predictions based on Array 3 data were equally distributed about the line of perfect agreement (Figure 4.156). The variation in the low and high temperature data from both arrays was typical of

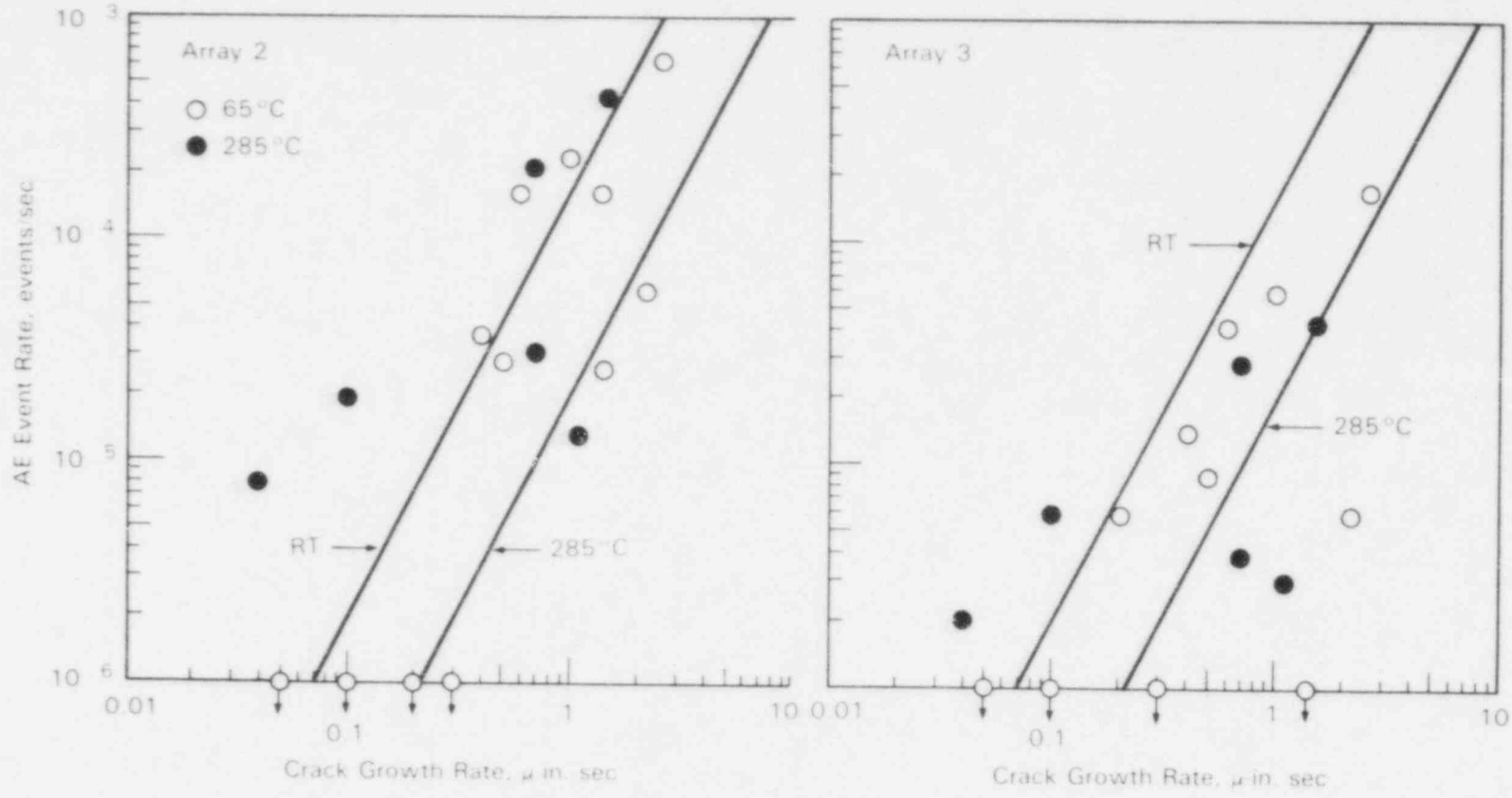

Figure 4.154. AE/Fatigue Crack Growth Rate Data from the ZB-1 Vessel, Arrays 2 and 3.

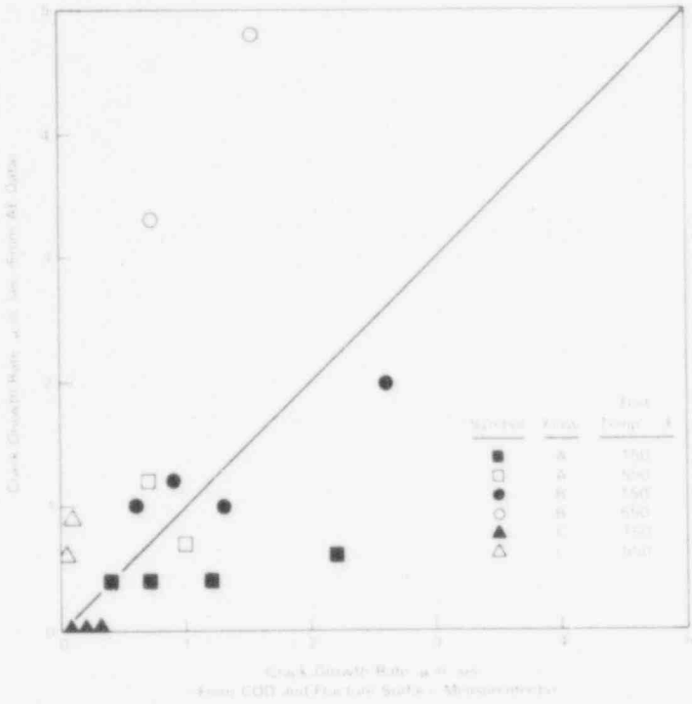

Figure 4.155. Evaluation of the AE/Flaw Severity Relationship for Array 2 Data.

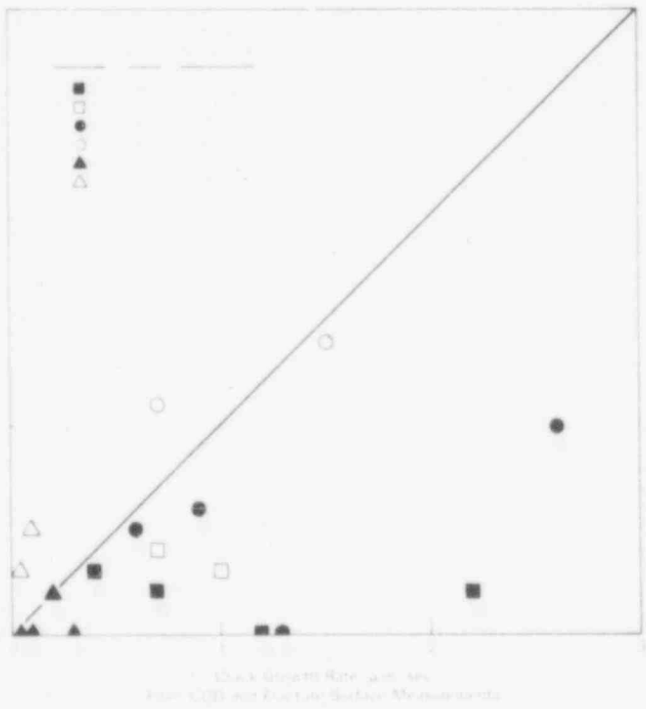

Figure 4.156. Evaluation of the AE/Flaw Severity Relationship for Array 3 Data.

laboratory test results (Figure 4.153). These data also suggest that calculated crack growth rates depend significantly on sensor sensitivity and the distance between the source and sensor.

Flaw severity estimates were also made for the KS07R flaw during Step 11 of the test. The AE data was filtered by load position between values of 65 to 80. During that step the average event rate was about 0.7 events/sec. From the relationship in Figure 4.153, this would predict a crack growth rate of about 230 micro-in./sec. The actual crack growth rate was estimated at between 1.5 and 2.2 micro-in./sec. for the deepest portion of the flaw. Thus, the flaw severity relationship greatly over estimated the crack growth rate. Section 4.4.3 gives some possible explanations for the greatly enhanced activity of this particular flaw.

4.5.4 Summary

Flaw growth characteristics for Flaws A, B, C, and KS07R weld cracking have been determined from NDE, crack-opening-displacement and fractographic measurements. This information was used to establish crack growth rates for comparison with predictions derived from the AE/flaw severity relationship. The near field array (Array 2) consistently detected more AE events than the far field array (Array 3). Both arrays failed to detect any notable AE from Flaw C at 65°C test conditions, but this was probably due to the small amount of crack growth produced by this defect. The amount of AE caused by large crack jumps varied widely, which matches experience from laboratory specimens. Detected AE could be approximately related to the volume of material swept out by the crack tip plastic zone. The high temperature data showed evidence of a threshold plastic zone volume for AE detection. The number of AE events per unit of crack area created or per unit of plastic zone volume swept out didn't depend on the crack growth rate. A test of the flaw severity relationship indicates that the model underpredicted crack growth rates at 65°C test temperature. This result was not anticipated but may not seriously impair the utility of the relationship for use at operating pressure and temperature. When the relationship was applied to 285°C data, the crack growth rate was consistently overpredicted by the near field array as was expected. The far field array results were not conservative in that the crack growth rate was underpredicted in half the cases. Clearly the source-to-sensor distance was largely responsible for this effect. The range of predicted crack growth rates were within the normal variation observed during laboratory testing. It is significant to note that the relationship tends to compensate for the wide range of absolute number of AE signals detected by the two arrays for the same two installed

flaws. A test of the relationship on the weld cracking in the KS07R replacement patch was attempted and indicated a significant overprediction of the crack growth rate. The magnitude of the overprediction was beyond our expectations based upon the laboratory data. Possible explanations for the difference in behavior were suggested in Section 4.4.3.

4.6 CRACK GROWTH AE SIGNAL IDENTIFICATION

One of the key elements of this program is to develop a method of separating AE signals produced by crack growth from acoustic signals produced by innocuous sources. Signal pattern recognition is the technique chosen for this purpose.[11] The underlying assumption in this work is that different sources of acoustic signals have different spectral characteristics. The approach taken is to use signal processing techniques to generate features related to spectral content of the signals. For instance, features from the power spectrum of the individual signal, the autocorrelation function, or statistical moments of the power spectrum of the signal itself. These features provide a reduced set of information that describes characteristics of the waveform of interest. Standard pattern recognition techniques are used to calculate decision rules for classifying the waveforms using these features.

The original set of features used in the ZB-1 test did not produce satisfactory results. Analysis using waveforms recorded on the ZB-1 test showed that it was working to separate many of the signal types but several of the more similar signal types were not being correctly identified.

A second set of features consisting of the parameters of a 10th order of autoregressive model of each waveform was developed out of this analysis. There are several potential advantages. First, they are not sensitive to waveform amplitude. They are mainly influenced by the spectral shape of the waveform, not the total amount of energy. This helps reduce the feature sensitivity to distance effects and differences in transducer gain. Second, this set of features has been successful in classifying seismic data and AE data from aluminum specimens. Third, these features can lead to a matched filter technique for classifying data that is amenable to hardware implementation. Finally, this representation of the power spectra leads to a linear model of the waveform that might be related to a model of the response function of the mechanical system.

The results using the second set of features showed improvement. The classification performance for the new features is given in Table 4.6 below. The classification of the noise data is improved about ten percent, while the crack data was about the same for both sets of features.

Table 4.6. Classification Results for Autoregressive Features

Signal Type	Percent Correctly Classified
Noise	75.7
Crack	78.5

Even though these results show improvement, they are still not acceptable. Statistical analysis has shown that a correct classification level of about 90% is needed to provide an effective working tool.

In the course of reassessing the problem, visual examination of the waveforms showed that one particular class of signal suspected of being caused by cracking was being classified as noise, while many types of apparent noise waveforms were classified as crack-produced. Waveform by waveform source location made possible the identification of a consistent three-pulse signal pattern present in practically all waveforms originating near known and suspected regions of crack growth (Figure 4.157).

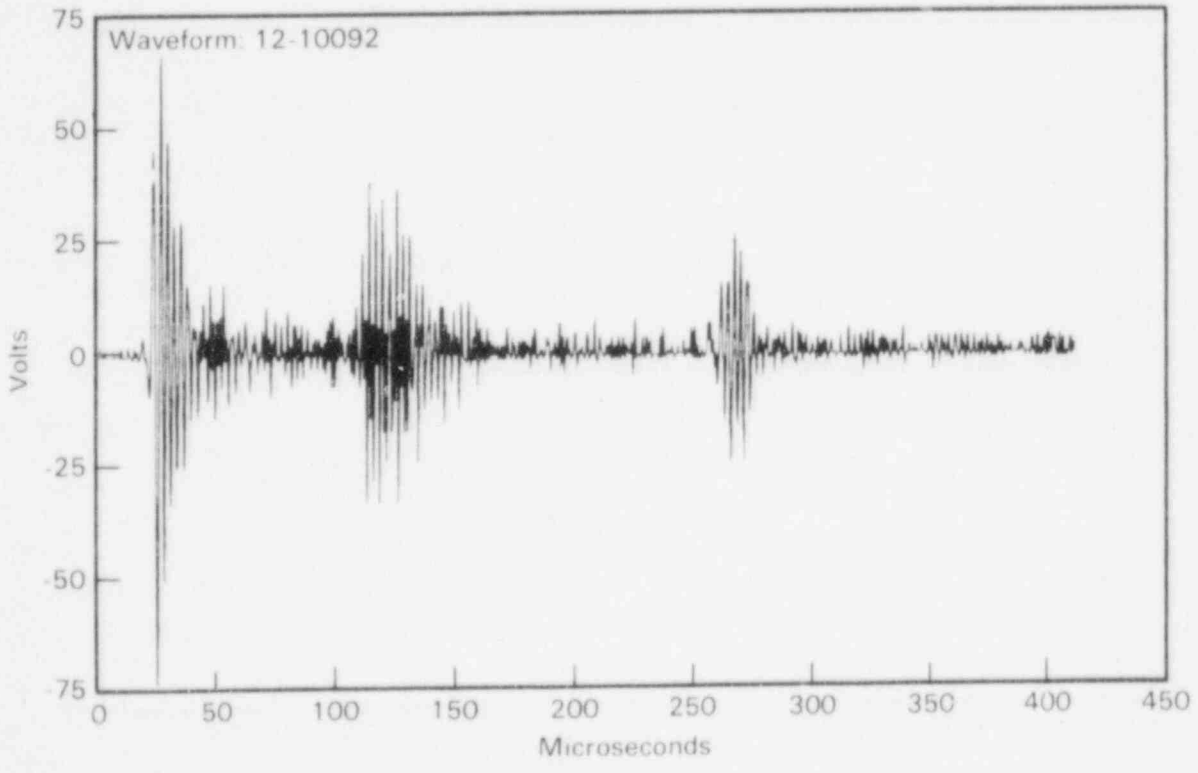

Figure 1.157. Example of Three-Pulse Waveform Produced by Crack Growth AE Signal.

The differences in pulse arrival time at the transducer are directly proportional to the length of the waveguide. Most suspected noise signals from the cold phase of ZB-1 pressure vessel testing did not show the three-pulse pattern.

It was determined experimentally that the three pulses are wave modes, traveling at different group velocities, and that separation of these wave modes takes place in the waveguide as a response to a high frequency, short duration input pulse. A short duration pulse is expected from inclusion fracture, which can occur during flaw growth, and is suspected of being the principal acoustic emission source during fracture of A533B steel. Other experiments were conducted to determine the effects of input signal frequency, source location, and waveguide coupling with the following general results:

1. Changing input pulse, frequency produces a definite beat behavior in the leading AE pulse at low frequencies.

2. It may be possible to determine source distance by wave mode separation produced in the test piece before reaching the waveguide.

3. Distinct and reproducible differences in the acoustic signal occur between sources located on the same surface as the waveguide and those on the opposite surface. This may allow identification of the surface on which the source occurred.

Work has continued on refinement of the pattern recognition method with focus on defining an implementation method for applying the technique to long-term monitoring.

From a standard cross-correlation and cross-variance with four templates representing known crack associated waveforms, the best correlation coefficient for each test signal with each template over a range of lags was found, and the resulting numbers were combined to produce a weighted linear least-squares sum computed in the statistical package ARTHUR, which is used as the discriminating feature. The cutoff least-squares result above which a signal is labelled noise and below which the signal is labelled crack was determined from a training set composed of 232 waveforms whose sources were determined through load position, source location, and visual examination. The training set contained representative waveforms from three distinct categories of crack signals, and samples of noise signals. The best cutoff value determined by ARTHUR correctly classified 97% of 226 out of 232 waveforms (95% correct using coefficients from cross-correlation alone). This breaks down to 140 of 141 crack

signals and 86 of 91 noise signals were correctly labelled. The method was then applied to 1989 waveforms from Step 5 of the ZB-1 test, of which 445 randomly chosen signals were carefully examined to check for proper classification. The test set was evaluated with the result that 212 of 219 crack-related waveforms were identified as cracks and 205 of 226 noise signals were labelled noise, giving 417 out of 445 or 94% correctly labelled signals. Two types of noise (of 1196 remaining waveforms) were labelled as cracks. The first type was composed of one or two short duration, very high bursts; and the second, low frequency (approximately 80 kHz), continuous signals. The low frequency signals contain a low amp, three-pulse burst pattern with the proper spacing. Using a filter to remove low frequency signals, the correct call percentage was increased to 97% or 417 of 430.

The same program including the screening procedure was next applied to Step 3 data, wherein a manhole located on the end of the vessel was known to be producing noise. After screening for saturation, visual examination indicated only 89% of the waveforms were classified correctly. Suspected manhole noise was being classified as crack-related despite low correlation coefficients due to a quirk of the weighting distribution used to classify the waveforms. By requiring that at least one coefficient exceed .60, 96% correct classification was achieved with minimal effect ($\approx$1%) on the classification of the Step 5 data.

Examination of waveforms taken from Watts Bar Unit 1 reactor monitoring indicate that the cross-correlation technique will be an effective discriminator on reactor data also. A calibration input is important to the field application where a variety of geometry must be accommodated.

The current implementation concept involves the following steps:

1. Digitize the signal and hold in memory.

2. Check for faulty representation; i.e., saturation, low amplitude, etc.

3. Detect wave front.

4. Perform cross-correlation; i.e., compare with wave template.

5. Classify the signal based on the cross-correlation result.

6. Store a signal identifier with the AE data.

This is a relatively slow process which would result in data sampling most of the time. The analog-to-digital conversion is the major time consuming step. Work is continuing on devising an approach to eliminate that step.

In summary, the original pattern recognition approach did not yield satisfactory results. It was performing a signal discrimination function correctly for many of the signals, but the total performance was not adequate. A modified approach which utilizes the response characteristics of the metal waveguide sensors is producing correct classification of data from the ZB-1 test at a level of about 95%. This meets the required level of accuracy for an effective working tool.

5.0 CONCLUSIONS

The ZB-1 test results provide strong support to the feasibility of flaw surveillance in reactor pressure boundaries using AE. Key points of the test results are highlighted below by topic.

5.1 MONITOR SYSTEM

The ability of an AE monitor system to perform over a long period under adverse conditions was demonstrated. Waveguide AE sensors are an effective answer to the high temperature (260-370°C) problem associated with continuous reactor monitoring. They have adequate sensitivity for detection of AE at a distance of at least 3 to 4-1/2 meters (10-15 ft.) even when tuned to about 400 kHz to control background noise plus being pressure coupled to simulate reactor installation. Achieving adequate coupling pressure, however, is vital to effective operation of the waveguide.

Although the data acquisition and analysis system developed some component problems at various times, in general it performed acceptably over the year-long period. This was in an environment of temperature and dust which was much less favorable than a reactor building.

Use of a high density cartridge tape for data storage was highly satisfactory. Three cartridges accommodated the data from the entire test except for digitized waveform recordings.

5.2 FLAW DETECTION

Generally, detection of AE from growing flaws was good at all stages of the test. One of the major achievements was detection of an unexpected crack growing in the KS07 replacement weld. This was clearly detected by AE well before it was confirmed by ultrasonics. Some of the AE sensors were 3 meters from the source.

Through the use of a flow noise simulator on the ZB-1 vessel and separate information from reactor monitoring, the capability to manage the flow noise problem and still detect AE was demonstrated. Information from the two sources was consistent.

One category of cracking that was not identified by the AE monitor system involved cracks growing radially from the bore of capped off nozzles on the vessel. The cracks were in the longitudinal plane of the vessel. It appears that failure to identify this cracking by AE was a problem of geometry wherein the nozzle bore and/or Flaw C acted to obstruct direct signal

propagation to one or more of the array sensors. This would result in the signal being classed as unlocated.

Little success was achieved in resolving potential affects of slag inclusions and cladding anomolies on crack growth AE identification. The slag inclusion was very small and attempts to install underclad cracking and an area of poor clad-to-base metal bond were unsuccessful.

5.3 AE SIGNAL IDENTIFICATION

Analysis of the test data to identify AE signals from crack growth has underscored the need for a method to isolate crack growth AE signals in real time. The parametric filtering method used in test data analysis is not suitable for reactor monitoring. The pattern recognition algorithms applied for this purpose during the test performed discrimination correctly for many of the signals, but the overall performance was not acceptable. Post test analysis of recorded waveforms has, however, produced a modified approach which achieves a correct classification level greater than 90% for the ZB-1 data. It now remains to implement the method in hardware to test the performance in a sequential signal analysis mode.

5.4 FLAW EVALUATION

A test of the flaw evaluation model using data obtained by Array 2 was performed. (A similar test using Array 3 data is planned.) The relationship underpredicted the crack growth rate at 65°C (150°F) test temperature and overpredicted the crack growth rate at 285°C (550°F) test conditions. The high temperature results were within the expected range based upon the observed variations in laboratory data. The low temperature results were below the expected range. This may be due to a change in the power-law relationship at low crack growth rates and/or that the relationship based on 20°C (70°F) data should be corrected for use on 65°C (150°F) data.

A test of the relationship on weld cracking in the KS07R replacement patch using Array 3 data was attempted and indicated a significant overprediction of the crack growth rate. The magnitude of the overprediction was beyond our expectations based on laboratory data. This result may have been due to differences in material chemistry, heat treatment, and flaw geometry.

5.5 HYDROSTATIC TEST MONITORING

Results from the hydrostatic tests lead to three conclusions.

- For preservice hydro testing to detect flaws where the vessel has not been previously stressed to operating conditions, AE should be sensitive to relatively small flaws. AE monitoring should be an effective technique to detect and locate flaws.

- Application of AE monitoring to inservice hydros limited to an overpressure of 1.15 x operating pressure as in the U.S. appears to be questionable. Results from the ZB-1 test hydros indicate that early detection of flaws by this means is improbable largely due to the fact that the flaws have already seen similar stress levels during operation.

- In the case where higher hydro overpressures are used - i.e., in the order of 1.4-1.5 x operating pressure - AE monitoring appears to offer a usable degree of flaw detection resolution.

5.6 TEMPERATURE AND MATERIALS EFFECTS

The AE event rate at a constant crack growth rate was not dependent upon temperature. Laboratory testing showed that the AE event rate was influenced by temperature. The event rate at constant crack growth rate was higher at room temperature than for 288°C (550°F) test conditions. This effect, however, was less pronounced at low crack growth rates. The ZB-1 data also suggests that at low crack growth rates, the affect of temperature may be less pronounced.

The high AE event rates from the KS07R weld cracks suggest that material chemistry and heat treat condition combined with complex flaw geometry may also significantly affect the AE event rate. Laboratory tests on A533B base and weld metal did not show a significant material dependence. Furthermore, no significant effect of flaw geometry was observed in lab testing. No lab tests were performed on unstress relieved HAZ material containing a complex crack network. This effect should be the subject of further investigation, since cracks often originate in weldments.

5.7 TECHNICAL AREAS REQUIRING SPECIAL ATTENTION

The results from the ZB-1 test have identified areas of technology which need to be improved. These areas do not preclude useful application of the technology at this time, but they are improvements needed to enhance the effectiveness and maturity of the technology.

- Source Location - Two dimensional point source location has been used for some time and it works well on simple geometries. Although it performed reasonably well on the ZB-1 vessel, in many cases there were source clusters which had no obvious relation to any flaws. This is a point of concern because, even with an effective method to identify crack growth AE signals, good source location remains to be important. Some of the possible avenues for improvement would be improved array configurations, improved algorithms, and sensors which favor a single propagation mode.

- Pattern Recognition - Pattern recognition for crack growth signal identification is vital to full achievement of program objectives. The current concept is producing good results with the ZB-1 data. It is important that the concept be incorporated into an instrument system to finally test the effectiveness when applied to serial analysis of AE data.

- Flaw Evaluation - The flaw evaluation method is producing reasonably good results for the machined flaws. There is need for refining the relationship to improve the consistency between low and high temperature data. The major question is in applying the relationship to the KS07R weld crack. This is important because the weld crack in some ways represents the type of circumstance that could arise in reactor monitoring. When the flaw evaluation relationship is applied to the KS07R weld crack, it appears to grossly overpredict the crack growth rate. This point needs further analysis to attempt to establish the true results.

5.8 INFORMATION NEEDED TO FINALIZE ANALYSIS OF ZB-1 TEST RESULTS

The primary area where additional information is needed to fully utilize the results from the ZB-1 vessel test is to relate those results to a detailed summary of the AE results obtained by KWU. KWU used equipment and techniques which differ from those used by Battelle, PNL. It is critical at this point to compare results obtained by the two test monitoring groups. Where they differ, the reason for the difference must be analyzed to determine why. The results from the test will be strengthened and both parties will benefit from such an exercise.

6.0 REFERENCES

1. P.H. Hutton, E.B. Schwenk, R.J. Kurtz, April 1979, Estimate of Feasibility to Develop Acoustic Emission-Flaw Relationships for Inservice Monitoring of Nuclear Pressure Vessels, NUREG/CR-0800, Pacific Northwest Laboratory, Richland, WA.

2. P.H. Hutton, R.J. Kurtz, June 1980, Reactor Safety Research Programs, Quarterly Report, October-December, 1979, pg. 73-96, NUREG/CR-1349, Pacific Northwest Laboratory, Richland, WA.

3. P.H. Hutton, T.T. Taylor, et al., June 1982, Acoustic Emission Monitoring of ASME Section III Hydrostatic Test, Watts Bar Unit 1 Nuclear Reactor, NUREG/CR-2880, Pacific Northwest Laboratory, Richland, WA.

4. P.H. Hutton, et al., June 1984, Acoustic Emission Monitoring of Hot Functional Testing - Watts Bar Unit 1 Nuclear Reactor, NUREG/CR-3693, Pacific Northwest Laboratory, Richland, WA.

5. Letter, Vessel Test Options, AE/Flaw Characterization Program, to Dr. J. Muscara, NRC from P.H. Hutton and R.J. Kurtz, Pacific Northwest Laboratory, March 11, 1980.

6. G.D. Whitman and R.H. Bryan, April 1978, Heavy Section Steel Technology Program, Quarterly Report for July-September 1977, NUREG/CR-0206, ORNL-TM166.

7. P.H. Hutton, "Summary Report on Investigation of Background Noise at the San Onofre Nuclear Power Reactor as Related to Structural Flaw Detection by Acoustic Emission," July 1971, published in Southwest Research Institute Project 17-2440, Biannual Progress Report No. 6, Vol. I, Projects I through IV, January 7, 1972.

8. J.R. Smith, G.V. Rao, and J. Craig, December 1979, Acoustic Monitoring Systems Tests at Indian Point Unit 1, C00/2974-2, Westinghouse Electric Corp., NTIS, PC A06/MF A01.

9. S.P. Ying, J.E. Knight, and C.C. Scott, "Background Noise for Acoustic Emission in a Boiling Water and a Pressurized Water Nuclear-Power Reactor," The Journal of the Acoustical Society of America, 53 (6), 1973.

10. E. Votava (Kraftwerk Union), P. Jax and J. Eisenblatter (Battelle, Frankfurt), "New Results on the Surveillance of Nuclear Reactor Components by Acoustic Emission during Hydrotests," Proceedings of the Third International Conference on Nondestructive Evaluation in the Nuclear Industry - 1981, pp. 437-461.

11. P.G. Doctor, T.P. Harrington, and P.H. Hutton, July 1979, Pattern Recognition Methods for Acoustic Emission Analysis, NUREG/CR-0910, PNL-3052, Pacific Northwest Laboratory, Richland, WA.

7.0 ACKNOWLEDGEMENTS

The ZB-1 vessel test was a major step in advancing AE technology to a stage of usefulness for continuous monitoring of reactor pressure boundaries. To my knowledge, no other test of this magnitude has been performed to evaluate flaw monitoring by AE under simulated reactor conditions. The success of this test was made possible by outstanding dedication and support from many sources. It goes without saying that the funding support provided by the U.S. Nuclear Regulatory Commission and the Staatliche Materialpruefungsanstalt (MPA)/West German government was a fundamental requirement for the test to take place. Performance of the test involved dedicated personal effort by many individuals - both German and American.

I wish to express my profound appreciation to:

U.S. Nuclear Regulatory Commission

Dr. J. Muscara

PNL - Battelle

D. A. Chaudier
L. S. Dake
J. F. Dawson
S. M. Faber
R. J. Kurtz
R. R. Lewis
R. A. Pappas
C. B. Perry
E. B. Schwenk
J. R. Skorpik
T. T. Taylor
K. E. Williamson

MPA

Prof. K. Kussmaul
R. Gillot
H. Beyer

Grosskraftwerk Mannheim

F. Bauemuller
Schweitzer
Spoehrer

Izfp

Prof. P. Hoeller
Dr. G. Deuster

I wish to also say "Thank You" to the many people in addition to those mentioned above who contributed in some way to the performance of the test.

P. H. Hutton
Project Manager
Pacific Northwest Laboratory
(Battelle Northwest)

APPENDIX A

Test Plan

for

U.S. - German

Cooperative Research to Acoustic Emission Monitor

German Pressure Vessel Test ZB-1

Revision 5
7/81

TEST PLAN

for

U.S. - GERMAN

COOPERATIVE RESEARCH TO ACOUSTIC EMISSION MONITOR

GERMAN PRESSURE VESSEL TEST ZB-1

P. H. Hutton
R. J. Kurtz
Battelle, Pacific Northwest Laboratory

Approved: _____ Date 8/4/81
For: Battelle, Pacific Northwest Laboratory

Approved: _____ Date 10/6/81
For: Engineering Technology Division, U.S. Nuclear Regulatory Commission

Approved: _____ Date 2/4/82
For: Materialpruefungsanstalt (MPA)

Approved: _____ Date 2/5/82
For: Institut für Zerstörungsfreie Prüfverfahren (IzfP)

TEST PLAN
for
U.S. - GERMAN
COOPERATIVE RESEARCH TO ACOUSTIC EMISSION MONITOR
GERMAN PRESSURE VESSEL TEST ZB-1

1.0 INTRODUCTION

The U.S. NRC, Engineering Technology Division has been conducting an extensive research program through one of their contractors (Battelle, Pacific Northwest Laboratory) to develop the application of acoustic emission (AE) to continuously monitor reactor pressure vessels for detection and evaluation of growing flaws. The initial work has been done primarily on laboratory specimens of Type A533-B Class 1 pressure vessel steel. The program has reached a point where it is recognized that further work must be conducted on heavy section vessels under simulated reactor conditions to adequately evaluate AE signal identification and flaw interpretation techniques developed. The forthcoming ZB-1 vessel test, to be performed at MPA Stuttgart, can meet the technical needs of the NRC program. Cooperative participation by the U.S. and Germany on this test also appears to offer mutually beneficial technical information exchange.

This test plan is intended to establish a technical and administrative understanding of the basis for U.S. NRC participation in the ZB-1 vessel test. Work in behalf of the U.S. NRC will be performed by its contractor, Battelle Pacific Northwest Laboratories (PNL).

2.0 TEST PLAN

2.1 PURPOSE

The purpose of this test is to measure and analyze acoustic emission (AE) data from fatigue crack growth in a heavy section (120 mm thick) steel pressure vessel. The conditions of the test

will attempt to simulate reactor pressure vessel (RPV) operation within practical limits. In the ZB-1 test, the primary AE data to be used by NRC/Battelle will be derived from fatigue crack growth in an insert of ASTM A533 Grade B, Class 1 steel in the vessel wall.

2.2 TEST VESSEL DESCRIPTION

Intermediate pressure vessel ZB-1 is a 120 mm thick, 1715 mm O.D. cylindrical vessel with hemispherical closure heads. The cylindrical section of the vessel is 2280 mm long. The vessel material is A508 steel. Two part cylindrical inserts shall be welded into the test vessel. One of the inserts shall be composed of KS07C (A508) degraded material 1500 mm long by 700 mm circumferential width (as measured on the outside surface of the vessel). This insert will be supplied by MPA. The level of material degradation will be determined by MPA. The second insert shall consist of A533B, Class 1 steel 1500 mm long by 750 mm circumferential width. The A533B insert will be provided by PNL. This insert will contain three part-circular surface flaws which will be fatigue presharpened by internal notch pressurization. Two of the flaws will be machined on the inside surface of the insert and one flaw will be on the outside surface. The longitudinal axes of the flaws shall be perpendicular to the circumferential stress in the vessel. Figure 1 shows the cylindrical portion of the vessel and gives the relative location of the two inserts. Figures 2 and 3 show the geometry of the A533B insert and the location and geometry of the three part-circular cracks.

2.3 VESSEL LOADING CONDITIONS

In order to simulate RPV loading conditions, the test vessel shall be internally pressurized with water at temperatures of 90 and 288^{o}C. About one-half of the planned test matrix shall be conducted at each test temperature. The water pressurization system will provide sinusoidal or sawtooth cyclic mechanical stressing of the vessel at a frequency near one cycle per minute. In addition, pressure cycling at R-ratios (R = minimum pressure/

maximum pressure) of 0.1, 0.33 and 0.6 shall be performed. The planned sequence is shown in Table I. High and low R-ratio load cycling shall be alternated to promote crack front marking at various stages of the test. Simulated hydrotests shall also be performed during the test sequence. The vessel loading rate for the hydrotests shall be 1 bar/minute.

TABLE I

Test Sequence for ZB-1 Vessel Test (Rev. 4)

STEP	PRESSURE, BAR		TEMP., °C	NUMBER OF CYCLES	COMMENTS
	MAX.	MIN.			
1	240	---	20 - 90	1	Hydro
2	240	24	20 - 90	See Note (1)	
3	240	144	20 - 90	10,000	Crack Mark
4	245	---	20 - 90	1	Hydro
5	240	24	20 - 90	2,000	
6	240	144	20 - 90	7,000	Crack Mark
7	250	---	20 - 90	1	Hydro
8	240	80	288	3,000	
9	240	144	288	5,000	Crack Mark
10	254	---	20 - 90	1	Hydro
11	240	80	288	2,000	
12	240	144	288	4,000	Crack Mark
13	264	---	20 - 90	1	Hydro
14	240	80	288	2,000	
15	340	---	20 - 90	1	Hydro
16	See Note (2)	---	Perform FRG hydro/fatigue test matrix. 20 - 90	1	Hydro
17	---	---	20 - 90	1	Burst

NOTES:

(1) Vessel pressure cycled until measurable crack growth is detected (~5 mm).

(2) Maximum hydrotest pressure increased until stable crack growth is obtained.

2.4 INNOCUOUS NOISE SOURCE SIMULATIONS

One of the important objectives of AE monitoring the vessel test is to evaluate the effect of various reactor background noise elements on AE monitoring. This relates to both basic detection of the AE signal and to identification of crack growth AE signals in the presence of similar noise signals.

One major source of noise is the reactor coolant circulation system. Measurements of this noise taken on operating reactors shows it to be very high relative to AE signal levels at low frequencies (< 100 kHz). However, with increasing frequency, it diminishes until at about 400 kHz, it is down near the electronic noise level of the measurement system. To evaluate flow noise effects on AE monitoring requires a noise field similar to reactor noise and a growing crack producing AE in that noise field. The planned approach to simulating reactor flow noise at a localized area is to drive a transducer located on the inside surface of the vessel with a shaped electrical input. This will require a penetration to the outside of the vessel for a metal sheathed lead wire. The outside diameter is expected to be approximately 4.75 mm.

Mechanical rubbing of thermal insulation on the exterior of the vessel is a potential noise source to be simulated. To produce this noise, the vessel should be covered with blanket-type glass fiber insulation except for an approximately 200 mm wide band of mirror insulation around the vessel cylinder.

Mechanical stressing of weld slag inclusions may produce noise similar to acoustic emission. To investigate this, a 100 mm long strip of slag inclusions shall be incorporated in the A533B insert-to-vessel weld denoted in Figure 4. The slag inclusions shall be located near mid-thickness of the vessel wall and involve approximately three consecutive weld passes. The size of the slag inclusions shall be determined prior to pressure cycling of the vessel by nondestructive means (e.g., x-ray and UT) for verification. Following the test, the slag inclusion and any associated crack growth will be characterized by destructive sectioning for correlation with AE results.

Potential base metal-to-weld cladding interface noise must also be investigated. To simulate this potential noise source, a 4 mm thick patch of stainless steel weld overlay cladding shall be deposited on the inside surface of the 750 mm circular repair patch (see Figure 4). Two 50 x 100 mm areas of intentionally defective weld cladding will be included on the plug. One area will contain underclad cracks and the other will have poorly bonded clad. The two defective areas shall be separated from each other by about 400 mm.

Electrical transients represent the last noise source to be introduced. These transients may be produced simply by methods such as spark discharge, or turning electric motors on and off. These noises will be inserted at random locations on the test sequence.

2.5 AE MONITORING

A fundamental requirement in AE monitoring is that it be performed by methods which can be directly applied on an operating reactor. This requires the use of sensors capable of monitoring a 288^{o}C surface. Other requirements are to obtain good quality data to be processed for source location, pattern recognition characteristics, and crack growth estimation. Digitized signal waveforms, plus conventional AE signal parameters such as signal peak time, amplitude, energy and duration must be recorded in a fashion which allows identification with test conditions and sequence.

To achieve the above requirements, NRC/Battelle will use an AE monitor system described schematically in Figure 5. Metal waveguide sensors will be employed in three arrays:

1. A sensor array located entirely on the A533B insert and encompassing the flaws. This will provide optimized AE data from the growing flaws.

2. One sensor array located to monitor the cylindrical portion of the vessel. These will provide a circumstance

more directly related to monitoring a reactor pressure vessel wherein attenuation and geometry effects can be evaluated and related to information from the optimized array in 1. above.

3. One magnetically mounted sensor array located on the KS07 insert.

Sensor locations are shown in Figure 4. The sensor array on the KS07 insert will be similar to that on the Battelle insert.

In addition to the sensor arrays described above, three sensors will be mounted temporarily on the A533B insert at selected times during the test to isolate on AE originating from a given flaw. The purpose of this technique is to provide periods of optimized waveform recording wherein the recorded signals are known to be originating from a flaw site. Since the use of these sensors will be intermittent and their location is flexible, they are not shown as part of the permanent sensor location plan.

The procedure planned for calibration and functional test of the Battelle AE system is:

A) Sensor Calibration

A secondary calibration referencing to a primary sensor calibrated by the U.S. National Bureau of Standards will be performed on all sensors. This will be performed in the laboratory prior to sensor installation on the vessel.

B) Installed Sensor - AE System Calibration

Upon completion of sensor installation on the vessel and AE monitor system hook up, sensor response and monitor system performance will be calibrated using a helium gas jet and Pentel pencil lead break. Although this will not provide an absolute calibration, it will provide for documentation of sensor and AE system response to reproducible input signals.

C) AE System Check During Test Monitoring

It is necessary to periodically check system performance during the course of test monitoring. A solenoid controlled mechanical impactor mounted on the vessel will be used to remotely introduce a known pulse signal into the vessel wall. This will provide a relative measure of the consistency of AE system response during the course of the test.

2.6 CRACK GROWTH MONITORING REQUIREMENTS

Methods for monitoring the crack propagation other than AE are required during the test. Crack opening displacement (COD) and ultrasonic (UT) inspection measurements will be used for this purpose. In order to perform COD measurements for the I.D. flaws, high temperature, water immersible MTS COD gages will be installed on the inside surface of the vessel. Thus, access to the interior of the vessel is required, as well as feedthroughs for lead wires. The O.D. flaw will also have an MTS COD gage in addition to a Shaevitz high temperature linear variable differential transformer (LVDT). Estimates of the extent of crack propagation shall be made after each loading block specified in the test sequence. Slow pressure ramps ($\sim$ 10 bar/min.) shall be run several times between minimum and maximum pressure. The output of the COD gages and the LVDT will be monitored on chart recorders to obtain plots of crack opening against test pressure. The slope of these curves can then be used to estimate the amount of crack growth.

Ultrasonic inspection of the flaws will also be performed following each load block. Both standard and advanced UT techniques shall be applied.

High temperature, water immersible Ailtech type strain gages are to be spot welded to the A533B insert at locations specified in Figure 6.

After the test is completed, the COD and UT inspection results will be confirmed by destructive examination of each flaw.

It will, therefore, be necessary to remove the A533B insert after the test is completed. Subsequent detailed sectioning of the flaws shall be performed at PNL.

2.7 BLIND TESTS

Blind tests of the AE monitoring system shall be performed at randomly selected times during the test sequence. In addition to monitoring crack growth in the presence and absence of various innocuous sources (see Section 2.4), it is also necessary to AE monitor the vessel in the presence of background noise when no crack growth is occurring. To produce this situation requires activating the various noise source mechanisms while cycling the vessel pressure between 24 bar and 120 bar. This pressure cycle should produce little, if any, crack growth and should be applied for only a limited number of cycles (a few hundred) at randomly selected points in the test sequence.

3.0 RESPONSIBILITIES

U.S. and German responsibilities in this cooperative test are:

U.S. (PNL)

1. Provide a finished insert of A533B material in accordance with dimensional specification and schedule requirements set forth by MPA. Flaws will be machined into the insert and precracked ready for testing. Insert is to be delivered to the vessel fabrication site.
2. Perform laboratory tests of samples of the degraded A508 material with microcracks prior to vessel testing to evaluate AE characteristics.
3. Provide a complete AE monitor/analysis system at the test site (MPA, Stuttgart), install AE sensors and prepare the system for testing in accordance with the schedule set forth by MPA.

4. Provide MTS COD gages, Ailtech high temperature strain gages and signal conditioning instruments required for the COD gages in support of crack growth monitoring, and the signal source for noise simulation. Provide a specific list of vessel wall penetration requirements for instrumentation leads.

5. Provide necessary mirror insulation for noise simulation.

6. Obtain NBS calibration of two AE sensors supplied by IzfP.

7. Provide the necessary qualified personnel to conduct AE and UT monitoring and analysis during the course of the test.

8. Record and provide to MPA any AE data from the KS07 insert to the extent practical without compromising AE monitoring of the A533 insert.

9. After removal of the A533 insert following the test, transport selected parts of the insert to PNL and perform destructive examination of the flaws to confirm crack growth characteristics.

10. Prepare a report describing AE monitoring results, physical measurement data, destructive examination results relevant to the AE monitoring and the correlations among these. This complete report, plus any supporting data is to be available to MPA, Stuttgart.

GERMANY

1. Provide samples of degraded KS07 material for laboratory testing by PNL to evaluate AE characteristics prior to the vessel test. The material is to be representative of that being inserted into the ZB-1 vessel.

2. Install the A533B insert provided by PNL in the ZB-1 vessel including necessary post weld stress relief and slag inclusion.

3. Install stainless steel cladding on section of vessel inner surface.

4. Keep PNL informed on test preparation and testing schedule.

5. Install strain gages, thermocouples and associated strain gage signal conditioning equipment, in addition to a sufficient number of chart recorders to monitor the output of the three MTS COD gages and the LVDT. The COD gages shall be installed by MPA personnel.

6. Provide output signal from a pressure transducer with the following characteristics:

Voltage range:	0-5 volts
Impedance:	50 ohm
Offset:	Zero
Connection:	Coaxial cable

7. MPA will supply a 240 to 120 volt, 50 Hz stepdown transformer with a 65 amp capacity.

8. IzfP will provide two AE sensors to PNL by September 1981 for calibration.

9. IzfP and MPA will provide all ultrasonic inspection equipment required to measure crack growth and perform the measurements.

10. Provide vessel test facilities and perform a test sequence in accordance with the test plan described herein. NOTE: In the event of problems with excessive crack growth rate or lack of growth in either insert, this test plan may be modified by mutual consent of PNL and MPA.

11. Remove selected parts of the A533B insert from the ZB-1 vessel following test completion.

12. Document physical test results and AE results by others in a report to be made available to PNL.

JOINT RESPONSIBILITIES

1. In the event of premature failure of either insert, the party responsible for that insert shall arrange for repair to facilitate completion of the test. Premature failure is defined as any throughwall penetration occurring prior to completion of the loading conditions specified in Table I.

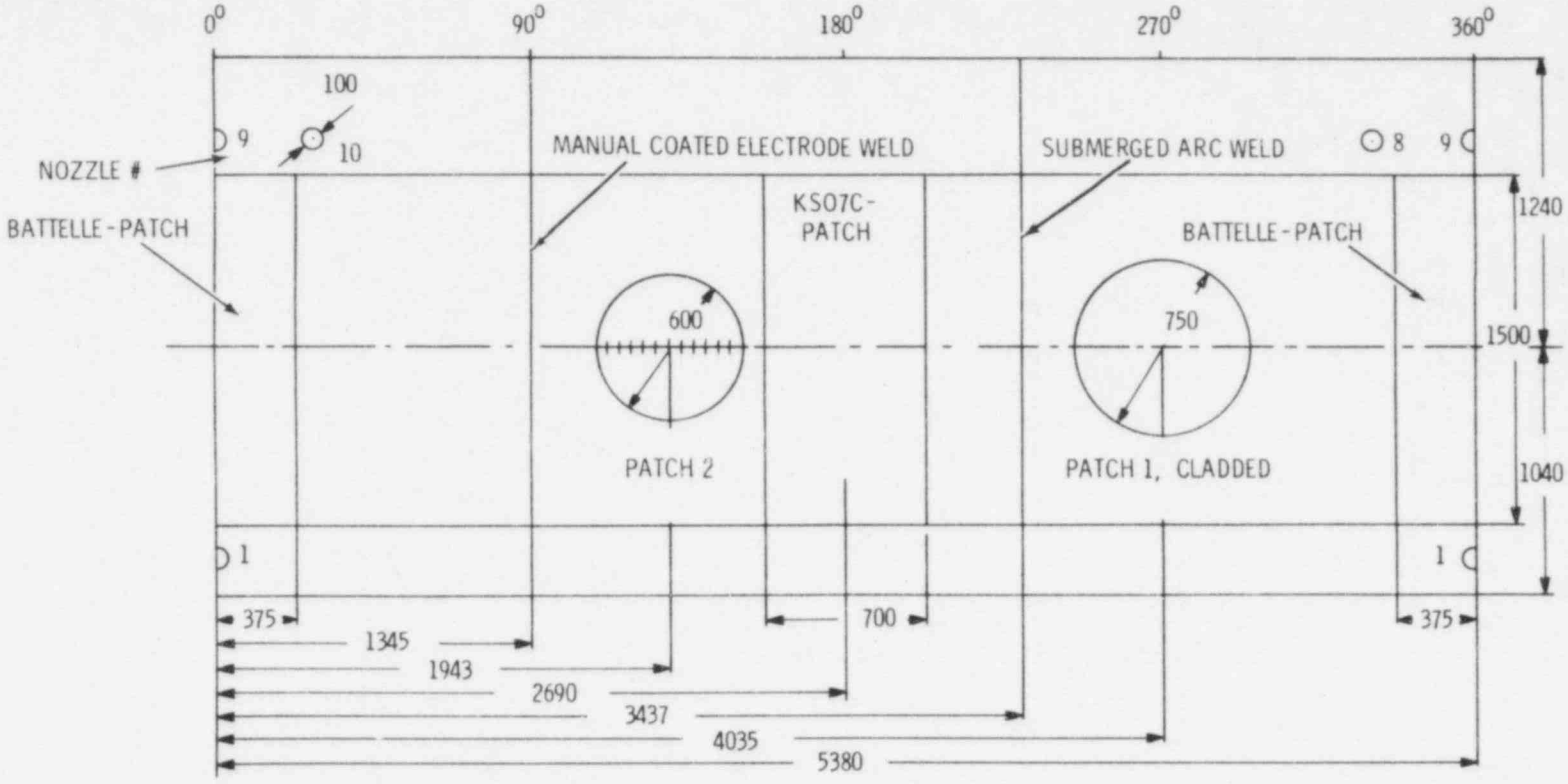

NOTE:

1) DIMENSIONS IN MILLIMETERS

Figure 1. Cylindrical Portion of ZB-1 Vessel

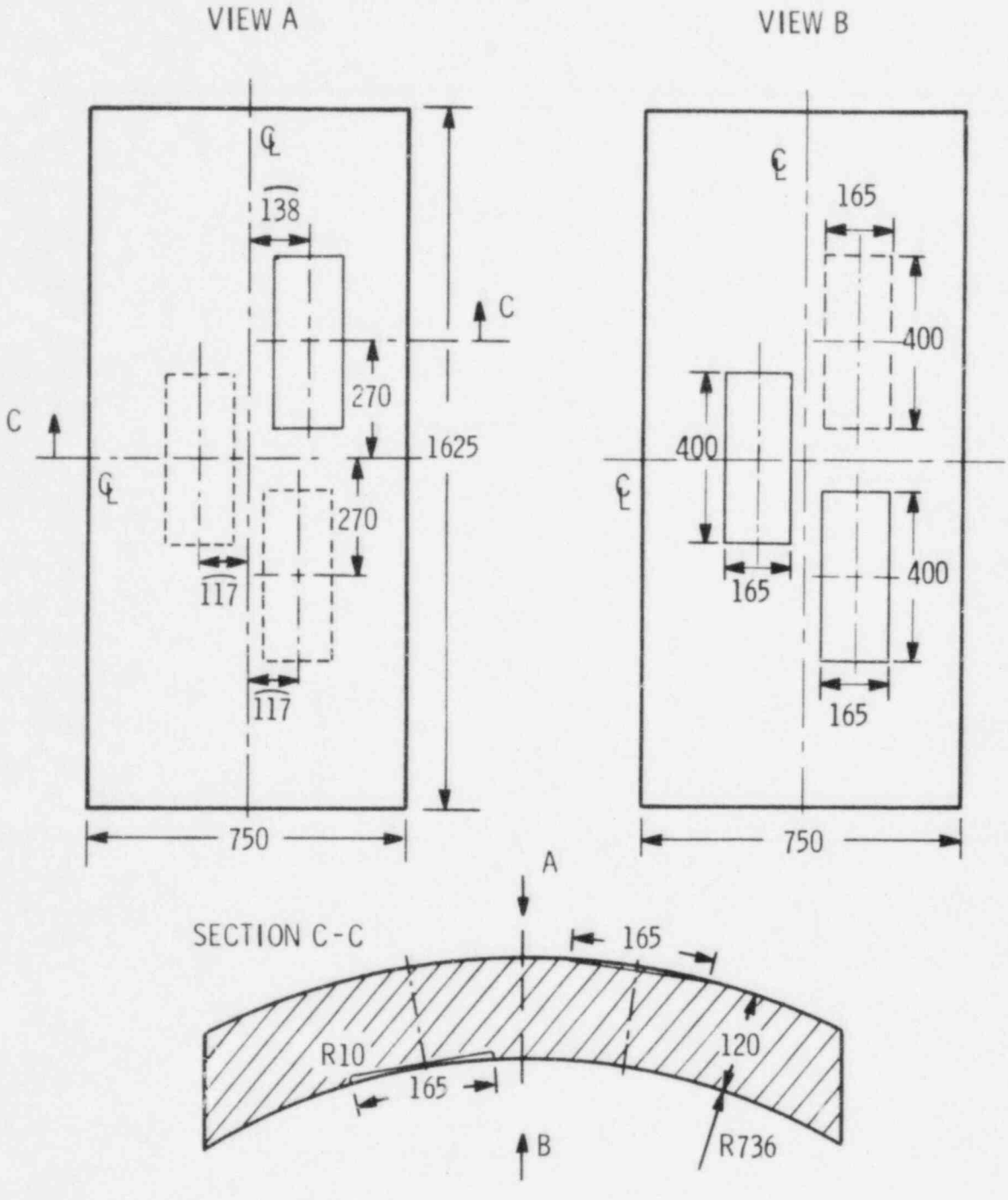

NOTES:

1) ALL DIMENSION IN MILLIMETERS

2) $\overset{\frown}{138}$ MEANS ARC LENGTH 138 mm

Figure 2. Geometry of A533B Insert

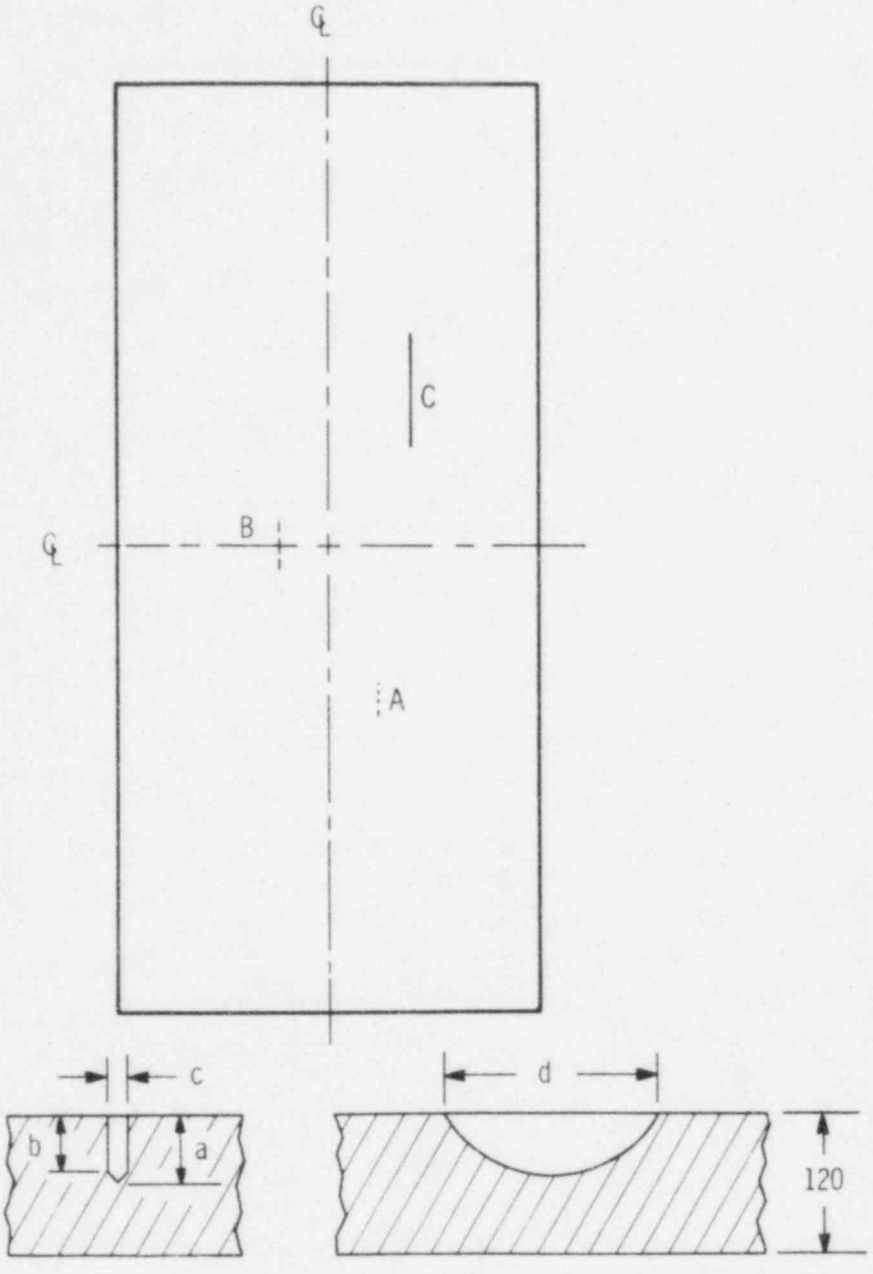

NOTCH	LOCATION	a	b	c	d	a/w
A	I.D.	22	16	3	54	0.18
B	I.D.	32	26	3	81	0.27
C	O.D.	48	36	6	190	0.40

NOTE: ALL DIMENSIONS IN MILLIMETERS

Figure 3. Geometry of Notches in A533B Insert

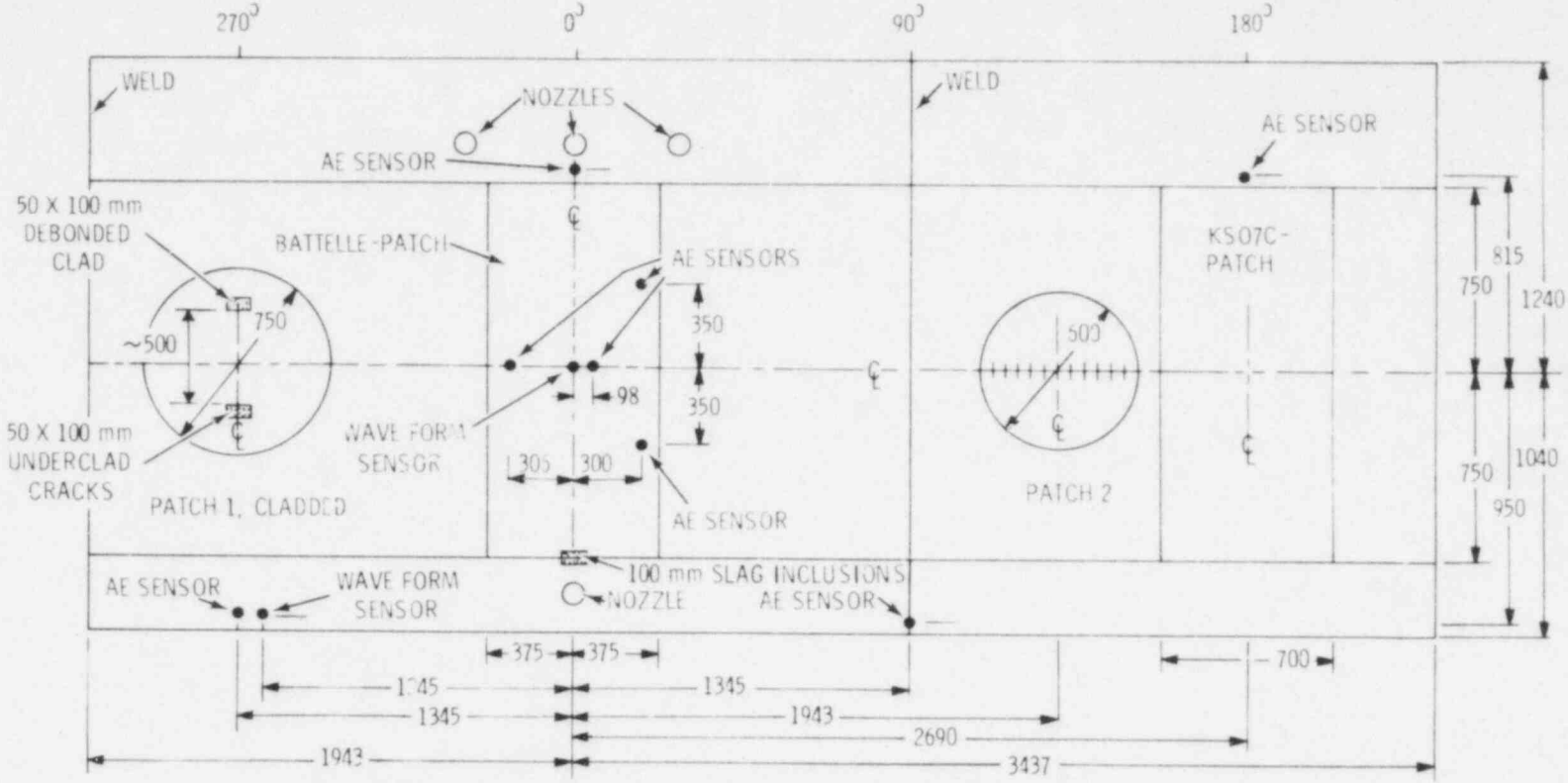

NOTE:

1) DIMENSIONS IN MILLIMETERS
2) AN ULTRASONIC NOISE SIMULATION TRANSDUCER WILL BE MOUNTED ON THE INSIDE CENTER OF THE PATCH
3) ALL AE SENSORS WILL BE METAL WAVE GUIDES
4) AE SENSORS ON THE PATCH WILL BE MOUNTED IN DRILLED AND TAPPED HOLES. ALL OTHER SENSORS WILL BE PRESSURE COUPLED USING MAGNETIC MOUNTS

Figure 4. Location of Battelle AE Sensors and Other Special Features - ZB-1 Vessel

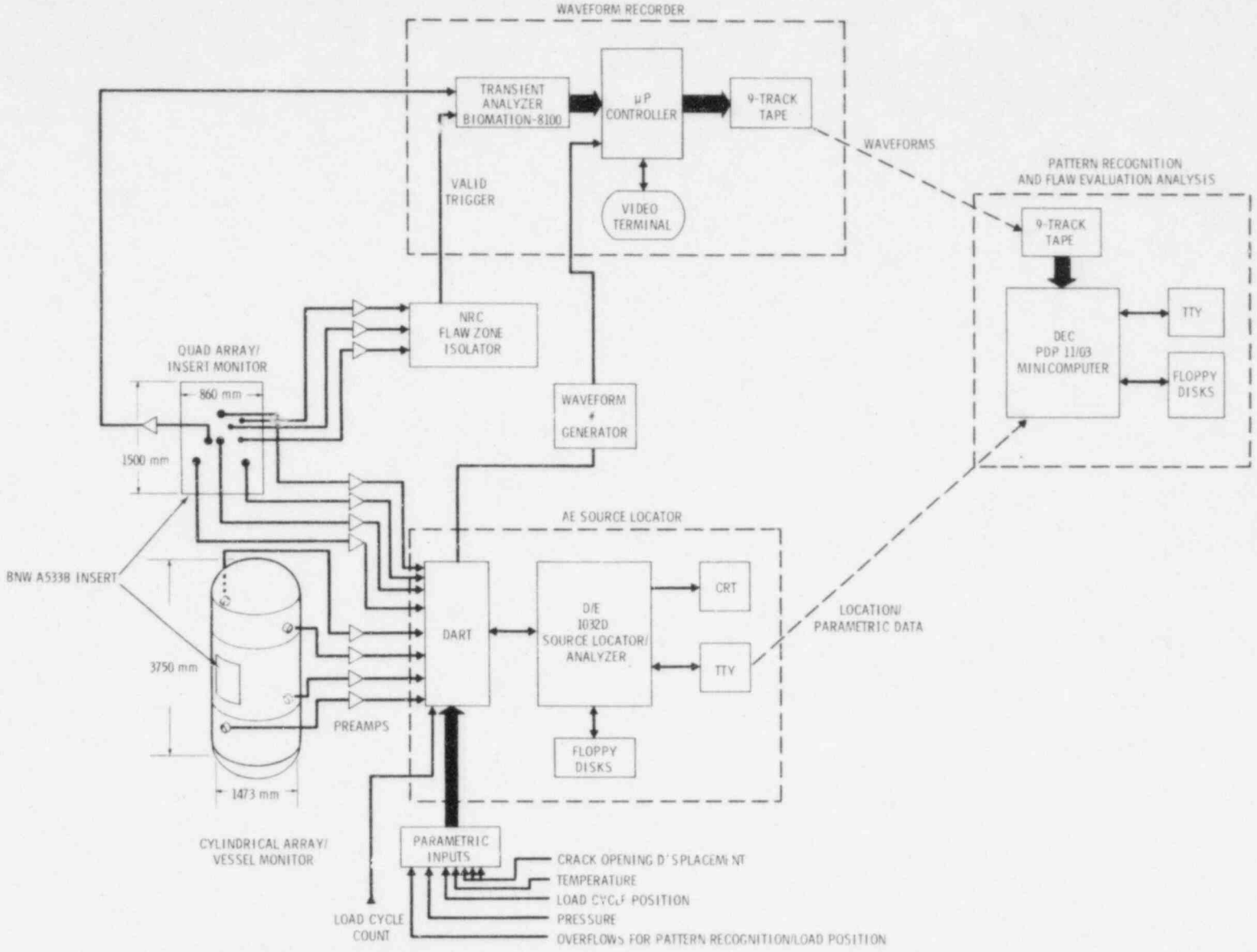

Figure 5. Battelle AE Monitor System - ZB-1 Vessel Test

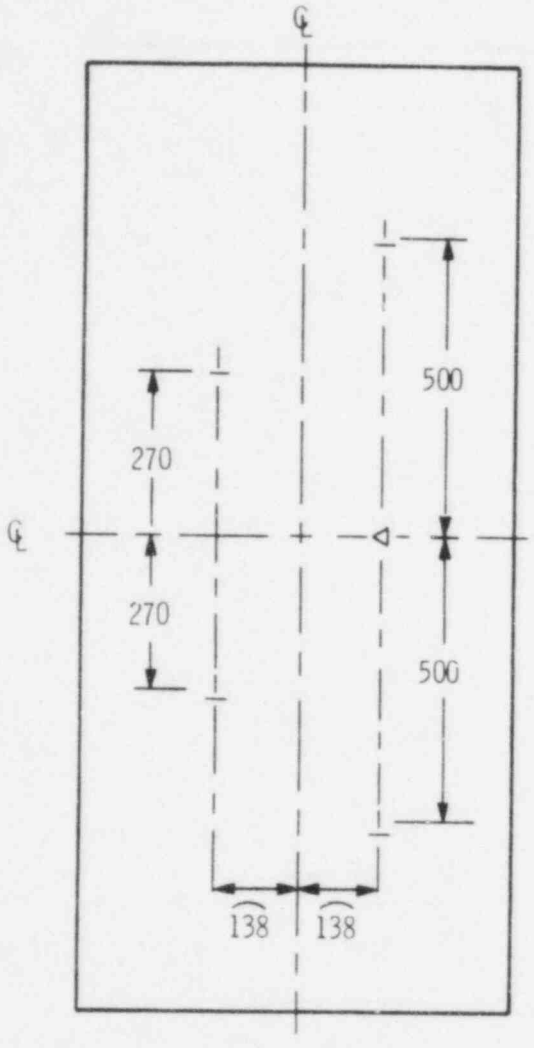

NOTES:

1) Δ = DELTA ROSETTE

2) ⊥ = BIAXIAL GAGES

3) DRAWING DEPICTS OUTSIDE SURFACE OF PATCH, IDENTICAL SERIES OF GAGES ON INSIDE SURFACE

4) DIMENSIONS IN MILLIMETERS

5) $\overset{\frown}{138}$ MEANS ARC LENGTH 138 mm

6) STRAIN GAGES: AILTECH TYPE SG 125

Figure 6. Strain Gage Plan for A533B Insert

APPENDIX B

Fabrication of A533B

Insert for ZB-1 Test Vessel

**Staatliche
Materialprüfungsanstalt**

Universität Stuttgart

**MPA
STUTTGART**

Prüfungsbericht

Zweitfertigung

Antragsteller:	Battelle Pacific Northwest Labs. P.O. Box 999 Richland, Washington 99 352 USA
Gegenstand:	Fabrication of a A 533 B cl. 1 Patch

Datum des Berichts:	Nov. 10, 1981
Auftrag	938 745 Gt/W
Textseiten:	7
Beilagen:	22
ausgefertigt:	3 x Battelle Pacific Northwest Labs.

**Staatliche
Materialprüfungsanstalt**

Universität Stuttgart

**MPA
STUTTGART**

Staatl. Materialprüfungsanstalt · Pfaffenwaldring 32 · 7000 Stuttgart 80 (Vaihingen)

Battelle Pacific Northwest Labs.
Attn. Mr. R. K u r t z
P.O.Box 999

Richland, Washington 99352
USA

Nov. 10, 1981

Re.: Fabrication of a A 533 B cl. 1 Patch
Purchase Order A 9578 AC
MPA Account Nr. 938 745

Abstract

By order of the Battelle Pacific Northwest Laboratories (BPNL) a patch was fabricated and fatigue cracks were grown from three premachined notches by locally applied hydraulic high-pressure cycling. After completion, the patch will be welded into the intermediate size vessel ZB 1 of the German Research Program "Integrity of Components" and tested by static and cyclic loading. The resulting crack initiation and crack growth will be monitored by accoustic emission.

The patch fabrication and the method used for the notch sharpening are described.

The crack growth was monitored by using a special ultrasonics technique. A pretest, which was conducted in order to verify the reliability of the loading apparatus and the NDE method, yielded good results.

1. Heat-Treatment and Patch-Fabrication

The material was supplied by BPNL in form of a A 533 B cl. 1 steel plate with the dimensions 1625 x 1040 x 210 mm^3, the approximate weight was 27 kN. Before machining, the plate was stress relief heat-treated at 593 °C ± 10 °C for 10 hours with a heating rate of 35 °C/h and a cooling rate of 20 °C/h (Fig. 1).

After heat-treatment the plate was cut to three parts (Fig. 2) : the blocks BNWA and most of BNWC are still available, from block BNWB the patch was machined. In order to check the mechanical properties of the A 533 B cl. 1 steel after heat-treatment, tensile and Charpy-V-specimens were testet (Fig. 3 to 5). The results of the tensile tests are shown in Table 1, the impact energy versus temperature is plotted in Fig. 6. The values, measured at room temperature, of approximately 600 N/mm^2 for the yield and 750 N/mm^2 for the ultimate tensile strength are almost 20 % higher than those from BPNL, taken before the heat treatment. The upper shelf impact energy is close to 200 J.

The dimensions of the curved patch, which was made from block BNWB, are shown in Fig. 7, the vessel ZB 1 with the patch in Fig. 8.

2. Notch Machining

The main test objects of the patch will be three pre-fatigued notches, two on the inner and one on the outer surface. In order to provide a flat and smooth surface for the seal plate, which is necessary for the local fatiguing method, three rectangular areas (400 x 165 mm^2, see Fig. 7) had to be machined around the location where the notches were planned. This was difficult to achieve, especially on the inner surface, since the true flatness was required to be within 0,05 mm.

In the next step, the part-circular notch C on the outer surface was machined mechanically by a milling cutter, according to BPNL drawing number SK-3-22708 (Fig. 9). The notch tip radius, which is important for the number of load cycles necessary to initiate a fatigue crack, is close to the specified value of 0,18 mm.

The notches A and B with an almost semicircular shape then were machined on the inner surface by using the electric discharge machining (EDM) process. Due to some unexpected difficulties with the spark erosion machine, the depth and radius of these two notches are approximately 1 mm larger than specified by the April 7, 1981 revision of R.J. Kurtz, while the width is significantly larger than the specification of 3,2 mm: it decreases from 5 mm on the surface to 3,5 mm at the transition to the notch tip angle for notch A and 6 mm respectively 4 mm for notch B (Fig. 10). However, for the fracture mechanics evaluation of the vessel test, only the depth and diameter of the prefatigued cracks are important.

3. Notch Sharpening by Local Fatigue

The method used for notch sharpening by locally applied hydraulic pressure cycling is described in references /1/ and /2/. To apply this method, a steel sealing block (Fig. 11) is pressed against the surface of the test plate by a frame or a testing machine (Fig. 12). The high oil pressure is kept in the cavity of the seal-block by an elastomer O-ring. In order to prevent damage to the O-ring and leakage in the system, the contact surfaces have to be flat with a smooth finish. The pulsating oil pressure acts like a wedge that is moved back and forth in the notch, causing a cyclically increasing respectively decreasing notch tip angle and finally a fatigue crack.

3.1. Analytical Backround

The hydraulic pressure necessary to grow a flaw can be calculated by the equation

$$\Delta p = \Delta K_I / C\sqrt{\pi a} ,$$

were C is the shape factor for uniform stress (C = 0,85 for notch A, 0,87 for notch B, and 1,05 for notch C) and a is the notch center depth (see Fig. 9 and 10). ORNL recommends a ΔK_I for crack initiation of less than 1400 N/mm$^{3/2}$ (40 ksi $\sqrt{in}$) and a 10 % lower value for crack propagation (/3/), Battelle proposed a ΔK_I

of 885 N/mm$^{3/2}$ for notch A and 1035 N/mm$^{3/2}$ for the notches B and C. This results in a p_{max} of 1250 bar for notch A, 1200 bar for notch B and 850 bar for notch C (Table 2). The minimum pressure during fatiguing was 50 bar for all three notches.

3.2. Crack Growth Monitoring

The most accurate method to measure the crack growth during the described cyclic loading of the patch seemed to be by a special ultrasonics technique, which is described in ref. /2/. In order to apply this technique, an UT-transducer has to be mounted exactly on the opposite side of the machined notch tip. The UT-signals have to be amplified to a level where considerable noise due to interactions with the grain boundaries of the base metal is visible. It is known from ORNL-experiments that this noise pattern oscillates with the frequency of the hydraulic pump in the region where the fatigue crack is growing, and that it is stationary in the range between the transducer and the fatigue crack tip. The length of the oscillating noise region is directly related to the actual depth of the growing crack. ORNL specifies the accuracy of the method to ± 1,5 mm.

3.3. Pre-Test

To test the cyclic loading system, the applicability of the technique and to get a better feeling for its accuracy a void with the dimensions of notch A was machined into a test block (Fig. 13) of the patch material by EDM and tested before the three notches in the patch were fatigued. An Aerotech transducer of 5 MHz, which was provided by BPNL, was used for the crack growth monitoring.

The seal block was loaded by a compressive force of 500 kN, the hydraulic pressure was cycled between 1250 and 50 bar (partially between 1500 and 50 bar) with a frequency of 200 cycles per minute. The pre-test was stopped after 220 000 cycles at a measured crack growth of 12 mm.

After heat-tinting the block was cut to several parts (Fig. 13). The cross-section of the notch (plate 1, section BNW 1) was investigated metallographically (Fig. 14, 15, 16), the other half of the fatigued notch (Fig. 13, plate 2, section BNW 2) was

cooled down to -30 °C and broken open (Fig. 17).

The actual dimensions of the fatigue crack were 12,1 mm at the point of maximum depth and 5 mm on the surface. These values are almost identical to the predicted ones, which shows that the accuracy of the UT-prediction seems to be much better than ± 1,5 mm, at least in this case.

3.4. Sharpening of Notch A, B and C

After the successfully conducted pre-test the notches A, B and C of the patch were fatigued without major problems. The front and side view of the patch and the loading apparatus are shown in Fig. 18 and 19.

The applied hydraulic pressure, the compressive load on the seal-block, the total number of load cycles and the fatigue crack depth, measured at the deepest point of the notch, are listed in Table 2.

Finally, a magnetic powder test was conducted to determine the dimensions of the fatigue cracks on the surface. The values are shown in Fig. 9 and 10, the dotted lines represent the anticipated shape of the crack front. Notch B does not have a fatigue crack on the surface, because the [illegible]us of the EDM notch was too large in this region, due to problems with the spark erosion machine (see chapter 2).

In Fig. 20 the number of load cycles is plotted versus the crack depth. Due to the lowest value of ΔK_I (see 3.1.), notch A has the highest number of load cycles, whereas the notches B and C with the same ΔK_I have almost identical load cycles.

4. Further Steps

After completion of the fatiguing the cracks were protected by spray lacquer in order to prevent corrosion. Then, the patch was sent to the vessel manufacturer. After the vessel test, selected parts of the patch will be mailed to BPNL for further destructive examination of the flaws to confirm crack growth characteristics.

Engineer in charge :

(gez.) Gillot

The Director:

(gez.) i. V. Krägeloh

References:

/1/ A.A. Abbatiello, R.W. Derby:
"Notch Sharpening in a Large Tensile Specimen by Local Fatigue",
ORNL-TM-3925, Oak Ridge National Laboratory

/2/ P.P. Holz:
"Flaw Preparations for HSST Program Vessel Fracture Mechanics Testing: Mechanical-Cyclic Pumping and Electron-Beam Weld-Hydrogen-Charge Cracking Schemes",
NUREG/CR-1274, ORNL/NUREG/TM-369, 1980

/3/ J.G. Merkle:
"An Analytical Basis for Notch Sharpening by Fatigue",
HSST Program 5th Annual Information Meeting, Paper No. 19,
Oak Ridge National Laboratory, 1971

Staatliche Materialprüfungsanstalt
Universität Stuttgart

test temp. (^{o}C)	specimen No.	yield strength (N/mm^2)	tensile strength (N/mm^2)	elongation (%)	reduction of area (%)
20	1	592	745	18,8	66,4
20	4	601	759	18,8	65,2
90	2	565	705	18,0	68,6
90	5	579	713	18,8	68,6
280	3	525	670	15,6	52,4
280	6	572	702	16,6	65,4

Table 1: Tensile test results of the patch material after heat-treatment

Staatliche Materialprüfungsanstalt
Universität Stuttgart

	pressure (bar) max	pressure (bar) min	load on seal-block (kN)	ΔK_I ($N/mm^{3/2}$)	number of load cycles	fatigue crack depth (mm)
notch A	1250	50	500	885	360 000	7
notch B	1200	50	700	1035	160 000	8
notch C	850	50	700	1035	155 000	8

Table 2: Characteristic values of the local fatiguing

Verteiler
NQT
QTW
QWW 2x

M·A·N GHH STERKRADE

QWW

Protokoll über Wärmebehandlung
Heat treatment record

Seite / Page 1 of

Lfd. Nr. / Consec No.

Besteller / Customer	MPA-Stuttgart
Projekt / Project	FKS
Komponente / Component	—
Prüfobjekt / Subject	1 Block 20MnMoNi55 für ZB1

GHH-Auftrags-Nr. / Order-No 505041

FP / FP SL vom 23.1.81

Schritt-Nr. / Seq. No. —

Prüf-Nr. / Test/Exam.No. —

Baugruppe / Assembly —

Glühofen-Nr. / Furnace-No 83016

Glühdatum / Annealing date 26.1.bis 28.1.81

QWW-Nr. / QWW-No 81/24

Werkstoff / Material	20MnMoNi55
Prüfobjektkennzeichnung / Stempelung / Subject designation / Marking	—
Fertigungs- / Wärmebehandlungszustand / Fabrication - / Heat treated condition	Spannungsarmglühung

Diagramm-Auswertung / Diagram analysis: gemessen am Bauteil / of measurements on component

Prüfung durch / Inspection by: [X] H [ ] K [ ] Inspector

Wärmebehandlung / Heat treatment

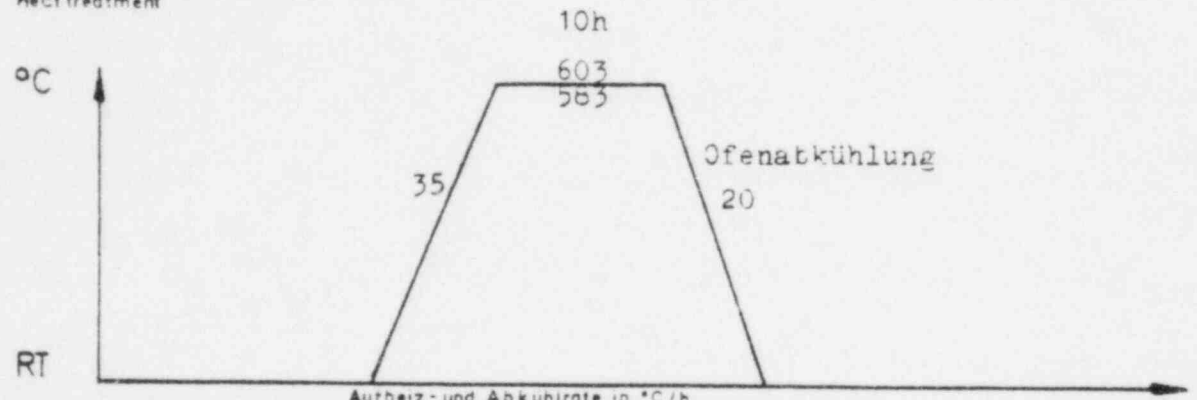

Die Wärmebehandlung entspricht dem / The heat treatment in accordance with WBP n.Angabe von NQT vom 23.1.81 [X] ja / yes [ ] nein / no

Bemerkungen / Remarks

Keine

Hersteller / Manufacturer	Prüfdatum / Date of Test	Unterschrift Prüfer / Signature Inspector	Datum / Date	Stempel / Stamp
	4.2.81	Hanbes, Hoff	4.2.81	QWW
	Prüfdatum / Date of Test	Unterschrift Prüfaufsicht / Signature Test or examination Supervisor		
	24.02.81	Ehrenfeld	24.02.81	QTW

UNIVERSITÄT STUTTGART

Figure 1: Heat-treatment of the A533 B steel plate

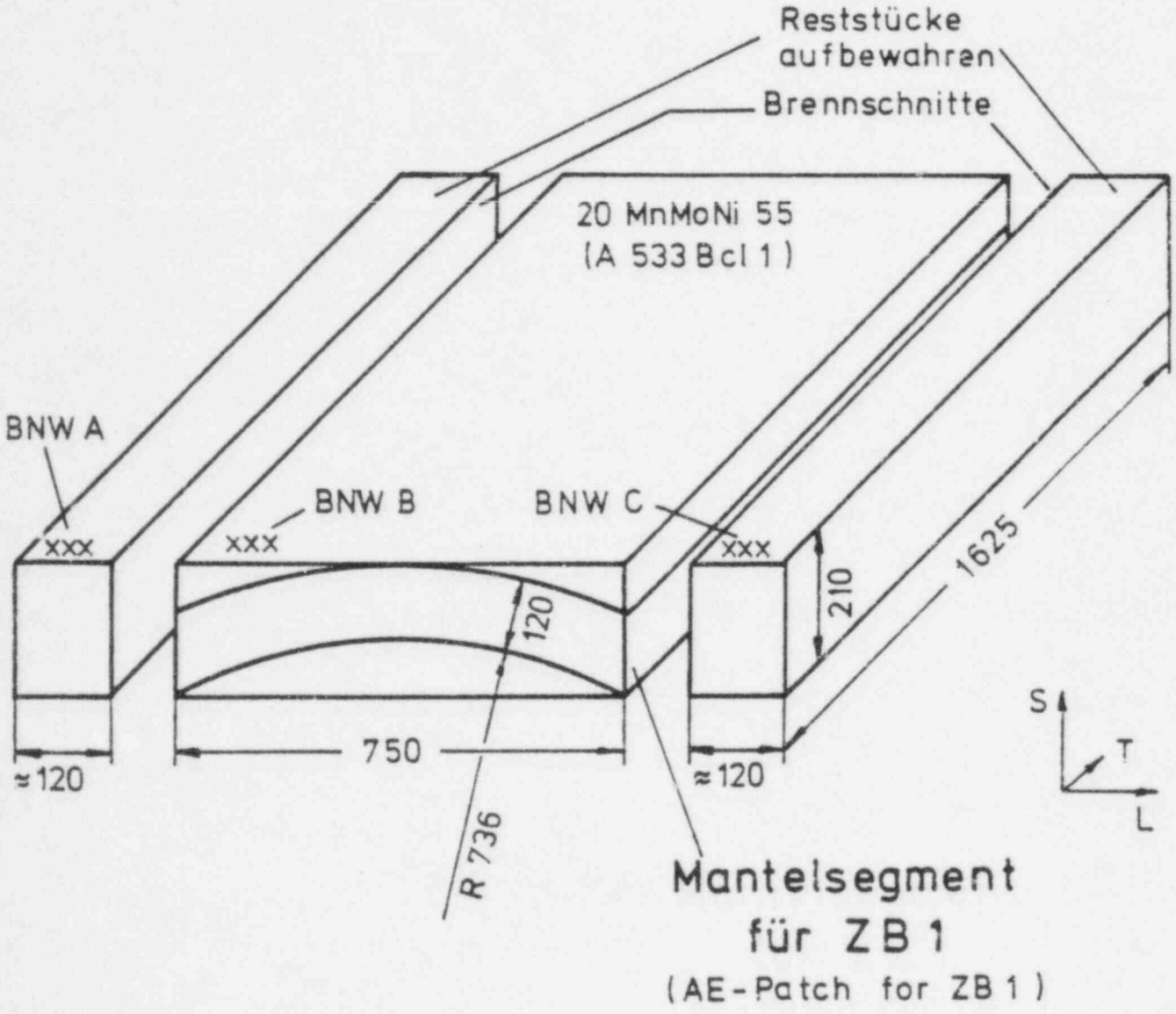

Figure 2: Cutting-plan of the A533 B steel plate

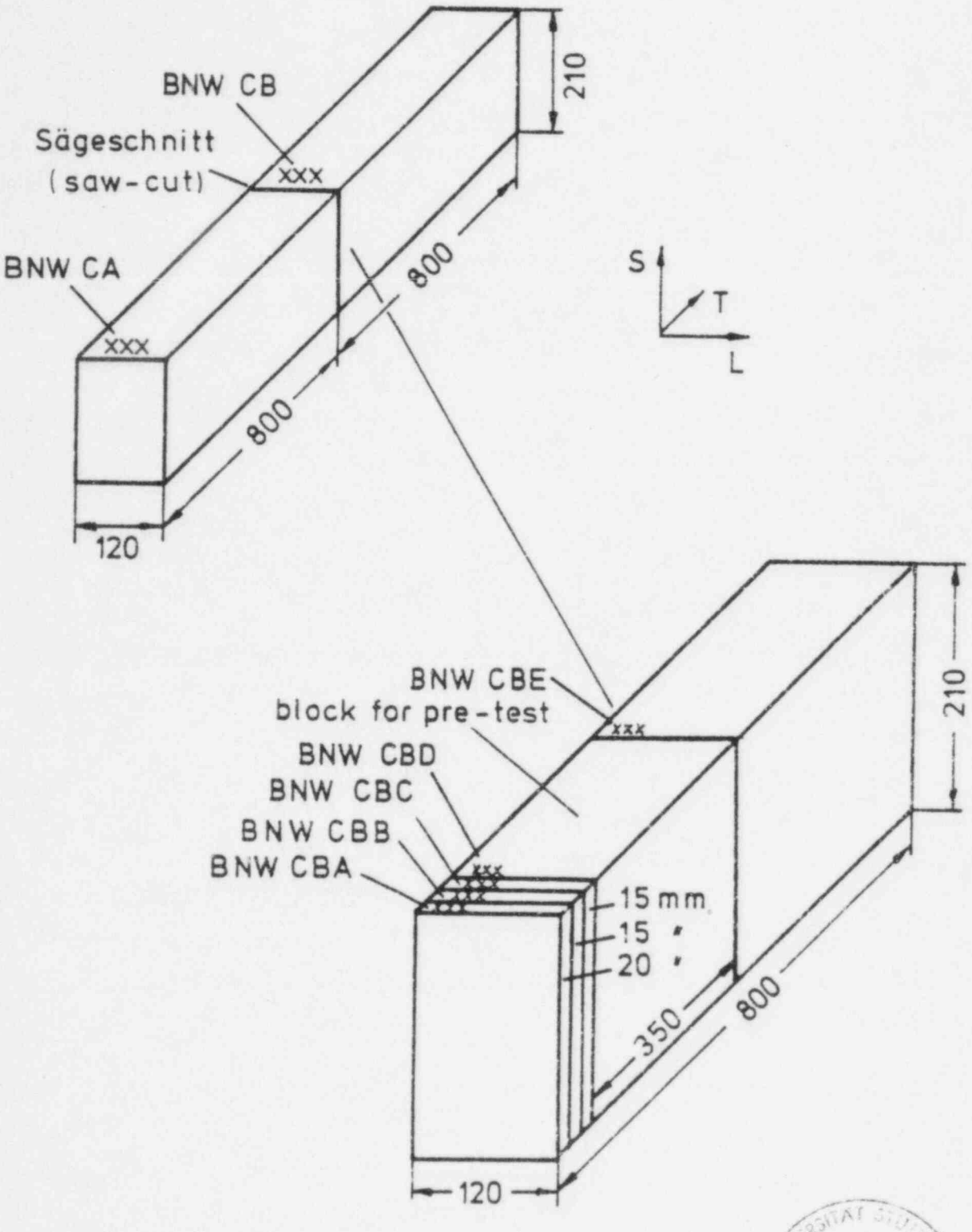

Figure 3: Cutting-plan of block BNW C

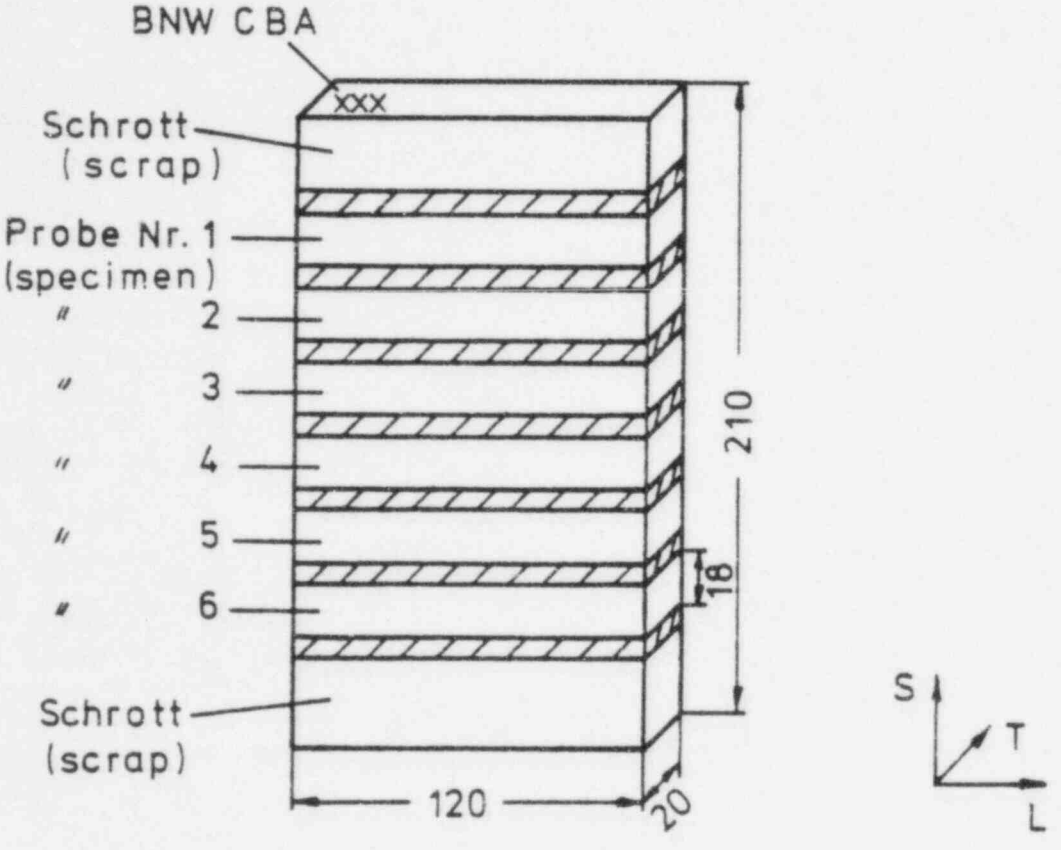

6 Zugproben (langs)
B 10 x 50 nach DIN 50 125
symmetrisch entnommen
(tensile specimens)

Figure 4: Location of the 6 tensile specimens

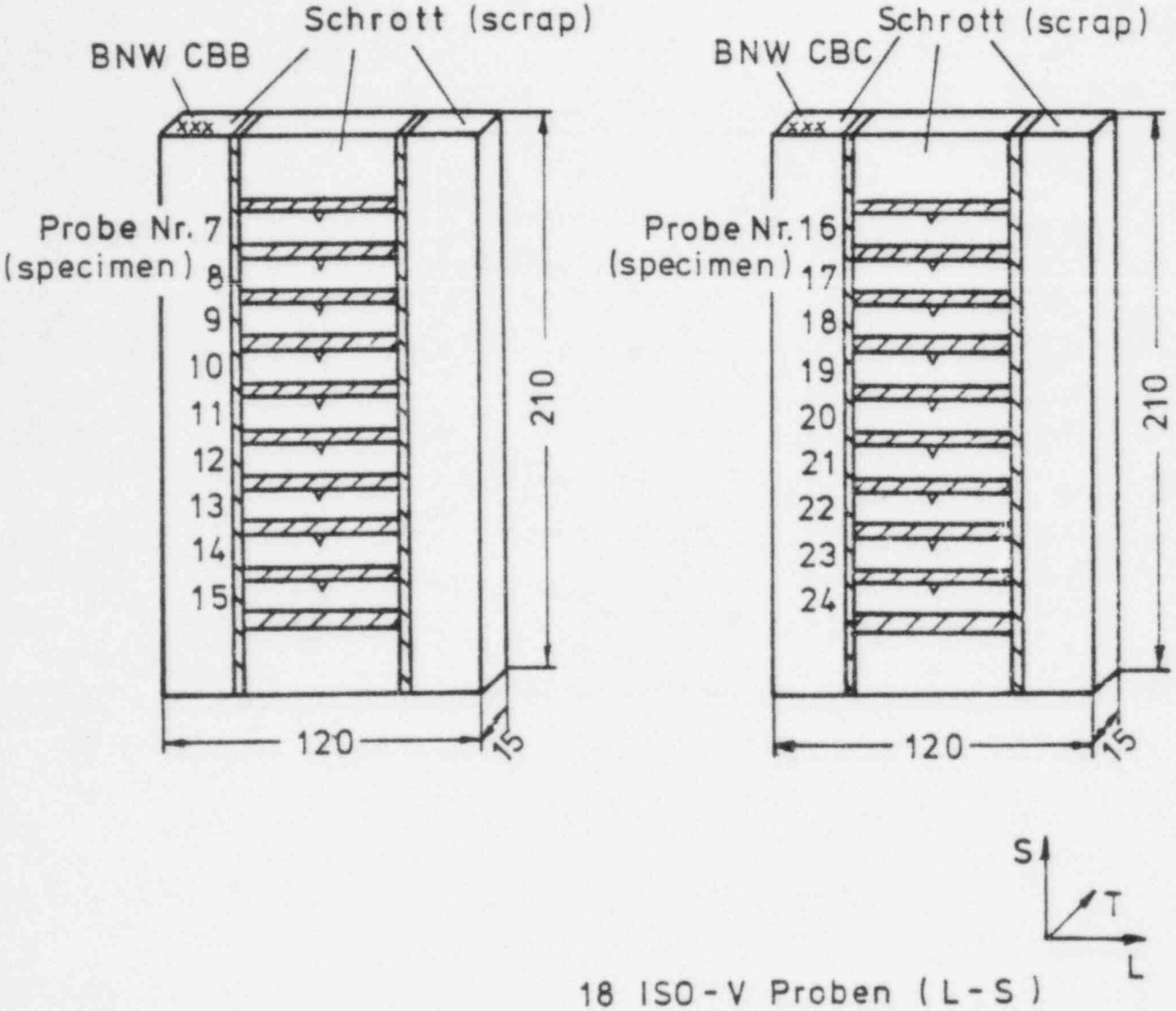

18 ISO-V Proben (L-S)
□ 10 x 55 nach DIN 50 115
symmetrisch entnommen
(Charpy-V specimens)

Figure 5: Location of the 18 Charpy-V- specimens

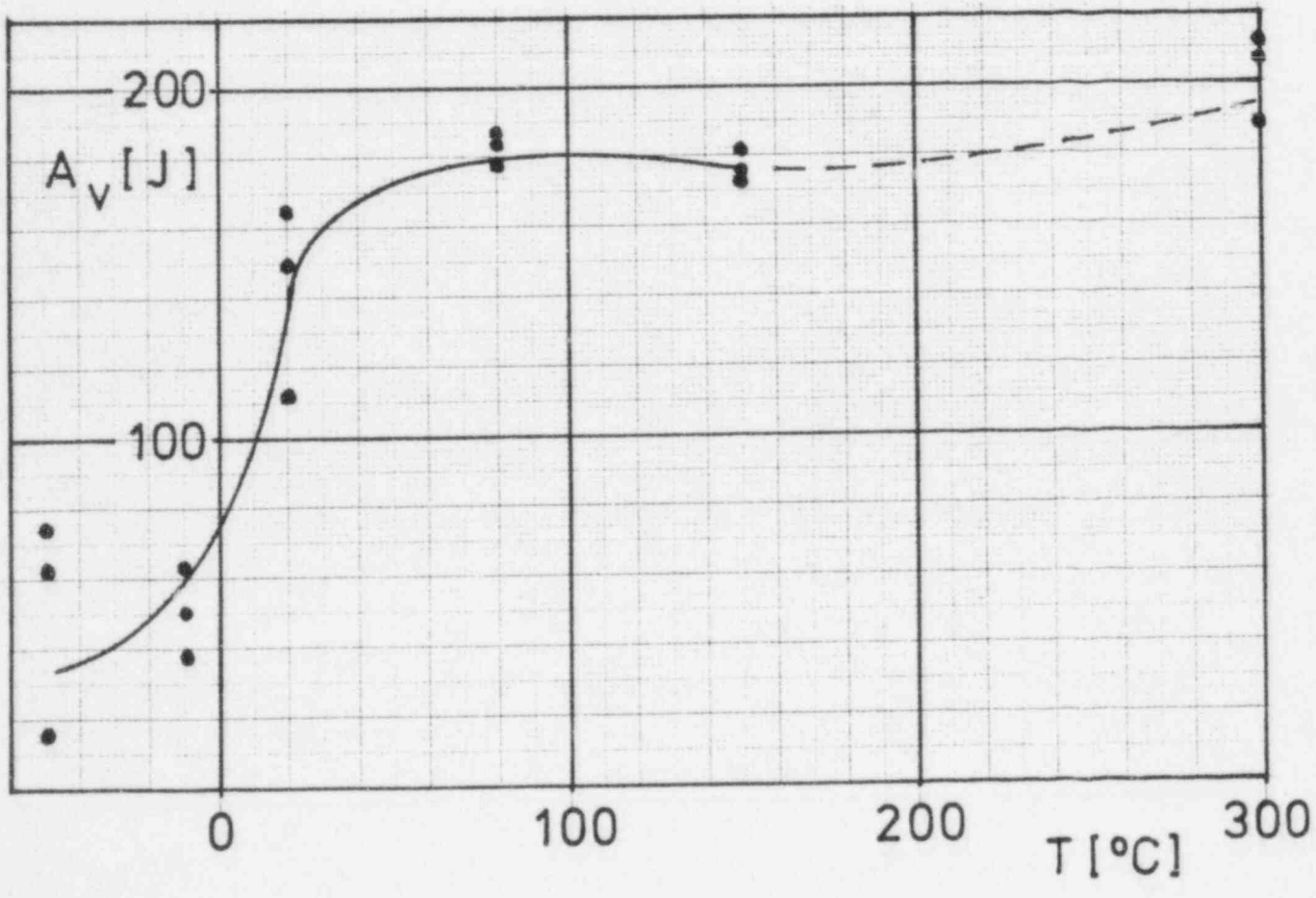

Figure 6: Impact energy after heat-treatment

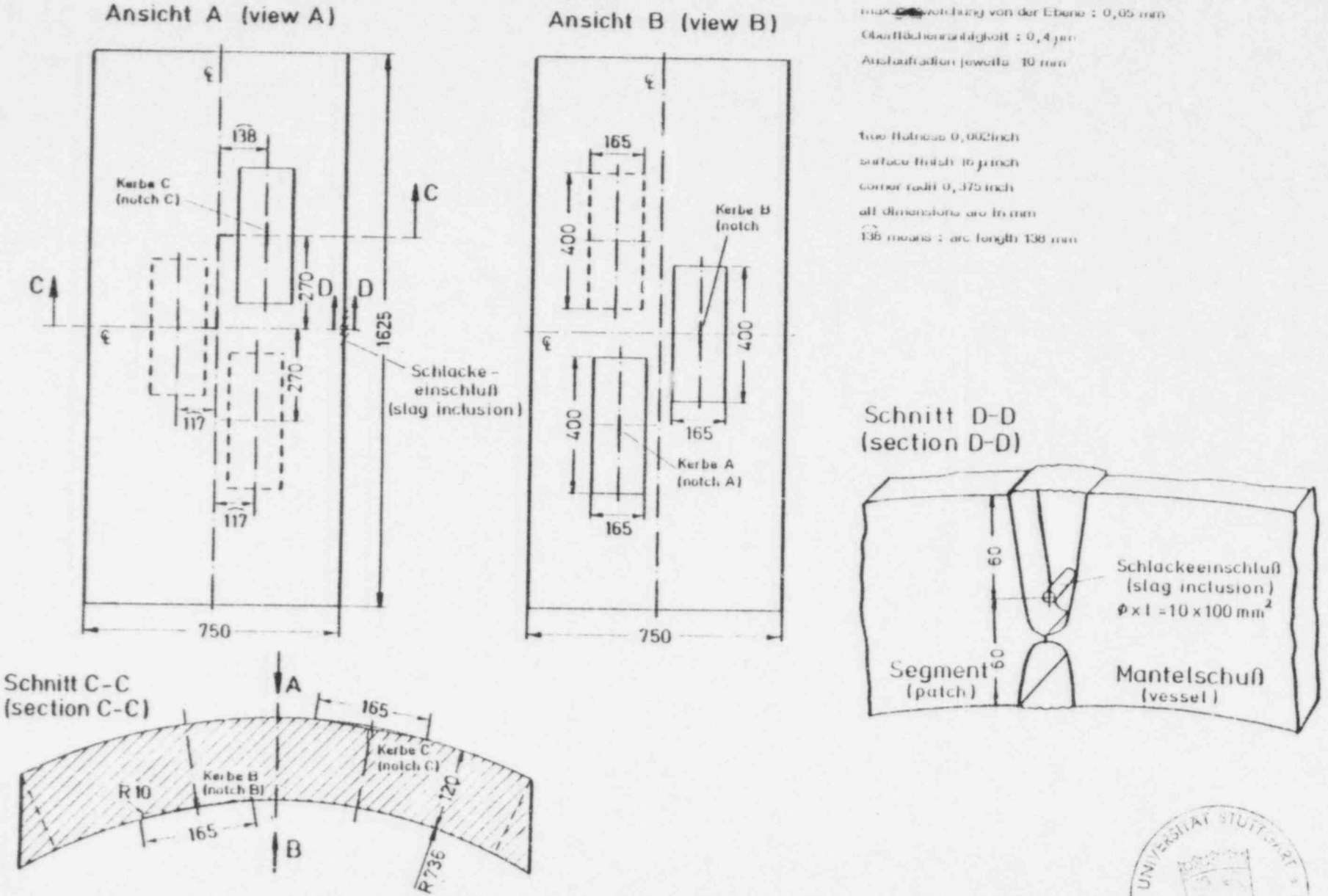

Figure 7: Dimensions of the patch with the location of the three notches

max. Abweichung von der Ebene : 0,05 mm
Oberflächenrauhigkeit : 0,4 µm
Anschaufradien jeweils 10 mm

true thickness 0,002inch
surface finish 16 µinch
corner radii 0,375 inch
all dimensions are in mm
138 means : arc length 138 mm

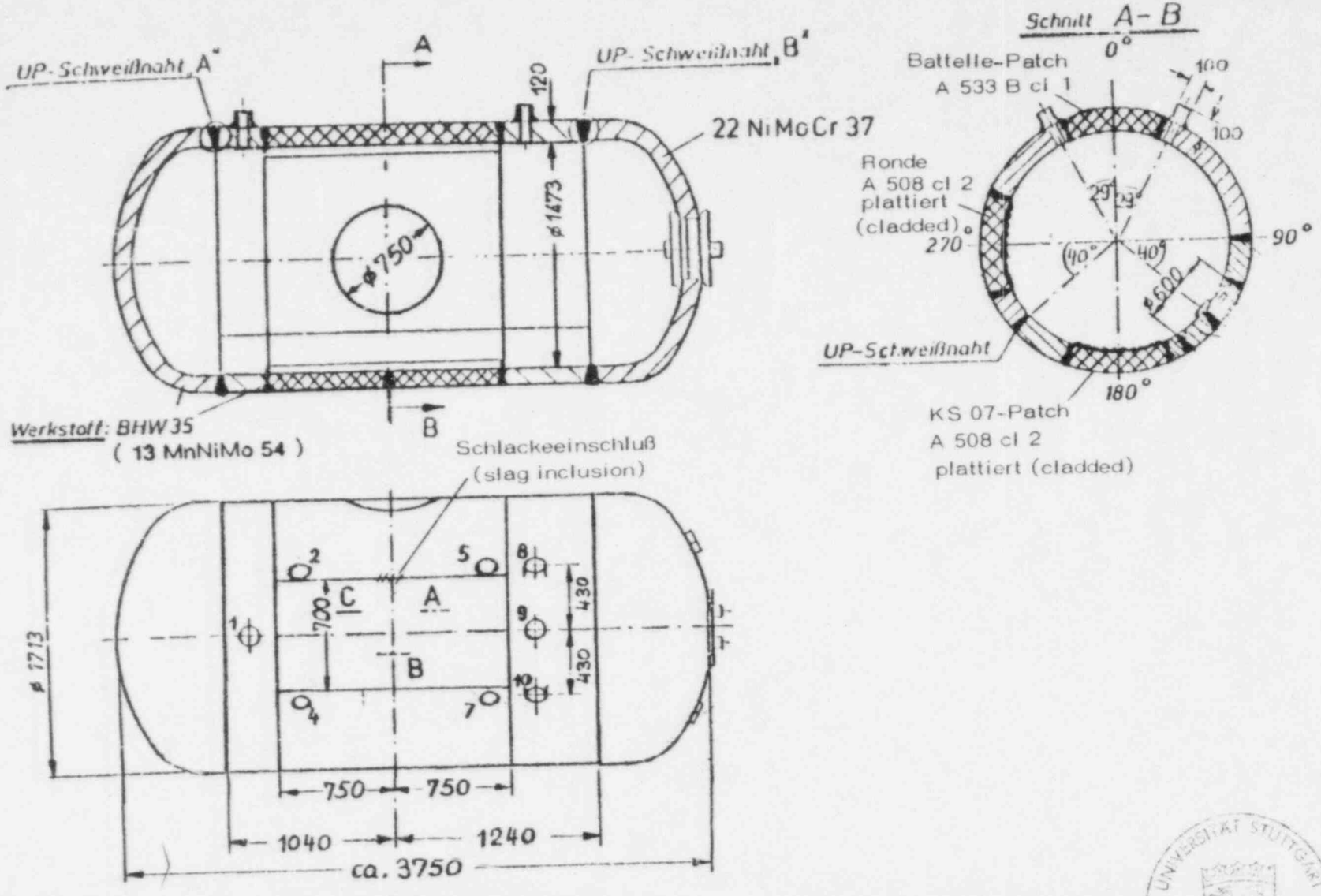

Figure 8: Vessel ZB 1 of the German Research Program "Integrity of Components"

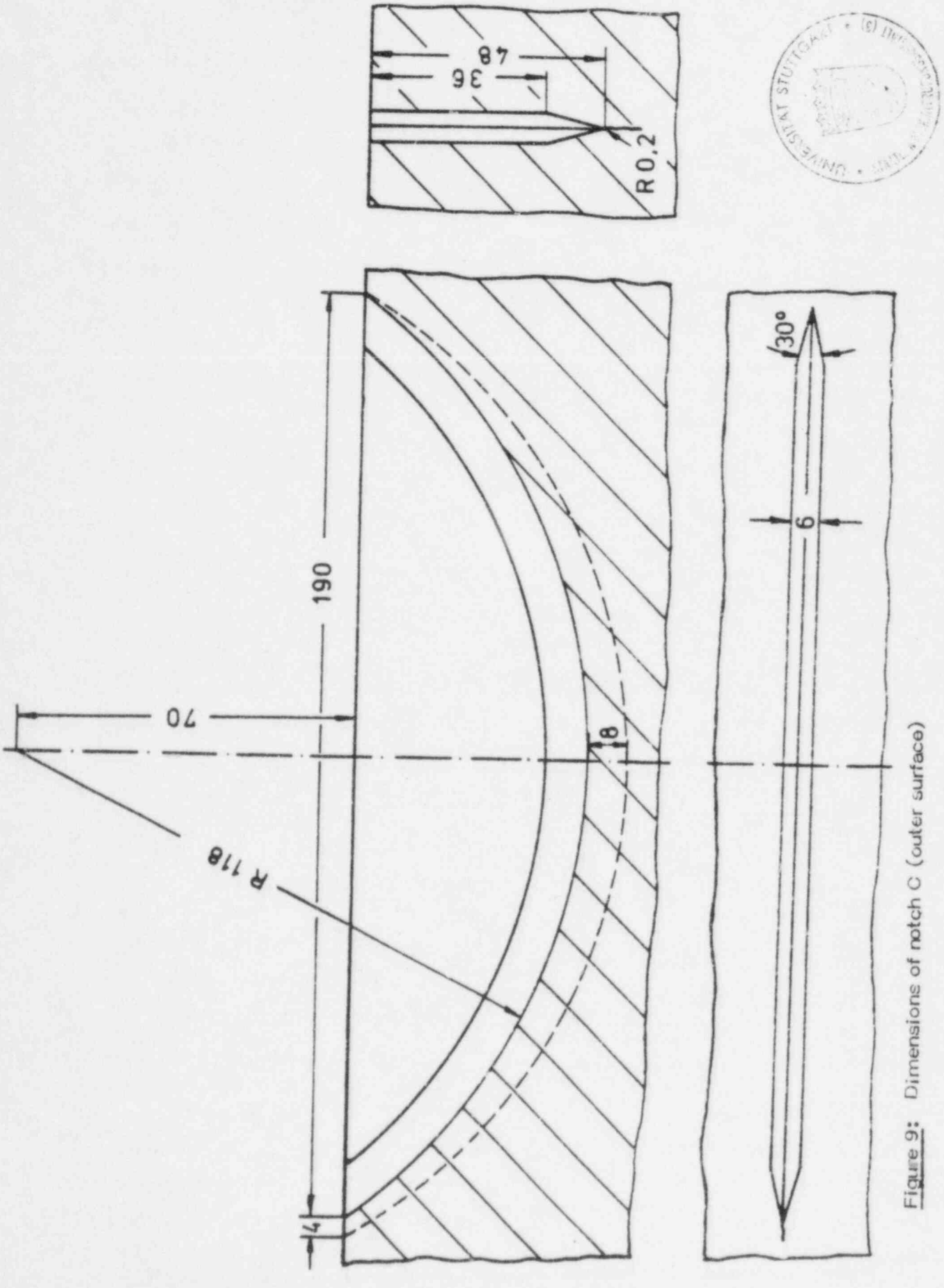

Figure 9: Dimensions of notch C (outer surface)

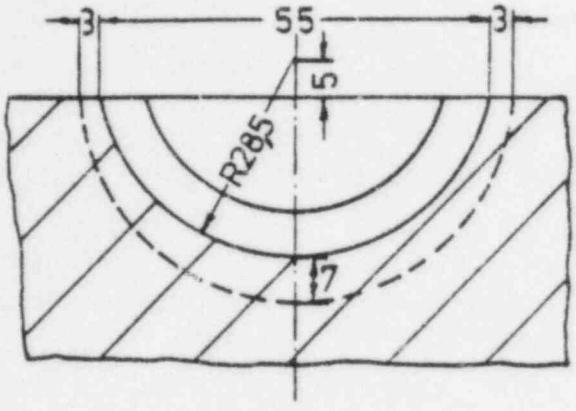

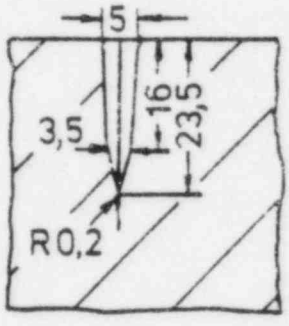

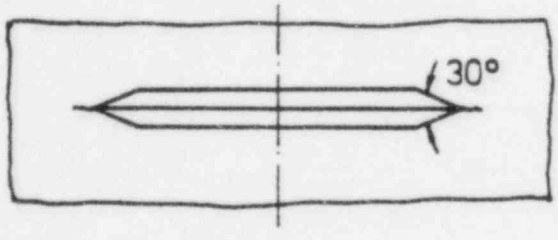

notch A

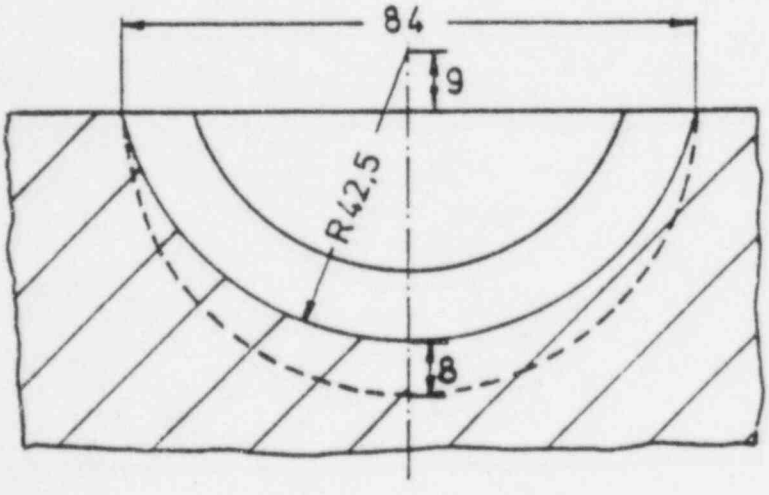

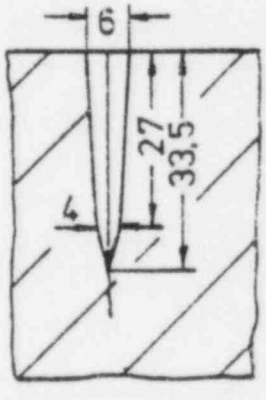

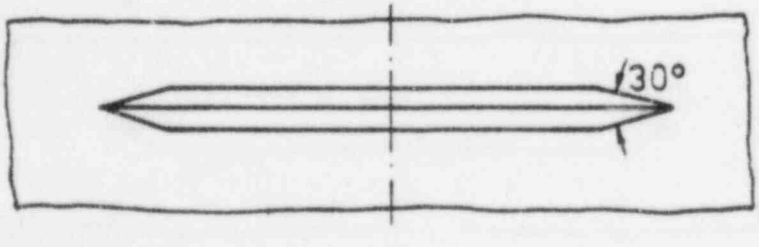

notch B

Figure 10: Dimensions of the notches A and B (inner surface)

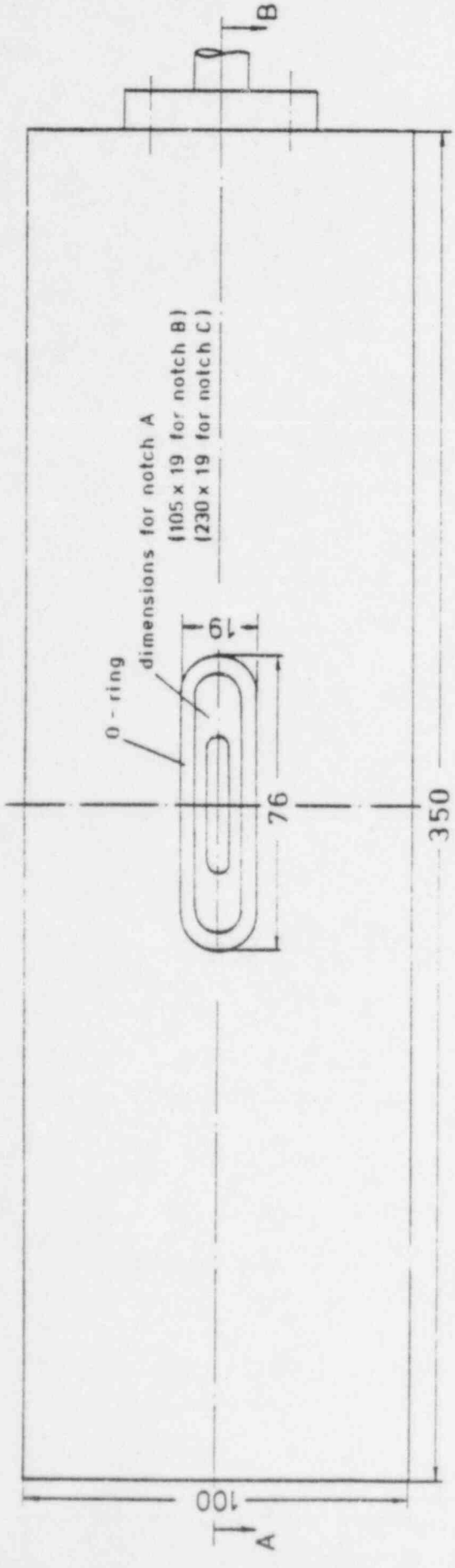

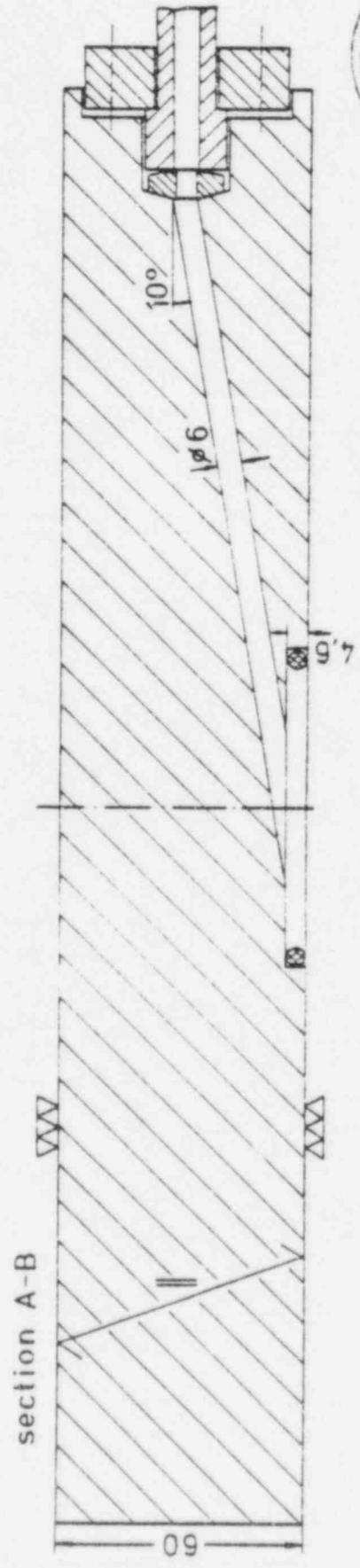

Figure 11: Seal-block used for local fatiguing

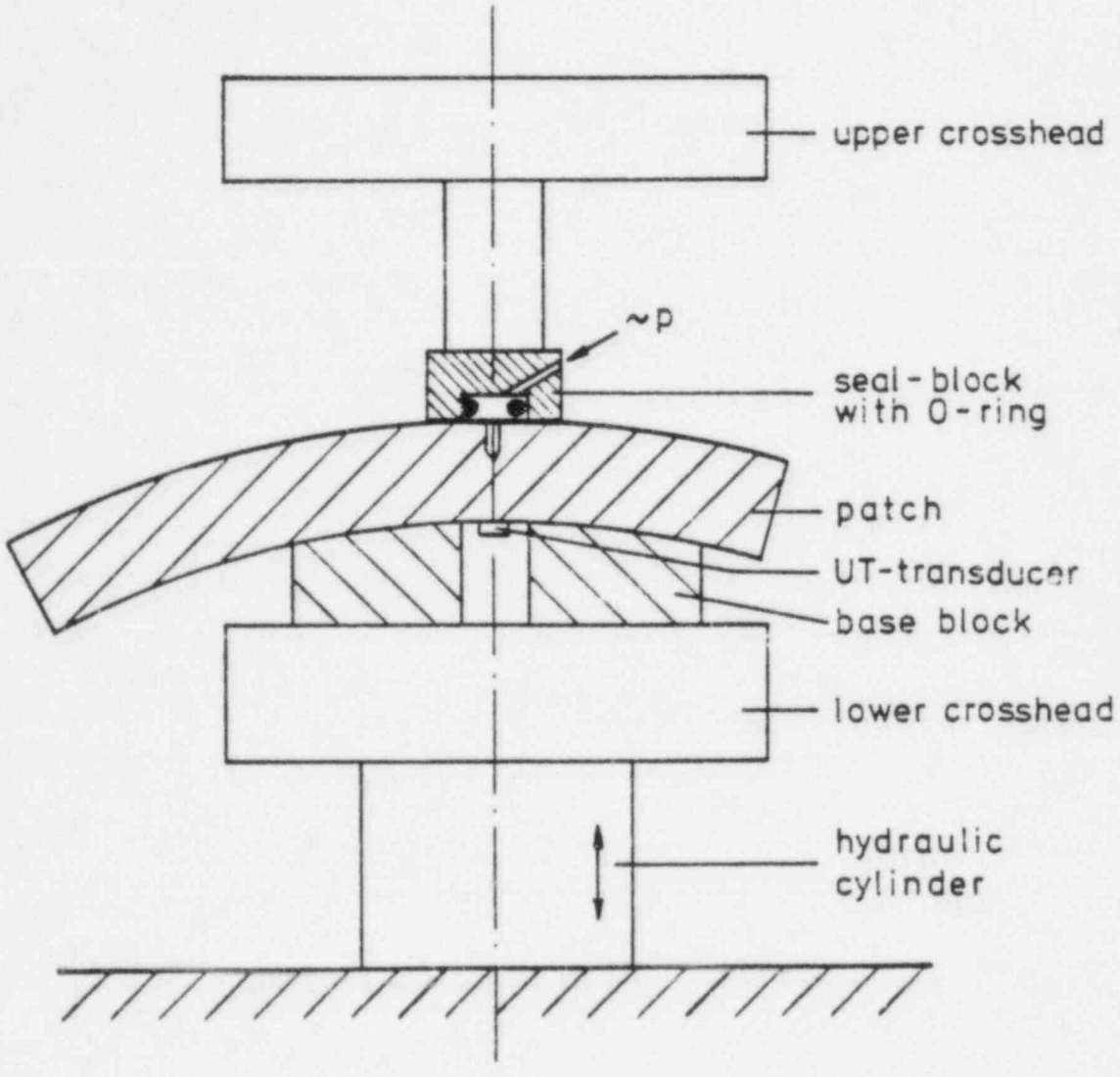

Figure 12: Schematic design of the loading apparatus

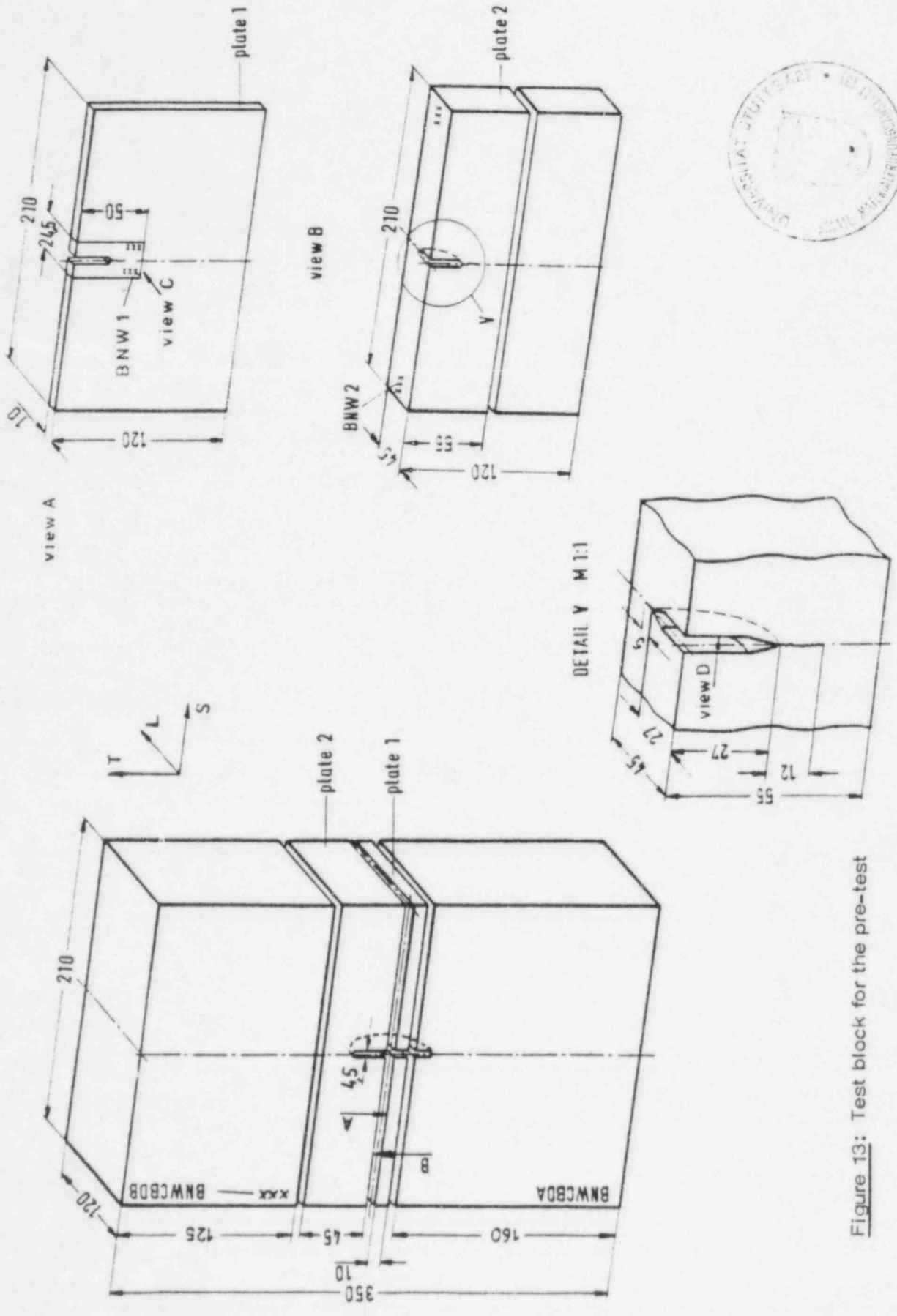

Figure 13: Test block for the pre-test

1 mm

Figure 14: Cross-section of notch A from pre-test (view C of Fig. 13, magnification 12,5 x)

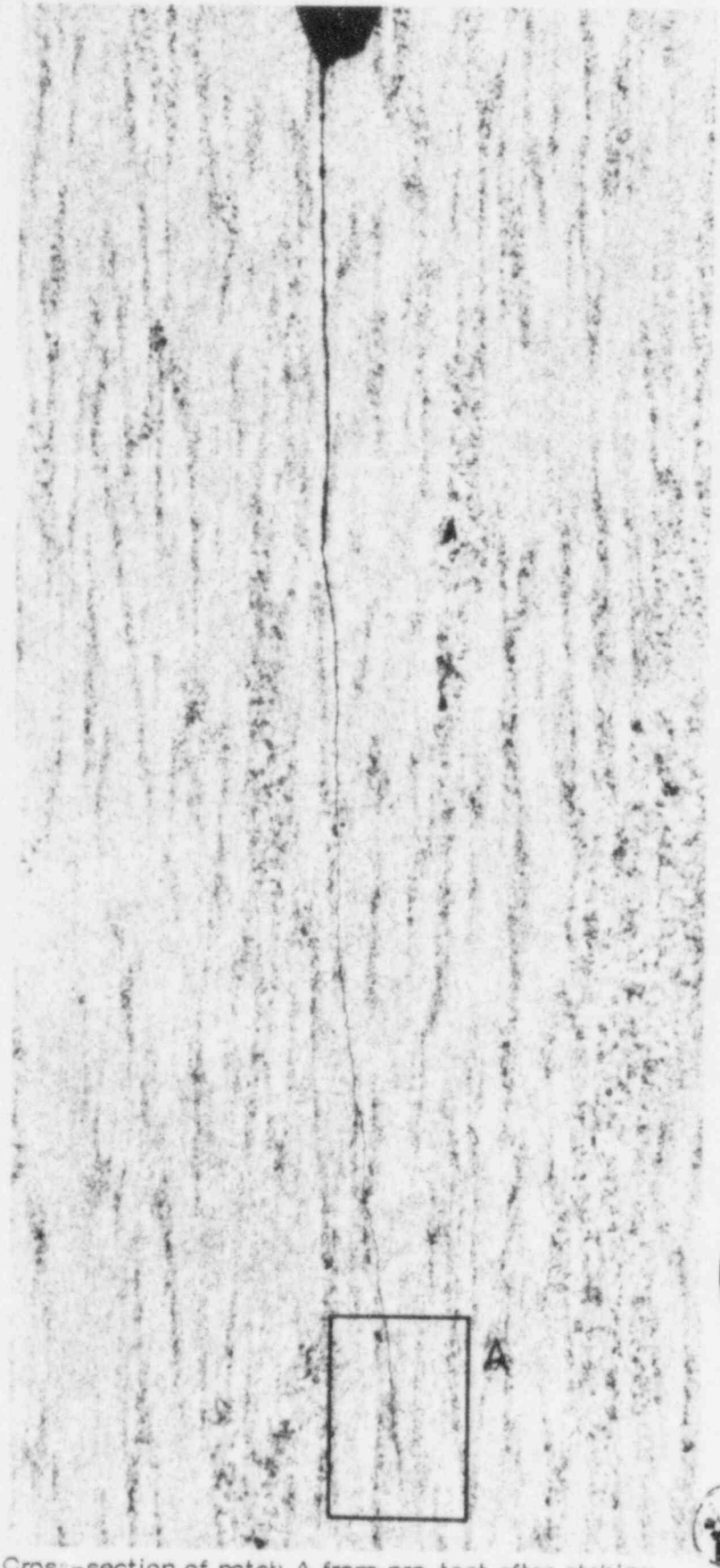

Figure 15: Cross-section of notch A from pre-test after etching (view C of Fig. 13, magnification 20 x)

Figure 16: Section A of Fig. 15 (magnification 100 x)

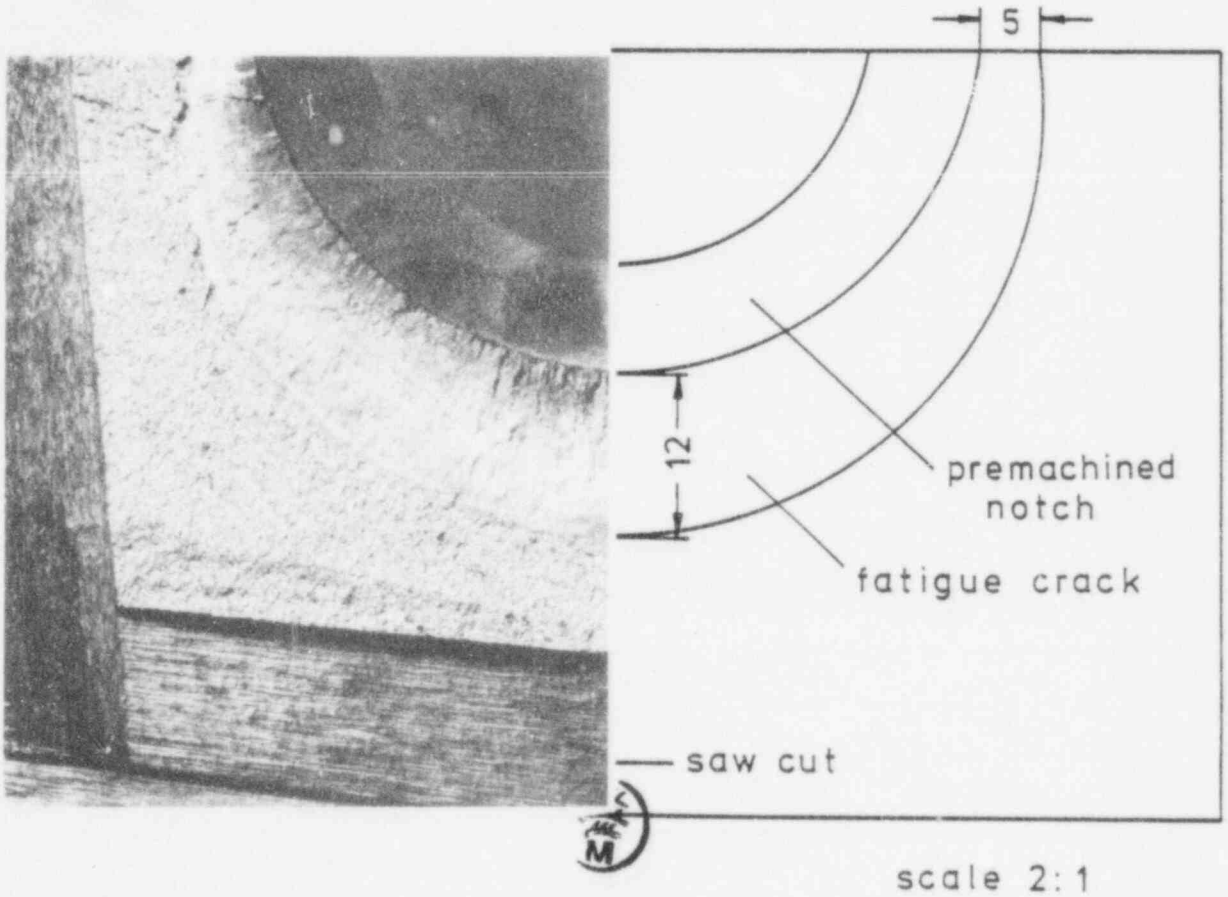

Figure 17: Fracture surface of notch A form pre-test (view D of Fig. 13, magnification 2 x)

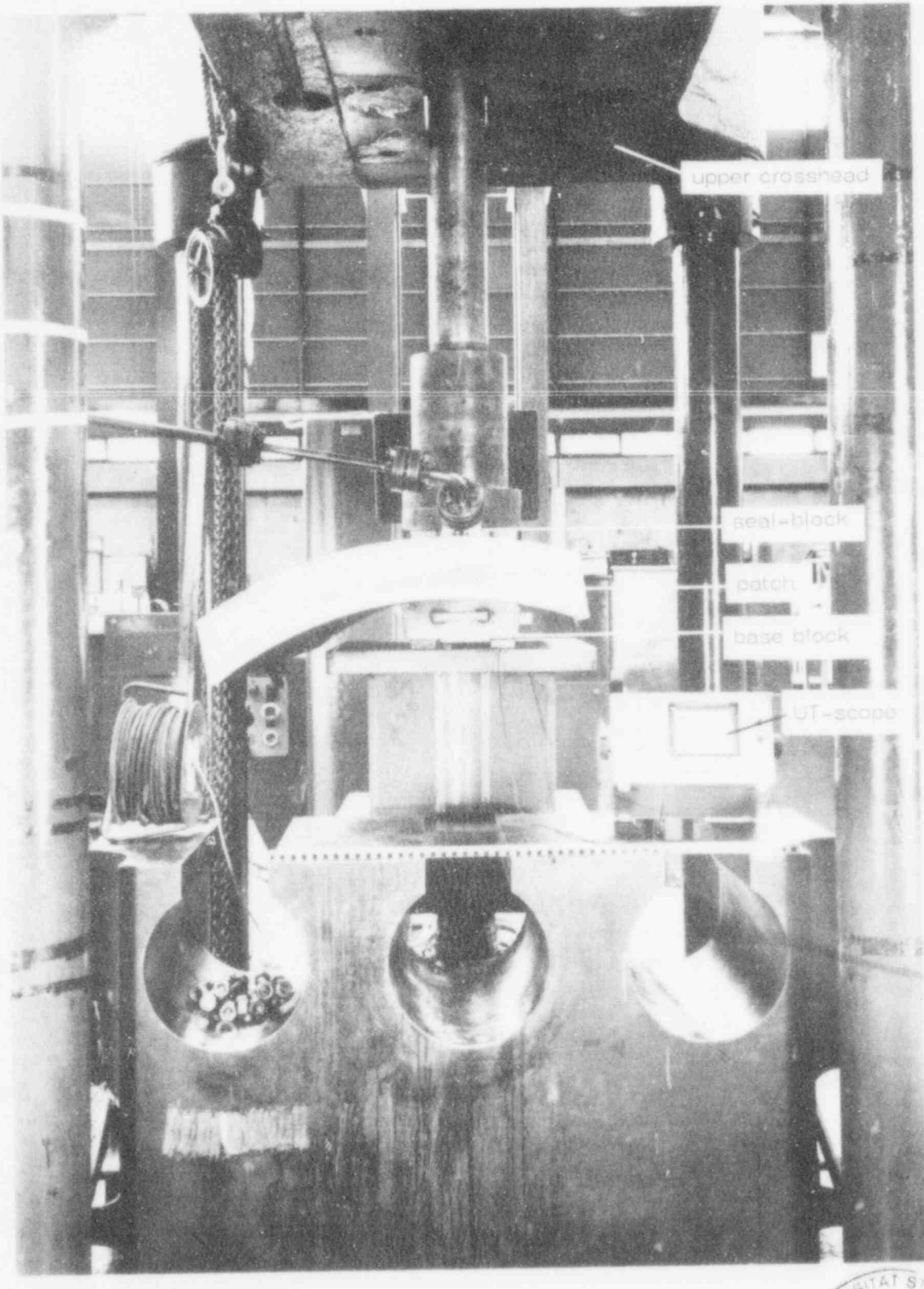

Figure 18: General front-view of the notch-sharpening apparatus

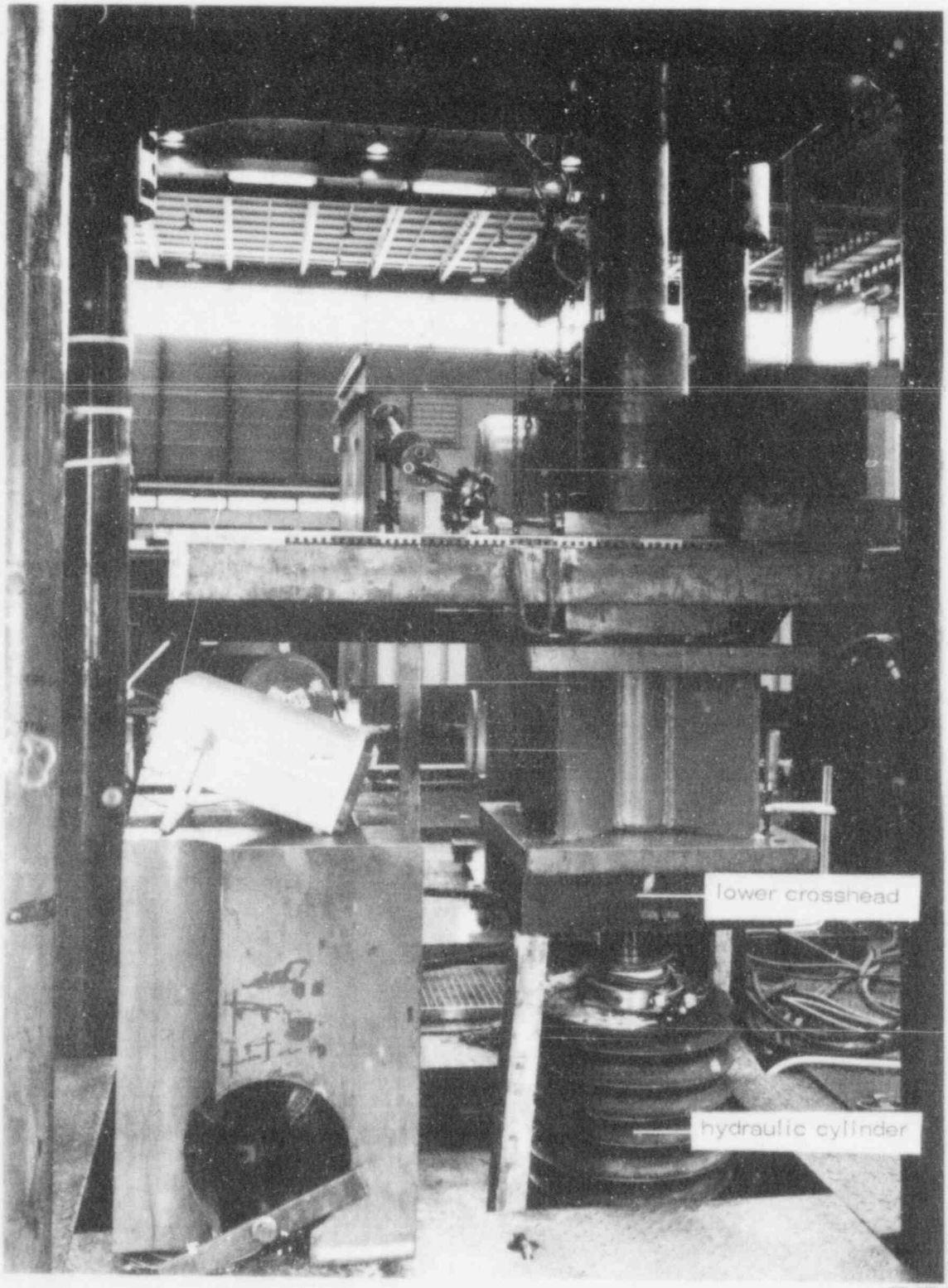

Figure 19: General side-view of the notch - sharpening apparatus

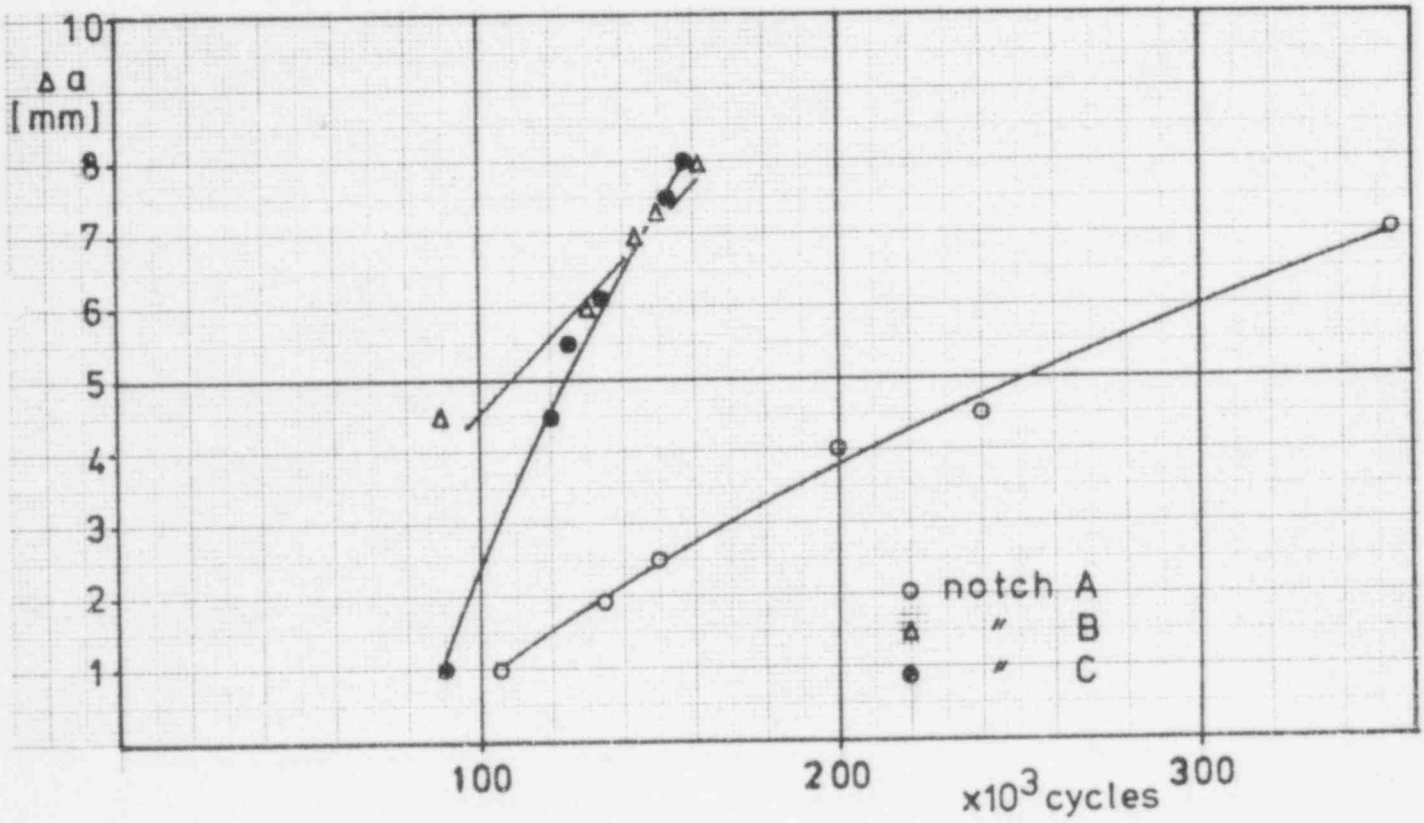

Figure 20: Crack-depth Δ a as a function of number of load-cycles for notch A, B and C

NUREG/CR-3915
PNL-5184
R5,GS

DISTRIBUTION

No. of Copies

U.S. Nuclear Regulatory Commission
Division of Technical Information and Document Control
7920 Norfolk Avenue
Bethesda, MD 20014

J. Muscara
U.S. Nuclear Regulatory Commission
Office of Nuclear Regulatory Research
M/S 5650NL
Washington, DC 20555

C.Z. Serpan
U.S. Nuclear Regulatory Commission
Office of Nuclear Regulatory Research
M/S 5650NL
Washington, DC 20555

2 John A. Raulston
Chief Nuclear Engineer, W10C126
Attn: Mr. E.A. Merrick, W3D194
Tennessee Valley Authority
400 West Summit Hill Drive
Knoxville, TN 37902

No. of Copies

31 Pacific Northwest Laboratory

L. S. Dake
J. F. Dawson
S. M. Faber
M. A. Friesel
P. H. Hutton (9)
R. J. Kurtz
R. R. Lewis
R. P. Marshall
R. A. Pappas
C. B. Perry
G. J. Posakony
E. B. Schwenk
J. R. Skorpik
R. A. Stokes
T. T. Taylor
K. E. Williamson
Tech. Information (5)
Publ. Coordination (2)

NRC FORM 335 (2-84) NRCM 1102, 3201, 3202

U.S. NUCLEAR REGULATORY COMMISSION

BIBLIOGRAPHIC DATA SHEET

SEE INSTRUCTIONS ON THE REVERSE

1. REPORT NUMBER (Assigned by TIDC, add Vol. No., if any)
NUREG/CR-3915
PNL-5184

2. TITLE AND SUBTITLE
Acoustic Emission Results Obtained from Testing the ZB-1 Intermediate Scale Pressure Vessel

3. LEAVE BLANK

4. DATE REPORT COMPLETED
MONTH: April YEAR: 1985

5. AUTHOR(S)
P.H. Hutton, R.J. Kurtz, R.A. Pappas, J.F. Dawson, L.S. Dake, J.R. Skorpik

6. DATE REPORT ISSUED
MONTH: September YEAR: 1985

7. PERFORMING ORGANIZATION NAME AND MAILING ADDRESS (Include Zip Code)
Pacific Northwest Laboratory
PO Box 999
Richland, WA 99352

8. PROJECT/TASK/WORK UNIT NUMBER

9. FIN OR GRANT NUMBER
B2088

10. SPONSORING ORGANIZATION NAME AND MAILING ADDRESS (Include Zip Code)
Division of Engineering Technology
Office of Nuclear Regulatory Research
U.S. Nuclear Regulatory Commission
Washington, DC 20555

11a. TYPE OF REPORT
Topical

b. PERIOD COVERED (Inclusive dates)
September 1982 - September 1983

12. SUPPLEMENTARY NOTES

13. ABSTRACT (200 words or less)

Acoustic emission (AE) monitoring of flaw growth in an intermediate scale vessel during cyclic loading at 65°C and 288°C is described in this report. The report deals with background, methodology, and results. The work discussed is of major significance in a program supported by NRC to develop and demonstrate application of AE monitoring for continuous surveillance of reactor pressure boundaries to detect and evaluate growing flaws. Several areas of technical concern are addressed. Results support the feasibility of effective continuous monitoring.

14. DOCUMENT ANALYSIS - a. KEYWORDS/DESCRIPTORS
Acoustic emission monitoring of reactor pressure boundaries for flaw detection.

b. IDENTIFIERS/OPEN-ENDED TERMS
acoustic emission, reactor pressure boundaries, continuous monitoring, flaw detection, intermediate scale vessel

15. AVAILABILITY STATEMENT
Unlimited

16. SECURITY CLASSIFICATION
(This page) Unclassified
(This report) Unclassified

17. NUMBER OF PAGES

18. PRICE

UNITED STATES
NUCLEAR REGULATORY COMMISSION
WASHINGTON, D.C. 20555

120555078877 1 1AN1R51GS
US NRC
ADM-DIV OF TIDC
POLICY & PUB MGT BR-PDR NUREG
W-501
WASHINGTON DC 20555